# ANALYSIS OF UPPER BODY BIOMECHANICS AND CONTROL IN MANUAL WHEELCHAIR USERS


**Hassanain Ali Lafta (B.Sc., M.Sc.)**

A thesis submitted in fulfilment of the requirements
for the degree of Doctor of Philosophy

**SCHOOL OF ENGINEERING**

**CARDIFF UNIVERSITY**

February 2018

# Abstract

Manual wheelchair propulsion involves repetitive shoulder range of motion and muscular activities. It is an important form of mobility for many people with lower limb disabilities who depend upon their upper body to provide means of locomotion for completion of their activities of daily living. As a result of greater than normal usage of the upper limbs, shoulder and wrist pain and pathology are common among manual wheelchair users.

This study provides a biomechanical analysis of the manual wheelchair mobility in control subjects during their functional activities of daily living. Non-experienced wheelchair users were recruited per this study for their feature of novice as they could determine their own self-selected speed and pattern of propulsion and to limit any variability that would be existed by a study group with multiple inter-individual differences.

In the context of manual wheelchair propulsion, biomechanics of upper body involves the study of how a manual wheelchair user imparts power to the wheels to achieve mobility. In general, the primary goal of biomechanical analysis of manual wheelchair propulsion is to generate knowledge that can be used to improve performance and/or prevent injuries.

The main objectives of this study were to investigate the impact of trunk and upper limb biomechanics associated with diverse wheelchair configurations in terms of adjusting vertical displacement (seat-to-floor height) and horizontal displacement (rear wheel axle position). A marker-based 3D motion analysis technique was used with more recently to the six degrees of freedom (6DOF) analysis, as an integrated feature in the software that was used to collect the motion capture data (Qualisys Track Manager, QTM, Qualisys, Sweden). Three-dimensional kinematics of trunk and upper limb joints were investigated during physiological range of motion (ROM), activities of daily living (ADL), and functional wheelchair mobility that includes starting up from the rest, propulsion and stopping a wheelchair during manual propulsion

The contribution of the shoulder complex muscles was investigated through the analysis of the surface electromyographic (sEMG) patterns of six stabilising muscles activity during physiological range of motion, activities of daily living and functional wheelchair mobility. Also, the interrelationship between the users' anthropometric characteristics and the biomechanics of their upper body were investigated in terms of kinematics, surface electromyography and spatiotemporal parameters during manual wheelchair propulsion.

This study showed an interrelationship between diverse wheelchair configurations of adjustable wheelchair rear wheel axle position and seat height and upper body kinematic behaviour, muscles recruitment and spatiotemporal patterns during manual wheelchair mobility. It was observed that changing rear wheel axle position posteriorly and raising the seat-to-floor distance (i.e. raising the seat height position) are correlated with higher upper body kinematics and release phase muscle activities and lower pushing patterns and push muscle activities during functional wheelchair mobility and so could be linked with higher risk of musculoskeletal disorders.

As the number of manual wheelchair users is developing around the world, it becomes very essential to increase the understanding of the biomechanics of upper body to enhance the performance and decrease the risk of injury. It is hoped that this knowledge will help both manufacturers and clinicians when designing and prescribing wheelchairs that are more proper to the users' functional features, needs and expectations, accordingly profiting users' independence and quality of life.

## *Acknowledgments*

I would like to express my appreciation towards everyone who made this work possible and real.

First, I would like to express a great deal of gratitude to my supervisors: Prof Cathy A. Holt and Dr Gemma M. Whatling for their support and guidance throughout my research study and for being a constant source of encouragement and motivation over these four years journey. It was a great experience working with them.

I would like to acknowledge my sponsor, The Higher Committee for Education Development in Iraq, HCED for sponsoring my study and giving me the opportunity to pursue my PhD degree at Cardiff University, United Kingdom.

My thanks also conveyed to my friends at the Cardiff School of Engineering who have contributed to the success of my experimental work, especially with their participation as volunteers in my study.

I would like to thank my beloved parents, brothers and sister for making me who I am today. Thank you for always being there for me.

Finally, I would like to thank my dearest wife, *Summer* and our loving daughter, *Mayan*. It was definitely not easy, but you both made these years a memorable journey full with love and support.

This accomplishment is dedicated to you.

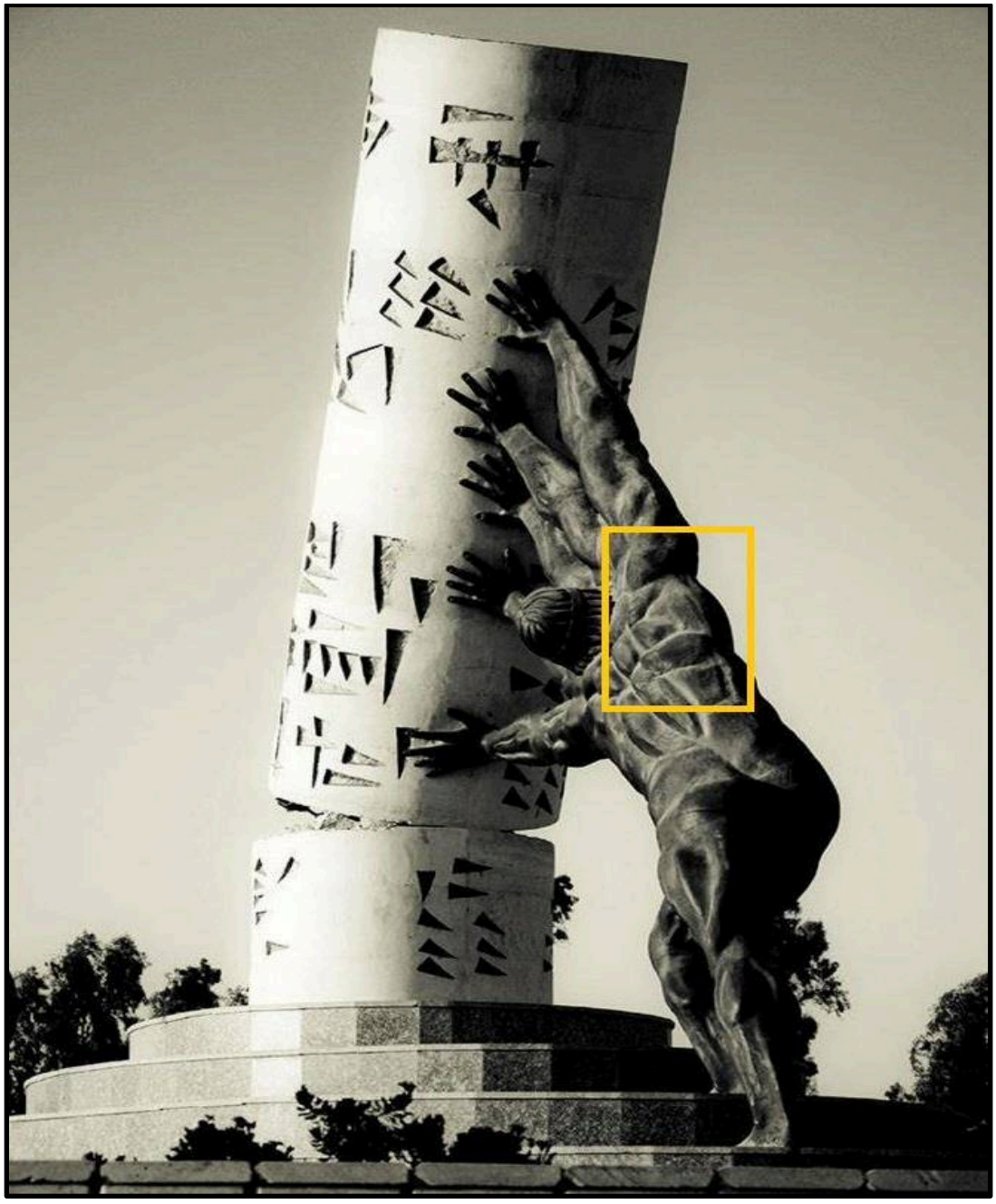

*"Iraq rises again"* is one of the most famous monuments in Baghdad, Iraq.

It was designed by the Iraqi sculptor Mohammed Ghani Hikmet (1929-2011). The broken pillar is engraved with Sumerian characters taken from the Cuneiform script. The translation of this script is *"the first written words started here"*. The pillar represents Iraq, and it is being held up by a man with multiple arms, representing the different ethnic groups of Iraqi people working together to rescue their homeland country.

# List of Contents

# List of Figures

# List of Tables

# Chapter 1

# Introduction

The human arm is, contrary to the human leg, not specialized. In contrast, the arm can be used for a large diversity of tasks, varying from manipulation of small objects to handling of heavy materials. In addition, the human arm has a large range of motion. From an anatomical view, the difference in function between arms and legs is well visible in the difference in structure between the shoulder and the pelvis.

The shoulder is the most complex while the most moveable joint in the human body. Because of this complexity, it has the greatest amount of motion than any other joint complex. In daily life, this mobility is used for a large number of different activities of daily living (ADLs) like cleaning, feeding and reaching activities. It can be seen as a perfect compromise between mobility and stability. This mobility is greater than that required for the majority of activities of daily living (ADLs). Manual wheelchair propulsion is an important form of mobility for many people with lower limbs disabilities who depend upon their upper limbs to provide means of locomotion during completion of their activities of daily living. As a result of greater than normal usage of the upper limbs, pain and pathology are common among manual wheelchair users (MWUs). This study focuses on understanding the kinematic and kinetic behaviour and muscles recruitment involved during interactions of the trunk and upper limbs with a propelling a manual wheelchair during daily mobility and use.

## 1.1 Literature Review

### *1.1.1. Biomechanics of Manual Wheelchair Propulsion*

Manual wheelchair propulsion biomechanics is the study of the way in which the wheelchair user powers the wheels for propulsion. Biomechanics study look at the loads on upper body joints and muscles during propulsion and on the kinematics of the stroking motion. Studies related to the biomechanics of manual wheelchair propulsion have increasingly been performed over the last two decades. In an effort to gain a better understanding of the relationship between manual wheelchair propulsion and upper limb joints kinematics and associated muscle activity,

researchers and clinicians have conducted biomechanical analyses of wheelchair propulsion.

Wheelchair propulsion is defined as a repetitive task that is typically described as two phases of hand and arm movement; the push phase and the recovery phase, see Figure (1.1). During the push (propulsive) phase, the individual's hands, in contact with the pushrim of the wheelchair, can be moved imparting a tangential force either upward with the elbow flexed (between the beginning and the middle of the push), or downward with the elbow extended (from the middle to the end of the movement) to the rim in order to increase or maintain velocity of the wheelchair, (Guo et al. 2013), see Figure (1.2). The recovery phase occurs after the propulsive phase and it is during this phase that the arms are brought back to a position where a new propulsive phase can begin (Sanderson and Sommer, 1985). These definitions have allowed researchers to compare findings during the push phase with those of the recovery phase and resulting biomechanical analyses have identified modifiable risk factors, which would hopefully aid in the development of prevention and treatment interventions.

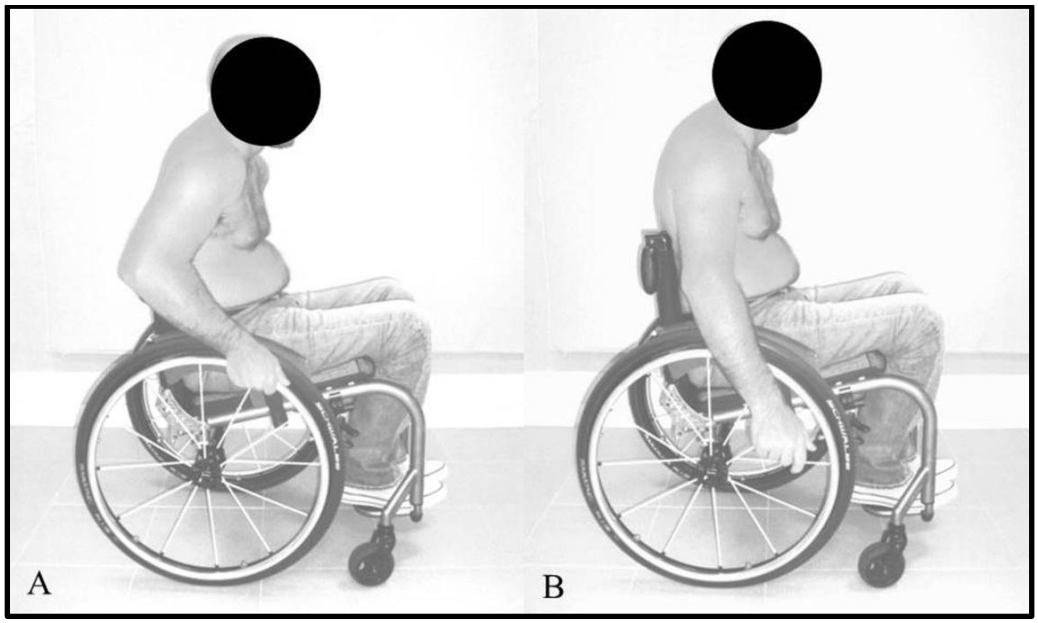


**Figure (1.1):** Phases of manual wheelchair propulsion cycle: (A) push phase and (B) recovery phase, (Dellabiancia et al. 2013).

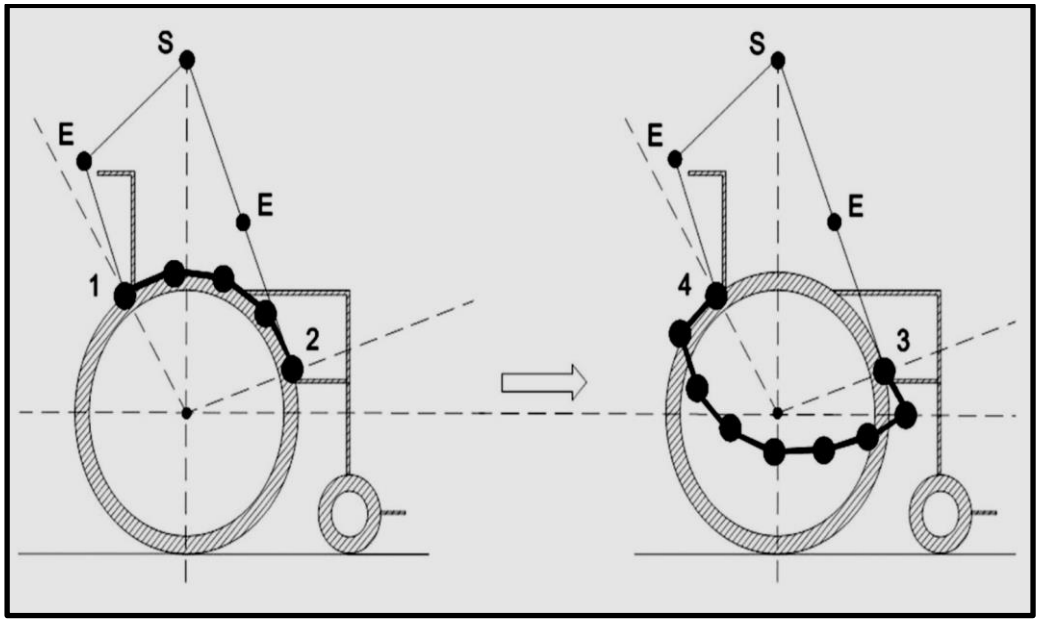


**Figure (1.2):** Trajectory of the hands during the two phases of manual wheelchair propulsion. S: shoulder, E: elbow, 1: start push, 2: end push, 3: start recovery, 4: end recovery. (Dellabiancia et al. 2013).

Although the greatest joint loads have been found to exist in the shoulder articulation, a further contribution of push is exerted by the wrist. The gradual change of the tangential force applied to the wheel has an injurious effect on the rotator cuff muscles. Also, it was found that those who rapidly load the pushrim during the propulsive stroke may be at risk for carpal tunnel syndrome, (Boninger et al. 1999). In a normal shoulder, the deltoid is the most powerful muscle and can generate a force up to six times the weight of the arm. It has the largest moment arm around the glenohumeral joint and is the most effective muscle in arm elevation, acting superiorly at (63°) when the arm is resting at the side of the body. The deltoid can alone provide (70%) of the torque at 30° of abduction and (85%) at (90°), the supraspinatus acts (15-20°) superiorly and can generate a force of 2.5 times the weight of the arm, the infraspinatus acts (40-45°) inferiorly and the force of the teres minor is also directed inferiorly at (55°). Together, the infraspinatus and teres minor can generate a force of five times the weight of the arm, (de Beer et al. 2007).

When abduction of the arm is initiated, the shear force on the glenohumeral joint generated by the deltoid is counteracted by the compressive force produced by the rotator cuff. Generally, the compressive force contributes towards joint stability while the shear force induces upward displacement of the humeral head. The

combination of shear and compressive forces allows efficient abduction by stabilising the humeral head within the glenoid fossa. The magnitude and direction of the resultant joint reaction force is dependent on the position of the arm. At (90°) of abduction, the joint reaction force is at its maximum and equates approximately the weight of the body, (de Beer et al. 2007).

During propulsion, the shoulder is maintained at approximately (70°) of abduction. At the onset of the propulsive phase of motion, the shoulder is extended and internally rotated and subsequently ends up flexed and externally rotated at the onset of the recovery phase. As a result of years of wheelchair propulsion, wheelchairs users often have well-developed shoulder flexors, internal rotators, and adductors, but may have poorly developed external rotators and thoracoscapular muscles, (Dellabiancia et al. 2013). This muscular imbalance and the repetitive nature of the wheelchair push predispose to the subacromial impingement.

The elbow is flexed throughout the pushing phase, starting from an angle of about (60°), gradually increasing until the hand assumes the most distant position from the ground and subsequently decreasing until to reach the minimum distance from the ground near by the recovery phase, (Dellabiancia et al. 2013), see Figure (1.3).

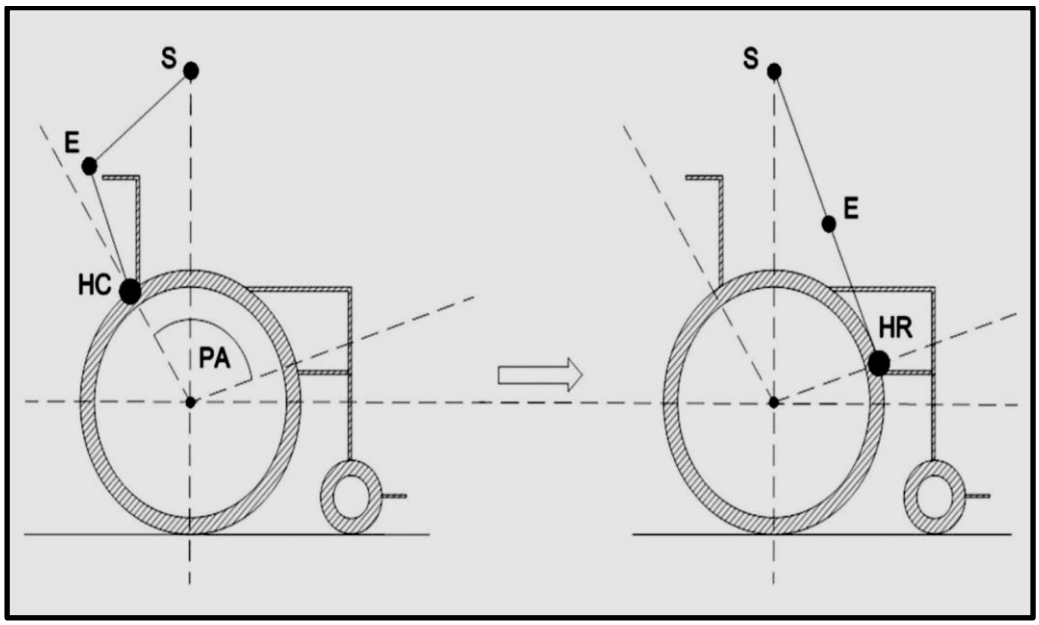


**Figure (1.3):** Sagittal view of the manual wheelchair propulsion and technique parameters. S:shoulder, E: elbow, HC: hand contact, PA: push angle, HR: hand release. (Dellabiancia et al. 2013).

### *1.1.2. Upper limb Pain in Manual Wheelchair Propulsion*

Upper limb pain is reportedly present in (40-70%) of manual wheelchair users with a spinal cord injury (SCI) (Curtis et al.1999), with (30-40%) of individuals experiencing pain during and within the first year after rehabilitation. Brose et al. (2008) observed an extremely high prevalence of supraspinatus tendinopathy (100%) and impingement (91.8%) in 49 active users with paraplegia, with (67%) symptomatic for pain.

Similarly, Medina et al. (2015) observed a similarly high prevalence of rotator cuff tendinopathy (>80%), bursitis (>55%) and acromioclavicular joint degeneration (>60%) in both active and sedentary males with tetraplegia. Mechanical impingement of the soft-tissue residing within the subacromial space of the glenohumoral (GH) joint (e.g. rotator cuff muscles, bicep tendon) is therefore considered a primary cause of shoulder pain and overuse pathology in manual wheelchair users (Brose et al. 2008; Medina et al. 2015; van Drongelen et al. 2006).

A high proportion of self-reported shoulder pain is unilateral in nature (Curtis et al. 1999). As a bilateral task, manual propulsion challenges upper limb motor control when repeatedly coupling the pushrim and maintaining a linear direction of travel (Vegter et al. 2013). Despite this, the reporting of bilateral data in wheelchair propulsion literature is limited, often due to increased cost of equipment for data collection or the assumption of symmetry in upper limb kinematics and kinetics. Even with bilateral data collection, studies often do not report results for both sides, they are either averaged or just reported for a single limb (Boninger et al. 2002).However, Boninger et al. (2002) previously observed around 40% of a subset of manual wheelchair users with paraplegia displayed bilateral asymmetries in hand recovery pattern during a propulsion cycle. Hurd et al. (2008) reported significant asymmetries in force and timing parameters in 12 wheelchair users free from pain, with increased magnitudes during propulsion up ramps and on uneven surfaces. In contrast, Soltau et al. (2015) found no difference in propulsion kinetics in80 manual wheelchair users with paraplegia, with only small differences in hand contact angle. Side to side differences (~5°) in joint range of motion were observed but these were smaller than differences between individuals and therefore not considered clinically meaningful (Soltau et al. 2015). However, even small differences in moments or

forces may result in cumulative differences during repetitive propulsion and risk factors for unilateral pain in manual wheelchair users have not yet been identified. Defining a range of scapular kinematic asymmetry may also be a useful tool when supporting the configuration and postural assessment of wheelchair propulsion and understanding shoulder girdle pathology.

### *1.1.3. Stroke Patterns in Manual Wheelchair Propulsion*

Stroke pattern refers to the trajectory of the hand during propulsion. During the propulsive phase, the hand follows the path of the handrim. However, during the recovery phase the user can choose any trajectory to prepare for the next push. Four stroke patterns have been identified for users of manual wheelchairs (Shimada et al. 1998; Boninger et al. 2002), see Figure (1.4):

(a) Arcing (ARC); the third metacarpophalangeal (MP) follows an arc along the path of the hand rim during the recovery phase.
(b)Single looping over propulsion (SLOP); the hands rise above the hand rim during recovery phase.
(c) Semicircular (SC); the hands fall below the hand rim during recovery phase.
(d) Double looping over propulsion (DLOP); the hands rise above the hand rim, then cross over and drop below the hand rim during the recovery phase.

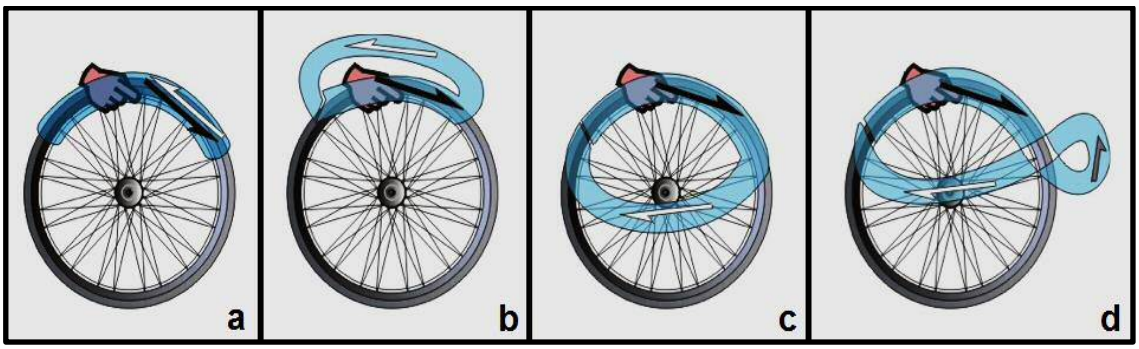


**Figure (1.4):** Stroke patterns in manual wheelchair propulsion; (a) Arcing (ARC), (b) Single looping over propulsion (SLOP), (c) Semicircular (SC) and (d) Double looping over propulsion (DLOP).

There are two studies that have investigated the effect of stroke pattern on wheelchair propulsion in the spinal cord injured population. Boninger et al. (2002) studied the stroke patterns of 38 individuals with paraplegia while propelling their own wheelchair on a dynamometer at two different steady state speeds. The SC and

DLOP patterns were found to have significantly lower cadence and least time spent in each phase of propulsion. The SC and ARC patterns had the greatest amount of time spent in propulsion relative to the recovery phase. A correlation has been found between cadence and the risk of median nerve injury (Boninger et al. 1999). They concluded a stroke pattern that minimized cadence may reduce the risk of median nerve injury.

Richter et al. (2007a) studied the stroke patterns of 25 individuals with paraplegia propelling their own wheelchairs at self-selected speeds on a treadmill set to level and at 3 and 6 degree grades. In this study, the SC pattern was not used by any of the subjects. For level propulsion, the number of subjects using the remaining 3 patterns was fairly even. However, once the subjects started going uphill (73%) were using the ARC pattern. No significant difference was found in the handrim biomechanics between the different stroke patterns. The authors caution against training wheelchair users to adopt a certain pattern until more is known about the consequences.

### *1.1.4. Wheelchair Weight*

Wheelchair propulsion may be affected by the weight of the wheelchair and/or the user. Wheelchairs are available in three general weight categories: standard, lightweight and ultralight. Bednarczyk and Sanderson (1995) studied the effect of adding weight to a wheelchair on the angular variables of wheelchair propulsion. Twenty individuals with paraplegia were tested propelling a wheelchair with no additional weight and then (5 kg) and 10 kg added. With the addition of the weight the proportion of the wheeling cycle spent in propulsion did not change. Also, there was no change in the angular kinematics (shoulder flexion/extension, elbow flexion/extension, shoulder abduction and trunk flexion/extension). The authors concluded that a change in the range of (5 kg) to (10 kg) in system weight of either the user or the wheelchair will probably not affect the wheeling motion in short distance, level wheeling.

Beekman et al. (1999) tested the propulsion efficiency of individuals with paraplegia and tetraplegia using an ultralight wheelchair and a standard wheelchair. Their results indicated that the use of an ultralight wheelchair by individuals with

paraplegia rather than a standard wheelchair increased speed, distance traveled and decreased oxygen cost. The use of an ultralight wheelchair for individuals with tetraplegia was also beneficial although the differences were not as great. However, the effect of weight was not clear. The different wheelchair features that would account for the increased efficiency with an ultralight wheelchair were not studied.

Boninger et al. (1999), who found a link between pushrim biomechanics and median nerve function, also found a link between body weight and median nerve function. Increased body weight was felt to increase the rolling resistance of the wheelchair and increase forces required to propel the chair. They also found that regardless of body weight, those who rapidly load the pushrim during the propulsive stroke may be at greater risk for carpal tunnel syndrome. They suggest that weight loss and training to incorporate smooth low impact strokes may reduce the chance of median nerve injury.

Collinger et al. (2008) investigated shoulder biomechanics during wheelchair propulsion in 61 persons with paraplegia. Their results indicate that shoulder pain does not affect the way a subject propels a wheelchair. This suggested pain or shoulder pathology did not affect propulsion patterns. They also found that at faster speeds shoulder joint forces and moments increased. When comparing the demographic variables between the subjects, body weight was the only indicator of shoulder joint forces. Heavier subjects experienced an increased loading and greater resultant forces. They suggested that manual wheelchair users maintain a healthy body weight and if that was not possible then the user be prescribed a lightweight wheelchair with an adjustable axle.

### *1.1.5. Wheelchair Propulsion Speed*

Shimada et al. (1998) investigated shoulder motion during two speeds (1.3 m/s and 2.2 m/s) of wheelchair propulsion. This study emphasized the differences of angular position, range of motion, and peak accelerations of the shoulder between two selected propulsion speeds. These results demonstrated that in the drive phase, the minimum shoulder abduction angle and range of motion in shoulder flexion/extension and abduction/adduction were significantly different between the speeds of (1.3 m/s) and (2.2 m/s). It was suggested that those changes in pushing

patterns with lower biomechanical efficiency revealed possible causes of shoulder injuries (Shimada et al., 1998).

Wang et al. (1995) concluded that the range of motion of the upper extremities increased when propulsion speed increased. The results of their study also showed an increase in trunk flexion at the faster speed, resulting in a larger contact angle and more elbow flexion during initial contact. The time during drive phase and recovery phase both decreased when the speed increased. Also, the percentage of drive phase time by cycle time decreased with increasing speed.

In a study to investigate the effects of handrim velocity on mechanical efficiency in wheelchair propulsion (Veeger, van der Woude and Rozendal, 1991), the findings revealed that when handrim velocity increased, the percentage of recovery phase time in a cycle increased, and the cycle time and drive time decreased, while recovery time remained constant. However, the increased stroke arc with increasing propulsion speed reported by Veeger, van der Woude and Rozendal (1991) was different from the result found in the study conducted by Wang which showed that the range of stroke arc was not a monotonic increase (Wang et al., 1995). This difference in findings may result from different analytical techniques, different wheelchair types, and different stroke patterns used by the participants.

Boninger, Cooper and Shimada (1998) reported shoulder motion at low speed (1.3 m/s) to be within the range of (64°) of flexion to (11°) of extension in the sagittal plane, (21°) to (47°) for abduction and (54°) to (91°) for internal rotation. Shoulder kinematics was speed dependent since increasing speed resulted in a marked increase in angular acceleration for flexion/extension and abduction/adduction movements (Boninger, Cooper and Shimada, 1998).

### *1.1.6. Upper Body Kinematics and Kinetics*

In order to understand motion of the shoulder during wheelchair propulsion, researchers investigated kinematics. Several researchers have recorded shoulder movement patterns during propulsion for various groups of wheelchair users. Many of the earlier studies presented a two-dimensional (2D) analysis of shoulder kinematics (Sanderson and Sommer, 1985; Bednarczyk and Sanderson, 1995).

Cerquiglini et al. (1981) found that a single plane analysis of wheelchair propulsion was insufficient. They conducted a three-dimensional (3D) kinematics analysis of the upper limb during wheelchair propulsion and determined that the shoulder joint exhibits the largest displacement. In order to further understand the significant arcs of motion that occur in all three planes of motion, other researchers investigated 3D shoulder kinematics during wheelchair propulsion. Three-dimensional (3D) analyses have been performed with axial rotation as a third articulation of the humerus (Rao et al., 1996; Boninger et al., 1998). These studies have documented that during the propulsion phase of the cycle, the shoulder exhibits internal rotation, abduction, and flexion and extension.

Reflective markers were placed on the anatomical landmarks of the trunk and upper limb and the location of these markers in 3D space were tracked throughout propulsion. Researchers used local coordinate systems to determine the joint angles for the shoulder, elbow, wrist, and trunk. However, a standard sequence for coordinate systems did not exist, so individual researchers chose their own sequence. For example, Cerquiglini et al. (1981) based their calculations on methods used in gait studies presented by Cappozzo et al. (1975; 1978).

Veeger and Rozendal (1992) described the global shoulder kinematics of five able-bodied participants during the drive phase as starting with a flexion of the shoulder from an extended position combined with abduction during the first part of the push, which changes into flexion and adduction during the last part of the drive phase. These findings were confirmed by Boninger, Cooper and Shimada (1998) and Newsam et al. (1999). A repetitive condition of an internal rotation position, combined with high external rotator and abductor load, would be a serious risk factor for supraspinatus tendon impingement (Boninger, Cooper and Shimada, 1998).

In order to understand the forces and moments generated at the shoulder during wheelchair propulsion, researchers investigated three-dimensional shoulder kinetics. Kulig et al. (1998) used an instrumented wheel, reflective markers, a standard wheelchair, and a wheelchair ergometer to study free, fast, and inclined wheelchair propulsion. They found increased shoulder joint loads during fast and

inclined propulsion. They suggested that these increased loads may lead to compression of subacromial structures against the overlying acromion.

Expanding upon their work, Koontz et al. (2002) investigated shoulder kinematics and kinetics during slow and fast speeds of wheelchair propulsion. Their experimental setup entailed instrumented pushrims, reflective markers and each study participant's wheelchair on a dynamometer. The authors reported that the net joint forces and moments were higher when the shoulder was near its end range of motion on the pushrim. They also reported that the shoulder was placed in a more compromise position during the fast propulsion speed.

Although these studies greatly contributed to the wheelchair propulsion biomechanics community, researchers also encountered difficulties with comparing shoulder kinetics results across studies due to differences in experimental setup and testing conditions. Moreover, there was no standard coordinate system for reporting shoulder joint kinetics, so researchers used different coordinate systems (Cooper et al., 1999; Finley et al., 2004; Koontz et al., 2002; Kulig et al., 1998; Mulroy et al., 2005). The coordinate system was issued by the International Society of Biomechanics (ISB) only for kinematic studies (Collinger et al., 2008; Wu et al., 2005). Morrow et al. (2009) and Desroches et al. (2010) explored expressions for upper limb joint kinetics during wheelchair propulsion.

Using the standardized ISB joint coordinate system and recognizing the inconsistencies in experimental setup and design across previous studies, Collinger et al. (2008) conducted a multisite study of persons with paraplegia to investigate shoulder biomechanics during the push phase of propulsion. They analysed shoulder kinematics and kinetics at two different speeds during wheelchair propulsion. Even though they reported shoulder kinematics in terms of the ISB standards, they recognized that there were no standards for reporting shoulder joint loading. Therefore, they used the same local coordinate systems for both kinematic and kinetic analyses. Due to the design of the multisite study (three biomechanics laboratories at research institutions: 61 study participants), they were also able to investigate the effect of pain and participant demographics on propulsion. Their findings suggested that body weight was the primary factor that affected shoulder

forces. They also observed peak shoulder joint loading when the arm is extended and internally rotated, suggesting that this position may be injurious to the shoulder (Collinger et al., 2008).Trunk instability due to the absence or impairment of abdominal and back muscle control or the long period of sitting usually leads to an increased kyphotic posture with flattened lumbar spine among individuals with spinal cord injury. Newsam et al. (1999) assessed upper extremity motion during wheelchair propulsion among persons with different levels of spinal cord injury (C6 tetraplegia, C7 tetraplegia, high paraplegia, and low paraplegia). They reported that participants with high cervical lesions yielded greater range of trunk motion during propulsion. They suggested that stabilizing the trunk might help participants who lose voluntary control of trunk musculature to maintain consistent propulsive stroke patterns.

Poor trunk control also limits the ability of manual wheelchair users to overcome fatigue during wheelchair propulsion. Rodgers et al. (1994) investigated the influence of fatigue on trunk movement during wheelchair propulsion. They reported a significant increase of trunk forward lean with fatigue. This increase in forward lean may aid the application of force to the pushrim and enable the transfer of propulsive power from the trunk and upper extremity to the pushrim (Sanderson and Sommer, 1985).

### *1.1.7. Upper limb muscles Electromyography (EMG)*

While some researchers were investigating shoulder kinematics and kinetics, others were investigating electromyography (EMG) to understand upper limb muscle recruitment patterns during wheelchair propulsion. Early studies by Cerquiglini et al. (1981) and Harburn and Spaulding (1986) used surface EMG to investigate muscle activity during wheelchair propulsion. However, the surface EMG technique was limited to recording the activity of the superficial shoulder muscles because electrodes were placed on the surface of the skin. Another disadvantage of this technique is that the quality of the signal is impaired due to electrode positioning, movement artefact, and adipose tissue.

Mulroy et al. (1996; 2004) improved upon these previous studies by performing fine-wire EMG. The fine-wire EMG technique can be used to record the

activity of deep muscles because small needles are inserted directly into the muscle belly. Mulroy et al. (1996) found that the pectoralis major, supraspinatus, middle and posterior deltoids, subscapularis, and middle trapezius were most vulnerable to fatigue in individuals with paraplegia and recommended endurance training. To further expand upon their work, Mulroy et al. (2004) investigated shoulder complex muscle activity in manual wheelchair users with paraplegia and tetraplegia. The researchers indicated that the middle trapezius and serratus anterior are active during wheelchair propulsion. Their studies suggest that the pectoralis major, supraspinatus, middle and posterior deltoids, subscapularis, middle trapezius, and serratus anterior have important roles in wheelchair propulsion.

Mulroy et al. (1996) identified two synergies of shoulder muscle function during wheelchair propulsion. The push phase synergy was dominated by muscles with shoulder flexion (anterior deltoid, pectoralis major), external rotation (supraspinatus, infraspinatus) and scapular protraction (serratus anterior) functions. The dominant functions of the recovery synergy were extension (posterior deltoid), abduction (medial deltoid, supraspinatus), internal rotation (subscapularis) and scapular retraction (middle trapezius). The push phase muscles (anterior deltoid, pectoralis major) were activated in the late recovery phase to decelerate the back swing of the arm and to prepare the hand (increasing hand speed) for the contact on the pushrim (Mulroy et al., 1996).

The same phenomenon was described for the recovery phase muscles, activated already at the end of the push phase to restrain shoulder flexion (posterior deltoid), adduction (medial deltoid) and external rotation (subscapularis). Mulroy et al. (1996) implied that with reduced activity of the rotator cuff muscles due to fatigue, contraction of the deltoid would result in upward gliding of the humeral head and possible impingement of the supraspinatus tendon against the subacromial arch. During the push phase, fatigue of pectoralis major would increase the risk of impingement due to the intra-articular force within the glenohumeral joint. During the recovery phase, the greater tubercle moved directly underneath the acromion due to increased shoulder internal rotation and this position would worsen the impingement syndrome (Mulroy et al. 2004).

At the elbow joint, biceps brachialis was activated in the late recovery phase and continued its action over a period where an elbow flexion torque would contribute to the propulsion. Likewise, triceps brachialis only became active when elbow extension would contribute to a propulsive force on the hand rim (Rodgers et al., 1994; Mulroy et al., 1996; Schantz et al., 1999; Guo, 2003).

It is believed that biceps brachialis and triceps brachialis are necessary for an effective force direction (Guo, 2003). After the hand has made contact with the pushrim, the pull phase starts with an initial elbow flexion, accompanied by activity of the biceps brachialis (Veeger, van der Woude and Rozendal, 1989). Anterior deltoid has a high activity at the beginning of hand contact, whereas pectoralis major has a more constant activity of longer duration. These two muscles are considered to be the prime movers in wheelchair propulsion (Veeger, van der Woude and Rozendal, 1989; Rodgers et al., 1994; Mulroy et al., 1996; Guo et al., 2003).

It was concluded by Schantz et al. (1999) that the brachial biceps and triceps, anterior deltoid and pectoralis major muscles could be anticipated to propel the wheelchair forward, whereas the posterior deltoid and trapezius muscles could be expected to play a role, especially during the recovery phase. However, individual differences exist. The posterior deltoid and trapezius muscles showed an unexpected and distinct activity during the push phase, possibly resulting from the function of stabilizing the shoulders. Regardless of the type of recovery movement (semicircular, loop or pumping), the posterior deltoid and trapezius muscles in particular were active during part of, or the whole, recovery phase (Schantz et al. 1999). The general order of activation of, first, the brachial biceps, thereafter the pectoralis major and anterior deltoid, and then the triceps brachial muscle at the normal velocity during the push phase is constant with findings in other studies (Schantz et al. 1999).

Although the integration of kinematics and kinetics provided a better understanding of the relationship between wheelchair propulsion and shoulder pain in SCI, researchers understood the importance of the findings from EMG studies and recognized the need to investigate kinematics, kinetics, and EMG simultaneously. A comprehensive analysis of kinematics, kinetics, and EMG in wheelchair propulsion

studies would provide a complete understanding of the relationship between wheelchair propulsion and shoulder pain in SCI. Cerquiglini et al. (1981) were the first to combine kinematics, kinetics, and EMG (in addition to electrocardiographic tracings, blood pressure estimations, oxygen consumption and pulmonary ventilation) to provide a method for describing upper limb biomechanics during wheelchair propulsion. However, they used an instrumented wheelchair that was propelled by a cranking arm, as opposed to the more conventional pushrim. Indeed, the pushrim style wheelchair is the most commonly used wheelchair in individuals with mobility impairment such as SCI, and therefore, warranted investigation (Sanderson and Sommers, 1985).

Expanding upon this work, Dubowsky et al. (2008) was able to integrate kinematics, kinetics, and EMG with an individual's own conventional pushrim style wheelchair to investigate the demands on the shoulder during wheelchair propulsion. The purpose of their study was to simultaneously compare pushrim forces, upper limb kinematics, and shoulder EMG during wheelchair propulsion in wheelchair users with paraplegia to able-bodied controls. Dubowsky et al. (2008) found that the able-bodied controls had no triceps activity in the early stages of propulsion while the individuals with paraplegia demonstrated triceps activity throughout propulsion.

While there have been multiple studies that compare a combination of participant kinematics, kinetics, and electromyography, there are limited number of studies where all three parameters are combined study.

### *1.1.8. Wheelchair Configurations*

Several studies have indicated that wheelchair configuration has a significant effect on wheelchair propulsion performance. The most common aspects of wheelchair components and configuration indicated as affecting manual mobility are those related to the geometry of the system assembly. In other words, the relative position of each component related to the others, and to the user, determines wheelchair mechanics, stability and the biomechanics of manual propulsion. Medola et al. (2014) reviewed the studies which have investigated how different wheelchair configurations, such as wheelchair seat height and rear wheels' vertical and horizontal position, impact the biomechanics of user mobility. Cowan's study (2009)

showed that the axle position relative to the shoulder is associated with significant differences in pushrim biomechanics. Hughes et al. (1992) tested the effect of seat position on wheelchair propulsion biomechanics. They found that biomechanics changed with seat position. Most lightweight and ultralight weight wheelchairs offer adjustable axle position. This allows the center of gravity to be adjusted appropriately for each individual and reduces the effort required to propel the wheelchair. There were four studies addressing the effect of rear axle position on wheelchair propulsion with individuals with a spinal cord injury.

Boninger et al. (2000) completed a study that showed axle position relative to the shoulder was associated with significant differences in pushrim biomechanics. They found that with the axle further back relative to the shoulder there is more rapid loading of the pushrim and increased stroke frequency was required. Additionally, individuals attained a slower speed when starting from a dead stop and there was a decrease in the push angle. An increase in the vertical distance between the axle and the shoulder resulted in a decrease in push angle. With a decrease in push angle, force was applied to the pushrim for a shorter period of time and thus the frequency of propulsion had to increase in order to maintain speed. They suggested that providing users with a wheelchair with adjustable axle position and setting up the chair to meet the user's needs could improve propulsion biomechanics and reduce the risk of secondary injuries as a result of wheelchair propulsion.

Mulroy et al. (2005) studied the effect of changing the fore-aft seat position on shoulder joint forces, moments and powers during three levels of effort of wheelchair propulsion. They found that the seat posterior position resulted in a statistically significant reduction in peak superior shoulder joint forces during free, fast and graded propulsion. They concluded that the posterior seat position may reduce the risk of rotator cuff tendinopathy. Rotator cuff muscles activity were not tested in our study as that requires using fine needle EMG electrodes and that will make the protocol more invasive and uncomfortable to the recruited healthy volunteers.

Samuelsson et al. (2004) also studied the effect of rear wheel position on wheelchair propulsion and seating aspects. A more forward position of the rear

wheel had a significant effect on stroke frequency and push angle. They also reported an increase in the weight distribution with the more forward position of the wheel. However, in their study they did not find any difference between the two wheel positions with respect to mechanical efficiency, estimated exertion, seating comfort, estimated propulsion qualities, pelvic position or activity performance.

Additionally, Freixes et al. (2010) assessed the changes in speed, acceleration, stroke frequency and shoulder range of motion in relation to four different axle positions. The study showed that the up and forward axle position resulted in an increase in speed and acceleration with a higher stroke frequency and a decreased shoulder ROM. The axle position of down and backward axle position resulted in a lower speed and acceleration with a lower stroke frequency and an increased shoulder ROM. The authors indicated that these were clinically important findings for wheelchair propulsion in their homes.

Tsai et al. (2012) investigated the effects of rear-wheel cambers on temporal-spatial parameters, joint angles and propulsion patterns on twelve inexperienced subjects. All those subjects propelled the same wheelchair, which had an instrumented wheel with cambers of 0°, 9° and 15° respectively at an average velocity of (1 m/sec). They found that the rear wheel cambers significantly affect the average acceleration, trunk, elbow and wrist movements, and propulsion patterns.

Further, Gorce and Louis (2012) examined the influence of the wheelchair settings on upper limb kinematics during wheelchair propulsion on ten experts and ten beginners' subjects propelled an experimental wheelchair on a roller ergometer system at a comfortable speed. They tested twelve wheelchair configurations of seat height and antero-posterior axle position and recorded kinematics for each configuration. Based on the hand position to the push rim, the main kinematic patterns were investigated on the whole propulsion cycle. The authors observed that low and backward wheelchair configurations allow greater propulsion efficiency.

Last, a summarised review of the most relevant studies involving biomechanics of manual wheelchair propulsion, illustrating the context, methods and impact derived per these studies is illustrated per the Appendix.

### *1.1.9. Prior Upper limb Studies at Cardiff University*

Most motion analysis research at Cardiff University has focused primarily on the assessment of lower limb function, in particular osteoarthritic knee function. The knee joint is modelled using the method described by Grood and Suntay (1983) which was designed to facilitate effective communication between biomechanicians and clinicians. The recommended standards of the International Society of Biomechanics (ISB), (Wu et al. 2005), are largely derived from the Grood and Suntay approach, and it was based on this that the initial attempts by Cardiff University researchers were made to measure shoulder kinematics (Jones et. al 2006).

A small number of undergraduate students adopted shoulder projects for their final year dissertations. Amy Bowles (2005-2006) helped develop the original measurement protocol to measure dynamic movements using skin markers attached to bony landmarks. Lindsay Stroud (2006-2007) introduced the Newcastle Scapula Locator to measure scapula function more accurately to the measurement protocol, Johnson et al. (1993). Robert Guppy (2015-2016) investigated simultaneously the shoulder kinematics and muscle actions of healthy individuals during their manual wheelchair propulsion.

Lovern (2010) expanded the study to include shoulder patients diagnosed with either shoulder injury or pathology as well as developing the use of an acromium marker cluster to measure dynamic scapula movements. Ferran (2010) aimed to measure glenohumeral (GH) joint translations on healthy volunteers and multidirectional instability patients.

Finally, Stroud (2011) developed the original Cardiff motion analysis protocol for measuring shoulder complex biomechanics using image registration and motion analysis methods to characterise healthy and pathological shoulder functions applying the Cardiff Dempster-Shafer (DS) objective classifier method.

All of the above studies where undertaken to understand and establish methods for quantifying upper limb and trunk kinematics at Cardiff using marker based on motion capture or low-dose X-rays. Bespoke software was developed to

Cardiff using Matlab (Mathworks), to understand the effects of changing the order off rotations in the calculations, the use of Euler and Cardin angles, and the limitations of these approaches due to Gimbal lock effects.

As well as identifying a number of limitations to this approach for measuring upper limb kinetics (identified by previous researchers), the results of the studies revealed differences when measuring upper limb kinematics for bilateral as compared to unilateral movements, and when using markers attached to the skin as compared to using mocha clusters or a scapula locator. They also identified the range of motion of common activities of daily living with respect to the wider physiological range of motion in the joints. None of the studies however introduced simultaneous EMG measurements to understand the contribution muscles two either physiological all activities of daily living joint range of motion and they were constrained to using the bespoke software.

More recently, new, more flexible approaches to the six degrees of freedom calculations have become available, as an integrated feature in the software that is used to collect the motion capture data (Qualisys Track Manager, QTM, Qualisys, Sweden). Although this allows greater flexibility in the calculations, a thorough understanding of the establishment of anatomical coordinate systems, in line with the ISB recommendations, is still required in order to ensure that the resulting joint range of motion outputs are sensible and can be benchmarked to the previous gold standard outputs.

## 1.2 Research Context

From research accomplished prior to this research study, it can be seen that this was the first time that upper limb investigations had been performed at Cardiff University, and this could provide a good foundation upon which further research can be developed to understand the biomechanics of manual wheelchair propulsion.

### *1.2.1. Aim and Objectives of the Study*

The basic aim of this study was to design an upper body robust model to simultaneously analyse the biomechanics of manual wheelchair mobility of able-

bodied non-experienced users (MWUs) during different functional activities of their daily living. Better understanding of the upper body biomechanics during manual wheelchair mobility will optimise the users' everyday activity that will improve their independence and quality of life, and also contribute to clinical knowledge, aiding who work with such field when prescribing, designing and selecting a device to provide the proper comfort and functionality for the user.

This aim has been achieved through setting the following objectives:

- Investigate the three-dimensional kinematics of trunk and upper limb joints during physiological range of motion (ROM), activities of daily living (ADL), that includes hygiene, feeding and reaching activities, and functional wheelchair mobility that includes starting up from the rest, propulsion and stopping a wheelchair during manual propulsion.
- Investigate the contribution of the shoulder complex muscles through the analysis of the surface electromyographic (sEMG) patterns of these stabilising muscles activation during physiological range of motion, activities of daily living and functional wheelchair mobility.
- Investigate the influence of adjusting wheelchair configurations, on trunk and upper limb joints kinematics and shoulder complex muscles recruitment during functional wheelchair activities. This includes vertically adjusting the wheelchair's seat to floor height and horizontally adjusting the rear wheel axle position.
- Investigate the interrelationship between the users' anthropometric characteristics and the biomechanics of their upper body in terms of kinematics, surface electromyography and spatiotemporal parameters during manual wheelchair propulsion.

One reason for preferring non-experienced user subjects is their feature of novice as they could determine their own self-selected speed and pattern of propulsion without any prior knowledge and experience influencing them. Experienced wheelchair users have already established their own motor behaviour, which may affect potential outcomes of true experiment. Also, well-experienced subjects usually have their own customized wheelchair.

Although experienced wheelchair users with disabilities have been shown to be more efficient in the wheelchair propulsion task and to differ in the wheelchair propulsion biomechanics, it was more practical to test the used experimental protocol on healthy subjects first, since they were easier to recruit and call back for repeat measurements when necessary.

Meanwhile, recruiting a group of controls has limited the variability that would be existed by a study group with multiple inter-individual differences and provided the following criteria:
(1) A constant level of experience and training status of all recruited participants in the different testing conditions, a homogenous participant group with controlled types of error.
(2) An understanding of upper body performance in a healthy subject as any pathological differences can be excluded.
(3) The wheelchair configuration remains constant throughout testing conditions removing the subsequent effect that different chair configurations would bring to the analysis.

Upper limbs kinematics is commonly investigated using three-dimensional (3D) motion analysis techniques. Advances in 3D motion analysis techniques have led to a wider adoption of motion capture as a highly sensitive, non-invasive and objective technique in which motion can be assessed during different activities of daily living and functional wheelchair mobility. This study introduced a bilateral measurement protocol for analysis the trunk and upper limb joints movement in the three planes of motion. It used a motion analysis technique and follows the recommendations of the International Society of Biomechanics (ISB) for the reporting of human joint motion.

Measuring shoulder 3D kinematics is challenging and its complexity becomes apparent as soon as one considers the following: firstly, shoulder motion is the result of the intricate interaction of four segments; this results in the greatest ROM as compared to any other joint complex in the human body. Secondly, movement is not cyclic and is much more unpredictable as compared, for example, to the lower limbs; furthermore, there is no one single way of performing a motor

task. Finally, soft tissue surrounding the joint complex complicates the reliability of the measurements. Upper body joints and particularly the shoulder are subjected to larger ranges of motion than the lower limb and involve highly complex three-dimensional task specific motions. In comparison, lower limb motion is primarily two-dimensional during gait, having more of a cyclic nature with relatively simple and consistent patterns of motion largely associated with a single activity.

### *1.2.2. Research Questions and Hypotheses*

The study reported in this thesis presents a novel aspect carried out at Cardiff University through using a 3D motion analysis protocol to assess the upper body functional kinematics and shoulder muscles activity during wheelchair mobility in able-bodied non-experienced users. This study basically questions how upper body biomechanics in manually propulsion users are impacted by adjusting wheelchair configurations? This could explore the following questions;

(1) What are the most influential upper limb joints kinematic movements during functional wheelchair mobility?

(2) What are the most influential muscles during functional wheelchair mobility?

(3) Which spatiotemporal parameters are more important in optimising wheelchair configurations for manually propulsion users during their functional mobility?

(4) Do varying anthropometric characteristics of the users affect potentially their upper body biomechanics during manual wheelchair mobility?

It was hypothesised that output parameters describe the 3D kinematics of upper body and associated spatiotemporal patterns would be significantly different between diverse wheelchair configurations and functional activities. Also, it was hypothesised that the EMG activity of the shoulder muscles predominantly involved with the push and recovery phases of the propulsion would be significantly different between wheelchair configurations and functional activities.

Furthermore, it was hypothesised that there is a significant correlation between the anthropometric characteristics of the users and their upper body biomechanics during manual wheelchair mobility. This significant correlation was presented per this study to quantify the association of upper body parts with the biomechanical behaviour during the repetitive usage of the upper limb of manual

wheelchair users. Anthropometric measurements whenever be considered for designing, can help in achieving comfortability, reduce musculoskeletal disorders and improve performance of the users. This information could potentially help clinical professionals and researchers to better optimise wheelchair prescription by knowing whether a user propelling more efficiently with a specific dimensions of upper body part or using a type of wheelchair over another to evaluate the effect of interventions such as adjusting wheelchair configuration.

### *1.2.3. Novelty of this Research Study*

The main objective of this study is to investigate the impact of trunk and upper limb biomechanics associated with diverse wheelchair configurations. Even though many researchers were worked on the manual wheelchair propulsion field, very few researchers were reported about a thorough simultaneous analysis of upper body three-dimensional bilateral kinematics, surface EMG and spatiotemporal patterns analyses during propelling a manual wheelchair during daily mobility and use. Though there is similar work, but in the present study some potential aspects were applied, in terms of data collection procedures and experimental set-up, that provide a feasible robust acquisition of the manual wheelchair propulsion for able-bodied non-experienced users in spite of the time consuming and laborious measurement protocol.

A marker-based 3D motion analysis technique was used with more recently to the six degrees of freedom (6DOF) analysis, as an integrated feature in the software that was used to collect the motion capture data (Qualisys Track Manager, QTM, Qualisys, Sweden). This allowed greater flexibility in calculating the joint angles, under a thorough understanding of identifying each segment anatomical coordinate system, in line with the ISB recommendations. This was important to ensure that the resulting joint range of motion outputs are sensible and can be benchmarked to the previous gold standard outputs.

A potential advantage of this study was that the experimental data were collected over ground but not on calibrated wheelchair ergometer or roller dynamometer. Stationary propulsion simulators do not perfectly replicate over ground propulsion. However, they result in similar propulsion mechanics while

providing greater control over experimental variables in a laboratory setting, (Knootz et al. 2012). Additionally, the use of these techniques eliminates examination of some viable metrics, such as right-left coupling of steering, (Vegter et al. 2013). In addition, a standard self-propelled wheelchair was utilized in the study instead of using instrumented or customised devices. All the recruited participants and adjustments were performed on the same device that limited the variability exist per the other related studies.

Another advantage concerns the fact that the designed kinematic model was unilateral, and therefore, a bimanual task could be analysed with the present method. Using a large number of cameras (9 cameras) within the motion capture system utilized in Cardiff University made possible the measurement of both upper limbs motion at the same time. Also, a rigorous non-invasive surface electromyography (sEMG) analysis method (in terms of normalised maximum voluntary contraction) was used simultaneously to analyse the muscle recruitment. Further, the relationship between the anthropometric characteristics of the recruited participants and their obtained biomechanical outcomes during manual wheelchair mobility was analysed exclusively in this study.

The findings of this study showed an interrelationship between adjusting wheelchair configurations (adjustable rear wheel axle positions and seat heights) and upper body kinematic behaviour, muscles recruitment and spatiotemporal patterns during manual wheelchair mobility. Appropriate wheelchair configuration should ensure the user's trunk and upper limb joints ROM fall within the normal range. Wheelchair configurations that cause joints to use maximum joint ROM considered inappropriate as the excessive movement may cause overuse injury due to joint impingement and tissue undue stress. Therefore, the optimisation of the wheelchair configuration, based on functional characteristics of the user, appears beneficial.

The improvement of manual wheelchair mobility has become increasingly important as the population of individuals using wheelchairs is growing and requires efficient mobility to maintain the user's independence and quality of life. Manual wheelchair propulsion, as the most common means of wheelchair mobility, has been considered a factor contributing to the high prevalence of upper limb injuries among manual wheelchair users. Providing a wheelchair that is suitable to the users'

characteristics, needs and preferences can benefit both mobility and satisfaction with the device. These are important ergonomic aspects influencing the successful use of assistive devices.

In order to improve the ergonomics of manual wheelchairs, adjustments in specific aspects of the equipment design are important factors contributing to the wheelchair suitability. Biomechanically, changes in users' relative position to the rear wheels' axle or seat height can affect important aspects of the user-wheelchair interaction, such as: upper limbs range of motion (ROM), handrim propulsion forces, system stability and rolling resistance. These are very relevant aspects of the ergonomics of manual wheelchair as, ultimately, they determine how easy or difficult it is to propel the wheelchair.

## 1.3 Outline of the Thesis

Basically, this research study aimed to simultaneously analyse the biomechanics of upper body in able-bodied individuals during performing different functional activities of daily living and manual wheelchair mobility. Therefore, the thesis is comprised of eight chapters aimed to address the research aim documented previously to provide a better understanding about why this research has been undertaken.

***Chapter One: Introduction.*** This chapter aimed to explain the relevant background information to the research, the study context, the aims and objectives. Also, it illustrated a literature review of the relevant previous studies of upper limb motion in general and in particular those involving studies of manual wheelchair propulsion.

***Chapter Two: Anatomy and Biomechanics of the Upper Limb.*** This chapter aimed to present an anatomical background through introducing a detailed illustration of the anatomy and biomechanics of the human upper limb. It described the structure, support and movements of the joints and articulations of the upper body and identified the muscular actions contributing to these joints. It also identified the common potential injuries to the shoulder, elbow, wrist and hand as associated with activities of daily living and manual wheelchair propulsion.

***Chapter Three: Anatomy and Biomechanics of Manual Wheelchair.*** This chapter aimed to present an overview background of manual wheelchair. It provided a detailed illustration of the anatomy and biomechanics of manual wheelchair that began with an overview of the types of manual wheelchair and briefly described its features and components and identified the function of each component. The following aspects focused on the mechanics of manual wheelchair propulsion and the methods used to predict the applied forces pattern and propulsion efficiency. It also presented a simplified approach to calculate the potential and kinetic energy during manual wheelchair propulsion.

***Chapter Four: Three-dimensional Kinematics of the Upper Body.*** This chapter aimed to describe the design concept of the methodology undertaken per this research study. It began with an overview of the kinematic analysis of rigid body in a three-dimensional space through defining its location and orientation. It also identified the methods used to define the body position and displacement in terms of translation and rotation matrices and Euler's angles. Approaches for estimation the centre of rotation of the glenohumeral joint were also illustrated. This chapter presented a detailed description of the kinematic analysis of the upper body joints and segments on the basis of International Society of Biomechanics (ISB) recommendations through defining the axes of the local coordinate system of each joint and segment of the upper body. It also provided the definition of rotation order of the thorax, clavicle, scapula, humerus and forearm with its articulations which were applied for the calculation of rotation matrices for the upper body joint rotations. The next two chapters will present a detailed demonstration of the general methods undertaken per this study through applying the described concept of three-dimensional motion analysis for quantifying the upper body functionality during activities of daily living and manual wheelchair use.

***Chapter Five: Motion Analysis Protocol for Quantifying Shoulder Complex Function.*** This chapter aimed to introduce the general procedure that was followed to quantify functionality of the shoulder complex joints in healthy individuals during physiological range of motion and common activities of daily living (ADLs) and arm elevation in the sagittal, frontal and coronal planes of motion. It began with a brief description of the motion analysis facilities at Cardiff University in terms of camera

setup and calibration, marker placement, camera and software operation when taking measurements, subsequent tracking of markers into 3D trajectories and importing this data into bespoke software to calculate the range of motion of the trunk and articulations in the shoulder. The ethical review process, participants and inclusion/exclusion criteria were explained in this chapter. It also presented a description of the methods developed previously at Cardiff and compared the outputs with those previously obtained in terms of kinematic range of motion using a different approach that calculate the 6 Degree of Freedom ROM developed during these studies. It is important to understand which joints or articulations of the shoulder are most important for performing each movement and how reliably those movements can be measured. However, it can be difficult to choose appropriate activities because the kinematic redundancy of the shoulder complex joints makes it possible to accomplish any task using a variety of movement strategies. In the next chapter, this protocol was developed and applied within manual wheelchair propulsion measurement through using the 6DOF analysis method to describe the kinematics of the trunk and upper limbs with propelling a manual wheelchair during daily mobility and use.

***Chapter Six: Motion Analysis Protocol for Quantifying Functional Wheelchair Use.*** This chapter is an extension of Chapter Five that aimed to introduce the general procedure that was followed to quantify functionality of the trunk and upper limbs in able-bodied individuals with propelling a manual wheelchair during daily mobility and use. The motion analysis facilities at Cardiff University were employed to investigate three-dimensional kinematics across a range of daily living activities, including manual wheelchair starting up, propulsion and stopping. The 6DOF analysis method was applied to quantify the kinematics of the trunk and upper limbs in terms of range of motion angles. Spatiotemporal parameters such as contact and release angles, as well as stroke cadence, time and velocity were used to assess variations across wheelchair diverse configurations as well as performance outcomes. Also, this chapter presented the general procedure that was followed to measure the surface electromyographic activity (sEMG) of the shoulder muscles which have a dominant role during the wheelchair mobility. It provided a detailed illustration about the instrumentation, surface electrodes placement and maximum voluntary contraction tasks used to investigate the activation patterns of the recruited

muscles during manual wheelchair daily mobility and use. The ethical review process, participants and inclusion/exclusion criteria were explained in this chapter.

***Chapter Seven: Impact of Wheelchair Configurations on Upper Body Biomechanics.*** This chapter is an extension of Chapter Six that aimed to present focused a development of the wheelchair-user interaction through investigating the impact of wheelchair diverse configuration on the upper body biomechanics. From a biomechanical perspective, the most important factors affecting manual wheelchair mobility are the position of the wheels and seat height relative to the user. Therefore, this chapter employed the methods described in the previous chapter six to address these features and how they influence the upper body biomechanics with propelling a manual wheelchair during daily mobility and use. This chapter presented a detailed calculation of three-dimensional kinematics of the trunk and upper limb joints, shoulder muscles EMG activity and spatiotemporal patterns during three displacements of rear wheel axle position and seat height including the manufacturer's set. These calculations were performed across a range of daily living activities, including manual wheelchair starting up, propulsion and stopping. The obtained results had implications for the design of wheelchair to improve the user performance and limit the risk of injury. It was found that changes in the users' relative position to the rear wheels and seat height affected important aspects of the user-wheelchair interaction in terms of the trunk and upper limbs range of motion (ROM), muscles activities and handrim propulsion patterns. A brief description of the results obtained per the established protocol was displayed.

***Chapter Eight: Discussion, Conclusions and Future Research.*** This chapter aimed to discuss the overall findings of the thesis and draws some more general conclusions. Also, recommendations for future research in this field are also presented in this chapter.

Upper limb function can be impaired by a variety of injuries to the neuromuscular or musculoskeletal systems, including spinal cord injury or stroke. Such impairments can greatly affect one's ability to perform activities of daily living (ADLs). Quantifying three-dimensional kinematics of the upper body during functional tasks could be a valuable method for assessing the upper limb function and provide an

important step towards understanding movement disorders of the upper limbs and evaluating the effect of rehabilitation interventions. The role of the shoulder complex in manual wheelchair users essentially becomes that of the hip joint in able-bodied individuals and provides locomotion by means of manual wheelchair propulsion. Forces applied to the wheelchair resulted in reactive loads acting on upper limb that may over time lead to pain and/or injury. In order to improve the ergonomics of manual wheelchairs, adjustments in the equipment configuration are important factors contributing to the wheelchair suitability. Biomechanically, changes in users' relative position to the rear wheels or seat height can affect important aspects of the user-wheelchair interaction, such as: upper limbs range of motion (ROM), handrim propulsion forces, system stability and rolling resistance. These are very relevant aspects of the ergonomics of manual wheelchair as, ultimately, they determine how easy or difficult it is to propel the wheelchair. Adjustments in specific aspects of the wheelchair design, such as frame design, tires, seat height and the position of the rear wheels' axle, can influence the users' performance and upper limb injury risk with propelling a manual wheelchair during daily mobility and use.

The following flow diagram in Figure (1.5) illustrates the overview of the thesis chapters' structure and how each chapter is linked.

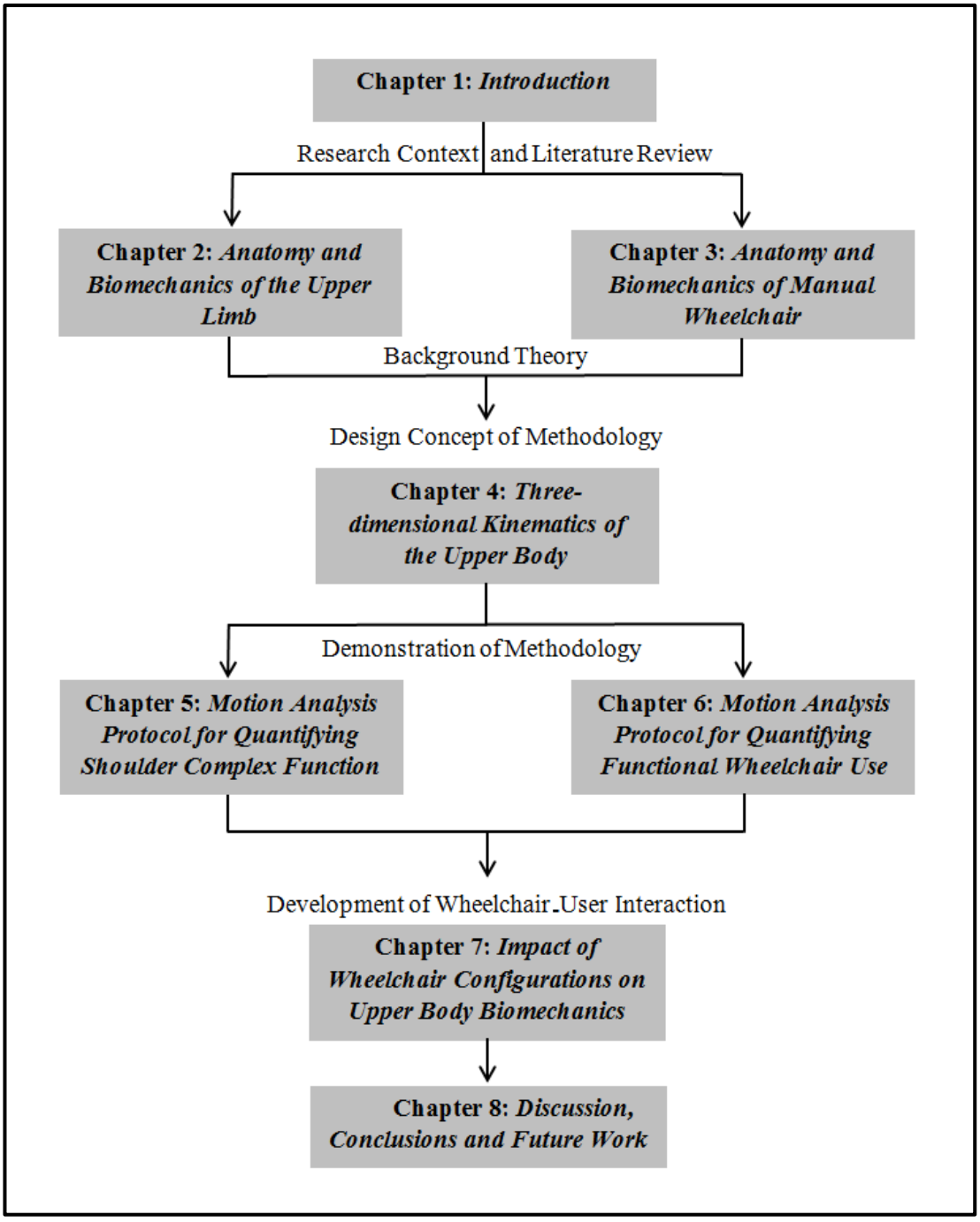


**Figure (1.5):** A flow diagram providing an overview of the thesis outline.

Finally, a complete list of publications and presentation at scientific conferences produced along the years of the PhD research study is given as final part of this thesis.

## 1.4 List of Presentations, Posters and Publications

- Analysis of Muscle Activation in the Shoulder Mechanism during Manual Wheelchair Propulsion. The 22nd ESB Congress, 10-13 July 2016, Lyon, France. (Podium Presentation).

- Kinematic Analysis of the Shoulder Mechanism in Able-bodied Non-experienced Manual Wheelchair users. The 1st ICSAE Conference, 20-21 October 2016, Newcastle, UK. (Podium Presentation and Published in the IEEE Xplore).

- Impact of Wheelchair Configurations on Upper body Biomechanics of Manual Wheelchair Users. The IMechE Conference - Engineering the Upper Limb, 12-13 December 2016, London, UK. (Podium Presentation).

- Towards better manual wheelchair mobility. Doctoral Academy – Images of Research Event, 6 December 2016, Cardiff, UK. (Poster Presentation).

- Analysis of Upper Limb Kinematics during Manual Wheelchair Mobility. CITER ASM, 18-19 September 2017, Cardiff, UK. (Podium Presentation).

- Lafta, H.A., Guppy, R., Whatling, G.M. and Holt, C.A. (2018). Impact of Rear Wheel Axle Position on Upper Limb Kinematics and Electromyography during Manual Wheelchair Use. International Biomechanics, 5(1):17-29.

# Chapter 2

## Anatomy and Biomechanics of the Upper Limb

The upper limb is interesting from anatomical and biomechanical perspectives because of the interplay among the various joints and segments necessary for smooth, efficient movement. Movements of the hand are made more effective through proper hand positioning by the elbow, shoulder joint, and shoulder girdle. Also, forearm movements occur in concert with both hand and shoulder movements, (Hamill et al. 2015). The upper limb is much more mobile than the lower limb, even though the limbs have structural similarities. There are similarities in the connection into girdles, the number of segments, and the decreasing size of the bones toward the distal end of the limbs.

This chapter aimed to present an anatomical background through introducing a detailed illustration of the anatomy and biomechanics of the human upper limb. It described the structure, support and movements of the joints and articulations of the upper body and identified the muscular actions contributing to these joints.

### 2.1 The Shoulder Complex

The shoulder is a complex joint with high mobility but a lack of stability. It is composed of three bones and the thorax, see Figure (2.1). The thorax can be defined as the sternum, ribcage and spine. The first bone is the *clavicle*, a small elongated bone connected to the sternum at one end and to the scapula at the other. The clavicle protects the neurovascular bundle (nerves and blood vessels) supplying the upper limb. It serves as a strut between the sternum and scapula, transmitting loads from the upper limb to the central skeletal axis of the body. The second bone is the *scapula*, a concave triangular bone connected to the clavicle and the humerus. The scapula's inner edge is called the medial border. The bony ridge running outwards from the upper end of the medial border is called the scapula's spine. It finishes at the acromion, the bony protrusion connecting the scapula to the clavicle. Below the acromion, is another bony protrusion called the coracoid process. This landmark is used as a muscle and ligament attachment site. Opposite the medial border is the lateral border running from the angulus inferior to the glenoid cavity. The clavicle

and scapula together with the thorax define the shoulder girdle. The third bone is the *humerus*, a long bone connected to the scapula, the radius and the ulna. Its upper end is called the humeral head, having a spherical shape. Between the humeral head and elbow, the humerus has a cylindrical shape. Its lower end is triangular. The external points of this shape are the lateral epicondyle and medial epicondyle.

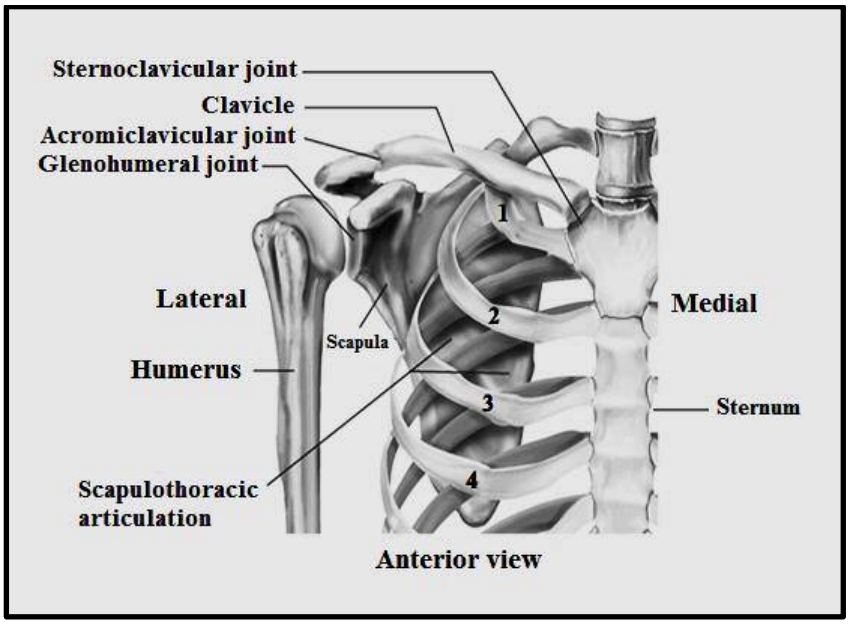


**Figure (2.1)**: Bones and articulations of the shoulder complex, anterior view. Copyrights 2007 McGraw-Hill Higher Education.

### *2.1.1. Shoulder Articulations*

The bones are joined together by three synovial articulations providing mobility, see Figure (2.1). The first articulation in the shoulder is called the sternoclavicular articulation (SC) between the sternum and clavicle, see Figure (2.2). The second articulation is called the acromioclavicular articulation (AC) between the clavicle and scapula, see Figure (2.3). The third articulation is the glenohumeral articulation (GH) between the scapula and humerus. This articulation is a synovial ball-and-socket joint that offers the greatest range of motion and movement potential of any joint in the human body. It is commonly referred to as the "shoulder joint" and is the shoulder's primary articulation. It contains a small, shallow socket called the glenoid fossa. This socket is only one quarter the size of the humeral head that must fit into it. When the joint is loaded, the round shape of the humeral head is pressed against the concave shape of the glenoid cavity on the scapula, see Figure (2.3). The glenoid has an elliptical shape with the long axis directed vertically. When

the joint is relaxed, there is a cavity between the bones. Surrounding the glenoid is the glenoid labrum, a fibro-elastic element protecting the edges of the glenoid cavity. At the other end of the humerus is the elbow and humerolulnar articulation.

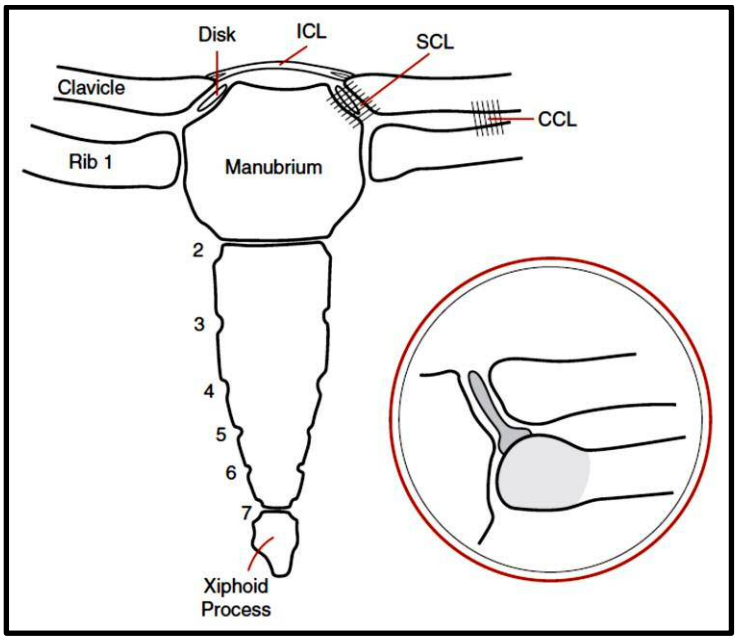


**Figure (2.2):** Sternoclavicular joint is formed by medial portion of clavicle articulating on manubrium sterni and also with cartilaginous end of first rib. Interclavicular (ICL), sternoclavicular (SCL), and costoclavicular ligaments (CCL) stabilize joint. There is fibroelastic disk between medial clavicle and sternum (inset). (Modified from Cailliet 2004).

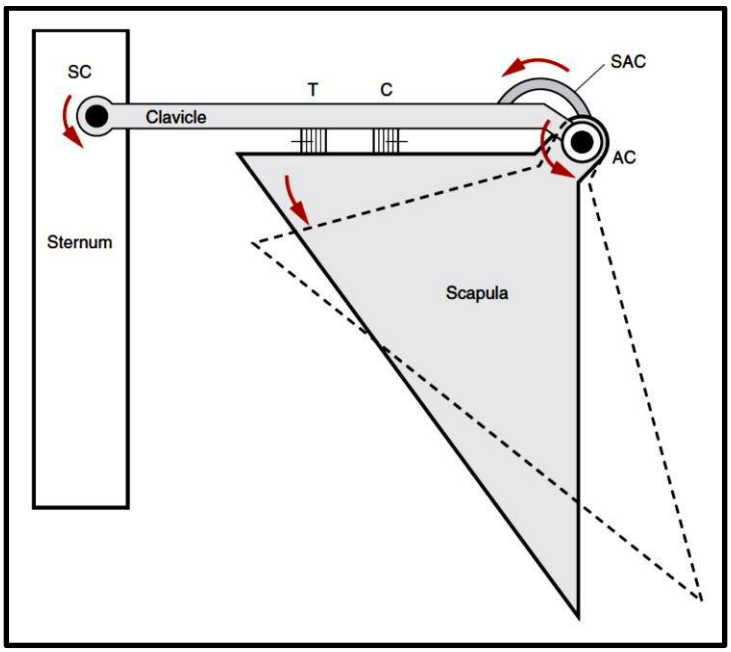


**Figure (2.3):** Clavicle acts as a strut from sternum at sternoclavicular joint (SC). Scapula articulates on end of clavicle at acromioclavicular joint (AC). By its eccentric weight, scapula should mechanically rotate about this AC joint (dotted lines on scapula) except for restraint by claviculoscapular trapezium (T) and conoid (C) ligaments. Superior acromioclavicular ligament (SAC) assists and replaces support of other ligaments when they are severed by any trauma. (Modified from Cailliet 2004).

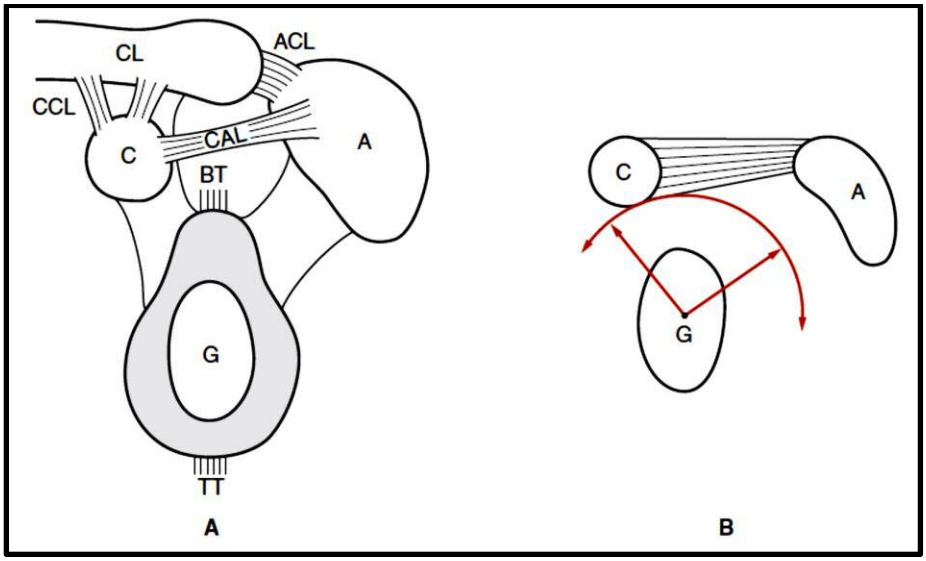


**Figure (2.4):** A, Glenoid fossa (G) is below and lateral to coracoid process (C) and below acromion (A). Biceps tendon (BT) originates from upper margin of fossa. B, Movement (arrows) of humeral head within fossa. ACL indicates acromioclavicular ligament; CCL, coracoclavicular ligaments; CL, clavicle; CAL, coracoacromial ligament; and TT, triceps tendon. (Modified from Cailliet 2004).

Additional structures of the shoulder associated with articulations include ligaments which are viscoelastic elements having a passive role. They are used to stabilise the motion of the bones relative to each other. There are capsular ligaments mentioned previously stabilising the synovial articulations. Stability is understood as keeping the bones of an articulation in the correct configuration such that the load passing through the articulation is not excessive or misaligned with the contact surfaces. Other ligaments in the shoulder provide added strength to the shoulder. For instance, the conoid ligament and coracohumeral ligament stabilise the motion of the scapula relative to the clavicle and humerus. Lastly, the flat concave shape of the scapula allows it to glide over the ribcage. This contact is called the scapulothoracic joint or gliding plane (ST) and is not a typical articulation, connecting bone to bone. Rather, it is a physiological joint (Zuckerman et al. 1989) because of the lack of connection between two bones. It is containing neurovascular, muscular, and bursal structures that allow for a smooth motion of the scapula on the thorax (Terry et al. 2000). The scapula actually rests on two muscles, the serratus anterior and the subscapularis, both connected to the scapula and moving across each other as the scapula moves. Underneath these two muscles lies the thorax.

### *2.1.2. Shoulder Combined Movements*

Although it is possible to create a small amount of movement at any one of these articulations in isolation, movement usually is generated at all of these joints synchronously as the arm is raised or lowered or if any other significant arm action is produced. Movement at the shoulder involves a complex integration of static and dynamic stabilisers. There must be free motion and coordinated actions between all four resulting articulations: the sternoclavicular (SC), acromioclavicular (AC), glenohumeral (GH) and scapulothoracic (ST) joints.

The shoulder complex has the greatest mobility of any region in the body, but as a consequence of this great mobility, it is an unstable area in which numerous injuries may occur. The shoulder motion and stability are dependent on at least three joints and a multitude of bony and soft-tissue structures. Because there is minimal contact between the glenoid fossa and the head of the humerus, the GH joint largely depends on the ligamentous and muscular structures for stability. Stability is provided by both static and dynamic components, which provide restraint and guide and maintain the head of the humerus in the glenoid fossa. The passive, static stabilizers include the articular surface, glenoid labrum, joint capsule, and ligaments. Dynamic support of the shoulder joint occurs primarily in the midrange of motion and is provided by the muscles as they contract in a coordinated pattern to compress the humeral head in the glenoid cavity, (Terry et al. 2000).

The movement of the scapula can occur in three directions, as shown in Figure (2.5). The scapula can move anteriorly and posteriorly about a vertical axis; these motions are known as *protraction* or *abduction* and *retraction* or *adduction*, respectively. Protraction and retraction occur as the acromion process moves on the meniscus in the joint and as the scapula rotates about the medial coracoclavicular ligament. There can be anywhere from 30° to 50° of protraction and retraction of the scapula, (Soderberg 1986). The second scapular movement occurs when the base of the scapula swings laterally and medially in the frontal plane. These actions are termed *upward* and *downward rotation*. This movement occurs as the clavicle moves on the meniscus in the joint and as the scapula rotates about the trapezoid portion of the lateral coracoclavicular ligament. This movement can occur through a range of motion of approximately (60°), (Zuckerman et al. 1989).The third and final movement potential, or degree of freedom, is the scapular movement up and down, termed *elevation* and *depression*. This movement occurs at the AC joint and is not

assisted by rotations about the coracoclavicular ligament. The range of motion at the AC joint for elevation and depression is approximately 30°, (Zuckerman et al. 1989).

The scapula movements also depend on the movement and position of the clavicle. The movements at the SC joint are opposite to the movements at the AC joint for elevation, depression, protraction, and retraction. For example, as elevation occurs at the AC joint, depression occurs at the SC joint and vice versa. This is not true for rotation because the clavicle rotates in the same direction along its length. The clavicle does rotate in different directions to accommodate the movements of the scapula: anteriorly with protraction and elevation and posteriorly with retraction and depression.

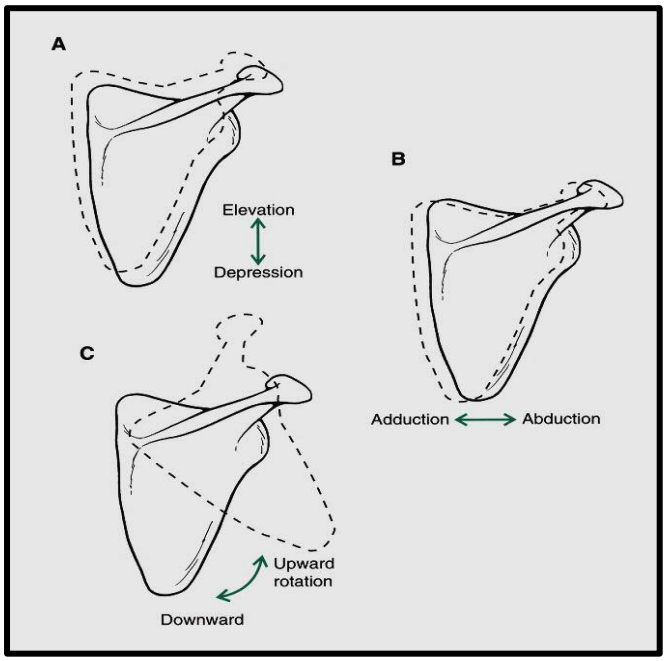


**Figure (2.5)**: Scapular movements take place in three directions. (A) Elevation and depression of the scapula occur with a shoulder shrug or when the arm raises. (B) Abduction (protraction) and adduction (retraction) occur when the scapulae are drawn away from or toward the vertebrae, respectively, or when the arm is brought in front or behind the body, respectively. (C) The scapula also rotates upward and downward as the arm raises and lowers, respectively. (Modified from Hamill 2015).

The shoulder has considerable range of motion of the humerus through flexion and extension, abduction and adduction, medial and lateral rotation, and combination movements of horizontal abduction and adduction and circumduction, see Figure (2.6). Motions at the GH joint are represented by the movements of the arm. The arm can move through approximately 165° to 180° of flexion to approximately 30° to 60° of hyperextension in the sagittal plane, (Zuckerman et al. 1989). The amount of flexion can be limited if the shoulder joint is also externally

rotated. With the joint in maximal external rotation, the arm can be flexed through only (30°). Also, during passive flexion and extension, there is accompanying anterior and posterior translation, respectively, of the head of the humerus on the glenoid.

The arm can also abduct through (150°) to (180°). The abduction movement can be limited by the amount of internal rotation occurring simultaneously with abduction. If the joint is maximally rotated internally, the arm can produce only about (60°) of abduction, but a certain amount of rotation is needed to reach (180°). As the arm adducts down to the anatomical or neutral position, it can continue past the neutral position for approximately (75°) of hyper-adduction across the body.

The arm can rotate both internally and externally (60°) to (90°) for a total of (120°) to (180°) of rotation. Rotation is limited by abduction of the arm. In an anatomical position, the arm can rotate through the full (180°), but in (90°) of abduction, the arm can rotate only through (90°). Finally, the arm can move across the body in an elevated position for (135°) of horizontal flexion or adduction and (45°) of horizontal extension or abduction, (Zuckerman et al. 1989).

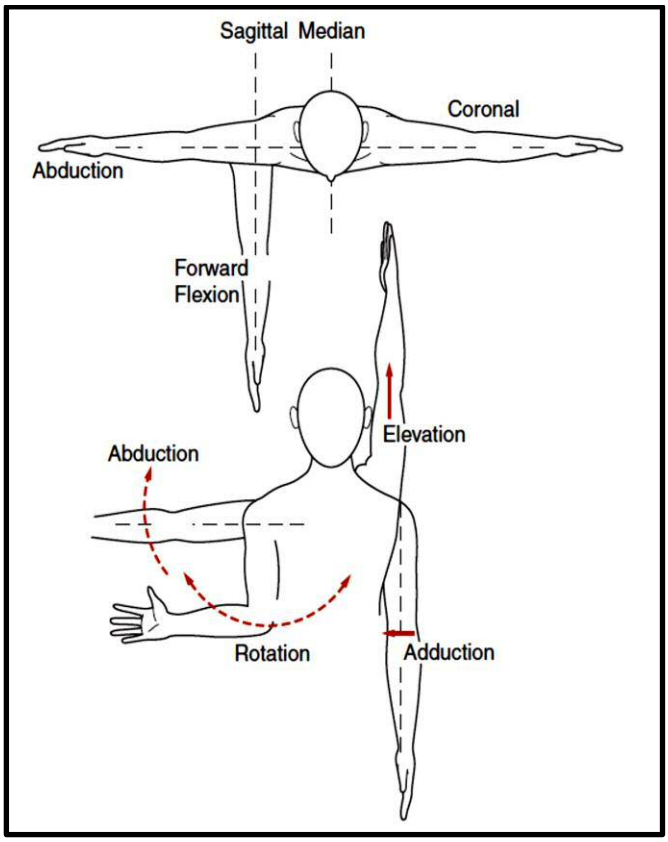


**Figure (2.6):** Planes of arm movement indicate direction of movement as relates to the body. All planes are related to those viewed from above and from front. (Modified from Cailliet 2004).

The four joints of the shoulder complex must work together in a coordinated action to create arm movements. Any time the arm is raised in flexion or abduction, accompanying scapular and clavicular movements take place. The scapula must rotate upward to allow full flexion and abduction at the shoulder joint, and the clavicle must elevate and rotate upward to allow the scapular motion, (Hamill et al. 2015).

There is a considerable movement of the arm at the shoulder joint. The arm can move through 180° of abduction, flexion, and rotation because of the interplay between movements occurring at all of the articulations. The timing of the movements between the arm, scapula, and clavicle is termed the *scapulohumeral rhythm*. The arm can move through only (30°) of abduction and (45°) to (60°) of flexion with minimal scapular movements. Past these points, the scapula movements occur synchronously with the arm movements. Through 180° of flexion or abduction, approximately (120°) of motion occurs in the GH joint and (60°) of motion occurs as a result of scapular movement on the thorax, i.e. 2:1 degrees of humeral movement to scapular movement, see Figure (2.7).

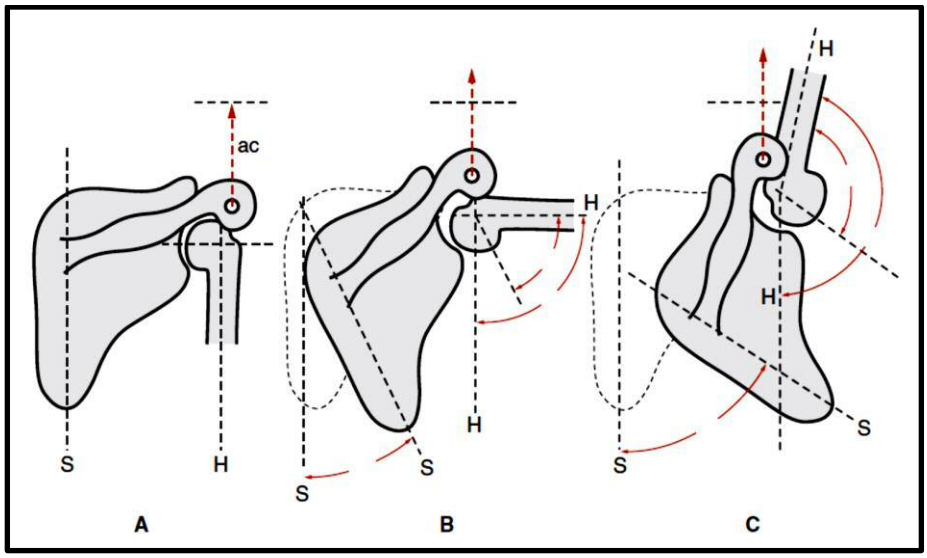


**Figure (2.7):** *Scapulohumeral Rhythm.* **A**, Dependent arm with vertical alignment of scapula (S) and humerus (H) about axis of acromioclavicular joint (ac). **B**, As abduction occurs, scapula rotates 30° and humerus rotates 60°, for a total of 90 degrees of arm abduction. **C**, For further arm overhead elevation (180°), scapula rotates 60°, and humerus rotates on glenoid fossa 120°. Ratio is thus 2:1. (Modified from Cailliet 2004).

### 2.1.3. Shoulder Muscles Actions

There are 16 muscles actuating the shoulder. The shoulder girdle muscles include: trapezius, serratus anterior, rhomboid minor, rhomboid major, levator scapulae, pectoralis minor. These muscles originate on the thorax and insert on the scapula. The superior part of the trapezius muscle inserts on the distal end of the clavicle. The trapezius and serratus anterior are the two major muscles of this group, see Figures (2.8) and (2.9).

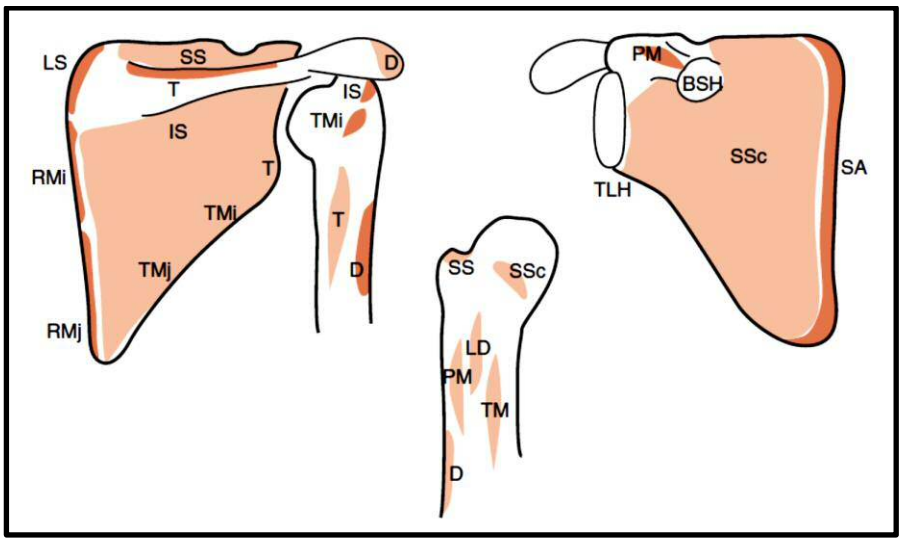


**Figure (2.8):** The muscles on and from the scapula are shown. SS indicates supraspinous; LS, levator muscle of scapula; D, deltoid; T, trapezius; RMi, rhomboid minor; RMj, rhomboid major; IS, infraspinous; TMi, teres minor; TMj, teres major; SSc, subscapular; BSH, biceps short head; TLH, triceps long head; PM, pectoralis major (greater pectoral); SA, anterior serratus; LD, latissimus dorsi. (Modified from Cailliet 2004).

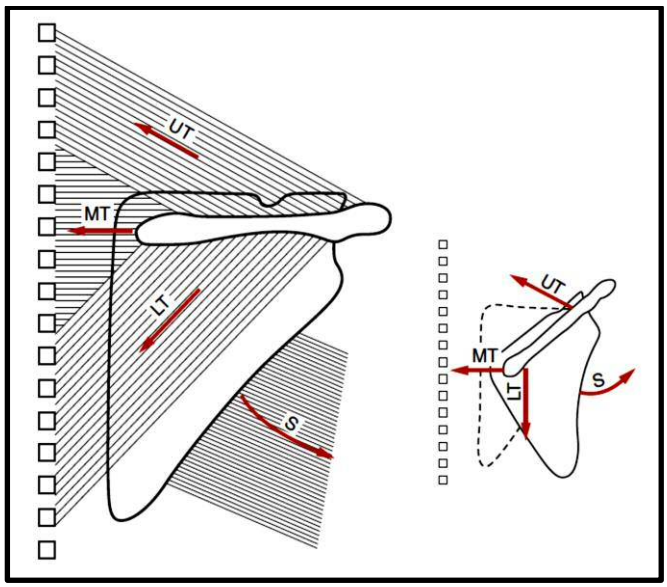


**Figure (2.9):** Muscles that support and rotate scapula are upper trapezius (UT), middle trapezius (MT), and lower trapezius (LT), and serratus (S). (Modified from Cailliet 2004).

The glenohumeral articulation muscles include: deltoid, infraspinatus, supraspinatus, subscapularis, teres minor, teres major, coracobrachialis.The deltoid is the primary muscle of this group. The infraspinatus, supraspinatus, teres minor and subscapularis form a group of muscles collectively known as the rotator cuff muscles, see Figure (2.10). The goal of these muscles is maintaining the stability of the glenohumeral articulation. Again, stability is understood as keeping the bones of an articulation in the correct configuration.

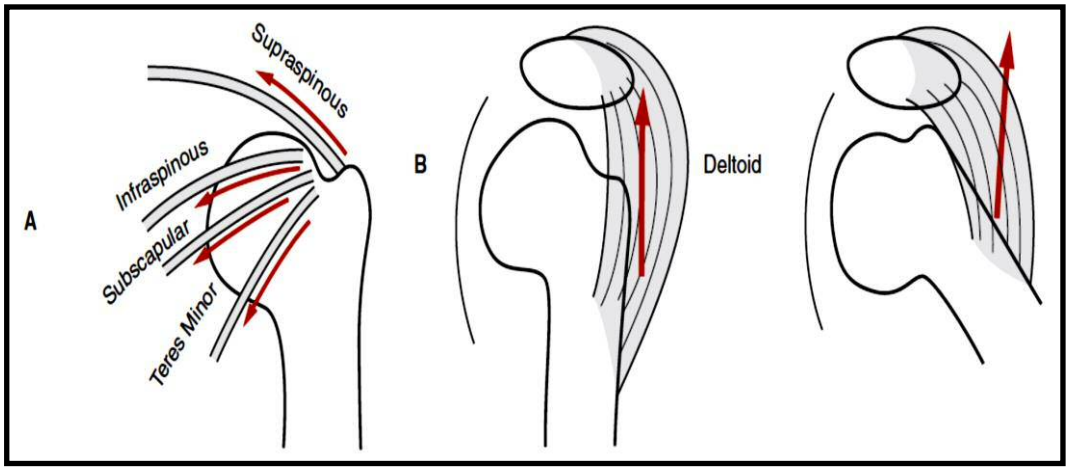


**Figure (2.10):** Muscles Acting on Humeral Head. **A**, Lines of pull of rotator cuff muscles. Supraspinous and infraspinous muscles abduct and rotate head of humerus. Subscapular muscle abducts to lesser degree but also rotates and depresses head of humerus. **B**, Assistance of deltoid muscle on humerus. (Modified from Cailliet 2004).

There are two additional muscles actuating the entire shoulder: the latissimus dorsi and pectoralis major. Both muscles originate on the thorax and insert on the humerus thereby influencing the motion of the entire shoulder. The subclavius muscle is of little importance in actuating the shoulder but rather plays a role of protecting certain arteries passing beneath the clavicle. If the clavicle breaks, this muscle protects the underlying arteries from puncture.

The muscles surrounding the shoulder joint are capable of generating high forces in the range of eight to nine times the weight of the limb. Table (2.1) illustrates the actions of shoulder muscles on the humerus and scapula, (Schenkman 1987).

**Table (2.1)**: Muscles actions at the shoulder complex.(Schenkman 1987).

| Muscle | Action | | | | | | | | | | | | | |
|---|---|---|---|---|---|---|---|---|---|---|---|---|---|---|
| | *Humerus* | | | | | | | *Scapula* | | | | | | |
| | Flexion | Extension | Internal Rotation | External Rotation | Abduction | Adduction | Horizontal Adduction | Elevation | Depression | Downward Rotation | Upward Rotation | Protraction | Retraction | Anterior Tilt |
| Biceps brachii (short head) | ● | | | | | | | | | | | | | |
| Biceps brachii (long head)[1] | ● | | | | ● | | | | | | | | | |
| Triceps brachii (long head) | | ● | | | | ● | | | | | | | | |
| Supraspinatus | | | | | ● | | | | | | | | | |
| Deltoid (Anterior) | ● | | ● | | | | | | | | | | | |
| Deltoid (Middle) | | | | | ● | | | | | | | | | |
| Deltoid (Posterior)[2] | | ● | | ● | | ● | | | | | | | | |
| Coracobrachialis | ● | | | | | ● | | | | | | | | ● |
| Lattissimusdorsi | | ● | ● | | | ● | | | | ● | | | | |
| Pectoralis major (upper fibers) | ● | | ● | | | | ● | | | | | ● | | |
| Pectoralis major (lower fibers) | | ● | ● | | | ● | ● | | | | | ● | | |
| Subscapularis | | | ● | | | | | | | | | | | |
| Infraspinatus | | | | ● | | | | | | | | | | |
| Teres major[3] | | ● | ● | | ● | ● | | | | | | | | |
| Teres minor | | | | ● | | | | | | | | | | |
| Pectoralis minor | | | | | | | | | ● | ● | | ● | | ● |
| Rhomboids | | | | | | | | ● | | ● | | | ● | |
| Levator scapulae | | | | | | | | ● | | ● | | | | |
| Trapezius (Upper) | | | | | | | | ● | | | ● | | | |
| Trapezius (Middle) | | | | | | | | | | | | | ● | |
| Trapezius (Lower)[4] | | | | | | | | | ● | ● | ● | | ● | |
| Serratus anterior (Upper fibers) | | | | | | | | ● | | | ● | ● | | |
| Serratus anterior (Lower fibers) | | | | | | | | | ● | | ● | ● | | |

[1] Biceps brachii long head may abduct the humerus if it is externally rotated.
[2] The joint angle will determine whether posterior deltoid can adduct the humerus.
[3] The joint angle will determine whether teres major abducts or adducts the limb.
[4]The joint angle will determine whether the lower trapezius upwardly or downwardly rotates the scapula.

In a flexed position, the shoulder muscles can generate the greatest strength output in adduction when muscle fibers of the latissimus dorsi, teres major, and pectoralis major contribute to the movement. The adduction strength of the shoulder muscles is twice that for abduction, even though the abduction movement and muscle group are used more frequently in activities of daily living and sports. The movement capable of generating the next greatest level of strength after the adductors is an extension movement that uses the same muscles that contribute to arm adduction.

The extension action is slightly stronger than its opposite movement, flexion. After flexion, the next strongest joint action is abduction, illustrating the fact that shoulder joint actions are capable of generating greater force output in the lowering phase using the adductors and extensors than in the raising phase, when the flexors and abductors are used. The weakest joint actions in the shoulder are rotational, with external rotation being weaker than internal rotation, (Zuckerman et al. 1989).

Two final movements of the arm which are important in performing manual wheelchair propulsion are actually combinations of elevated arm positions are horizontal flexion or adduction and horizontal extension or abduction. Because the arm is elevated, the same muscles illustrated earlier for abduction and flexion also contributes to these movements of the arm across the body, (Zuckerman et al. 1989). Muscles contributing more significantly to horizontal flexion are the pectoralis major and the anterior head of the deltoid. This movement brings the arms across the body in the elevated position and is important in power movements of upper extremity skills (i.e, pushing the wheelchair handrim). Horizontal extension in which the arm is brought back in the elevated position is produced primarily by the infraspinatus, teres minor, and posterior head of the deltoid. This joint action is common in the backswing and preparatory actions in upper limb skills, (i.e, releasing the wheelchair handrim).

## 2.2 The Elbow

The elbow and the radioulnar joints assist the shoulder in applying force and placing the hand in a proper position for a desired action. The elbow is considered a stable joint, with structural integrity, good ligamentous support, and good muscular support. It has three joints allowing motion between the three bones of the arm and forearm (humerus, radius, and ulna). Movement between the forearm and the arm takes place at the ulnohumeral and radiohumeral articulations, and movements between the radius and the ulna take place at the radioulnar articulations, (Soderberg 1986). Landmarks on the radius and ulna and theulnohumeral, radiohumeral, and proximal radioulnar articulations are shown in Figure (2.11).

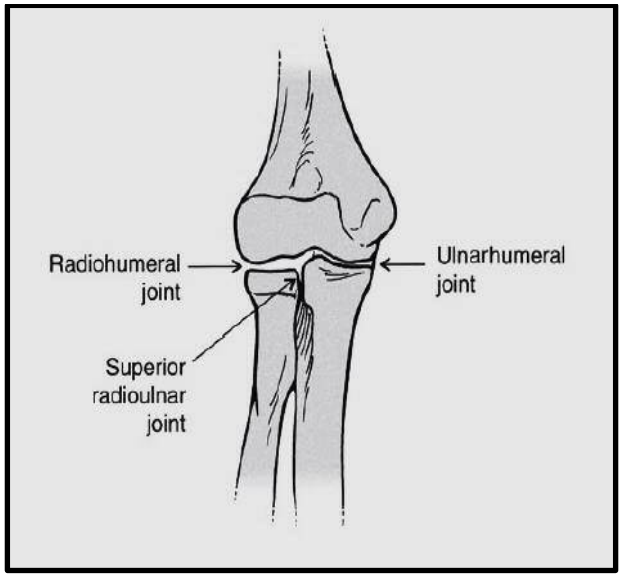


**Figure (2.11)**: The elbow joint complex. The radius and ulnar articulate with the humerus to form the radiohumeral and ulnar humeral joints. (Modified from Hamill 2015).

### *2.2.1. Elbow Articulations*

The ulnohumeral joint is the articulation between the ulna and the humerus and is the major contributing joint to flexion and extension of the forearm. The joint is the union between the spool-like trochlea on the distal end of the humerus and the trochlear notch on the ulna. On the front of the ulna is the coronoid process, which makes contact in the coronoid fossa of the humerus, limiting flexion in the terminal range of motion. Likewise, on the posterior side of the ulna is the olecranon process, which makes contact with the olecranon fossa on the humerus, terminating extension. An individual who can hyperextend at the elbow joint may have a small olecranon process or a large olecranon fossa, which allows more extension before contact occurs.

The trochlear notch of the ulna fits snugly around the trochlea, offering good structural stability. The trochlea is covered with articular cartilage over the anterior, inferior, and posterior surfaces and is asymmetrical, with an oblique posterior projection. In the extended position, the asymmetrical trochlea creates an angulation of the ulna laterally referred to as a valgus position. This is termed the *carrying angle*and ranges from (10°) to (15°) in males and (15°) to (25°) in females. Measurement of the carrying angle is shown in Figure (2.12). As the forearm flexes, this valgus position is reduced and may even result in a varus position with full flexion, (Hamill et al. 2015).

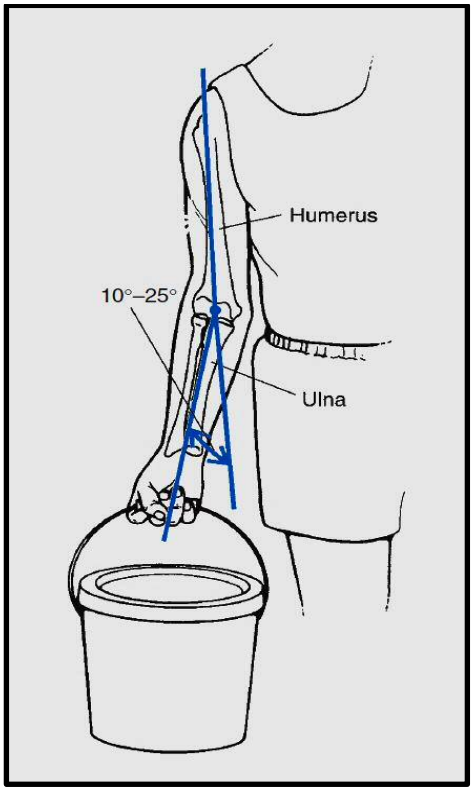


**Figure (2.12)**: In the extended position, the ulna and humerus form the carrying angle because of asymmetry in the trochlea. The carrying angle is measured as the angle between a line describing the long axis of the ulna and a line describing the long axis of the humerus. It ranges from 10° to 25°. (Modified from Hamill et al. 2015).

The radiohumeral joint is the second joint participating in flexion and extension of the forearm. At the distal end of the humerus is the articulating surface for this joint, the capitulum, which is spheroidal and covered with cartilage on the anterior and inferior surfaces. The top of the round radial head butts up against the capitulum, allowing radial movement around the humerus during flexion and extension. The capitulum acts as a buttress for lateral compression and other rotational forces absorbed during throwing and other rapid forearm movements.

The third articulation, the radioulnar joint, establishes movement between the radius and the ulna in pronation and supination. There are actually two radioulnar articulations, the superior in the elbow joint region and the inferior near the wrist. Also, midway between the elbow and the wrist is another fibrous connection between the radius and the ulna, recognized by some as a third radioulnar articulation. The superior or proximal radioulnar joint consists of the articulation between the radial head and the radial fossa on the side of the ulna. The radial head rotates in a fibrous osseous ring and can turn both clockwise and counter clockwise, creating movement of the radius relative to the ulna, (Bowling et al. 1985). In the

neutral position, the radius and ulna lie next to each other, but in full pronation, the radius has crossed over the ulna diagonally. As the radius crosses over in pronation, the distal end of the ulna moves laterally. The opposite occurs during supination.

Two final structural components in the elbow region are the medial and lateral epicondyles. These are prominent landmarks on the medial and lateral sides of the humerus. The lateral epicondyle serves as a site of attachment for the lateral ligaments and the forearm supinator and extensor muscles, and the medial epicondyle accommodates the medial ligaments and the forearm flexors and pronators. These extensions of the humerus are also common sites of overuse injury.

### *2.2.2. Movement Characteristics*

The three joints of the elbow complex do not all reach a close-packed position (i.e., position of maximum joint surface contact and ligamentous support) at the same point in the range of motion. A close-packed position for the radiohumeralis achieved when the forearm is flexed to (80°) and in the semi pronated position. The fully extended position is the close-packed position for the ulnohumeral joint. Thus, when the ulnohumeral articulation is most stable in the extended position, the radiohumeral articulation is loose packed and least stable. The proximal radioulnar joint is in its close-packed position in the semi pronated position, complementing the close-packed position of the radiohumeral, (Bowling et al. 1985).

The range of motion at the elbow in flexion and extension is approximately (145°) of active flexion, (160°) of passive flexion, and (5°) to (10°) of hyperextension. An extension movement is limited by the joint capsule and the flexor muscles. It is also terminally restrained by bone-on-bone impact with the olecranon process. Flexion at the joint is limited by soft tissue, the posterior capsule, the extensor muscles, and the bone-on-bone contact of the coronoid process with its respective fossa. A significant amount of hypertrophy or fatty tissue will limit the range of motion in flexion considerably. Approximately (100°) to (140°) of flexion and extension is required for most daily activities, but the total range of motion is (30°) to (130°) of flexion, (Bowling et al. 1985). The range of motion for pronation is approximately (70°), limited by the ligaments, the joint capsule, and soft tissue compressing as the radius and ulna cross. Range of motion for supination is (85°) and is limited by ligaments, the capsule, and the pronator muscles.

Approximately (50°) of pronation and (50°) of supination are required to perform most daily activities, (Zuckerman et al. 1989).

### *2.2.3. Elbow Muscles Actions*

Twenty-four muscles cross the elbow joint. Some of them act on the elbow joint exclusively; others act at the wrist and finger joints. Most of these muscles are capable of producing as many as three movements at the elbow, wrist, or phalangeal joints. One movement is usually dominant, however, and it is the movement with which the muscle or muscle group is associated. These muscles can be further classified into four main muscle groups which are anterior flexors (biceps brachii, brachioradialis, brachialis, pronator teres, and extensor carpi radialis), posterior extensors (triceps brachii and anconeus), medial flexor-pronators (pronator quadrates and pronator teres), and lateral extensor-supinators (biceps brachii and supinator). The flexor muscle group is considerably stronger than the extensor group. Maximum flexion strength can be developed from the semiprone forearm position. Extension strength is maximum in a flexion position of 90°. Pronation and supination strength is also maximum from the semiprone position, see Figure (2.13) and Table (2.2), (Hamill et al. 2015).

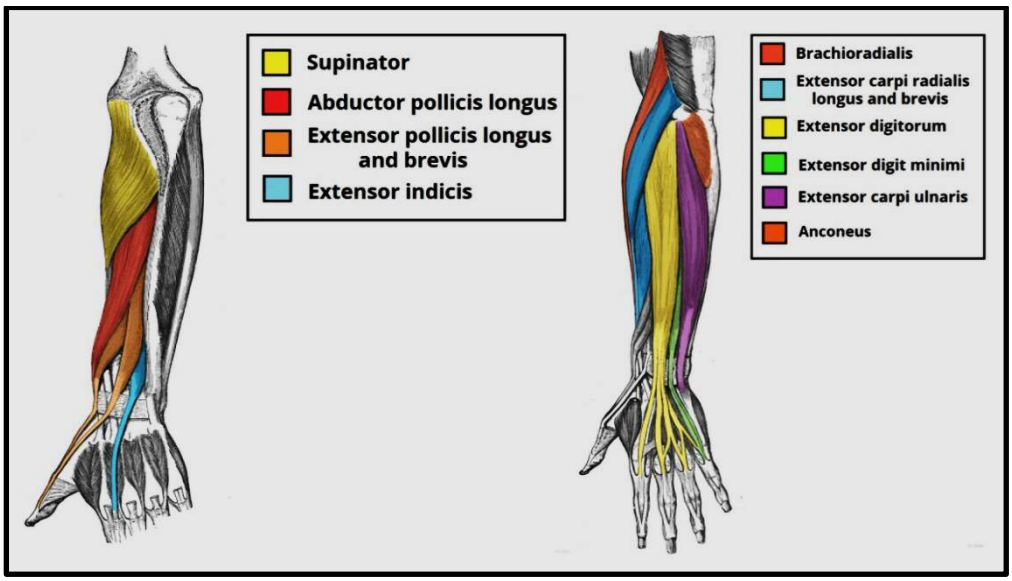


**Figure (2.13)**: Muscles acting on the elbow. (Right) the anterior and (Left) posterior surfaces of the forearm. (Modified from www.anatomybody101.org).

**Table (2.2)**: Muscles actions at the elbow and radioulnar joints. Along with origin and insertion, the principal muscles causing the joints movement are illustrated. (Hamill 2015).

| Movement | Prime Mover Muscle | Origin | Insertion |
|---|---|---|---|
| Flexion | Biceps brachii* | Scapula | Radius |
| | Brachialis* | Humerus | Ulna |
| | Brachioradialis* | Humerus | Radius |
| | Extensor carpi | Humerus | Metacarpals |
| | Pronator teres | Humerus | Radius |
| Extension | Triceps brachii* | Scapula and Humerus | Ulna |
| | Anconeus* | Humerus | Ulna |
| Pronation | Pronator quadratus/teres* | Humerus and Ulna | Radius |
| | Flexor carpi radialis/longus | Humerus | Metacarpals |
| | Brachioradialis | Humerus | Radius |
| Supination | Supinator* | Humerus and Ulna | Radius |
| | Biceps brachii | Scapula | Radius |
| | Abductor/extensor pollicislongus | Radius and Ulna | Metacarpals |
| | Brachioradialis | Humerus | Radius |

* The principal muscles causing the joints movement.

The flexor muscle group is almost twice as strong as the extensors at all joint positions, making us better pullers than pushers. The joint forces created by a maximum isometric flexion in an extended position that is equal to approximately two times body weight. The semiprone elbow position is the position at which maximum strength in flexion can be developed, followed by the supine position, and finally, the pronated position. The supine position generates about (20%) to (25%) more strength than the pronation position. The semiprone position is most commonly used in daily activities. Semiprone flexion exercises should be included in a conditioning routine to take advantage of the strong position of the forearm. Extension strength is greatest from a position of (90°) of flexion, (Zuckerman et al. 1989). This is a common forearm position for daily living activities and for power positions in upper extremity sport skills. Finally, pronation and supination strength is greatest in the semiprone position, with the torque dropping off considerably at the fully pronated or fully supinated position.

## 2.3 The Wrist

The hand is primarily used for manipulation activities requiring very fine movements incorporating a wide variety of hand and finger postures to perform daily activities. Consequently, there is much interplay between the wrist joint positions and efficiency of finger actions. The hand region has many stable yet very mobile

segments, with complex muscle and joint actions. The main joints of the hand are the radiocarpal joint, inferior radioulnar joint, midcarpal and intercarpal joints, carpometacarpal (CMC) joints, metacarpophalangeal (MCP) joints, andinterphalangeal (IP) joints, see Figure(2.14), (Hamill et al. 2015).

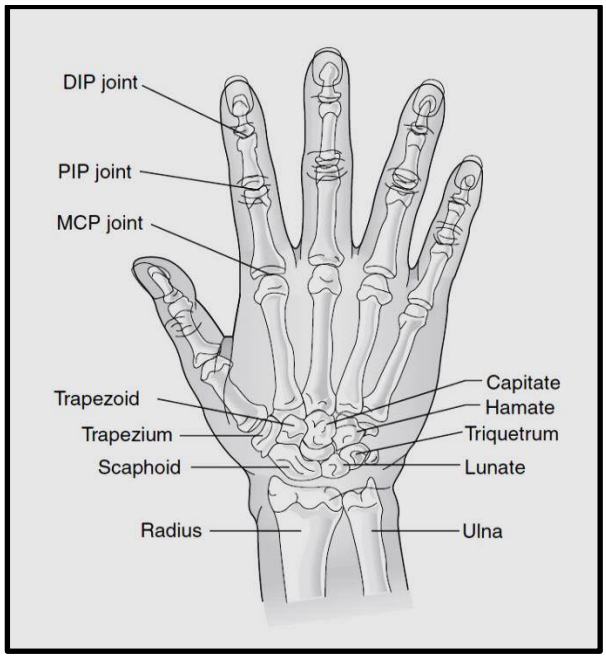


**Figure (2.14)**: The wrist and hand can perform both precision and power movements because of numerous joints controlled by a large number of muscles. DIP, distal interphalangeal; MCP, metacarpophalangeal; PIP, proximal interphalangeal, (Hamill 2015).

### *2.3.1. Wrist Articulations*

The wrist consists of ten small carpal bones but can be functionally divided into the radiocarpaland the midcarpal joints. The *radiocarpal joint* is the articulation where movement of the whole hand occurs. The radiocarpal joint involves the broad distal end of the radius and two carpals, the scaphoid and the lunate. There is also minimal contact and involvement with the triquetrum. This ellipsoid joint allows movementin two planes: flexion–extension and radial–ulnar flexion. It should be noted that wrist extension and radial and ulnar flexion primarily occur at the radiocarpal joint but a good portion of the wrist flexion is developed at the midcarpal joints.

Adjacent to the radiocarpal joint but not participating in any wrist movements is the *distal radioulnar articulation*. The ulna makes no actual contact with the carpals and is separated by a fibrocartilage disk. This arrangement is important so

that the ulna can glide on the disk in pronation and supination while not influencing wrist or carpal movements.

To understand wrist joint function, it is necessary to examine the structure and function at the joints between the carpals. There are two rows of carpals, the proximal row, containing the three carpals that participate in wrist joint function (lunate, scaphoid, and triquetrum), and the pisiform bone, which sits on the medial side of the hand, serving as a site of muscular attachment. In the distal row, there are also four carpals: the trapezium interfacing with the thumb at the saddle joint, the trapezoid, the capitate, and the hamate. The articulation between the two rows of carpals is called the midcarpal joint, and the articulation between a pair of carpal bones is referred to as an intercarpal joint. All of these are gliding joints in which translation movements are produced concomitantly with wrist movements. However, the proximal row of carpals is more mobile than the distal row. A concave transverse arch runs across the carpals, forming the carpal arch that determines the floor and walls of the carpal tunnel, through which the tendons of the flexors and the median nerve travel. The scaphoid may be one of the most important carpals because it supports the weight of the arm, transmits forces received from the hand to the bones of the forearm, and is a key participant in wrist joint actions. The scaphoid supports the weight of the arm and transmits forces when the hand is fixed and the forearm weight is applied to the hand. Because the scaphoid interjects into the distal row of carpals, it sometimes moves with the proximal row and at other times with the distal row.

### *2.3.2. Combined Movements of the Wrist*

The wrist position influences the position of the metacarpal joints, and the metacarpal joints influence the position of the IP joints. This requires a balance between muscle groups. The wrist movements are usually reverse to those of the fingers because the extrinsic muscle tendons are not long enough to allow the full range of motion at the wrist and fingers, (Tubiana et al. 1988). Thus, complete flexion of the fingers is generally only possible if the wrist is in slight extension, and the extension of the fingers is facilitated with synergistic action from the wrist extensors. Although many different hand movements are possible, the hand contains relatively few of the muscles that control these various movements, these muscles being in the forearm. This helps the hand to be less bulky and more manoeuvrable.

The hand is capable of moving through (70°) to (90°) of wrist flexion, (70°) to (80°) of extension, (15°) to (20°) of radial flexion, and (30°) to (40°) of ulnar flexion.

### *2.3.3. Wrist Muscles Action*

Most of the muscles that act at the wrist and fingers joints originate in the forearm and enter the region as tendons. These muscles are termed extrinsic muscles. During wrist and finger movements, the tendons move through considerable distances but are still maintained by the retinacula. Thirty nine muscles work the wrist and hand, and no muscle works alone; antagonists and agonists work in pairs, (Tubiana et al. 1988). The extrinsic muscles provide considerable strength and dexterity to the fingers without adding muscle bulk to the hand, see Figure (2.15) and Table (2.3), (Hamill et al. 2015).

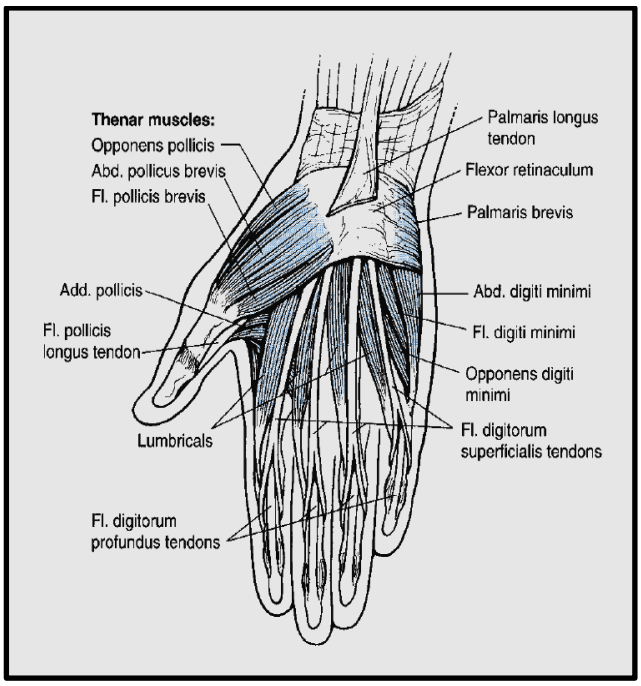


**Figure (2.15)**: Muscles of the wrist and hand, (Hamill et al. 2015).

The muscles work in groups to produce wrist flexion (flexor carpi ulnaris, flexor carpi radialis, and palmarislongus), extension (extensor carpi ulnaris, extensor carpi radialislongus, and extensor carpi radialis brevis), ulnar deviation flexor carpi ulnaris and extensor carpi ulnaris), and radial flexion (flexor carpi radialis, extensor carpi radialislongus, and extensor carpi radialis brevis).

**Table (2.3)**: Muscles actions at the wrist and fingers joints. Along with origin and insertion, the principle muscles causing the joints movement are illustrated.

| Movement | Prime Mover Muscle | Origin | Insertion |
|---|---|---|---|
| Palmar Flexion | Digitorum superficialis/profundus | Humerus, Radius and Ulna | Phalanges |
| | Carpi ulnaris | Humerus | Metacarpals |
| | Palmaris longus | Humerus | Palmar aponeurosis |
| | Carpi radialis | Humerus | Metacarpals |
| | Abductor pollicislongus | Radius and Ulna | Metacarpals |
| Dorsi Flexion | Digitorum | Humerus | Phalanges |
| | Carpi radialislongus/brevis | Humerus | Metacarpals |
| | Palmaris longus | Humerus | Palmar aponeurosis |
| | Digitiminimi | Humerus | Phalanges |
| Radial Abduction | Extensor carpi radialislongus | Humerus | Metacarpals |
| | Abductor pollicislongus | Radius and Ulna | Metacarpals |
| | Extensor pollicislongus | Radius and Ulna | Thumb |
| | Flexor carpi radialis | Humerus | Metacarpals |
| | Flexor pollicislongus | Radius | Thumb |
| Ulnar Abduction | Extensor/flexor carpi ulnaris | Humerus and Ulna | Metacarpals |
| | Extensor digitorum | Humerus | Phalanges |
| | Extensor digitiminimi | Humerus | Metacarpals |

## 2.4 Injury Potential of the Upper Limb

Injuries of the upper limb have a considerable impact on the biomechanical aspects of individuals because of their potential for the resulting lifelong functional disorders. These injuries commonly imply a reduction in the upper limb function which complicates, or even constrains, the performance of basic activities of daily living (ADL) and then lead to decrease in quality of life.

Moreover, manual wheelchair propulsion is essential for many individuals with lower limb impairments who wish to maintain an active, independent life style. However, it is also one of the activities related to the high prevalence of upper limb pain in manual wheelchair users. Over half of all manual wheelchair users experience pain and injuries primarily in their shoulder and wrist areas, (Jensen et al. 2005 and Alm et al. 2008). Although less frequent, pain at the elbow and neck is also common amongst manual wheelchair users. Shoulder pain, carpal tunnel syndrome and other upper limb injuries are common problems in manual wheelchair users (Boninger et al. 1999). They result from high mechanical stress accompanying the propulsion of manual wheelchairs.

Therefore, to help reduce the incidences of pain, it is initially important to understand the common injuries to the shoulder, elbow and wrist to generate the knowledge that can be used to improve upper limb performance and/or prevent injuries.

### *2.4.1. Injury Potential of the Shoulder Complex*

The shoulder complex is subject to a wide variety of injuriesthat can be incurred in two ways. The first type of injury is through trauma. This type of injury usually occurs when contact is made with an external object, such as the ground or another individual. The second type of injury is through repetitive joint actions that create inflammatory sites in and around the joints or muscular attachments.

Many injuries to the shoulder girdle are traumatic, a result of impacts during falls or contact with an external object. The sternoclavicular joint can sprain or dislocate anteriorly if an individual falls on the top of the shoulder in the area of the middle deltoid. An individual with a sprain to this joint has pain in horizontal extension movements of the shoulder, such as in the golf swing or the backstroke in swimming (Hamill et al. 2015). Anterior subluxations of this joint in adolescents have also occurred spontaneously during throwing because they have greater mobility in this joint than adults. A posterior dislocation or subluxation of the sternoclavicular joint can be quite serious because the trachea, esophagus, and numerous veins and arteries lie below this structure. This injury occurs as a consequence of force to the sternal end of the clavicle.

The clavicle is frequently a site of injury by direct trauma received through contact in football and some other sports. The most common injury is a fracture tothe middle third of the clavicle. This injury is incurred by falling on the shoulder or outstretched arm or receiving a blow on the shoulder so that a force is applied along the shaft of the clavicle. Other less common fractures occur to the medial clavicle as a result of direct trauma to the lateral end of the clavicle or as a result of direct trauma to the tip of the shoulder (Hamill et al. 2015).

Clavicular fractures in adolescents heal quickly and effectively; but in adults, the healing and repair process is not as efficient or effective. This is related to the differences in the level of skeletal maturation. In adolescents, new bone is being formed at a much faster rate than in mature individuals.

Injuries to the acromioclavicular joint can cause a considerable amount of disruption to shoulder movements. Again, if an individual falls on the point of the shoulder, the AC joint can subluxate or dislocate. This can also occur because of a fall on the elbow or on an outstretched arm. This joint is also frequently subjected to overuse injuries in sports using the overhand pattern, such as throwing, tennis, and swimming.

The scapula rarely receives sufficient force to cause an injury. If an athlete or an individual falls on the upper back, however, it is possible to fracture the scapula and bruise the musculature so that arm abduction is quite painful. Another site of fracture on the scapula is the coracoid process, which can be fractured with separation of the AC joint. Throwers can also acquire bursitisat the inferomedial border of the scapula, causing pain as the scapula moves through the cocking and acceleration phases in the throw. The pain is diminished in the follow through phase. Bursitis is the inflammation of the bursa, a fluid-filled sac found at strategic sites around the synovial joints that reduces the friction in the joint.

The shoulder joint is commonly injured either through direct trauma or repeated overuse. Dislocation or subluxation in the glenohumeral joint is frequent because of the lack of bony restraint and the dependence on soft tissue for restraint and support of the joint. The glenoid fossa faces anterolaterally, creating more stability in the posterior joint than the anterior. Thus, the most common direction of dislocation is anterior. Anterior and inferior dislocations account for 95% of dislocations (Hamill et al. 2015).

The usual cause of the dislocation is contact or some force applied to the arm when it is abducted and externally rotated overhead. This drives the humeral head anteriorly, possibly tearing the capsule or the glenoid labrum. The rate of recurrence of dislocation depends on the age of the individual and the magnitude of the force producing the dislocation (Hamill et al. 2015).

Recurrent dislocations also depend on the amount of initial damage and whether the glenoid labrum was also damaged. A tear to the glenoid labrum, similar to tearing the meniscus in the knee, results in clicking and pain with the arm overhead (Hamill et al. 2015). An anterior dislocation also makes it difficult to rotate the arm internally, so that the contralateral shoulder cannot be touched with the hand on the injured side. Posterior dislocations of the shoulder are rare and are usually associated with a force applied with an adducted and internally rotated arm with the

hand below shoulder level. The clinical signs of a posterior dislocation are inability to abduct and externally rotate the arm.

Soft-tissue injuries at the shoulder joint are numerous and are most often associated with overhead motions of the arm, such as in throwing, swimming, and racket sports. Because of the extreme range of motions and high velocities in throwing, the dynamic stabilizing structures of the shoulder joint are at great risk for injury (Hamill et al. 2015). Injuries in this category include examples such as posterior and anterior instability, impingement, and glenoid labrum damage. The rotator cuff muscles, which are active in controlling the humeral head and motion during the overhand pattern, are highly susceptible to injury.

The most common mechanism of injury to the rotator cuff occurs when the greater tuberosity pushes against the underside of the acromion process. This subacromial impingement syndrome occurs during the acceleration phase of the overhand throwing pattern when the arm is internally rotating while still maintained in the abducted position. Impingement is commonly injured in wheelchair users. It can also occur in the lead arm of golfers and in a variety of other activities that use the overhead pattern. The rotator cuff, subacromial bursa, and biceps tendon are compressed against the anterior undersurface of the acromion and coracoacromial ligament (Hamill et al. 2015).

Another injury that is a consequence of impingement is subacromial bursitis. This injury results from an irritation of the bursae above the supraspinatus muscle and underneath the acromion process. It also develops in wheelchair propulsion because of greater-than-normal pressures in the joint and abnormal distribution of stress in the subacromial area (Hamill et al. 2015).

Finally, the tendon of the long head of the biceps brachii can become irritated when the arm is forcefully abducted and rotated. Bicipital tendinitis develops as the biceps tendon is subluxated or irritated within the bicipital groove. Irritation to the biceps tendon is manifested in a painful arc syndrome similar to that of the rotator cuff injury.

In summary, the shoulder complex has the greatest mobility of any region in the body, but as a consequence of this great mobility, it is an unstable area in which numerous injuries may occur. Despite the high probability of injury, successful rehabilitation after surgery is quite common. It is important to maintain the strength and flexibility of the musculature surrounding the shoulder complex because there is

considerable dependence on the musculature and soft tissue for support and stabilisation.

### *2.4.2. Injury Potential of the Forearm*

The elbow and forearm are vulnerable to injury as a result of falling or repetitive overuse. There are two categories of injuries at the elbow joint: traumatic or high-force injuries and repetitive or overuse injuries. The elbow joint is subjected to traumatic injuries caused by the absorption of a high force, such as in falling, but most of the injuries at the elbow joint result from repetitive activities, such as throwing and throwing-type actions. The high-impact or traumatic injuries are presented first, followed by the more common overuse injuries.

One of the injuries occurring as a consequence of absorbing a high force is a dislocation. These injuries usually occur in sports such as gymnastics, football, and wrestling. The athlete falls on an outstretched arm, causing a posterior dislocation. With the dislocation, a fracture in the medial epicondyle or the coronoid process may occur. The elbow is the second most common dislocated joint in the body (Hamill et al. 2015). Other areas that may fracture with a fall include the olecranon process; the head of the radius; and the shaft of the radius, the ulna, or both. Additionally, spiral fractures of the humerus can be incurred through a fall.

A high muscular force can create a rupture of the long head of the biceps brachii, commonly seen in adults. The joint movements facilitating this injury are arm hyperextension, forearm extension, and forearm pronation. If these three movements occur concomitantly, the strain on the biceps brachii may be significant. The repetitive or overuse injuries occurring at the elbow can be associated with throwing or some overhead movement, such as the tennis serve. Throwing places stringent demands on the medial side of the elbow joint. Through the high-velocity actions of the throw, large tensile forces develop on the medial side of the elbow joint, compressive forces develop on the lateral side of the joint, and shear forces occur on the posterior side of the joint. The elbow joint is injured because of the change in a varus to a valgus angle, greater forces, smaller contact areas, and contact areas that move more to the periphery as the joint moves through the throwing action (Hamill et al. 2015).

Medial epicondylitis is an irritation of the insertion site of the wrist flexor muscles attached to the medial epicondyle. The lateral overuse injuries to the elbow usually occur as a consequence of overuse of the wrist extensors at their attachment site on the lateral epicondyle. The overuse of the wrist extensors occurs as they eccentrically slow down or resist any flexion movement at the wrist.

### *2.4.3. Injury Potential of the Wrist*

Many injuries can occur to the hand as a result of absorbing a blunt force, as in impact with a ball, the ground, or another object. Injuries of this type in the wrist region are usually associated with a fall, forcing the wrist into extreme flexion or extension. In this case, extreme hyperextension is the most common injury. This can result in a sprain of the wrist ligaments, a strain of the wrist muscles, a fracture of the scaphoid (70%) or other carpals (30%), a fracture of the distal radius, or a dislocation between the carpals and the wrist or other carpals (Hamill et al. 2015).

The distal end of the radius is one of the most frequently fractured areas of the body because the bone is not dense and the force of the fall is absorbed by the radius. A common fracture of the radius, *Colles fracture*, is a diagonal fracture that forces the radius into more radial flexion and shortens it. These injuries are associated mainly with activities such as hockey, fencing, football, rugby, skiing, soccer, bicycling, parachuting, mountain climbing, and hang gliding in which the chance of a blunt macro trauma is greater than in other activities.

There is also overuse injuries associated with repetitive use of the hand in sports, work, or other activities. A disabling overuse injury to the hand is carpal tunnel syndrome. Next to low-back injuries, carpal tunnel syndrome is one of the most frequent work injuries reported by the medical profession. The floor and sides of the carpal tunnel are formed by the carpals, and the top is formed by the transverse carpal ligament. Travelling through this tunnel are all of the wrist flexor tendons and the median nerve. Through repetitive actions at the wrist, usually repeated wrist flexion, the wrist flexor tendons may be inflamed to the point where there is pressure and constriction of the median nerve. The median nerve innervates the radial side of the hand, specifically the thenar muscles of the thumb. Impingement of this nerve can cause pain, atrophy of the thenar muscles, and tingling sensations in the radial side of the hand.

It is recommended that the wrist be maintained in a neutral position while performing tasks in the workplace to avoid carpal tunnel syndrome. Ulnar nerve injuries can also result in loss of function to the ulnar side of the hand, specifically the ring and little fingers. Damage to this nerve can occur as a result of trauma to the elbow or shoulder region. Ulnar neuropathy is associated with activities such as cycling (Hamill et al. 2015).

## 2.5 Summary

This chapter aimed to present an anatomical background through introducing a detailed illustration of the anatomy and biomechanics of the human upper limb. It described the structure, support and movements of the joints and articulations of the upper body and identified the muscular actions contributing to these joints. It also identified the common potential injuries to the shoulder, elbow, wrist and hand as associated with activities of daily living and manual wheelchair propulsion. The next chapter will introduce another background theory about the anatomy and biomechanics of manual wheelchairs.

# Chapter 3

## Anatomy and Biomechanics of Manual Wheelchair

### 3.1 Background

A wheelchair is one of the most commonly used assistive devices that provide wheeled mobility and seating support for people who have impairments with their ability of walking or moving around. Statistics of the World Health Organisation on the number of wheelchair users worldwide indicate that about 10% of the population, approximately 650 million people worldwide, have disabilities. Of that disabled population, some (10%) are in need of a wheelchair (WHO, 2008). Such a large number of current and potential users represent a major public health concern. In undeveloped countries, the number of people who need wheelchairs is much higher than in developed countries (because of the higher prevalence of disease and injury) but only (5–15%) of those will actually have a wheelchair.

Wheelchair users can be divided into three groups: (1) persons who have lost some or all of their lower limb function (i.e. spinal cord injury (SCI), arthritis, cerebral palsy, poliomyelitis, multiple sclerosis, muscular dystrophy, stroke/brain trauma, bilateral amputation), (2) persons with insufficient postural stability (i.e. brain damage, cerebral palsy, cancer of the spine), or (3) persons with general debilitation (i.e. aging, obesity, temporary illness), (Wilson 1986).

A manual wheelchair has the impossible task of replacing lower limbs as well as supplying a comfy seat. According to the World Health Organization, a wheelchair is appropriate when it:

• meets the user's needs and environmental conditions;

• provides proper fit and postural support;

• is safe and durable;

• is available in the country; and

• can be obtained, maintained and services sustained in the country at an affordable cost.

This chapter aimed to present a background theory of manual wheelchair. It provided a detailed illustration of the anatomy and biomechanics of manual

wheelchair that began with an overview of the types of manual wheelchair and briefly described its features and components and identified the function of each component and mechanical properties that can influence the performance of manual wheelchair propulsion.

## 3.2 Types of Wheelchairs

About 90% of all wheelchairs are basic manual pushrim-propelled wheelchairs, (van der Woude et al. 2001). They are the most commonly prescribed type of chair because they are inexpensive, easy to manoeuvre on flat surfaces (such as those in a home) and convenient to transport, being light and foldable. They vary from the most simple 'transport' chair which is mostly used in hospitals for short-term use to modern styles for permanent use, See Figure (3.1).


**Figure (3.1)**: Pushrim-propelled wheelchairs. (a) A 'transport' chair. Invacare Corporation. Used with permission. (b) Modern style wheelchair. Otto Bock Healthcare GmbH. Used with permission. (www.adaptivespecialities.com).

Van der Woude et al. (2006) described handrim propulsion as having 'the closest interaction with the human system (of all propulsion methods) with direct visual, proprioceptive and kinaesthetic feedback to the user, directly expressing information on position, speed and spatial orientation of the body'. There are two main disadvantages with the standard pushrim-propelled wheelchair; first, it is inefficient and second it is straining. This means that even physically strong users will struggle to travel up ramps and on rough surfaces such as outdoor paths and that their limited environment will restrict their participation in activities of daily living. The inefficiency arises from the fact that only a small part of the stroke cycle

actually pushes the chair forward. The remaining part of the stroke cycle is the 'recovery' part where the user's arm moves into position for the next push phase.

The long-term repetitive strain associated with pushrim propulsion will cause chronic use of the shoulders and wrists resulting in pain that may eventually force the person to use powered propulsion.

No single model or size of wheelchair can meet the needs of all users, and the diversity among users creates a need for different types of wheelchair. The ability to adjust or customize a wheelchair to meet the user's physical needs will vary, depending on the type of wheelchair. Generally, choosing the right configuration of the wheelchair is the first step in prescribing it. A few of the factors which need to be considered when choosing a configuration for a wheelchair are; the user's environment, prognosis, abilities and activities. The wheelchair should be functional in the user's environment, adaptable to the users prognosis, enhance their abilities and enable their participation in desired their activities. Based on variations in the basic design, there are many types of wheelchairs, with being highly customized to suit individual needs.

• Manual wheelchairs are mostly propelled by the user. Other features such as foot/leg rests, front caster outriggers, adjustable backrests and controls can be added to the basic model. The seat size (width and depth), seat-to-floor height, seat angle (also called seat dump or squeeze) relative to the horizontal plane can be modified. Users who have specialized needs may opt for a custom-built wheelchair, (WHO 2011).

• Attendant-propelled chairs are designed to be propelled by an attendant using the handles, and thus the back wheels are often rimless and smaller. These chairs are often used as 'transfer chairs' possibly within a hospital or airport to move a mobility-impaired person when a better alternative or a user's standard chair is unavailable, (WHO 2011).

• A rigid frame wheelchair is usually a non-folding type with a base of support on which the person sits. In some models, the backrest of the chair can be folded down,

and the wheels have a quick release mechanism to enable easy transportation and storage, (WHO 2011).

• A folding frame wheelchair is one whose frame is collapsible sideways by the use of an "X" mechanism in the frame. This mechanism is lockable, and the wheelchair folds on release of two locking levers on the chair, (WHO 2011).

• A motorized wheelchair, power chair, electric wheelchair or electric-powered wheelchair is propelled by means of an electric motor rather than manual power. Motorized wheelchairs are useful for those unable to propel a manual wheelchair or who may need to use a wheelchair for distances or over terrain which would be fatiguing in a manual wheelchair. They may also be used by people with cardiovascular and fatigue-based conditions, (WHO 2011).

## 3.3 Wheelchairs Features and Components

Manual wheelchairs have many features to make the equipment more functional for the end user, but there are variations on these features and reasons why each variation is important to each user. There are many decisions to make when prescribing a wheelchair and most of them concern the choosing of the components that will work best for the user. Understanding of how each decision will affect other decisions is important. Often choosing the right wheelchair configuration for a wheelchair is a seemingly never ending series of compromises. Traditional manual wheelchairs have consisted of tubular construction, sling seats and backs suspended from a horizontal and vertical cross brace folding mechanism, front casters and rear drive wheels and brakes with hand rims mounted on the rear vertical frame (Brubaker 1986). Advances in wheelchair technology have made some improvements on this design. Some of these advances include rear wheel axle adjustment; using materials such as aluminum, carbon fiber and titanium to reduce the weight and size of the wheelchair, hand rim technology reduction in vibrations transmitted to the user, transportability and transportation and improved propulsion methods (Di Giovine et al. 2006). Together, these parts of the wheelchair help the user to maintain a comfortable and functional posture and to provide pressure relief. The basic wheelchair parts are illustrated in the schematic figure (3.2).

### *3.3.1. Wheelchair Frames*

The wheelchair frame is the main component of a wheelchair that connects all the other components together and determines the type of wheelchair that will result from a tubular structure that can last a long time. Currently, two types of frame design are commercially available: folding and rigid frames. When selecting the frame type, one should consider the user's functional and physical features and lifestyle. For a less active user, wheelchairs with folding frames may be the best choice, since they are, in general, larger and therefore more stable, and allow disassembly of components that may facilitate transportation.

Moreover, Liu et al. (2010) showed that folding-frame wheelchairs are more stable in the forward direction, and they suggested that this may be a consequence of the footrest position being more forward in folding chairs than in rigid-frame wheelchairs. Rigid frames, in turn, are generally lighter and provide improved mobility performance, but stability is affected.

The frame mass plays an important role in the mechanics of a manual wheelchair. Ultralight chairs are most appropriate for those users who have an active lifestyle, since the reduced mass helps with the preservation of upper limb function by reducing the handrim forces during manual propulsion. Aluminium is widely used in wheelchairs, since it has a better strength-to-weight ratio than steel and does not require special manufacturing techniques, (Cooper et al. 2010). More recently, titanium and carbon fibre have been used to make wheelchair frames. Titanium has advanced properties in terms of absorbing shocks and vibration, and a better strength-to-weight ratio than aluminium, (Boninger et al. 2006). Similarly, carbon fibre has an improved strength-to-weight ratio, and the fibres can be molded in a way that increases the strength in one direction while increasing flexibility in another direction. However, both titanium and carbon fibres are significantly more expensive than aluminium, and they also require specialized manufacturing techniques.

### *3.2.2. Wheelchair Seat Frames*

The wheelchair seat frame consists of simply a seat and attached backrest without arms or footrests however if the wheelchair arms are fixed (not removable) then they are part of the seat frame as well. Older wheelchairs and some institutional

wheelchairs are the only chairs seen these days with fixed arms. Push Handles are extensions to the top of the backrest, they project and overlap backwards from the wheelchair and permit a caretaker to help propel the chair from behind. The seat frames of most wheelchairs are available in many dimensions for the seat width, seat depth and back height.

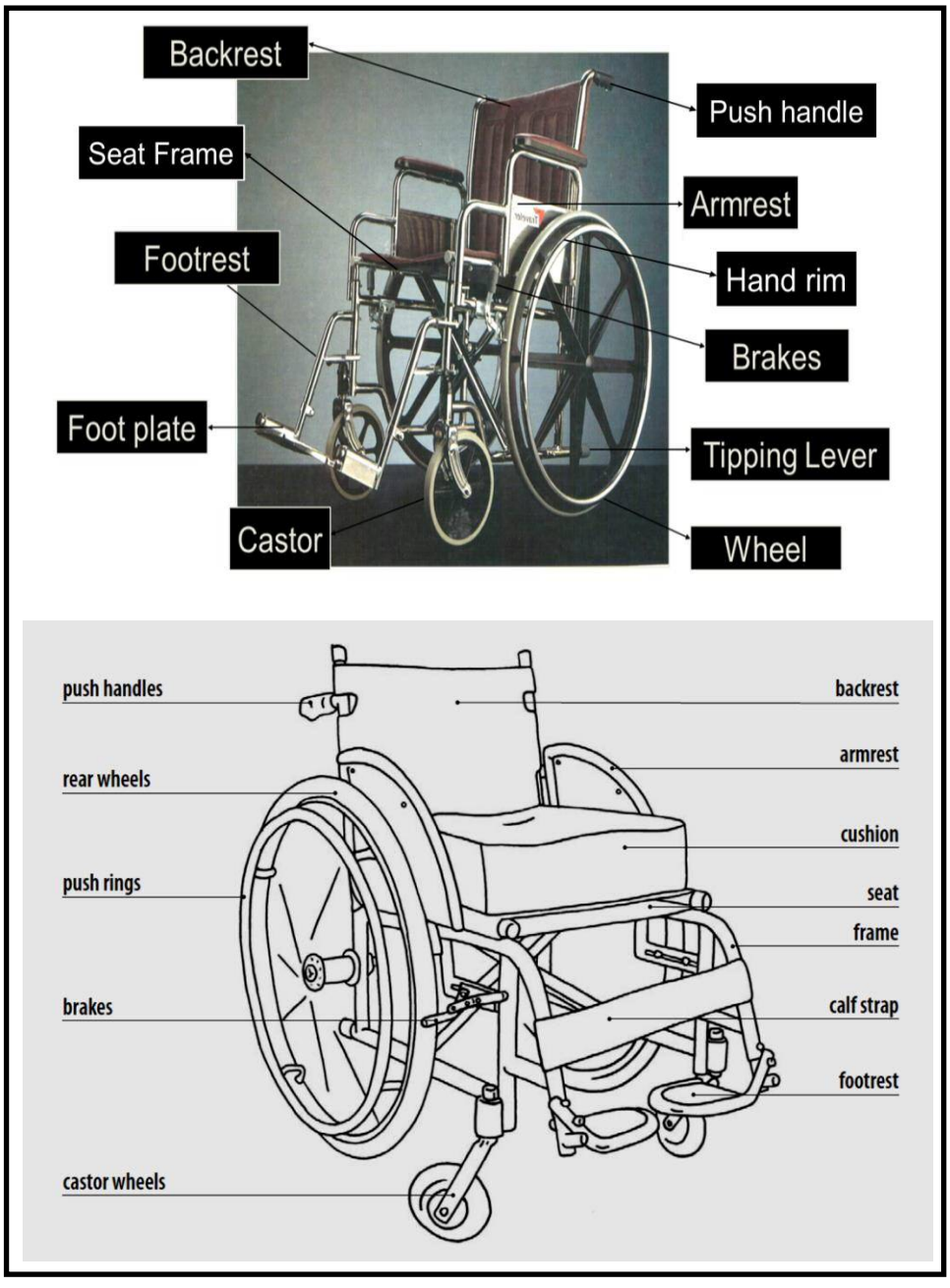


**Figure (3.2)**: Schematic basic components of a manual wheelchair, (WHO 2008).

The vertical distance between the rear wheels and the seat greatly influences the biomechanics of manual propulsion. Having a lower seat benefits manual

propulsion because it results in increased push angle. However, it results in increased upper limbs' ROM, which is potentially harmful if physiological limits are exceeded, (van der Woude et al. 1989). On the other hand, when the user is too high above the wheels (i.e. in a higher seat), he/she can only push the hand rims over a short distance (small push angle), and to maintain the desired speed, the user has to increase push frequency, (Boninger et al. 2000), which may lead to muscular fatigue. The relation between seat height, push angle and push frequency has been investigated by Richter et al. (2001).

The optimal seat height is determined by the elbow angle when the user holds the handrim at its top position. Previous studies have shown that elbow angles ranging from (100°) to (120°) are related to improved propulsion efficiency and lower energy expenditure, (Veeger et al. 1990). Lower seat heights (elbow angles ranging from 80° to 90°) have been shown to be less efficient in terms of handrim forces and cardiorespiratory parameters (van der Woude et al. 2009). Therefore, in order to preserve upper limb function, it is recommended to set up the chair with the seat positioned at such a height that the elbow angle ranges from (100°) to (120°).

### *3.2.3. Wheelchair Backrest*

Wheelchair backrest is the suspension between the upright components of the seat frame against which the user rests his or her back. It provides users the necessary postural support. Some users require more support from a backrest than others. It should support the normal curvature of the spine. The backrest configuration influences the trunk support and upper limbs' ROM. These aspects are counter posed when one considers the two extreme situations: while a higher backrest provides greater support, it limits shoulder extension, which is particularly undesirable, since it is necessary to posteriorly grip the hand rims of the wheel when starting to push a wheelchair. On the other hand, lower backrests allow the upper limbs to move freely, but back support and posterior stability are limited.

A study by Yang et al. (2012) found that a lower backrest (20 cm, versus the highest 40.6 cm) allowed greater shoulder ROM and greater push angle and push time, thus reducing push frequency. However, backrest height did not significantly affect the forces applied to the handrim. Cherubini et al. (2012) advised that users

with impaired trunk control would benefit from higher backrests, which should be positioned (2 cm) below the scapulae inferior angle. Those with intact trunk control should use lower backrests, taking the top of the lumbar spine as a reference.

### *3.2.4. Wheelchair Armrests*

There are a variety of wheelchair armrests to meet the needs of various types of wheelchair users. Users should use armrests only for temporary postural support. If needed, other postural support options should be used to keep the user's arms free for activities such as propelling. Armrests on wheelchairs have various functions depending on the user's needs. They assist in transferring into and out of the wheelchair, for example by pushing up on the armrest. Many users find it easier to transfer into and out of their wheelchair if the armrests are "low-profile" (closely following the profile of the rear wheel) or removable. In other words, armrests should be removable, folding or low-profile for easy transferral in and out of the wheelchair. The height of the wheelchair arms should be sufficient to rest the elbows on without forcing the shoulders to either hunch up or sag down for the best comfort for most users.

### *3.2.5. Wheelchair Footrests*

The footrest provides users with support for their feet and legs. Footrests must be individually adjusted for each user. There are two types of foot support for a wheelchair. The two most common are generally known as "footrests" and "legrests". A footrest consists of a footrest hanger and a footplate for the user's foot to rest on and a legrest has a "calf pad" mounted on an elevating hanger to support the lower leg when elevated and the same options for a footplate as the footrest will have. Correctly adjusted, the footplate reduces pressure on the user's seat and puts the user in a healthy sitting posture. Sufficient ground clearance needs to be maintained to prevent the footrest hitting obstacles or catching and tipping the wheelchair on uneven ground. The height of the footrest should be adjustable. Footrests need to be long or wide enough to support the foot but, at the same time, should not create difficulty while folding or moving around. Proper support of the feet and legs is important to the comfort of the wheelchair user and long term use of footrests/legrests that are not set up properly can lead to pain in the lower back and excess pressure on the buttocks or the lower thigh area.

### *3.2.6. Wheelchair Casters*

Caster wheels are important components of the system, influencing the system's stability, rolling resistance, maneuver ability and users' comfort. The casters are usually located at the front of the wheelchair, but on wheelchairs where the drive wheels are in the centre or front of the wheelchair, the casters are usually located at the rear of the wheelchair. The tires on the casters can be a huge factor on how easily the wheelchair will roll over all terrain. Similar to the rear wheels, pneumatic and solid caster wheels are commercially available. Although pneumatic wheels have been shown to reduce rolling resistance, they do require extra attention regarding pressure control and maintenance. Therefore, solid casters are still the most commonly used type of caster in manual wheelchairs. Generally the harder the caster tire, the easier the wheelchair will roll and turn corners. The softer the caster tire, the harder it will be to propel the wheelchair and the harder it will be to turn the wheelchair.

Caster wheels and stem assembly can influence a wheelchair in motion in many aspects. First, the diameter of the caster wheels affects rolling resistance: smaller wheels increase rolling resistance, thus requiring the user to push harder to maintain an average velocity. The position of the caster assembly in the wheelchair geometry is also an important aspect of wheelchair mechanics. The shorter the distance between the rear wheel and caster, the lower the rolling resistance due to the increased weight upon the rear wheels, (Boninger et al. 2006). Furthermore, more mass is located near the centre of the system and, therefore, rotational inertia is reduced, making turning maneuvers easier. However, this requires reduced wheelchair length, which may have an impact on system stability.

Finally, the transmission of shock and vibration is an important aspect of the casters' size and composition. Smaller casters with solid tires have limited shock and vibration absorption and, therefore, the user's comfort is affected. In an effort to reduce vibration and improve user's comfort, damping materials may be used inside the casters' stem. Similarly, the use of suspension in the casters' assembly is an efficient way of reducing vibration transmission to the user, (Cooper et al. 2003).

### *3.2.7. Wheelchair Rear Wheel*

Design of the rear wheels plays an important role in the system's mass and vibration transmission. The rear wheel should be in a position that allows the user to have the best push stroke as possible and keeps the user safely balanced according to his or her skill level and ability. The rear wheel spokes are responsible for keeping the wheelchair wheel in a round position through connecting the wheel rim and tire at the axle. The wheel hub is the centre of the wheel where the spokes are connected to. The wheel hub also contains the axel of the wheel. The axle plate is located next to the wheelchair hub on either side of the chair. The axle plate connects the wheel to the frame, it is adjustable that permits the wheelbase to be extended to increase the chair stability or shortened to increase the user mobility.

From a mechanical standpoint, heavier wheels make it harder to start moving from a standing position; lighter wheels allow users to accelerate faster. Furthermore, because the rear wheels are located on the outer side of the chair, the mass greatly influences the rotational inertia of the system. Traditionally, rear wheels have been produced in either plastic or steel. More recently, carbon fibre has been used to produce lighter wheels. In addition to weight reduction, carbon fibre wheels minimize the transmission of vibration to the user's body, (Boninger et al. 2006), which is highly beneficial since vibration may cause discomfort, nausea, dizziness and fatigue.

The ***anterior–posterior position*** of the rear wheels influences two important aspects of wheelchair mobility: stability and manual propulsion. While positioning the wheels rearward improves stability, it limits the user's ability to reach the hand rims in this rearward position, thus reducing the push angle. Alternatively, moving the wheels forward improves propulsion biomechanics but reduces stability. The optimal position of the rear wheels is a client-dependent decision, based on the user's perception of stability and ease of chair propulsion. However, there are some objective guidelines to support this decision. The rear wheels should be positioned in the most forward position that does not compromise system stability. Gorce et al. 2012 showed that, when moving the rear wheels forward, push angle and shoulder ROM are increased, thus reducing both push frequency and handrim forces, minimizing the risk of upper limb injuries, (Knootz et al. 2005). In addition to the biomechanical benefits, moving the rear wheels forward diminishes the wheelchair

length and, as a result, facilitates turning maneuvers by reducing the rotational inertia of the system.

### *3.2.8. Wheelchair Tires*

Wheelchair tires provide friction between the chair and the ground. When selecting rear wheel tires, two options are available: pneumatic and solid tires. Pneumatic tires provide good impact and vibration absorption, thus improving users' comfort. Solid tires, however, are still commonly used because they are almost maintenance free, and pose no risk of being flat or emptying due to punctures they won't likely wear out in the life of the wheelchair. Solid tires are most suitable for wheelchairs that are expected to stay indoors most of the time such as nursing home use. Pneumatic tires have been shown to significantly reduce rolling resistance compared to solid tires (Kwarciak et al. 2009), and this facilitates manual propulsion by keeping the wheels rolling for a longer distance until another push is need, thus contributing to mobility efficiency. The disadvantage of pneumatic tires is they will go flat if punctured and they will go soft even without any damage eventually that makes the wheelchair hard to push and causes excessive wear on the tires. An important aspect of the tire type affecting wheelchair mobility is the force opposing the movement of the tire rolling on a surface. This force, known as rolling resistance, is dependent on the tire design, material composition, mass of the tires, and interactions with the surface. Generally the harder the tire, the easier the wheelchair will roll and turn corners. The softer the tire, the harder it will be to propel the wheelchair.

### *3.2.9. Wheelchair Handrims*

Wheelchair hand rim is the interface through which the user drives manual wheelchairs by pushing or pulling their hands. The handrims which are sometimes known as pushrims, play an important role in terms of both the comfort and efficiency of manual propulsion. In the majority of manual wheelchairs, the handrims are two metallic round tubes located on the outer side of the wheels. The small size of conventional handrims leads to two main problems: increased pressure on the areas of the hands' surface where contact with the handrim occurs; and reduced mechanical efficiency due to inability to hold the handrim with the entire

hand, which requires additional muscle contraction to stabilize the hands on the rim, (van der Woude et al. 2003). Not surprisingly, many wheelchair users hold the handrim and tire simultaneously when propelling the wheelchair.

Previous studies have proposed different handrim designs in order to optimize propulsion comfort and efficiency. Veeger et al. (1996) found that handrims with a greater tube diameter showed greater efficiency and lower physiological costs. Richter et al. (2006) found reduced finger and wrist flexor activity during manual propulsion with the use of a flexible handrim, a metallic tube connected to the wheels through a flexible rubber membrane that reduces peak forces during initial contact.

### *3.2.10. Wheelchair Wheel Locks*

Contrary to popular belief, wheel locks on wheelchairs are not brakes. Brakes would be used to slow down and stop a wheelchair but that is not the purpose of wheel locks. Wheel locks are more like parking brakes; designed to permit the wheels to be locked in place, which prevents any unwanted movement when waiting or transferring in and out of the wheelchair. They can be positioned in many different locations depending on what they are used for. All locks extend from the frame to the wheels and always use some form of manual mechanical locking or lever system.

***Push/Pull to Lock*** brakes are the industry standard on most wheelchairs. They come in either a push to lock version, meaning the user pushes to lock the wheels, or pull to lock, meaning the user pulls to lock the wheels. These wheel locks are located on the top side frame rail in front of each rear wheel.***Scissor lock*** brakes are chosen on the sportier wheelchairs for very active users. These wheel locks are mounted on the top rail of the side frame of the wheelchair however when not in use are completely under the seat. Very active users who propel their wheelchairs quickly have been known to hurt their hands on the push/pull to lock wheel locks because of their close proximity to the wheels. These scissor locks solve this issue by being well out of the way when the wheelchair is being propelled.***Foot lock*** wheel locks are only available on tilt wheelchairs with non-folding frames. Foot locks are not accessible to the wheelchair user and for the use of the caregiver.

They are mounted below the back of the seat on the lower side rail bars and each brake is connected to a centre brake lever that most people use their foot on.

### *3.2.11. Rear Wheel Cambers*

Stability is enhanced with wheel camber, especially when moving over lateral slopes. Therefore, majority of sports wheelchairs are equipped with cambered rear wheels. In addition, the hands are better protected against trauma because the wheels touch the floor spanning a wider area than the hands have in contact with the handrims. Maneuver ability is also enhanced by wheel camber, which facilitates turning maneuvers.

Previous studies have investigated the effects of wheel camber on propulsion biomechanics. Camber angles wider than (15°) increase the elbow ROM, reduce wrist radial deviation and increase wrist ulnar deviation. The changes in wrist kinematics are a consequence of the contact and release positions of the hand rim happening in a more forward position. Camber angles ranging from (0°) to (9°) have been shown not to affect the cardiopulmonary parameters of manual propulsion. Rolling resistance is reduced by cambers up to (9°), compared to wheels with no camber, (Veeger et al. 1989). Perdios et al. (2007) indicate that (6°) is the optimal angle for rear wheel camber, in terms of lateral stability in inclined planes, comfort during hand rim propulsion, maneuver ability and the general preferences of manual wheelchair users. However, rear wheel camber increases the system's overall width, which may lead to problems when moving in tight spaces.

## 3.3 Mechanics of Manual Wheelchair Propulsion

To efficiently propel a manual wheelchair, the shoulder should be in vertical alignment with (or slightly in front of) the axle of the wheel (Schmeler et al. 1999). When the axle is in the correct position and the upper body is in balance, users reach as far back as possible on the rim of the wheelchair and initiate a propulsion stoke that typically has two parts (flexion and extension) rather than just one.Wheelchair propulsion includes the actual push as well as a recovery phase. The push phase (PP) is a closed chain event, during which the hand is in contact with the rim and it consists of pull and push segments, see Figure (3.4). It begins with when the hands

contacting the top of the rim or at a point just behind the top and ends when the hands leave the rim, usually when the arms are extended. The contact involves grasping the rim just behind the top dead centre (TDC) then stronger muscles (e.g. biceps) can be recruited to create forward propulsion. If hand placement is far behind the TDC then there is danger of damaging the joint capsule of the shoulder through the effects of the combined movement of internal rotation and shoulder extension. During the push phase, the hand centre has passed the TDC and it should be vertically aligned with the shoulder to place the hand in an optimal position for exerting forward force on the wheelchair push-rims, (Moon et al. 2013).

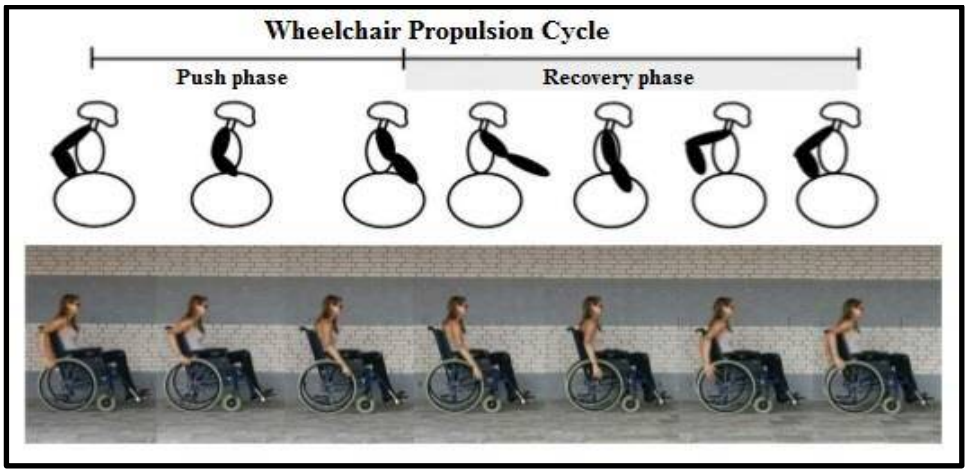


**Figure (3.4)**: The propulsion cycle, which is divided into the push and the recovery phases, (Moon et al. 2013).

The recovery phase (RP) is an open chain event during which no force is exerted on the push-rim. It begins as the hands go further down the rim to complete the stroke with maximum efficiency, and requires lifting the hands off the wheel and counter-balancing the inertia of the arms. The RP continues with the hands swinging back past the line of the shoulders leaving them adjacent to the rim, and ends with the humerus at its most posterior position, (Moon et al. 2013).

### *3.3.1. Methods for Measuring Wheelchair Propulsion*

Given the above, wheelchair propulsion is accomplished by the bilateral, simultaneous, repetitive motion of the upper extremities. Over the last decade, researchers have demonstrated that the biomechanics of wheelchair propulsion varies in relation to the subjects' levels of spinal cord injuries (SCI) (Kulig et al. 2001).

The methods used in these studies for measuring wheelchair propulsion ability included the determination of biomechanical characteristics, such as upper-limb kinematics and push-rim force application. First, the test environment determined the test apparatus chosen. While measuring wheelchair propulsion in an actual outdoor environment was considered ideal, simulation in a laboratory was preferred because body movement could be better controlled and more accurately assessed. Therefore, stationary wheelchair ergometers and dynamometer systems were widely used to study propulsion abilities of wheelchair users, see Figure (3.5), (Finley et al. 2004).

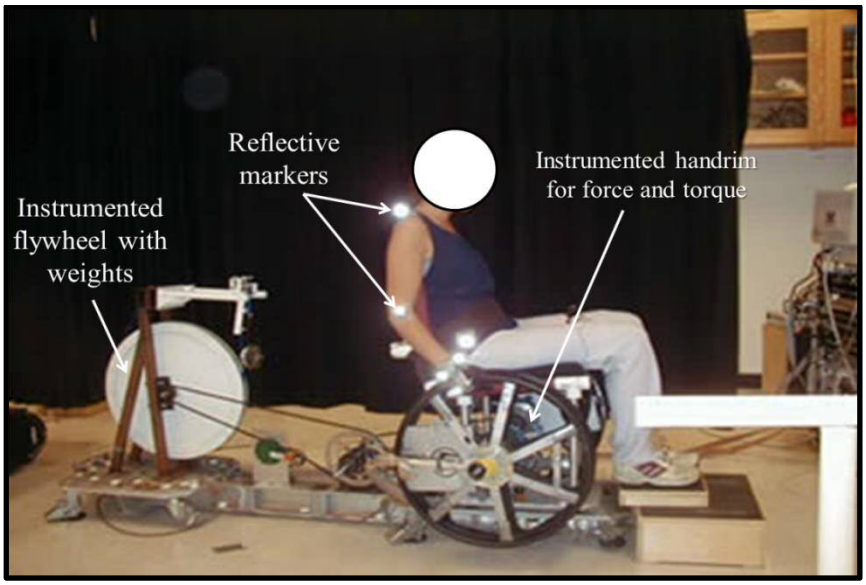


**Figure (3.5)**: Instrumented wheelchair ergometer and 3D motion analysis system used for test setup, (Finley et al. 2004).

Furthermore, researchers investigated different wheel-based measurement systems, which allowed for the collection of propulsion kinetics and wheelchair kinematics. Newsam et al. (1999) introduced the strain gauge force transducer for determining forces and torque applied to the push rim to identify the start and end of hand and push rim contact. Cooper et al. (2009) described the Smart$^{Wheel}$, a commercial force- and torque- sensing push-rim wheel that has been used in several studies to examine three-dimensional (3D) propulsion forces, moments, and temporal characteristics over different surfaces and inclines. The Smart$^{Wheel}$contains an onboard optical encoder that determines the rotational angle of the wheel, which can determine average velocities, distances travelled per stroke.

The major advantage of an instrumented wheel will be the analysis of daily activities and wheelchair-related tasks that cannot be met with stationary ergometry technology. However, Smart$^{Wheel}$is heavier than a traditional wheelchair wheel and requires the user to push on the rim, see Figure (3.5), (Cooper 2009).

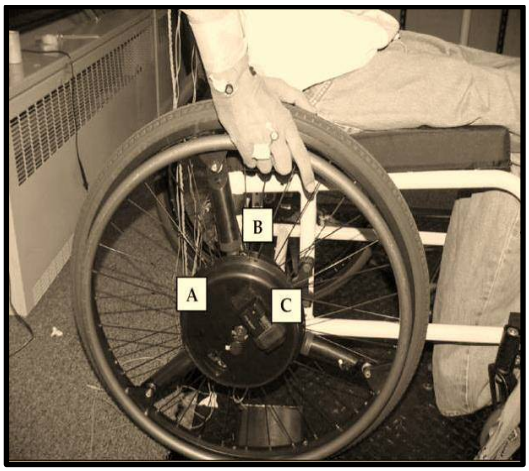


**Figure (3.6)**: The Smart$^{Wheel}$ device for recording kinetic wheelchair propulsion data. (A) Hub with cap enclosing all the electronics. (B) Sleeve to cover the strain gauge bridges. (C) Battery in its receiver. (Copper 2009).

The Smart$^{Wheel}$measures three-dimensional forces (tangential, radial, and axial) and moments applied to the pushrim. Its design is based on equations for a 3-beam (120° apart) system for pushrim force and moments detection utilizing strain gages. The output of the Smart$^{Wheel}$ consists of forces and moments in three dimensions determined by a frame coordinate system.These forces $F_x$, $F_y$, $F_z$ and associated moments $M_x$, $M_y$, $M_z$ are depicted in Figure (3.7), (Boninger et al. 1997).

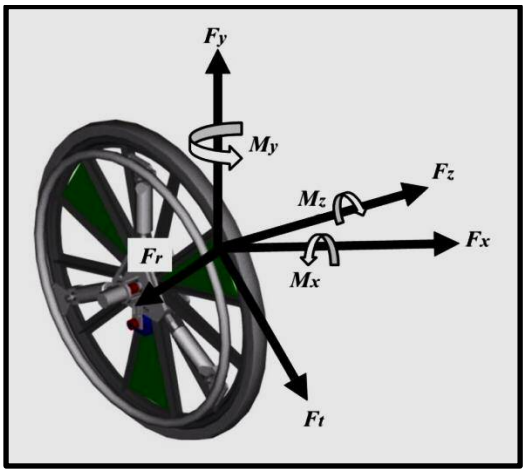


**Figure (3.7):** Orientation of force and moments. The orientation of pushrim forces and hub moments are shown. The direction of the arrows indicates the directions of the forces and

moments applied by the subject. $F_t$ and $F_r$ were calculated from $F_x$ and $F_y$ and used in the analysis (Boninger et al., 1997).

Finally, video cameras were employed for capturing the upper body motions during the test process and a 3D capturing system was generally used for generating better arcs. The development of biomechanical model is also essential. To clarify how the body segments, which includes shoulder, elbow, wrist and trunk, interact mechanically to execute motor tasks, mathematical models have been applied and updated initially from the sagittal plane in two dimensional (2D) to three dimensional (3D) kinematic analyses.

### *3.3.2. Predicting Wheelchair Propulsion Forces*

Apart from using sensors, such as strain gauge force transducers and the Smart$^{Wheel}$discussed above, wheelchair propulsion forces also can be predicted by theassumption of propelling a wheelchair with constant velocity on a slope. Theimportant quantities in measuring wheelchair propulsion ability are listed below,which include wheelchair mass properties, kinematics, resistance forces, wheelchair energies and propulsion efficiency.

#### *3.3.2.1. Wheelchair mass properties*

Figure (3.8) shows the mass properties for the wheelchair, with the vertical ground forces written in the form:

—— …… (**3.1**)

—— …… (**3.2**)

Where $R_F$ and $R_R$ are the vertical reaction forces at the front and rear wheels respectively (in N),

$m$ is the mass of the wheelchair and the user (in kg),

$g$ is the gravitational acceleration = 9.81 m/s$^2$,

$I$ is the mass moment of inertia (in kg m$^2$),

$F_N$ is the normal wheel force at ground (in N).

$l_1$ and $l_2$ are length in horizontal direction from the rear and front wheel centres to the system centre of gravity (in m) and

$\hat{l}_1$ and $\hat{l}_2$ are length in the ‘x’ direction from the rear and front wheel centres to the system centre of gravity (in m).

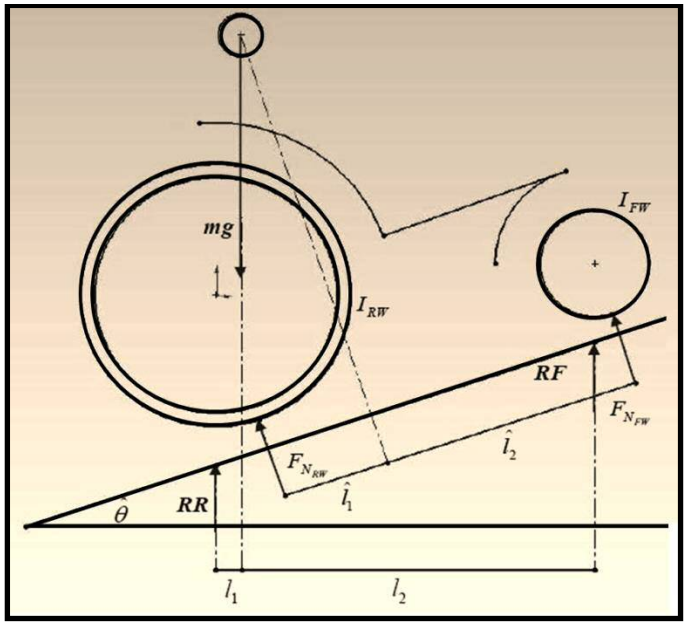


**Figure (3.8):** Mass properties for the wheelchair.

*3.3.2.2. Wheelchair kinematics*

The linear wheelchair displacement, velocity and acceleration are defined as $x$, and respectively. Wheelchair kinematics can also be described in terms of angular wheel displacement, velocity and acceleration as listed below:

$x = \theta r$ ..... **(3.3)**

$= \boldsymbol{r}$ ..... **(3.4)**

$= r$ ..... **(3.5)**

where $x$ is the linear wheelchair displacement (in m),

is the linear wheelchair velocity (in m/s),

is the linear wheelchair acceleration (in m/s$^2$),

$\theta$ is the angular wheelchair displacement (in rad),

is the angular wheelchair velocity (in rad/s),

is the angular wheelchair acceleration (in rad/s$^2$) and

$r$ is the wheel radius (in m).

*3.3.2.3. Wheelchair resistance forces*

In order to sustain a constant velocity, the wheelchair user must overcome resistance forces associated with tire contact losses, aerodynamic drag and mechanical losses. Tire contact forces are caused by surface/tire deformation, and

result in resistive force acting in the opposite direction to the applied wheel torque. Resistance due to tyre deformation is shown schematically in Figure (3.9).

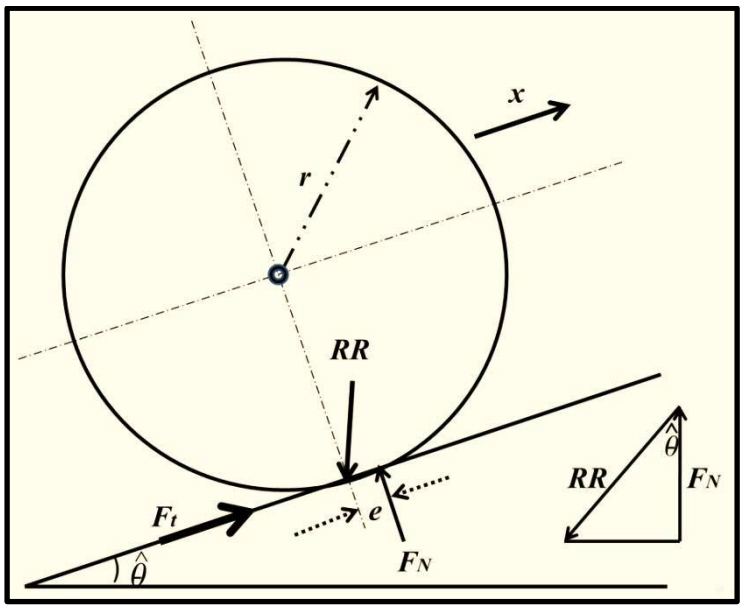


**Figure (3.9):** Schematic of wheelchair resistance due to the tire deformation.

The total resistance due to tire deformation will be the sum of the resistance from all four wheels, namely: $F_{NRW} = R_R\ Cos$ ——+ $R_F\ Cos$ ——…… (**3.6**)

Aerodynamic drag will be calculated as: $F_D =$ ——……...…… (**3.7**)

where $e$ is the distance from the wheel centre line (normal to ground) to the applied normal ground force $F_N$ (in m),

is the density of Air = 1.23 kg/m$^3$,

$F_t$ is the tractive force (in N),

$F_D$ is the aerodynamic force (in N),

$A$ is the frontal wheelchair area including the user (in m$^2$) and

$F_W$ and $R_W$ refer to the front wheel and rear wheel respectively.

*3.3.2.4. Force patterns and propulsion efficiency*

Considering the figure (3.10), to relate the forces to the rear wheel of the wheelchair, $F_x$ and $F_z$ forces are rotated in such a way that they can be measured as a force tangential to the pushrim, ($F_t$), and a force radial to the pushrim, ($F_r$). The tangential force component ($F_t$) is the only force that contributes to the forward motion of the wheel. The radial force component ($F_r$) and the axial force component ($F_z$) create the friction necessary to allow ($F_t$) to be applied.

The resultant force ($F_{tot}$), which is the total force applied to the hand rim, is mathematically calculated by taking the vector sum of the three force components ($F_x$), ($F_y$) and ($F_z$). Using hand position data from video recordings and the ($F_x$), ($F_y$) and ($F_z$) applied on the hand rim, the effective force ($F_{eff}$) can be calculated, according to:

$$F_{eff} = F_x Cos\alpha + F_y Sin\,\alpha\, Sin\,\beta + F_z Sin\,\alpha Cos\beta \quad \textbf{(3.8)}$$

where α is the angle between the line from the hand marker through the wheel axle, relative to the vertical line through the wheel axle, and β is the wheel camber angle.

Veeger et al. (2002) introduced a parameter termed 'fraction of the effective force' (FEF) as a measure for the effectiveness of force application. FEF is the ratio of the effective propulsion moment measured at the wheel hub ($M_{hub}$) to the resultant force: $FEF = M_{hub}\, r^{-1}\, F_{tot}\, -1 * 100\%$ **(3.9)**

where *r* is the radius of the rear wheel (in m).

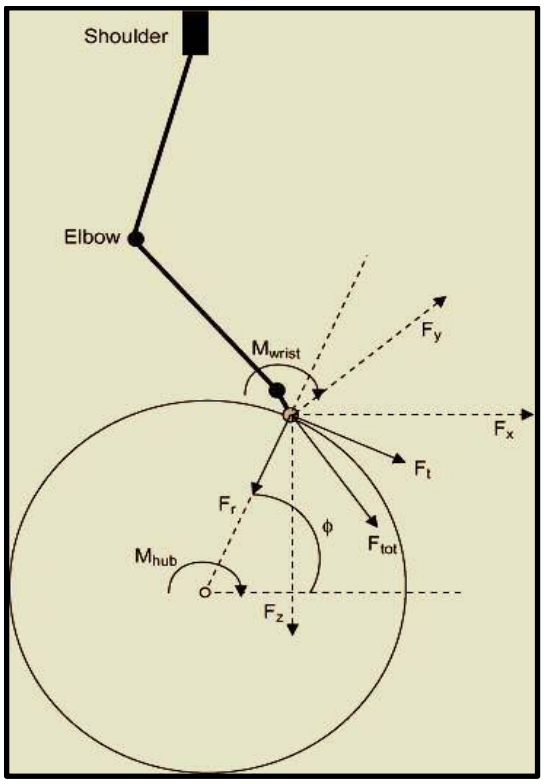


**Figure (3.10)**: Definition of forces (in N) in wheelchair propulsion. $F_r$= radial component of $F_{tot}$; $F_t$= tangential component of $F_{tot}$; $F_{tot}$= total force; $F_x$, $F_y$, $F_z$= global reference frame; $F_x$, $F_y$ and $F_z$ are defined as directed horizontally forwards, horizontally outwards and vertically downwards, respectively, in a right-hand coordinate system. $M_{wrist}$= wrist torque (in Nm); $M_{hub}$= hub torque (Nm); φ = point of force application referenced with respect to the horizontal (°), (Vanlandewijck et al. 2001).

A comparable, although slightly different, measure of effectiveness of force application was introduced by Boninger et al. (1999). The mechanical effective force (MEF) is the percentage of the resultant force leading to forward motion:

$MEF = F_t^2 / F_{tot}^2 * 100\%$…… (**3.10**)

Besides a propulsive force, the hands can also apply a torque on the hand rims. If only a force was applied by the hands to the rims, the tangential component of that force ($F_{eff}$) would equal the torque divided by the wheel radius. The difference between both equals the hand moment ($M_{hand}$). According to Cooper et al. (1997), $M_{hand}$ can be estimated by assuming that the point of force application (PFA) coincides with a metacarpophalangeal joint (MP) or the calculated PFA based on the three-dimensional moments: $Tan \quad = M_x / M_z$…… (**3.11**)

Where$M_x$ and $M_z$ are moments (in N.m) generated by the hand, around the x- and z-axis of the coordinate system, respectively.

A simplified approach to understand the propulsive force applied by the user during manually propelling the wheelchair is presented. A marker-based on motion analysis was used to record the trajectories of retro-reflective markers where placed on the wheelchair wheels, see Figure (3.11). More detailed description about will be presented in Chapter Six.An integrated feature in the used software (Qualisys Track Manager QTM Software, Qualisys, Sweden) was used applied to estimate the velocity and acceleration during the propulsion cycles.


**Figure (3.11):** Retro-reflective markers placement on the wheel.

Considering the below schematic figure (3.12), applying Newton's second law, the equation of motion for the manual wheelchair can be written in the following form:

$F_p = m\,a$ ..... (**3.12**)

Assuming the resistive forces such as the rolling friction and aerodynamic drag are negligible. Using Newton's second law to relate the force $F_p$ to the angular acceleration $\alpha$:

$F_p = m\,a = m\,r\,\alpha$ ..... (**3.13**)

where m is the mass (in kg),

$a$ is the linear acceleration (in m/sec$^2$),

$\alpha$ is the angular acceleration (in rad/sec$^2$),

$F_p$ is the propulsion force (in N) that is created by the user's action, namely a force applied to the wheelchair push rim, and

$r$ is the wheel radius (in m).

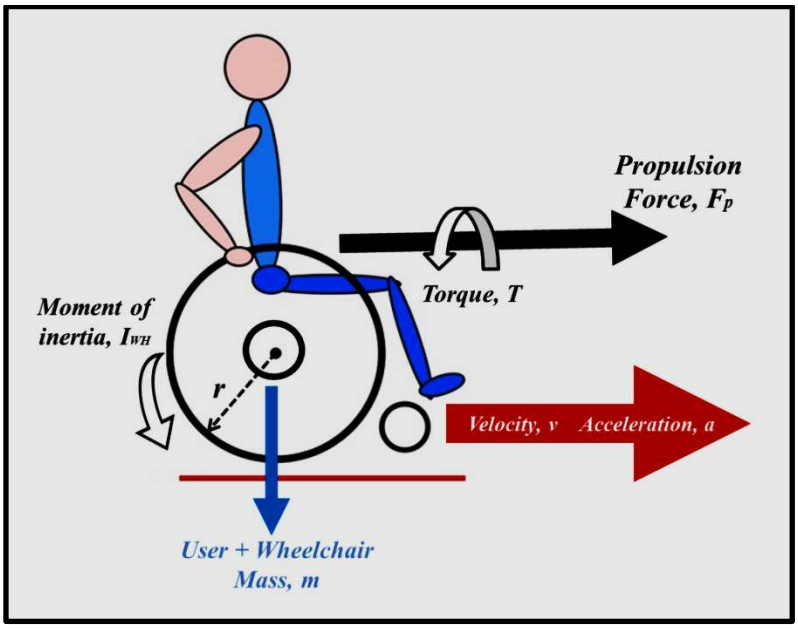


**Figure (3.12):** Simplified description of the wheelchair propulsive force.

Due to this propulsion force, the torque about the wheel axle has been applied to move the wheelchair. This torque can be calculated as follows:

$Torque\ (T) = F_p\,r$ ..... (**3.14**)

When a torque is applied to an object it begins to rotate with acceleration inversely proportional to its moment of inertia. This relation can be thought of as Newton's second law for rotation. The moment of inertia is the rotational mass and the torque is rotational force. Therefore, the torque (*T*) applied by the hand to the wheel can be calculated in terms of moment of inertia as follows:

*Torque (T) = I α = I* **–**…….…….. (**3.15**)

Angular motion obeys Newton's first law.If no outside forces act on an object, an object in motion remains in motion and an object at rest remains at rest.

The wheelchair is a combination of wheels and rigid bodies maintained at fixed orientations to each other. The wheel is considered as a solid disk of given radius, constant density, and mass, which locates the centre of mass at the hub. A solid, uniform disk has moment of inertia (about an axis through its centre and perpendicular to the disk) equal to half the product of the radius squared and the mass.Therefore, the moment of inertia (*I*) of the wheel can be calculated as follows:

$I = \mathbf{-}\, m\, r^2$ ..... (**3.16**)

The wheelchair used per this study was a traditional manual self-propelled device manufactured by Invacare Action$^2{}_{NG}$ and has the following specification;

Rear Wheel diameter = 610 mm

Handrim diameter = 520 mm

Overall wheelchair mass = 16.4 kg

Both wheels mass = 8.7 kg

By applying the equations (3.15) and (3.16) then substituting in equation (3.14), the propulsive force will be evaluated in terms of time as illustrated in Figure (3.13). An average force was presented for fifteen healthy volunteers (two left-arm dominant, mean age 32.13 ± 9.17 years, height 178.14 ± 6.74 cm, mass 89.1 ± 16.17 kg and body mass index 28.17 ± 5.54) who performed five strokes of manual propulsion cycle. Both starting up and stopping strokes were excluded from the analysis.

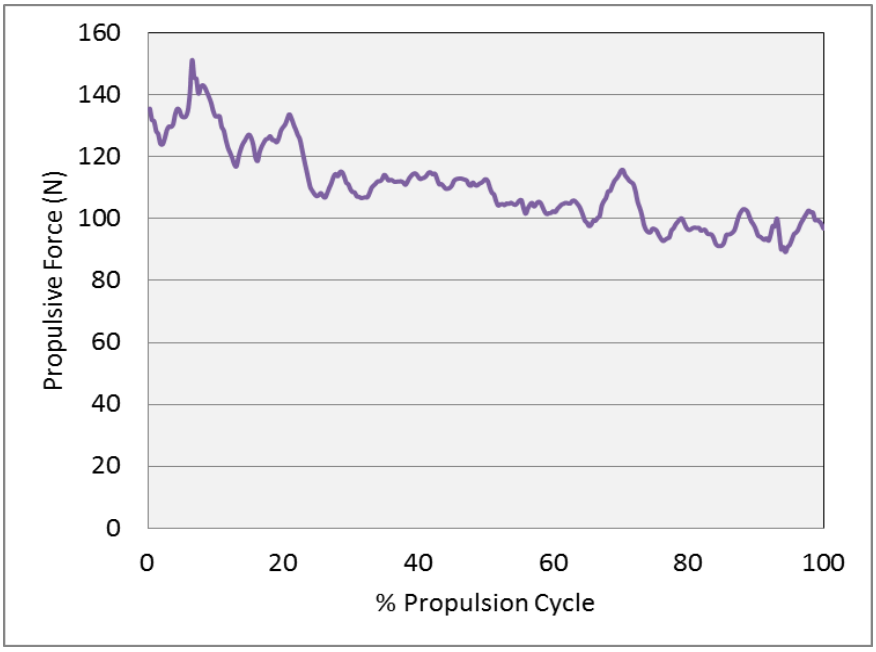


**Figure (3.13)**: Average propulsive force during five strokes of manual wheelchair propulsion.

It was observed that the propulsive force and wheel rotation speed are kinematically linked, and this ratio remains true whenever the chair moves straight. While starting the propulsion cycle, the trunk and upper limbs musculature apply effort to propel the wheel forward so that the upper body segments are moved forward quickly. Positive acceleration was obtained by the applied propulsive forces on the wheels overcoming the resistive ones. The wheelchair propulsive force exerts with the push on the handrim, generating motion (i.e. the applied force by the ground in the wheel). When the mass gets accelerated, it produces an inertial force. During terminal propulsion, the upper body segments are decelerated (for preparation of repositioning the hand) by eccentric muscle activity during the recovery phase, even though the segments are still moving downward and forward.

*3.3.2.5. Wheelchair energy calculations*

Expressions for components of the system's total mechanical energy, including the potential energy and kinetic energy of the wheelchair, are given in this section. The energy acquired through a change in configuration of the body and is called the *Potential Energy ($E_p$)* and it can be calculated as follows:

$E_p = m\ g\ h$ ……...……...…… (**3.17**)

where h is the vertical displacement of the body, and g is gravitational force.

As the subject is seated in the wheelchair, wheel motion is affected by the mass of the entire user/chair system. It is assumed that the mass, $m_{syst}$, is consisting of the user body mass and plus the chair mass. This mass is equally distributed at the two hubs. In two dimensions, the wheel is a circular lamina with a given radius. Each wheel's centre of mass is located at the centre of its circle (its hub). Therefore, the masses involved in computing the mechanical potential energy of one side of the wheelchair are actually the mass of one wheel and half $m_{syst.}$ Where is located at each wheel hub. Then the computed potential energy will equal the product of the sum of half *m-rest* and the mass of one wheel, the gravitational constant (9.81 m/s$^2$), and the wheel's hub height from the floor. Therefore, the wheel's potential energy can be computed as follows:

$E_p$ = – ……...…… (**3.18**)

The kinetic energy ($E_{k)}$ can be defined as the energy possessed by a body in motion. The wheel can move in only one direction, namely it rotates about the wheel axle. Computation of the wheel's kinetic energy requires the moment of inertia and the angular velocity of the wheel about its axle.

To determine this angular velocity, the velocity of the marker on the wheel was first evaluated by using the motion analysis software (Qualisys Track Manager QTM Software, Qualisys, Sweden) to record the trajectories of retro-reflective markers where placed on the wheelchair wheelsduring the propulsion cycles. The angular velocity of the wheel, $\omega_{wh,}$ was determined by calculating the quotient of the hub marker's velocity and the distance from the hub to the marker, as indicated in

$_{wh}(t)$ =——— ……..…… (**3.19**)

A solid, uniform disk has moment of inertia (about an axis through its centre and perpendicular to the disk) equal to half the product of the radius squared and the mass. Therefore, the wheelchair's kinetic energy, at time *t,* can be determined as one-half the moment of inertia times the angular velocity squared.

$E_k(t)$ = – – ———} – ……..…… (**3.20**)

where $m_{wh}$ is the mass of one wheel (in kg),

$v_{wh}$ is the wheel's velocity (in m/sec),

and $I$ is the wheel's moment of inertia (in kg.m$^2$).

For the wheelchair used per this study was a traditional manual self-propelled device manufactured by Invacare Action$^{2}_{NG}$ and has the following specification;
Wheel's hub height from the floor = 290 mm
Rear Wheel diameter = 610 mm
Overall wheelchair mass = 16.4 kg
Both wheels mass = 8.7 kg

Figures (3.15) and (3.16) indicate the average potential and kinetic energies results, respectively, of an analysis of five strokes of manual propulsion cycle performed by the same fifteen healthy volunteers. A highly correlated relationship was observed between the wheelchair's potential energy and the users' body mass.

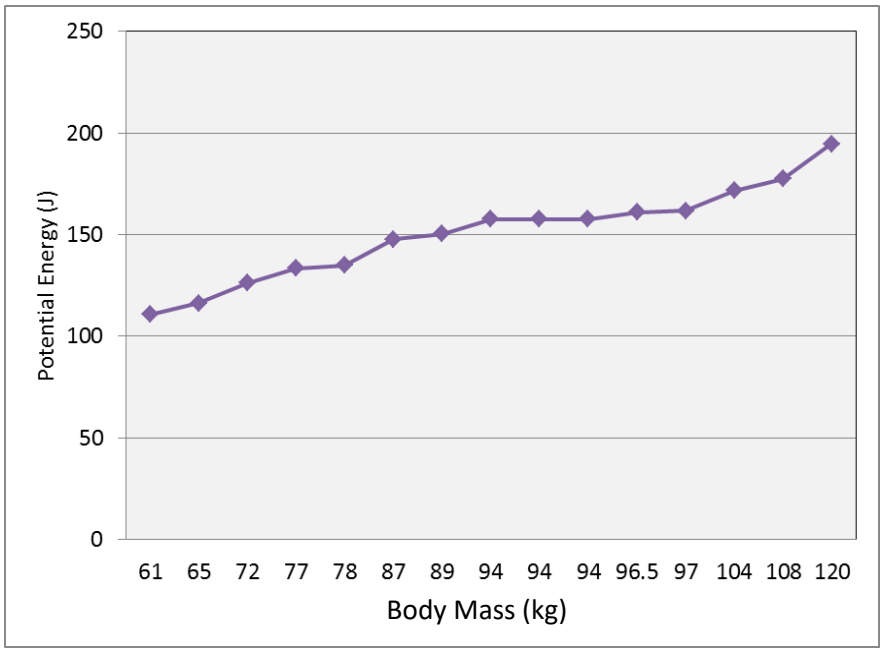


**Figure (3.14)**: Wheelchair average potential energy versus users body mass during five strokes of manual propulsion.

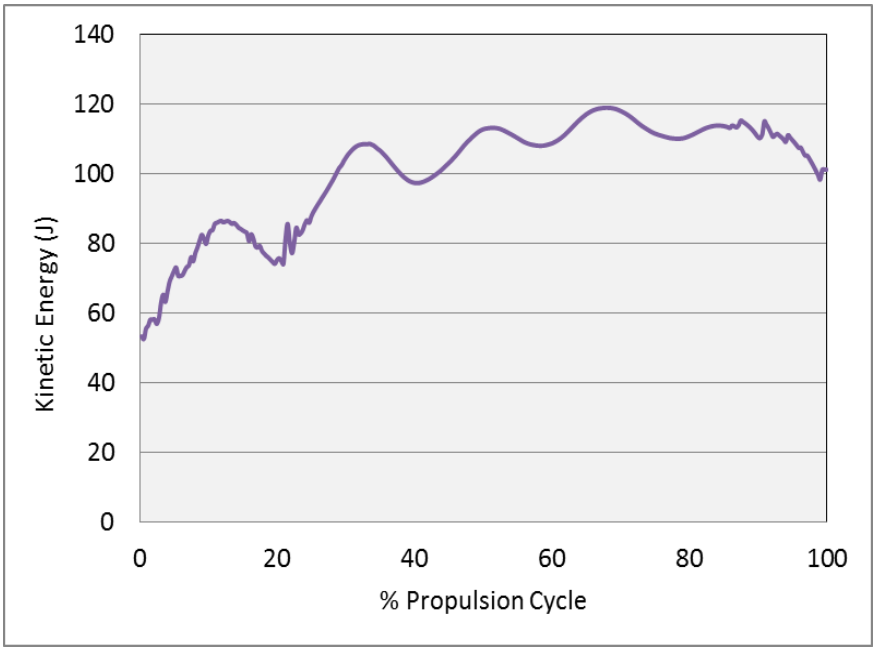


**Figure (3.15)**: Wheelchair average kinetic energy during five strokes of manual propulsion.

## 3.4 Summary

This chapter aimed to present an overview background of manual wheelchair. It provided a detailed illustration of the anatomy and biomechanics of manual wheelchair that began with an overview of the types of manual wheelchair and briefly described its features and components and identified the function of each component. The following aspects focused on the mechanics of manual wheelchair propulsion and the methods used to predict the applied forces pattern and propulsion efficiency. It also presented a simplified approach to calculate the potential and kinetic energy during manual wheelchair propulsion.

While performing the pushing phase of propulsion cycle, the trunk and upper limbs musculature apply effort to propel the wheel forward so that the upper body segments are moved forward quickly. Therefore, the total mechanical energy during this phase increased, primarily due to increases in kinetic energy. Due to the movement constraint that the hand must follow the contour of the handrim during propulsion, the upper body segments have to move downward, causing the potential energy to decrease. During the recovery phase, the segments have to be repositioned on the handrim for the next propulsion cycle. The segments move backward and upward slowly so the restoration of the total mechanical energy is mainly from potential energy. The mechanical energy pattern showed a complementary trend

during most of the propulsion cycle, i.e. when kinetic energy increased, potential energy decreased over time. This complementary trend was not demonstrated in terminal propulsion phase, however, because the potential and kinetic energy decreased simultaneously. During terminal propulsion, the upper body segments are decelerated (for preparation of repositioning the hand) by eccentric muscle activity during the recovery phase, even though the segments are still moving downward and forward. This may be a potential explanation for the inefficiency of handrim wheelchair propulsion.

# Chapter 4

## Three-dimensional Kinematics of the Upper Body

The position of a rigid body in a three-dimensional space is defined by the location of a point on that body and the body's orientation. The human body can be viewed as a series of rigid finks connected by joints. Human body parts are not actually rigid structures, but they are assumed to be so to facilitate studies of human motion. Accordingly, human body position can be defined by its location, orientation, and joint configuration, (Zatsiorski 1998).

This chapter describes the design concept used to process the three-dimensional kinematics of the trunk and upper limb in terms of joints and segments chosen for analysis on the basis of International Society of Biomechanics (ISB) recommendations and establishing joint coordinate systems and segment rotation sequences. Adopting this concept will lead to computethe 3D kinematics of each joint during different activities.

### 4.1 Defining Body Location and Orientation

The location of a body in space is described by using a coordinate method. Various coordinate systems can be used, such as Cartesian, oblique, spherical or cylindrical, with the Cartesian coordinate system (three orthogonal axes) being the most commonly used.

A coordinate method description to define body location is performed in three steps:

1. A Global Coordinate System (GCS) is defined.
2. A point P in the body is specified. It is convenient to choose the origin of the Local Coordinate System (LCS).
3. The location of this point in the GCS is specified.

The global coordinate system is by convention described as a right handed orthogonal triad. Usually the positive X-axis is horizontal and forward, the positive Y-axis vertical and upward, and the positive Z-axis horizontal and to the right. This can cause complications when examining the left and right extremities, as adduction of the right arm is in a positive direction, while adduction of the left arm is in a

negative direction. To avoid this complication, a "forward, outward, upward" system is recommended, which can be designated as left or right handed.

Three steps are performed to describe body orientation:

1. Define the GCS.
2. Attach a LCS to the body.
3. Determine the orientation of the LCS relative to the GCS.

### *4.1.1. Defining a Local Coordinate System in a Rigid Body*

A body is considered rigid or solid if the distance between any two points within the body does not change. True rigid bodies are a mathematical abstraction and do not occur in nature. However, it can be a very useful assumption to model something as a rigid body, i.e. a bone.

To fix an orthogonal local coordinate system to a rigid body, the coordinates of three non-collinear points within the body must be known, see Figure (4.1). The following procedure can be carried out to fix the reference frame:

1. The cross product of vectors $r_1$ and $r_2$defines the vector $r_3$, ($r_1 \times r_2 = r_3$).
2. The cross product of vectors $r_3$ and $r_1$ defines the vector $r_4$, ($r_3 \times r_1 = r_4$).
3. Each vector is divided by its own length to determine the unit vectors. The unit vectors of $r_1$ (—), $r_4$ (—), and $r_3$ (—) correspond to the x, y, and z axes of the orthogonal LCS.

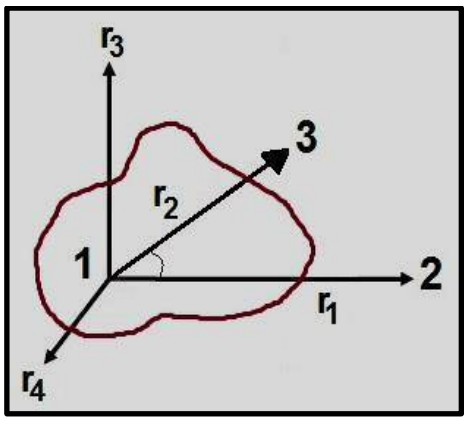


**Figure (4.1)**: Within a rigid body of arbitrary dimensions, three points 1, 2, and 3 are known. Vectors $r_1$ and $r_2$are from point 1 to points 2 and 3 respectively. Vectors $r_3$and $r_4$are then determined as cross products, $r_1$ corresponds to the x-axis of the LCS, $r_3$to the y-axis, and $r_4$to the z-axis.

The LCS is thus defined by the three mutually orthogonal unit vectors. The orientation of the LCS relative to the GCS describes the orientation of the body in the global reference system, (Zatsiorski 1998).

## 4.2 Defining Body Position and Displacement

The orientation of a moving reference system, fixed within a body, relative to a global reference system can be determined by two methods; the Matrix Method and Euler's Method.

### *4.2.1. The Matrix Method*

Using the *Matrix Method*, both the translation and rotation of a LCS with respect to the global system can be defined. Correspondingly, the translation and rotation of a LCS relative to a different LCS in another rigid body can be calculated in the same manner.

Taking O-XYZ and o-xyz as the GCS and LCS respectively, then $L_G$ is the vector giving the origin of the LCS in the GCS, otherwise known as the 'location vector', see Figure (4.2). $L_G$ also defines the translation from point O to point o.

Each unit vector (x, y, z) of the LCS is represented by its components in the GCS. By dividing each component by the length of the vector (which is l, as it is a unit vector), the cosine of the angle that the vector makes with each of the axes of the GCS is determined. These angles are referred to as the 'direction angles' and the cosines are called the 'direction cosines'. The matrix of direction cosines, also known as the 'rotation matrix' [R] is as follows:

..... (**4.1**)

The columns of [R] are 3 x 1 unit vectors, which correspond to the orientation of the local axes in the global frame. The columns correspond to the axes of the LCS, and the rows match the axes of the GCS.

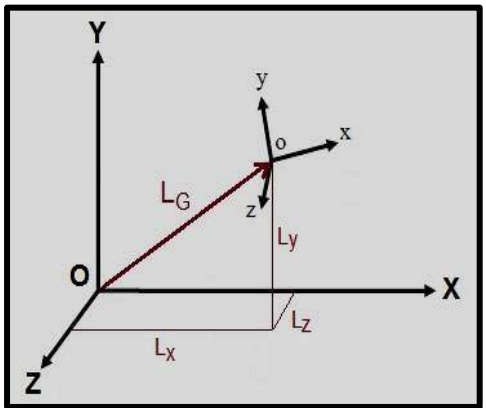


**Figure (4.2)**: The three components of the vector L define the location of the LCS within the GCS.

### *4.2.2. Translation and Rotation*

The position of a local coordinate system (LCS) with respect to the global coordinate system (GCS) can be expressed as a sequence of translation and rotation described by a 3 x 1 column matrix for translation and a 3 x 3 matrix of direction cosines for rotation. A row consisting of elements (1, 0, 0, 0) (which simply means *l=1* so doesn't affect anything) is added to homogenise the matrix, making it a 4 x 4 matrix, known as a transformation matrix [T]:

..... (**4.2**)

This transformation matrix will describe any given position of a LCS relative to the GCS, or potentially relative to any other LCS. Hence if the local coordinate system is attached to a rigid body, the matrix [T] is the same for all points of the body.

### *4.2.3. Euler's Method*

The matrix method is the basic mathematical tool used for computing body position or movement. However, it is not easy to associate it directly with the relative movement between two bodies. Obviously the position of a body in space can be described by a smaller number of angles than nine, so some of the direction cosines are redundant. Finite rotations in three-dimensional space must be performed in a specific order, i.e. they are non-commutative. As such, they cannot be considered as vectors. The change in orientation can be described as a sequence of three successive rotations from an initial position where the global coordinate system and the local coordinate system coincided. These three successive angles of rotation are Euler's angles, (Zatsiorski 1998).

The general succession for Euler's method is defined as follows:

1. The first rotation is defined relative to an axis in the GCS
2. The second axis of rotation is not fixed with respect to the GCS and the LCS, so is commonly called the "floating" axis. It is always orthogonal to the first and third axes. It is denoted by a single prime (').
3. The third rotation is defined with regard to an axis fixed within the rotating body and it is denoted by a double prime (").

The second and third rotations are about local axes transformed by the previous rotations. For example, the sequence X y'x" means that the second rotation is around the local y axis which was previously rotated around the global X axis; and the third rotation is around the local x axis which was previously rotated around the global X axis and then around the local y axis.

The final axis in the rotation sequence can be identical to the initial rotation axis (e.g. Xy'x", Zx'z"), or different (e.g. Xy'z", Yx'z"). The term '*Euler's Angles*' is often used to denote the use of an identical axis, and is referred to as the *two axis system.* The term '*Cardan Angle*' is likewise used to denote the use of a different final axis. This convention is referred to as the three axis system or the *gyroscopic system.* In total there are 12 sequences of rotations. However the general succession is the same. Six of the sequences are Euler's Angles, and six of the sequences are Cardan Angles. It is important to realise that the same body orientation measured with various Euler/Cardan sequences gives different angular values.

Euler's/Cardan angles have the advantage of being easily understood, as the angles between two segments of the human body can be measured with a goniometer. However, only the orientation of the segment is defined, meaning that Euler's/Cardan angles do not form a homogeneous system, meaning that translation and rotation must be calculated separately. But, the Euler's/Cardan angles can be expressed as elements of a 3 x 3 rotation matrix, $[R] = [R_1]\ [R_2]\ [R_3]$, where $[R_1]$,$[R_2]$ and $[R_3]$ are the matrices of sequential rotations. An augmented 4 x 4 transformation matrix [T] can be constructed and used as previously discussed in the Matrix Method. The following is an example for a Zy'x" rotation sequence:

..... (**4.3**)

The elements of the combined matrix [R] represent the direction cosines between the axes of the two reference systems, expressed as functions of the Euler's angles. This is known as *decomposition* of the Euler's angles, meaning that the axes are decomposed into their projections onto the axes of the global frame, (Zatsiorski 1998).

Conversely, when a rotation matrix [R] is given rather than the Euler/Cardan angles, the elements of the matrix can be interpreted in terms of the Euler/Cardan angles if a certain order of rotations is assumed. When the angle of tilt (about the second rotation axis) is zero, and the first and third axes axe parallel, the Euler's/Cardan angles cannot be defined. This results in a *singularity* or *gimbal lock.* If a body is in a singular position, the values of the first and third angles cannot be determined, only their sum (or difference) is measurable, leading to very high errors. This is a very common problem when assessing the GH joint, particularly at low and high levels of arm elevation.

## 4.3 Upper body Joints and Segments

In 2005, Wu et al. proposed an advantageous approach for defining the coordinate systems of various upper limb joints, (Wu et al. 2005). Its recommended standards were based on the work of Grood and Suntay (1983) who developed a methodology to calculate relative movement of two body segments and applied it to the knee. The bones of the body can be viewed as a series of rigid links whose positions can be defined by the location of a point on the bone and the bone's orientation in space. The basic premise is that three non-collinear bony landmarks on a given bone segment are needed to generate a three dimensional orthogonal coordinate system for that bone. There are three segments of the upper limb attached to the thorax by the scapula: the humerus, forearm and hand. Within these are several joints: sternoclavicular (SC); acromioclavicular (AC); scapulothoracic (ST); glenohumeral (GH); elbow, superior and inferior radioulnar, wrist, carpometacarpal and interphalangeal joints.

### *4.3.1. Anatomical Bony Landmarks*

Bony landmarks are used for the location of markers to set up the local coordinate systems of the upper limb joints as recommended by the International Society of Biomechanics (ISB) are shown in Figure (4.3) and Table (4.1).

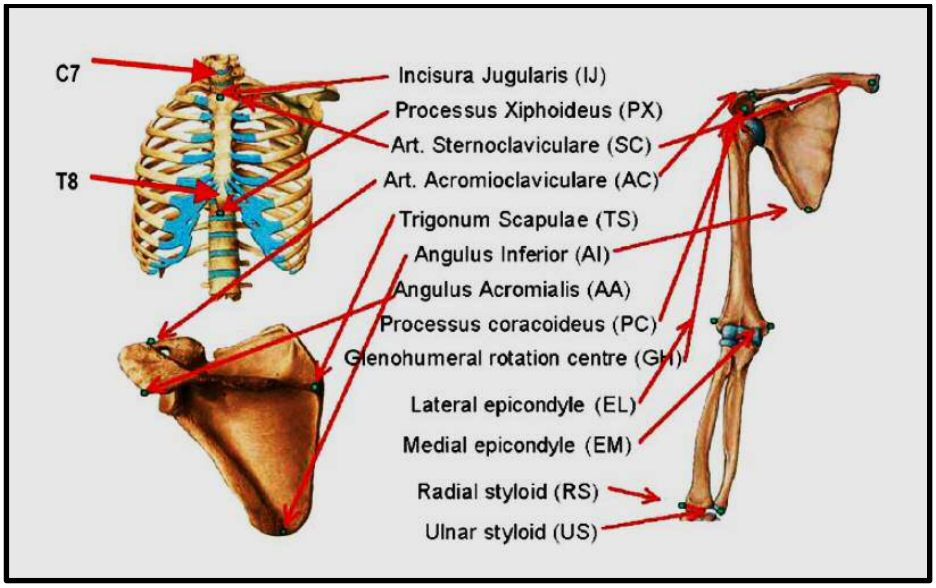


**Figure (4.3)**: Bony landmarks and local coordinate systems of the thorax, clavicle, scapula, humerus and forearm as established by the ISB to define each segment and joint of the upper limb, (Wu et al. 2005).

**Table (4.1)**: Anatomical landmarks of the upper limb segments as proposed by the ISB.

| Segment | Bony Landmark | Description of Location |
|---|---|---|
| **Thorax** | C7 | Spinous process of the 7$^{th}$ cervical vertebra |
| | T8 | Spinous process of the 8$^{th}$ cervical vertebra |
| | IJ | Deepest point of IncisureJugularis |
| | PX | Processus Xiphoideus, most caudal point on the sternum |
| **Clavicle** | SC | Most ventral point on the sternoclavicular joint |
| | AC | Most dorsal point on the sternoclavicular joint |
| **Scapula** | TS | Trigonium Spinae, the midpoint of the triangular surface on the medial border of the scapula in line with the scapular spine |
| | AI | Angulus Inferior, most caudal point of the scapula |
| | AA | Angulus Acromialis, most laterodorsal point of the scapula |
| | PC | Most ventral point of processuscoracoideus |
| **Humerus** | GH | Glenohumeral rotation centre, estimated by regression or motion recordings |
| | EL | Most caudal point on lateral epicondyle |
| | EM | Most caudal point on medial epicondyle |
| **Forearm** | RS | Most caudal-lateral point on the radial styloid |
| | US | Most caudal-medial point on the ulnar styloid |
| **Hand** | MC3 | Most dorsal point on dorsal styloid process of the 3$^{rd}$ metacarpal |
| | MCP2 | Distal head of the 2$^{nd}$ metacarpal |
| | MCP3 | Distal head of the 3$^{rd}$ metacarpal |
| | MCP5 | Distal head of the 5$^{th}$ metacarpal |

For the clavicle only two bony landmarks can be discerned: SC and AC. Hence, the axial rotation of the clavicle cannot be determined through non-invasive palpation measurements, but can be estimated on the basis of optimization techniques (Van der Helm and Pronk, 1995). In contrast to Van der Helm (1996), the use of the landmark AA is now proposed instead of the acromioclavicular joint (AC joint). This choice will reduce the occurrence of complications due to gimbal lock (Groot, 1998). The humerus was defined by three points: the medial humeral epicondyle (EM), lateral humeral epicondyle (LM) and the glenohumeral (GH) joint rotation centre.

### *4.3.2. Glenohumeral Joint Centre*

For the kinematics analysis of human motion, three non-collinear landmarks must be identified to create an anatomical coordinate system (ACS) on a segment. Only two landmarks can be identified on the humerus by means of palpation, the medial (EM) and lateral (EL) epicondyles. The third landmark, the glenohumeral (GH) joint centre of rotation must be estimated. Technically, the GH joint rotation centre is not a bony landmark, that cannot be located using palpation, but it is required to define the longitudinal axis of the humerus. The ability to accurately determine the GH joint rotation centre can lead to improved kinematic measurements of the shoulder complex because it is essential for the definition of the embedded humerus anatomical coordinate system. There are currently multiple methods used to model the location of the glenohumeral joint centre.

Campbell et al. (2009) sought to determine and compare the accuracy of these well-established methods as well propose two new predictive methods. The methods Campbell chose for comparison include: the (7 cm) drop method (Schmidt et al. 1999), the two Vicon standard method versions, the UWA (University of Western Australia) method (Lloyd et al. 2000), and the original and updated ISB recommended regression equation methods, (Meskers et al. 1998, Wu et al. 2005).

Schmidt et al. (1999) used a ruler to determine the average distance between the acromion marker and the shoulder joint centre. The shoulder joint centre was then assumed to be inferior to the acromion marker by the (7 cm) average. Vicon (Vicon Oxford Metrics, Inc.) developed two methods similar to that of Schmidt for

glenohumeral joint centre determination. The first method takes a two dimensional measurement of the distance between the acromioclavicular joint and the glenohumeral joint and subtracts this amount from the AC joint location. The second Vicon method measures the two dimensional shoulder widths and subtracts half of this value from the AC joint location (Campbell et al. 2009). The UWA method uses markers placed on shoulder to represent the anterior and posterior portion of the glenohumeral joint. Lloyd et al. (2000) then used the point halfway between these markers to designate the glenohumeral joint centre.

Campbell et al. (2009) uses the intersection of the vector between these markers and a vector perpendicular to it from the centre of the acromial lateral ridge (Campbell et al. 2009). The last method(s) included in Campbell's investigation are the original predictive method as developed by Meskers et al. (1998) and an updated version put forth by the International Shoulder Group (ISG). Both methods require the use of multiple scapula marker locations in three regression equations to determine the glenohumeral joint location (Campbell et al. 2009).

Meskers et al.'s original equations that were developed, used the positions of the acromioclavicular (AC), trigonum spinae (TS), inferior angle (AI), acromial angle and coracoid process (PC) of 36 sets of cadaver scapulae and humeri. The location of the glenohumeral joint centre was then estimated using a sphere fitting technique, Meskers et al. (1998). The three dimensional positions of the scapular bony landmarks, as well as all 10 distances between the markers were then used as potential variables in the linear regression model to predict the estimated location of the glenohumeral joint centre. The resulting regression equations determine the x, y and z location of the glenohumeral joint centre in the scapula coordinate system defined by Meskers as: x-axis from the TS to the AC; z-axis perpendicular to the plane formed by the AC, TS and AI markers, pointing backwards; y-axis perpendicular to the x and z axes, pointing upwards.

The regression equations follow:

$GH_{Cxl} = 18.9743 + 0.2434\ (m_{PCx}) + 0.2341\ (m_{AIx}) + 0.1590\ (m_{AI}\text{-}m_{AA}) + 0.0558\ (m_{PCy})$ ……..…….... **(4.4)**

$GH_{Cyl} = -3.8791 - 0.3940\ (m_{AC}\text{-}\ m_{AA}) + 0.2341\ (m_{AIx}) + 0.1732\ (m_{PCy}) + 0.1205\ (m_{AIx}) - 0.1002\ (m_{AC} - m_{PC})$ ..……..……..……..…… **(4.5)**

$GH_{Czl} = 9.2629 + 1.0255\ (m_{PCz}) - 0.2403\ (m_{PCy}) + 0.1720\ (m_{TS}\text{-}\ m_{PC})$ …….……...…….. **(4.6)**

Where $GH_{Cxl}$ is the x-coordinate of the glenohumeral joint centre in the local scapular coordinate system, $m_{markerx}$ is the denoted axis coordinate of the specified marker and ($m_{marker1}$ - $m_{marker2}$) is the Euclidean distance (ED, equation below) between marker 1 and marker 2.

$$ED = \sqrt{\qquad\qquad\qquad\qquad}$$ ……..……..…….. **(4.7)**

The resulting low fitting and validation errors led Meskers et al. to conclude that this model adequately predicts the location of the GH joint centre for upper arm coordinate system creation (Meskers et al. 1998). Lastly, Campbell included the amended version of Meskers regression equations by the ISG. They proposed the following regression equations:

$GH_{Cxl} = 26.896 + 0.614\ (m_{TSx}) + 0.295\ (m_{AI}\text{-}\ m_{PC})$……..……...……. **(4.8)**

$GH_{Cyl} = -16.307 + 0.825\ (m_{ACy}) + 0.293\ (m_{PCz})$ …….……..…… **(4.9)**

$GH_{Czl} = -1.740 - 0.899\ (m_{AA}\text{-}\ m_{PC}) - 0.229\ (m_{TSx})$……..…...…….…….. **(4.10)**

Additionally, Campbell et al. (2009) sought to create two new predictive methods to compare to these six established equations. First, a new regression model was created based on the following five possible predictive variables: subject height, subject mass, the Euclidean distance between the IJ and C7, the Euclidean distance between the midpoint of the lateral ridge of the acromial plateau and the midpoint of the IJ and C7 markers, and lastly the Euclidean distance between a marker on the anterior portion of the shoulder and a marker on the posterior portion of the shoulder (in line with the glenohumeral joint).The stepwise linear regression provided the following three equations, (Campbell et al. 2009):

$GH_{Cx} = 96.2 - 0.302\ (m_{IJ} - m_{C7}) - 0.364\ (\text{subject height}) + 0.385\ (\text{subject mass})$ ……..... **(4.11)**

$GH_{Cy} = -66.32 + 0.30\ (m_{IJ} - m_{C7}) - 0.432\ (\text{subject mass})$ ……...…...……...…...…… **(4.12)**

$GH_{Cz} = 66.468 - 0.531\ (m_{ACrLR} - m_{PC}) + 0.571\ (\text{subject mass})$ ……..…….. **(4.13)**

where $GH_{Cx}$ is the x-coordinate of the glenohumeral joint centre location with respect to an acromion reference technical coordinate system (TCS), ($m_{marker1}$ - $m_{marker2}$) is the Euclidean distance between marker 1 and marker 2 (in mm), the subject height is in cm and the subject mass is in kg.

## 4.4 Joints and Segments Coordinate System for the Shoulder Complex

Once the anatomical bony landmarks have been defined, the local coordinate systems for the shoulder complex segments can be identified as follows:

***4.4.1. Thorax coordinate system*** — $X_tY_tZ_t$, see Figures (4.3) and (4.4)

$O_t$: The origin coincident with IJ.

$Y_t$: The line connecting the midpoint between PX and T8 and the midpoint between IJ and C7, pointing upward.

$Z_t$: The line perpendicular to the plane formed by IJ, C7, and the midpoint between PX and T8, pointing to the right.

$X_t$: The common line perpendicular to the $Z_t$ and $Y_t$ axes, pointing forwards.

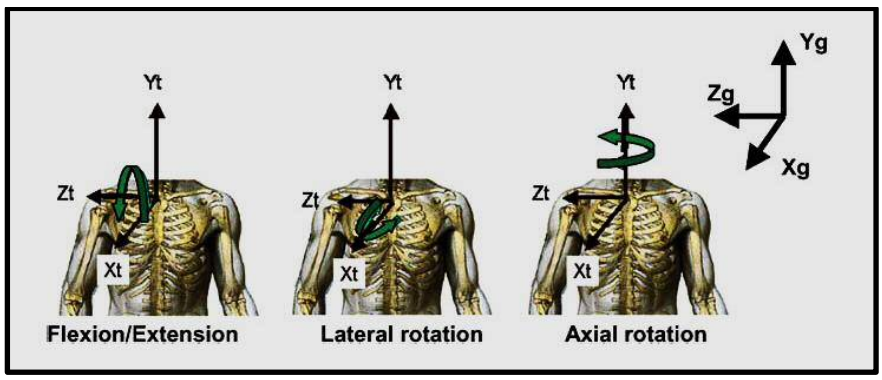


**Figure (4.4)**: Thorax coordinate system and definition of motions, (Wu et al. 2005).

***4.4.2. Clavicle coordinate system*** — $X_cY_cZ_c$, see Figures (4.3) and (4.5)

$O_c$: The origin coincident with SC.

$Z_c$: The line connecting SC and AC, pointing to AC.

$X_c$: The line perpendicular to $Z_c$ and $Y_t$, pointing forward. Note that the $X_c$ axis is defined with respect to the vertical axis of the thorax ($Y_t$ axis) because only two bony landmarks can be discerned at the clavicle.

$Y_c$: The common line perpendicular to the $X_c$ and $Z_c$ axis, pointing upward.

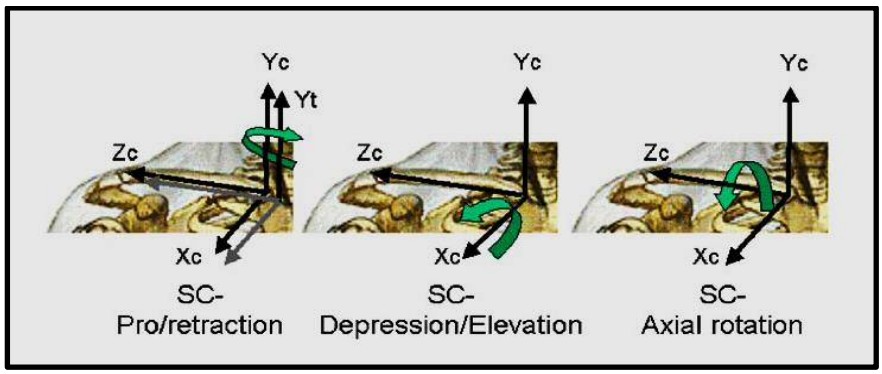


**Figure (4.5)**: Clavicle coordinate system and definition of SC motions. $Y_t$ is the local axis for the thorax coordinate system, which is initially aligned with $Y_c$ of the clavicle, (Wu et al. 2005).

***4.4.3. Scapula coordinate system*** — $X_sY_sZ_s$, see Figures (4.3) and (4.6)

$O_s$: The origin coincident with AA.

$Z_s$: The line connecting TS and AA, pointing to AA.

$X_s$: The line perpendicular to the plane formed by AI, AA, and TS, pointing forward. Note that because of the use of AA instead of AC, this plane is not the same as the visual plane of the scapula bone.

$Y_s$: The common line perpendicular to the $X_s$ and $Z_s$ axis, pointing upward.

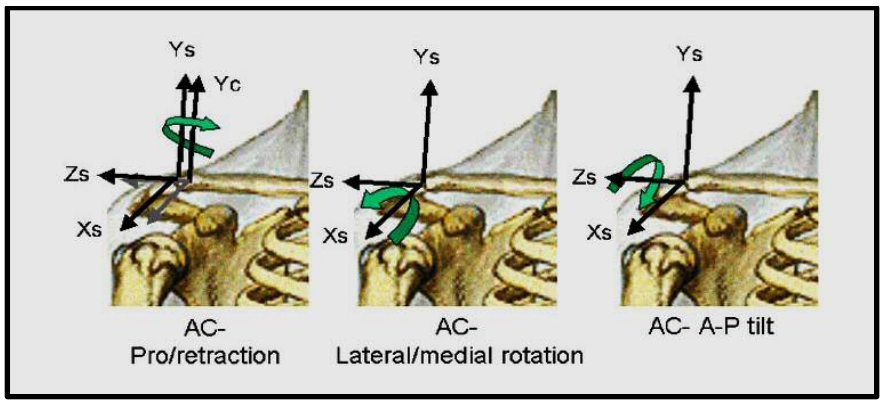


**Figure (4.6)**: Scapula coordinate system and definition of AC motions. $Y_c$ is the local axis for the clavicle coordinate system (Please note, the origin, shown here at AC, should be placed at AA), (Wu et al. 2005).

### *4.4.4. Humerus coordinate system*

Due to the relatively short distance between the EM and EL the effect of measurement errors, in particular on humeral axial rotation ($Z_h$ axis), can be problematic (Veeger et al., 2003). Two options for defining the humeral coordinate system are recommended by the ISB (Wu et al., 2005). The first option uses the plane formed by EL, EM, and GH joint rotation centre pointing forward to estimate the $Z_h$ local coordinate axis. The second option uses the plane formed by the upper arm and the forearm (elbow flexed to 90 , forearm pronated) to estimate the same axis.

- ***1st option*** — $X_{h1}Y_{h1}Z_{h1}$, see Figures (4.3) and (4.7); see also notes (1) and (2)

$O_{h1}$: The origin coincident with GH.

$Y_{h1}$: The line connecting GH and the midpoint of EL and EM, pointing to GH.

$X_{h1}$: The line perpendicular to the plane formed by EL, EM, and GH, pointing forward.

$Z_{h1}$: The common line perpendicular to the $Y_{h1}$- and $Z_{h1}$-axis, pointing to the right.

- ***2nd option*** — $X_{h2}Y_{h2}Z_{h2}$

$O_{h2}$: The origin coincident with GH.

$Y_{h2}$: The line connecting GH and the midpoint of EL and EM, pointing to GH.

$Z_{h2}$: The line perpendicular to the plane formed by $Y_{h2}$ and $Y_f$ , (see Fore coordinate system), pointing to the right.

$X_{h2}$: The common line perpendicular to the $Z_{h2}$- and $Y_{h2}$-axis, pointing forward.

***Note 1***: The second definition of humerus coordinate system is motivated by the high error sensitivity of the direction connecting EL and EM due to the short distance between them. Since it cannot be assured that the $Z_{h2}$ axis is equal to the joint rotation axis, its orientation depends on the position of the upper arm and forearm as well as the forearm orientation (Wang, 1996). Therefore, by definition, the $Z_{h2}$ axis is taken with the elbow flexed 90° in the sagittal plane and the forearm fully pronated.

***Note 2***: We are faced with two difficulties in defining $Z_h$: (1) the anatomical definition of neutral humeral internal/external rotation is unclear; and (2) the numerical and practical inaccuracies in defining EL and EM may swamp the

accuracy of our definition. The 1st and 2nd definitions will not agree if the true EM–EL line is rotated with respect to the forearm axis (in pronation). For the humerus, the difference will only affect the value for internal/external rotation; for the forearm it will affect all three angles to some degree, most significantly pro/supination. The ISB recommended using the second option when the forearm is available for recording and otherwise to use the first option, (Wu et al. 2005).

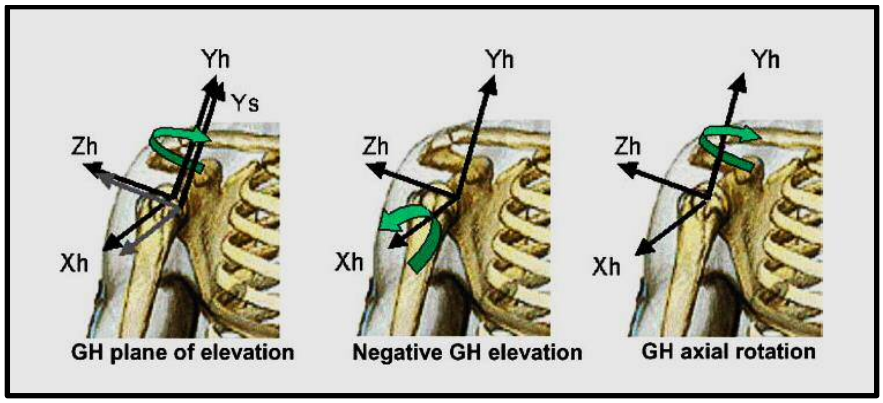


**Figure (4.7)**: Humerus coordinate system and definition of GH motions. $Y_s$ is the local axis for the scapula coordinate system, (Wu et al. 2005).

***4.4.5. Forearm coordinate system*** — $X_fY_fZ_f$, see Figures (4.3) and (4.8)

$O_f$ : The origin coincident with US.

$Y_f$ : The line connecting US and the midpoint between EL and EM, pointing proximally.

$X_f$ : The line perpendicular to the plane through US, RS, and the midpoint between EL and EM, pointing forward.

$Z_f$ : The common line perpendicular to the $X_f$ and $Y_f$ axes, pointing to the right.

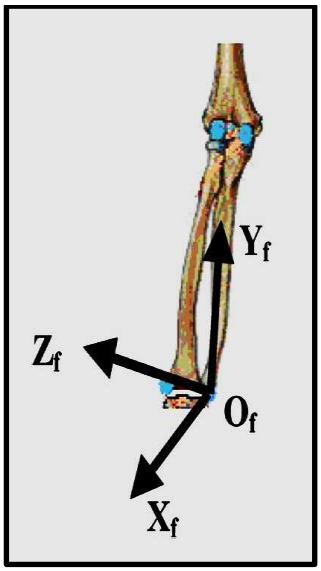


**Figure (4.8)**: Definition of forearm coordinate system, (Wu et al. 2005).

## 4.5 Segments Rotation for the Shoulder Complex

For the shoulder complex, it can be useful to describe two types of rotations. One is the *joint rotation*, i.e., rotation of one segment relative to another proximal articulating segment, including the clavicle relative to the thorax (SC joint), the scapula relative to the clavicle (AC joint), and the humerus relative to the scapula (GH joint). The other is segment rotation, i.e., rotation of the clavicle, scapula, or humerus relative to the thorax (the non-existent thoracohumeral joint, often loosely defined as the shoulder joint). The definition of joint displacements is only useful if it is defined with respect to the proximal segment. Many rotation orders are possible such as X-Y-Z in Cardan angles or Y-Z-Y in Euler angles. Rotation orders follow the recommendations of the ISB, (Wu et al. 2005), which were chosen so that angles remain as close as possible to clinical definitions of joint and segment rotations.

The rotations for each joint and segment rotation are summarised in Table (4.2), α is around the Z axis, $\beta$ around the X axis and γ around the Y axis, regardless of the order of rotation, (Wu et al. 2015).

***4.5.1. Thorax relative to the GCS,*** Z–X–Y order, see Figure (4.4).

$e_1$: The axis coincident with the $Z_g$ axis of the global coordinate system.

Rotation ($\alpha_{GT}$): flexion (negative) or extension (positive).

$e_3$: The axis fixed to the thorax and coincident with the $Y_t$ axis of the thorax coordinate system.

Rotation ($\gamma_{GT}$): axial rotation to the left (positive) or to the right (negative).

$e_2$: The common axis perpendicular to $e_1$ and $e_3$, i.e., the rotated $X_t$ axis of the thorax.

Rotation ($\beta_{GT}$): lateral flexion rotation of the thorax, to the right is positive, to the left is negative.

***4.5.2. Clavicle relative to the thorax (SC joint)***, Y–X–Z order, see Figure (4.5).

$e_1$: The axis fixed to the thorax and coincident with the $Y_t$ axis of the thorax coordinate system.

Rotation ($\gamma_{SC}$): retraction (negative) or protraction (positive).

$e_3$: The axis fixed to the clavicle and coincident with the $Z_c$ axis of the clavicle coordinate system.

Rotation ($\alpha_{SC}$): axial rotation of the clavicle; rotation of the top backwards is positive, forwards is negative.

$e_2$: The common axis perpendicular to $e_1$ and $e_3$, the rotated $X_c$ axis.

Rotation ($\beta_{SC}$): elevation (negative) or depression (positive).

***4.5.3. Scapula relative to the clavicle (AC joint),*** Y–X–Z order, see Figure (4.6).

Note: The following sequence is supported by Karduna et al. (2000), who studied the six possible Euler sequences for scapular motion. They found that the proposed sequence is ‘‘consistent with both research and clinical-based 2D representations of scapular motion’’. They also found that changing the sequence resulted in ‘‘significant alterations in the description of motion, with differences up to 50° noted for some angles’’. Since the scapular coordinate system is initially aligned with the clavicular coordinate system even though this position is never assumed anatomically, typical angle values are offset from zero (either positive or negative).

$e_1$: The axis fixed to the clavicle and coincident with the $Y_c$ axis of the clavicle coordinate system.

Rotation ($\gamma_{AC}$): AC retraction (negative) or AC protraction (negative); the scapula is usually retracted.

$e_3$: The axis fixed to the scapula and coincident with the $Z_s$ axis of the scapular coordinate system (scapular spine).

Rotation ($\alpha_{AC}$): AC-anterior (negative) or AC posterior (Positive) tilt; the scapula is usually tilted posteriorly.

$e_2$: The common axis perpendicular to $e_1$ and $e_3$, the rotated $X_s$ axis of the scapula coordinate system.

Rotation ($\beta_{AC}$): AC-lateral (negative) or AC medial (positive) rotation; the scapula is usually laterally rotated.

***4.5.4. Humerus relative to the scapula (GH joint),*** Y–X–Y order, see Figure (4.7).

Note: This is the one joint that is based on an Euler rotation sequence. Since $e_1$ and $e_3$ start in the same direction, the standard Grood and Suntay (1983) (floating-axis) equations cannot be used. Instead, Euler decomposition is used to find the corresponding angles. As stated before, we have avoided the clinical terms flexion and abduction because flexion followed by abduction would give radically different results than abduction followed by flexion. Furthermore, these terms are only

defined relative to the thorax, not the scapula. For comparison, flexion is elevation parallel to the sagittal plane and abduction is elevation in the coronal (frontal) plane.

$e_1$: The axis fixed to the scapula and coincident with the $Y_s$ axis of the scapular coordinate system.

Rotation ($\gamma_{GH1}$): GH plane of elevation.

$e_3$: Axial rotation around the $Y_h$ axis.

Rotation ($\gamma_{GH2}$): GH-axial rotation, endo- or internal-rotation (positive) and exo- or external-rotation (negative).

$e_2$: The axis fixed to the humerus and coincident with the $X_h$ axis of the humerus coordinate system.

Rotation ($\beta_{GH}$): GH elevation (negative).

As a consequence of the chosen direction of axes (ISB choice, but not preferred by the ISG), the second rotation elevation is by definition in the negative direction. The clinical term ‘‘elevation’’ corresponds to negative rotations around the $e_2$-axis.

***4.5.5. Scapula relative to the thorax (ST articulation),*** Y–X–Z order

$e_1$: The axis fixed to the thorax and coincident with the $Y_t$ axis of the thorax coordinate system.

Rotation ($\gamma_s$): retraction (negative) or protraction (positive).

$e_3$: The axis fixed to the scapula and coincident with the $Z_s$ axis of the scapular coordinate system.

Rotation ($\alpha_s$): anterior (negative) or posterior (positive) tilt.

$e_2$: The common axis perpendicular to $e_1$ and $e_3$.

Rotation ($\beta_s$): lateral (negative) or medial (positive) rotation.

***4.5.6. Humerus relative to the thorax*** (Y–X–Y order), see Figure (4.9)

$e_1$: The axis fixed to the thorax and coincident with the $Y_t$ axis of the thorax coordinate system.

Rotation ($\gamma_h$): Plane of elevation, 0° is abduction, 90° is forward flexion.

e3: Axial rotation around the $Y_h$ axis.

Rotation $(\gamma_h)_2$: axial rotation, endo- or internal rotation (positive) and exo- or external-rotation (negative).

$e_2$: The axis fixed to the humerus and coincident with the $X_h$ axis of the humerus coordinate system.Rotation ($\beta_h$): elevation (negative).

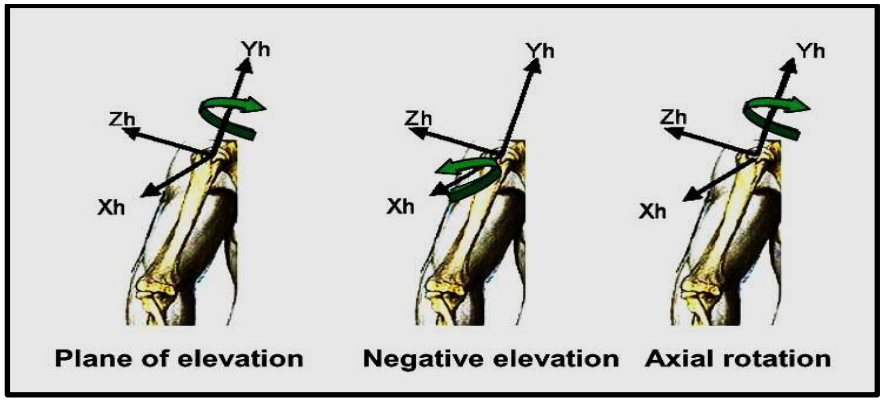


**Figure (4.9)**: Definition of thoracohumeral rotations, (Wu et al. 2005).

## 4.6 Joints and Segments Coordinate System for the Elbow

To make a kinematic description of the elbow joint useful and practical, we use the following anatomical approximations, see Figure (4.3):

1. The GH joint is a ball joint.
2. The humeroulnar joint is a hinge joint.
3. The radioulnar joint (contacting proximally and distally) is a hinge joint. The centre of the capitulum on the humerus and the axes of the two radioulnar joints (proximal and distal) are on the joint axis.

A special problem is posed to the definitions of the segment coordinate systems of the ulna and radius, in that there are only a few palpable bony landmarks. Therefore, bony landmarks of other bones are needed for definitions, which result in position-dependent definitions of the segment coordinate systems.

***4.6.1. Humerus coordinate system*** — $X_{h1}Y_{h1}Z_{h1}$ (1st option) or $X_{h2}Y_{h2}Z_{h2}$ (2nd option)

Previously described in Section 4.4.4 as a description of the two options for humerus coordinate systems. Since the forearm is obviously needed when studying the elbow, we recommend using the second definition.

***4.6.2. Forearm coordinate system*** — $X_fY_fZ_f$

Previously described in Section 4.4.5 as a description of the two options for humerus coordinate systems.

***4.6.3. Ulna coordinate system*** — $X_uY_uZ_u$ (defined at elbow flexed 90° in the sagittal plane).

$O_u$: The origin is at US.

$Y_u$: The line pointing proximally from US to the midpoint between EM and EL.

$X_u$: The line perpendicular to the plane formed by US, EM, and EL, pointing forward.

$Z_u$: The common line perpendicular to the $X_u$- and $Y_u$-axis, pointing to the right.

***4.6.4. Radius coordinate system*** — $X_rY_rZ_r$ (defined with forearm in the neutral position and elbow flexed 90° in the sagittal plane).

$O_r$: The origin is at RS.

$Y_r$: The line pointing proximally from RS towards EL.

$X_r$: The line perpendicular to the plane formed by RS, US, and EL, pointing forward.

$Z_r$: The common line perpendicular to the $X_r$ and $Y_r$ axis, pointing to the right.

## 4.7 Segments Rotation for the Elbow

Realistically, the elbow joint and radioulnar joint do not coincide with the axes of the segment coordinate systems. However, in situations where simplifications are allowed, the axis of rotation for each of these joints can be assumed to coincide with the local axes of the humerus ($Z_{h1}$ or $Z_{h2}$) or ulna ($Y_u$). For a detailed study of the joint kinematics, the orientation of the hinge axis with respect to the proximal coordinate system should be determined; approximations of these are available from the literature. Only joint rotations with respect to the proximal segment coordinate system are defined here, as segment rotations with respect to the thorax would be meaningless.

***4.7.1. Forearm relative to the humerus (elbow joint),*** Z–X–Y order

$e_1$: The axis fixed to the proximal segment and coincident with the $Z_h$ axis of the humerus coordinate system (preferably an approximation of the elbow flexion/extension axis).

Rotation ($\alpha_{HF}$): flexion (positive) and hyperextension (negative).

$e_3$: The axis fixed to the distal segment and coincident with the $Y_f$ axis of the forearm coordinate system.

Rotation ($\gamma_{HF}$): axial rotation of the forearm, pronation (positive) and supination (negative).

$e_2$: The floating axis, the common axis perpendicular to $e_1$ and $e_3$, the rotated $X_f$ axis of the forearm coordinate system.

Rotation ($\beta_{HF}$): carrying angle, the angle between the longitudinal axis of the forearm and the plane perpendicular to the flexion/extension axis. The carrying angle occurs due to both a tilt in the humeral (flexion/extension) axis at the humeroulnar joint and an angulation of the ulna itself. It is therefore a passive response to elbow flexion/extension. Since the carrying angle is passive, it is rarely reported.

### *4.7.2. Ulna relative to the humerus (humeroulnar joint),* Z–X–Y order

$e_1$: The axis fixed to the proximal segment and coincident with the $Z_h$axis of the humerus coordinate system (preferably an approximation of flexion/extension axis).

Rotation ($\alpha_{HU}$): flexion (positive). Hyperextension is defined negative.

$e_3$: The axis fixed to the distal segment and coincident with the $Y_u$ axis of the ulnar coordinate system.

Rotation ($\gamma_{HU}$): axial rotation of the ulna (negligible).

$e_2$: The common axis perpendicular to $e_1$ and $e_3$, the rotated $X_u$ axis of the ulnar coordinate system.

Rotation ($\beta_{HU}$): carrying angle, the angle between the longitudinal axis of the ulna and the plane perpendicular to the flexion/extension axis.

### *4.7.3. Radius relative to the humerus (Radioulnar joint),* X–Z–Y order

$e_1$: The axis fixed to the proximal segment and coincident with the $X_u$ axis of the ulnar coordinate system (describing the orientation of the pro/supination axis with respect to the ulna). It is implicitly assumed that the pro/ supination axis intersects the elbow flexion/ extension axis, although in reality this is not the case.

Rotation ($\beta_{UR}$): orientation of the pro/supination axis relative to the ulna (constant).

$e_3$: The axis fixed to the distal segment and coincident with the $Y_r$ axis of the radius coordinate system.

Rotation ($\gamma_{UR}$): pro/supination of the radius with respect to the ulna.

$e_2$: The common axis perpendicular to $e_1$ and $e_3$, the rotated $Z_r$ axis of the radius coordinate system.

Rotation ($\alpha_{UR}$): abduction/adduction of the radius (negligible).

## 4.8 Joints Coordinate System for the hand and wrist

Separate coordinate systems have been developed for each bone that is distal to the elbow, so that relative motion between any two adjacent segments maybe described. These systems are then also applicable to global wrist motion as well as to motion of the individual components that cause the global motion. Global wrist motion is typically considered as the motion of the second and/or third metacarpal with respect to the radius (here, we use the third metacarpal) and is achieved by movement of the carpal bones with respect to the radius as well as the numerous articulations of the eight carpal bones with respect to each other. Some researchers, who only examine global wrist motion and have no need to examine carpal motion, can still use the definitions given for the radius and the metacarpal bones to describe wrist motion.

### *4.8.1. Standard wrist positions*

*Neutral wrist position*: Position of the wrist relative to the radius is defined as in neutral flexion/ extension and neutral radial/ulnar deviation when the third metacarpal long axis is parallel to the $Y_r$ axis in the radius.

*Neutral forearm rotation*: Position of the radius relative to the ulna when the elbow is flexed 90° and the thumb is pointing to the shoulder.

For each bone, a coordinate system is given, assuming that the forearm is initially in the standard anatomical position, with the palm forward (anterior), and the thumb lateral. The dorsum of the hand and forearm face posteriorly. In general for a right arm, the positive $Y_i$ axis is directed proximally, the positive $X_i$ axis is directed volarly, and the positive $Z_i$ axis is directed to the right in the anatomical position (radially), see Figures (4.10) and (4.11). In order to have the same sign convention for clinical motion of left and right arms, for a left arm, $Y_i$ is directed distally, $X_i$ is directed dorsally, and $Z_i$ is directed to the right in the anatomical position (ulnarly). The following radius and ulna coordinate systems differ from those given in the elbow section above. Here, we are primarily concerned with studies that are based on all available bony landmarks. If a more general motion is of interest, similar to the artificial humerothoracic joint, one can use the forearm and 3$^{rd}$ metacarpal axes to create a simplified wrist joint.

### *4.8.2. Radius coordinate system* — $X_rY_rZ_r$

$O_r$: The origin is located midway between the distal radius at the level of the ridge between the radioscaphoid fossa and the radiolunate fossa, and the proximal radius at the level of the depression in the proximal radial head. If the distance to the ridge between the radioscaphoid and radiolunatefossas varies, then the location halfway between the dorsal and volar extremes of the ridge will be used to define the distal landmark on the radius. In the transverse plane it will be at the approximate centre of the tubular bone (along its principal axis of inertia).

$Y_r$: The line parallel to the long shaft of the radius from $O_r$ to intersect with the ridge of bone between the radioscaphoid fossa and the radiolunate fossa (midway dorsally and volarly along the ridge).

$Z_r$: The line perpendicular to the $Y_r$ axis, and in a plane defined by the tip of the radial styloid, the base of the concavity of the sigmoid notch and the specified origin.

$X_r$: The common line perpendicular to the $Y_r$ and $Z_r$ axes.

### *4.8.3. Ulna coordinate system* — $X_uY_uZ_u$

$O_u$: The origin is located midway between the distal ulna at the level of the dome of the ulnar head, and the proximal ulna at the level of the coronoid process. In the transverse plane it is at the approximate centre of the tubular bone (along its principal axis of inertia).

$Y_u$: The line parallel to the long shaft of the ulna from $O_u$ to intersect with the centre of the dome of the ulnar head.

$X_u$: The line parallel to $X_r$ when the radius is in neutral forearm rotation.

$Z_u$: The common line perpendicular to the $X_u$ and $Y_u$ axes.

### *4.8.4. Carpal bones coordinate system* — $X_cY_cZ_c$

The eight carpal bones, scaphoid, lunate, triquetrum, pisiform, trapezium, trapezoid, capitate, and hamate, will be considered simultaneously. Most researchers only report angular changes in carpal bone motion and use the neutral wrist position as a neutral reference position. The neutral wrist position is when the wrist is in neutral flexion/extension and neutral radial/ulnar deviation such that the third metacarpal long axis is parallel with the $Y_r$ axis in the radius.

These researchers define the motion relative to the radius and typically not the ulna. Therefore, the orientation of the coordinate systems for each carpal bone should be parallel with the radial coordinate system when the wrist is in the neutral wrist position, see Figure (4.10). Thus, Y carpal bone will be parallel to $Y_r$ and similarly for X carpal bone and Z carpal bone. At present, most researchers who need to define a coordinate system origin in a carpal bone use the volumetric centroid of the bone. Therefore it is proposed that, when necessary, the origin of a coordinate system in a carpal bone be located at the volumetric centroid of the bone.

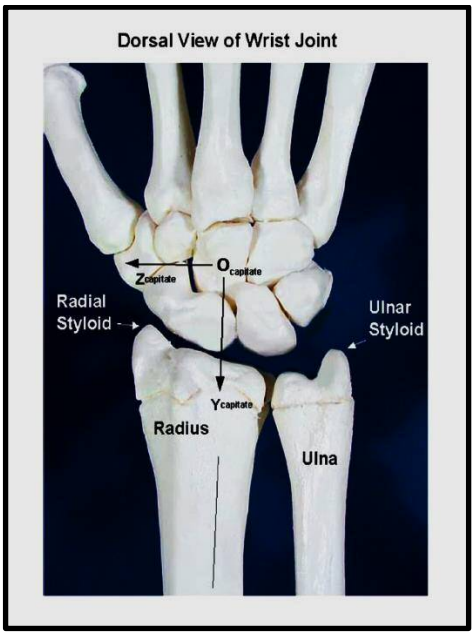


**Figure (4.10)**: Dorsal view of a right wrist joint illustrating the capitate coordinate system as an example of the carpal coordinate systems. X-axis is pointing volarly. (For a left arm X-axis is dorsal, Y-axis is distal, Z-axis is to the right (ulnarly) in the anatomical position.), Wu et al. 2005.

### *4.8.5. Metacarpals coordinate system* — $X_mY_mZ_m$

The five coordinate systems for the five metacarpals are described in the same manner. The major differences in the metacarpals are in the shape of their bases where ‘‘contact’’ with the carpals is made and their relative movement capabilities. In this regard, the first metacarpal has a very large range of motion. The third metacarpal has special significance because of its use in the definition of global wrist motion. Most researchers consider either the second or third metacarpal as representative of hand motion.

$O_m$: The origin for each of these coordinate systems is located midway between the base and head of each metacarpal. In the transverse plane, it will be at the approximate centre of the tubular bone (at its moment of inertia).

$Y_m$: The line parallel to a line from the centre of the distal head of the metacarpal to the midpoint of the base of the metacarpal.

$X_m$: The $X_m$ and $Y_m$-axis will form a sagittal plane that splits the metacarpal into mirror images.

$Z_m$: The common line perpendicular to the $X_m$- and $Y_m$-axis.

### *4.8.6. Phalanges coordinate system* — $X_pY_pZ_p$

The 14 coordinate systems for the phalanges of the five digits can be described in a manner that is analogous to the description used for the metacarpal systems. The proximal and middle phalanges for the five digits are similar in shape as are the five distal phalanges.

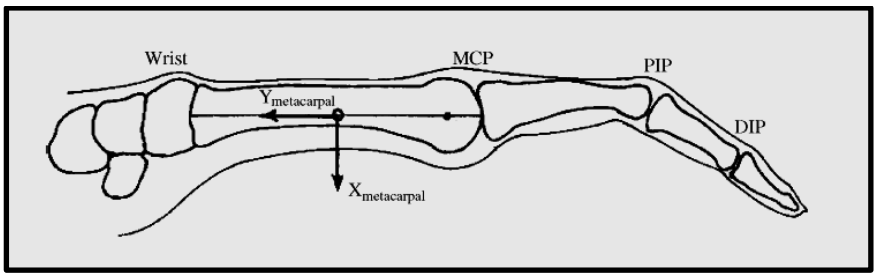


**Figure (4.11)**: Sagittal view of a right finger illustrating the metacarpal coordinate system as an example of phalangeal and metacarpal coordinate systems. X-axis is directed volarly and Y-axis is directed proximally. (For a left arm X-axis is dorsal, Y-axis is distal, and Z-axis is to the right in the anatomical position.), Wu et al. 2005.

## 4.9 Segments Rotation for the Hand and Wrist

$e_1$: The axis fixed to the proximal segment and coincident with the Z-axis of the proximal segment coordinate system.

Rotation (α): flexion or extension (flexion is positive).

$e_3$: The axis fixed to the distal segment and coincident with the Y-axis of the distal segment coordinate system.

Rotation (γ): rotation (pronation–supination).

Zero degrees of rotation are defined to be at the neutral forearm position. Pronation is a positive rotation. Supination is a negative rotation.

$e_2$: The common axis perpendicular to e1 and e3.

Rotation (β): adduction or abduction, or radial or ulnar deviation (ulnar deviation is positive).

For the interphalangeal, first metacarpophalangeal, intercarpal, and radiocarpal joints, a neutral posture is defined as the position where the orientations of the proximal and distal segmental systems are aligned. For the second through fifth metacarpophalangeal joints, a neutral posture is defined as the position where the orientation of the distal segmental system is identical to that of the third metacarpal. The third carpometacarpal joint will be neutral when the third metacarpal system is aligned with the wrist system. For the first carpometacarpal (trapeziometacarpal) joint, a neutral posture will be defined as the position where the orientations of the proximal segmental system (as defined by Cooney et al., 1981) and distal segmental system are identical. The neutral posture for the second, fourth, and fifth carpometacarpal joints can be defined in an analogous manner.

## 4.10 Summary

This chapter aimed to describe the design concept of the methodology undertaken per this research study. It began with an overview of the kinematic analysis of rigid body in a three-dimensional space through defining its location and orientation. It also identified the methods used to define the body position and displacement in terms of translation and rotation matrices and Euler's angles. Approaches for estimation the centre of rotation of the glenohumeral joint were also illustrated. This chapter presented a detailed description of the kinematic analysis of the upper body joints and segments on the basis of International Society of Biomechanics (ISB) recommendations through defining the axes of the local coordinate system of each joint and segment of the upper body. It also provided the definition of rotation order of the thorax, clavicle, scapula, humerus and forearm with its articulations which were applied for the calculation of rotation matrices for the upper body joint rotations. The next two chapters will present a detailed demonstration of the general methods undertaken per this study through applying the described concept of three-dimensional motion analysis for quantifying the upper body functionality during activities of daily living and manual wheelchair use.

# Chapter 5

## Motion Analysis Protocol for Quantifying Shoulder Complex Function

Measuring the range of motion (ROM) of the shoulder complex is important in the diagnostic and therapeutic approach to patients with shoulder disorders. Clinical assessments of joint ROM usually concern measurements made in one or two dimensions. The shoulder joint is, however, a complicated structure involving a number of motion segments, which move in relation to each other in various planes. Therefore, motion analysis of the shoulder complex requires a system that can measure movements in three dimensions.

Van der Helm and Pronk (1995) implied that such methods should meet three criteria. First, a full description of the shoulder kinematics should be obtained, i.e., rotations of all four bony structures of the shoulder kinematic chain, namely, thorax, clavicle, scapula and humerus together with the interrelations between the bones: the rotations at the scapulathoracic (ST), sternoclavicular (SC), acromioclavicular (AC) and glenohumeral (GH) joints. Furthermore, a complete kinematic description allows for the assessment of important clinical parameters as rotations at especially the glenohumeral joint. Second, the measurements should be standardised to allow for comparisons of results. Standardization implicates both parametrisation of the kinematics according to a well-defined protocol and description of the motions of the LCSs with respect to reference coordinate systems. Third, the method should allow for fast and easy to perform measurements, so it becomes possible to measure larger groups of individuals, (van der Helm and Pronk 1995).

The initial set of measurements for this study were undertaken to ensure a complete understanding of the methods developed previously at Cardiff and to compare the outputs with those previously obtained. Since this study was developed to enable quantification of trunk and upper limb movements during wheelchair propulsion, obtaining an insight to the methods developed previously in studies that did not involve wheelchair propulsion, and how they could potentially be adapted for people who are using wheelchairs was important.

This chapter aimed to demonstrate the general procedure that was followed to quantify functionality of the shoulder complex joints in healthy individuals during physiological range of motion and common activities of daily living (ADLs) and arm elevation in the sagittal, frontal and coronal planes of motion. It presents an introduction to the motion analysis facilities at Cardiff; camera setup and calibration, marker placement, camera and software operation when taking measurements, subsequent tracking of markers into 3D trajectories and importing this data into bespoke software to calculate the range of motion of the trunk and articulations in the shoulder. It also allowed a clear understanding of the expected range of motion output in terms of kinematic waveforms for physiological range of motion and activities of daily living. This in turn provided a comparison with previous results generated at Cardiff and other laboratories in terms of mean ranges of motion and kinematic waveforms. Finally, it generated data for comparison of results produced using a different approach to calculate the 6 Degree of Freedom ROM developed during these studies.

## 5.1 Instrumentation

The Motion Analysis laboratory at Cardiff University was used for this analysis through an opto-electronic motion capture system, (Oqus Cameras and QTM Software, Qualisys, Sweden). It is equipped with nine Qualisys Pro-Reflex Oqus Cameras arranged around the periphery of the laboratory's walls. Each camera is equipped with an array of LEDs with a sampling frequency of (60 Hz), which emit infrared ashes to illuminate retro-reflective markers used to identify important bony landmarks or marker clusters attached tosegments. The shoulder complex has a very large ROM. The visible workspace of the cameras needs to be accordingly large to ensure that all markers are visible (by at least two cameras) throughout the shoulder's full ROM in order to determine its position in three-dimensional space, see Figure (5.1).

Three-dimensional (3D) marker positions are obtained from the triangulation of the two-dimensional (2D) marker positions recorded by each camera. Two or more cameras must record a marker in a calibrated camera layout for the Qualisys software to perform the triangulation. Qualisys' proprietary tracking software,

Qualisys Track Manager (QTM), is used to record and identify marker trajectory data. The QTM software configuration and settings are changed in the Workspace Options. Synchronised QTM and video recordings are taken for visual feedback and qualitative analysis.


**Figure (5.1):** Layout of the Motion Analysis Lab at Cardiff University showing Qualisys Pro-Reflex Oqus Cameras arranged around the periphery of the laboratory's walls.

## 5.2 Calibration

Once the cameras are positioned, the system can be calibrated to define a global coordinate system (GSC) for the laboratory. The calibration is performed using a (750 mm) T-shaped wand kit provided by Qualisys (www.qualisys.com) with a 60 seconds capture period prior to the participant's arrival to the laboratory. An L-shaped calibration frame is placed on a stool, where the subject would be positioned, which is placed in the centre of the laboratory. The frame has fourreflective markers with known and fixed positions, so that all of its markers are seen in the 2D view of every camera.

The long arm of the L-frame defines the X-axis of the GCS pointing to the right, the short arm of the L-frame defines the Y-axis of the GCS pointing forward, and the Z-axis is vertically upward, perpendicular to the X and Y axes. The origin of

the GCS is located in the marker on the centre of the L-frame. The T-wand was moved over the frame for a period of 30 seconds to calibrate a bounding volume large enough to capture the movement of a subject's upper limbs during full ROM movement, see Figure (5.2).

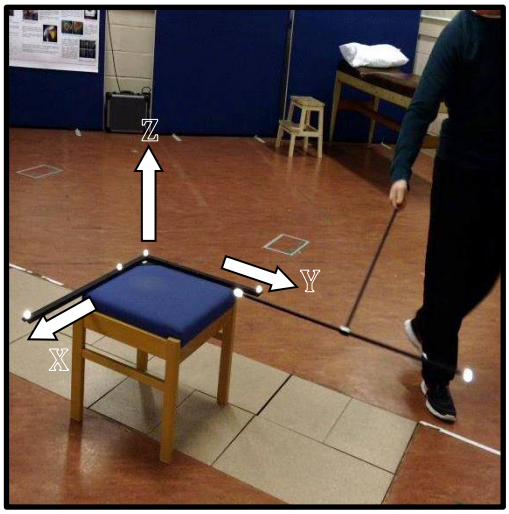


**Figure (5.2)**: The L-shaped frame and T-shaped wand were used for system static calibration to define the lab's global coordinates system.

## 5.3 Subjects

Five healthy male novice individuals, (two left-arm dominant, mean age 30 ± 7.84 years, height 176.72 ± 0.03 cm, mass 80.6 ± 13.2 kg and body mass index 30.37 ± 3.95), participated in this research study after giving their written informed consent in accordance with the approval obtained from the Cardiff University Ethics Committee. An informal interview was conducted at the start of the laboratory session. During the interview, the participant's date of birth, age and arm dominance are documented in the protocol sheet. Criteria for inclusion were: being able-bodied and having no previous history of shoulder pathologies or injuries. The exclusion criterion was the presence of any severe medical conditions that could have an influence on parameters measured in this study, based on a physical activity readiness questionnaire (PAR-Q). The consent and questionnaire forms used per this study are attached in the Appendix.

## 5.4 Anthropometric measurements

Once the participants have signed the consent form, their anthropometric data were collected. The subject's height (m) is measured with a Seca Ltd. wall mounted

measuring tape. Weighing scales are used to measure the participant's mass (kg). Trunk circumference and upper arm circumference, both when the arm is flexed and when it is extended, are measured with measuring tape (cm) to provide an indication of muscle mass. The measurement sheet used per this study is attached in the Appendix.

## 5.5 Markers Placement

Retro-reflective markers were attached to the skin overlying specific bony landmarks of the thorax, clavicle, scapula, and humerus. These bony landmarks were recommended by the International Society of Biomechanics (ISB) for to establish body segment and joint coordinate system of the shoulder complex (Wu et al., 2005). During the landmark identification process, subjects are asked to adopt the neutral position (NP) that is standing up straight, elbows flexed at 90°, hands pronated. The bony landmarks are identified by means of palpation. Markers are attached onto the landmark using double-sided tape. Additionally, individual markers are attached to the upper arm on the deltoid insertion (DI), the biceps belly (BB) and the brachioradialis insertion (BI), which provides a more accurate representation of axial rotation and allows compensatory techniques for soft tissue artefacts to be implemented when measurement of humerus axial rotation is of specific concern. The identified bony landmarks are represented graphically in Figure (5.3).

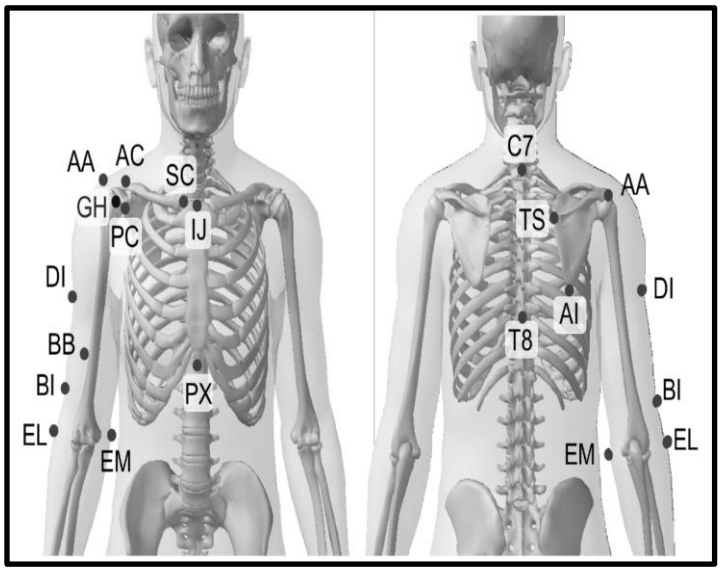


**Figure (5.3):** Anatomical bony landmarks of the thorax, clavicle, scapula, and humerus segments of the shoulder complex according to the ISB recommendations, (Wu et al. 2005).

The size (diameter in mm) of the markers used to identity each landmark is provided in the below table (5.1). By default, (19.2 mm) diameter markers are used to identify all bony landmarks. For bony landmarks that are prone to "marker swapping" such as SC and IJ, PC, AC and AA, and RS and US, (9.6 mm) markers were used to minimise this occurrence. For DI, BB and BI landmarks, (9.6 mm) markers were used as it was felt that the increased diameter of the (19.2 mm) markers would make it more difficult to accurately place the markers on the muscle insertion points. The anatomical description and marker diameter of the identified bony landmarks are summarised in the table (5.1).

**Table (5.1):** Trunk and upper limb markers set placement with their anatomical description and markers diameters.

| Segment | Bony Landmark | Description of Location | Diameter of Markers |
|---|---|---|---|
| **Thorax** | C7 | Spinous process of the 7$^{th}$ Cervical vertebra | 19.2 mm |
| | T8 | Spinous process of the 8$^{th}$ Thoracic vertebra | 19.2 mm |
| | IJ | Deepest point of IncisureJugularis | 9.6 mm |
| | PX | Processus Xiphoideus, most caudal point on the sternum | 19.2 mm |
| **Clavicle** | SC | Most ventral point on the sternoclavicular joint | 9.6 mm |
| | AC | Most dorsal point on the sternoclavicular joint | 9.6 mm |
| **Scapula** | TS | TrigoniumSpinae, the midpoint of the triangular surface on the medial border of the scapula in line with the scapular spine | 19.2 mm |
| | AI | Angulus Inferior, most caudal point on the scapula | 19.2 mm |
| | AA | AngulusAcromialis, most laterodorsal point on the scapula | 9.6 mm |
| | PC | Most ventral point on the Processus Coracoideus | 9.6 mm |
| **Humerus** | EL | Most caudal point on Lateral Epicondyle | 19.2 mm |
| | EM | Most caudal point on Medial Epicondyle | 19.2 mm |
| | GH | Glenohumeral joint centre of rotation. Most caudal point on the Acromion. | 19.2 mm |
| | DI | Deltoid insertion | 9.6 mm |
| | BB | Biceps brachii belly | 9.6 mm |
| | BI | Brachioradialis insertion | 9.6 mm |
| **Forearm** | RS | Most caudal-lateral point on the Radial Styloid | 9.6 mm |
| | US | Most caudal-medial point on the Ulnar Styloid | 9.6 mm |

A scapula locator (SL), developed at Newcastle University, is used in the measurement protocol to accurately track scapula movement during static arm elevations, (Johnson 1993). The SL consists of a Perspex (Perspex, Ltd.) device with three palpating legs. The legs are adjusted along slots on the base plate to match and have the best contact with the individual's scapula bony landmarks. The legs are fixed in place by tightening the screws on them to keep a fix relationship between

the landmarks. A retro-reflective marker is attached on top of each peg to record the SL's position. The SL is held in place by the observer during each static measurement, see Figure (5.4).

An acromion marker cluster (AMC) was built in the Mechanical Workshop at the School of Engineering and used by Stroud (2011). The AMC enables unconstrained 3D measurements of scapula kinematics during dynamic arm movements. It consists of a (10 mm) diameter plastic base and three carbon fibre rods with (9.6 mm) diameter retro-reflective markers attached onto them. The AMC can be accurately placed in the flat part of the acromion using Velcro. Its accuracy has been reported up to 90° of arm elevation using optoelectronic systems, see Figure (5.4).

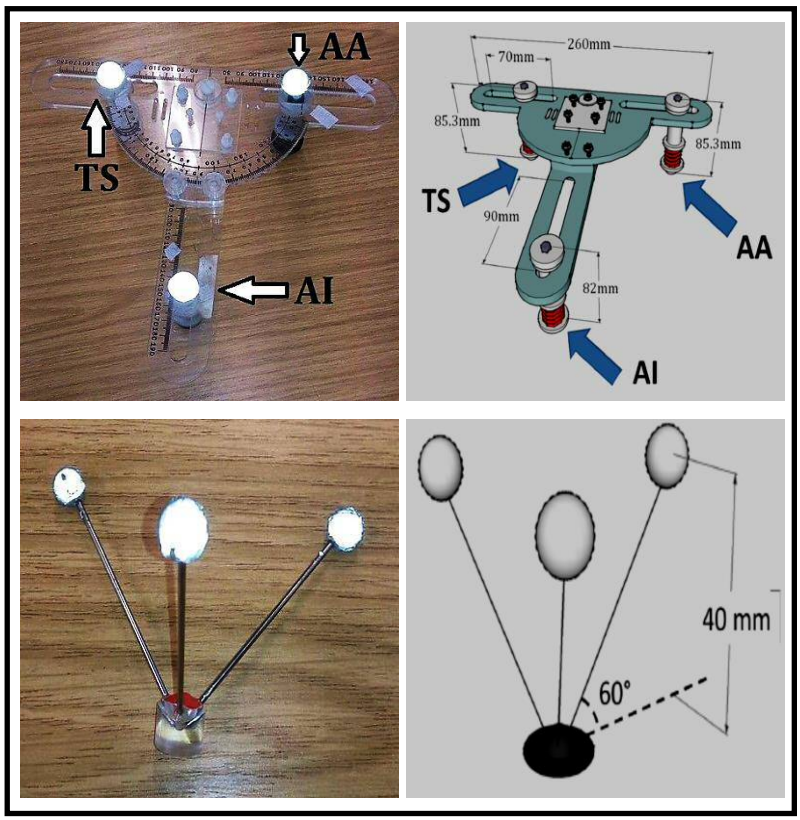


**Figure (5.4)**: Scapula locator (Up) and acromion marker cluster (Down). The right upper rod of the scapular locator is to be placed on AA, the left upper one on TS and the caudal one on AI, (Stroud 2011)

## 5.6 Shoulder Complex Function Measurements

### *5.6.1. Neutral Position Measurement*

During the one second neutral position (NP) measurement, subjects maintain both arms by the side of the body with the elbows flexed to 90°, hands pronated. During the recording, the system measures the positions of the AMC and the individual markers attached to bony landmarks in the GCS, see Figure (5.5). The neutral position measurement was repeated as any maker falls off and has to be repositioned to avoid the markers position changes.

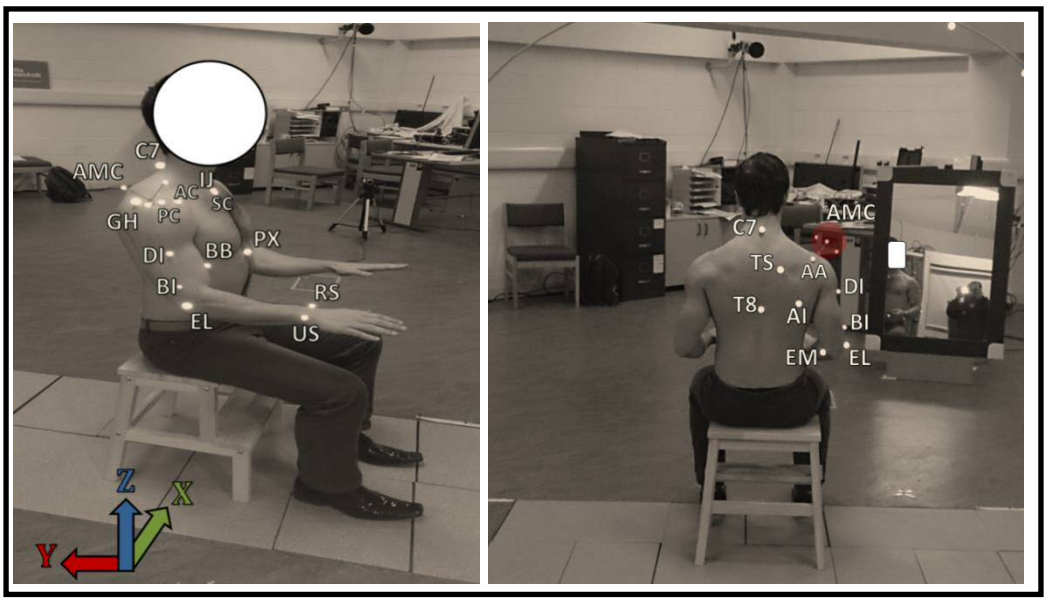


**Figure (5.5)**: Neutral position measurement with fixed skin markers on scapula landmarks.

### *5.6.2. Circumduction Measurement*

A 10 seconds recording of the healthy volunteers performing passive circumduction was made. Participants maintained their elbow flexed to 90° whilst the observer moved their dominant arm in small circular movements. They were instructed neither to move their arm themselves nor to oppose the movement that was performed by the observer. The observer also applied pressure on the scapula whilst rotating the volunteer's upper arm to minimise scapula rotation during the measurement, see Figure (5.6). During the measurement, the system records the movement of the scapula tracking markers.

**Figure (5.6)**: Circumduction recording.

### *5.6.3. Activities of Daily Living Measurement*

All healthy volunteers were instructed to perform twelve functional tasks of daily living and four ROM by their dominant arms at a speed and manner with which they felt comfortable, see Figure (5.7). Each task began and finished in the "neutral position". All movements were performed seated on a stool in order to isolate the movement of the arm from that of the trunk. A more detailed description of the shoulder complex movement during these tasks performed during hygiene, feeding and reaching activities is illustrated below:

***Reach to opposite axilla;*** during this task, the clavicle elevates then depresses. The AC joint rotates laterally then medially, and tilts posteriorly then anteriorly. The GH joint elevates then depresses and rotates externally then internally. Relative to the thorax, the scapula rotates laterally then medially, and tilts posteriorly then anteriorly, whilst the humerus elevates and depresses, rotating axially externally then internally.

***Reach to opposite side of neck;*** during this task, the thorax rotates axilla to the left then to the right on returning. The SC joint elevates. The AC joint tilts posteriorly, with slight medial rotation. The GH joint elevates, rotating externally. The scapula protracts, rotates laterally and tilts posteriorly with respect to the thorax whilst the humerus elevates and rotates externally axially.

***Reach to side and back of head;*** during this task, the thorax relative to the global coordinate system (GCS) exhibits extension followed by flexion, and left and right

lateral flexion. The SC joint exhibits retraction and elevation followed by protraction and depression. The AC joint protracts, rotates laterally and tilts posteriorly, then returns. The GH joint elevates, rotating externally. Relative to the thorax, the scapula retracts and rotates laterally, whilst the humerus elevates, rotating externally axially.

***Eat with hand to mouth*;** during this task, the position of the thorax remains fairly constant. The SC joint retracts and elevates, whilst the AC joint tilts posteriorly. The GH joint elevates and rotates externally. The scapula tilts posteriorly and rotates laterally and the humerus elevates and rotates externally relative to the thorax.

***Drink from a mug;*** during this task, the thorax moves to quite an extent, caused by having to reach to the table to pick up the mug. It flexes on reaching to the table, extends when raising the mug to the mouth, then flexes again as the mug is placed on the table. It also rotates axilla both left and right and flexes laterally both left and right. The SC joint retracts, protracts then retracts again, whilst the AC joint tilts posteriorly. The GH joint elevates and rotates externally, as does the humerus relative to the thorax. The scapula protracts when reaching forwards, retracts then protracts again, whilst rotating laterally and tilting posteriorly.

***Answer phone*;** during this task, the thorax flexes, rotates axially and flexes laterally both left and right. The SC joint retracts and protracts, and the AC joint tilts posteriorly and anteriorly. The GH joint repeatedly elevates and depresses, rotating axially both internally and externally, as does the humerus relative to the thorax, although extension is to a lesser extent. The scapula relative to the thorax repeatedly retracts and protracts.

***Cross body;*** during this task, the thorax rotates axilla to the left then to the right on returning. The SC joint elevates. The AC joint tilts posteriorly, with slight medial rotation. The GH joint elevates, rotating externally. The scapula protracts, rotates laterally and tilts posteriorly with respect to the thorax whilst the humerus elevates and rotates externally axially.

***Brush opposite side of head*;** during this task, the thorax remains fairly steady for all subjects. With each stroke of the comb there is elevation and depression of the SC joint, posterior and anterior tilt along with lateral and medial rotation of the AC joint, and elevation and depression of the GH joint; although external rotation of this joint

remains fairly constant. Also the scapula retracts and protracts whilst tilting posteriorly and anteriorly with each stroke.

***Clean upper back;*** during this task, the thorax relative to the global coordinate system (GCS) exhibits extension followed by flexion, and left and right lateral flexion. The SC joint exhibits retraction and elevation followed by protraction and depression. The AC joint protracts, rotates laterally and tilts posteriorly, then returns. The GH joint elevates, rotating externally. Relative to the thorax, the scapula retracts and rotates laterally, whilst the humerus elevates, rotating externally axially.

***Lift object (20 N) to shoulder height*;** during this task, the thorax showed very slight extension, and axial rotation to the right in the middle of the task. The SC joint protracted whilst the AC joint held a fairly constant position, although showed posterior tilt in the middle of the task for some subjects. The GH joint elevated and exhibited both internal and external rotation. The scapula relative to the thorax protracted and tilted posteriorly in the middle of the task for most subjects. The humerus relative to the thorax showed elevation and external axial rotation for the middle of the task.

***Lift object (20 N) to head height*;** during this task, the thorax axially rotated to the right then to the left. The SC joint retracted as the object was being raised, protracted as it was placed on the shelf, then retracted again on returning to the side of the body. The AC joint tilted posteriorly whilst the GH joint elevated and externally rotated. Relative to the thorax, the scapula rotated laterally, tilted posteriorly and protracted as the object was place on the shelf.

***Internal/External Rotation*;** during external rotation, the thorax extends and flexes to the right. The SC joint retracts and depresses and the AC joint tilts posteriorly. The GH joint rotates externally, as does the humerus relative to the thorax and the scapula retracts and tilts anteriorly. Internal rotation was performed by reaching as far up the back as possible with the thumb pointing upwards.

***Abduction/Adduction;*** during abduction the thorax extends in global space, whilst flexing laterally and rotating axially to the right. The SC joint retracts and elevates. The AC joint protracts, rotates laterally and tilts posteriorly. The GH joint elevates and rotates externally, and the scapula retracts, rotates laterally and tilts posteriorly.

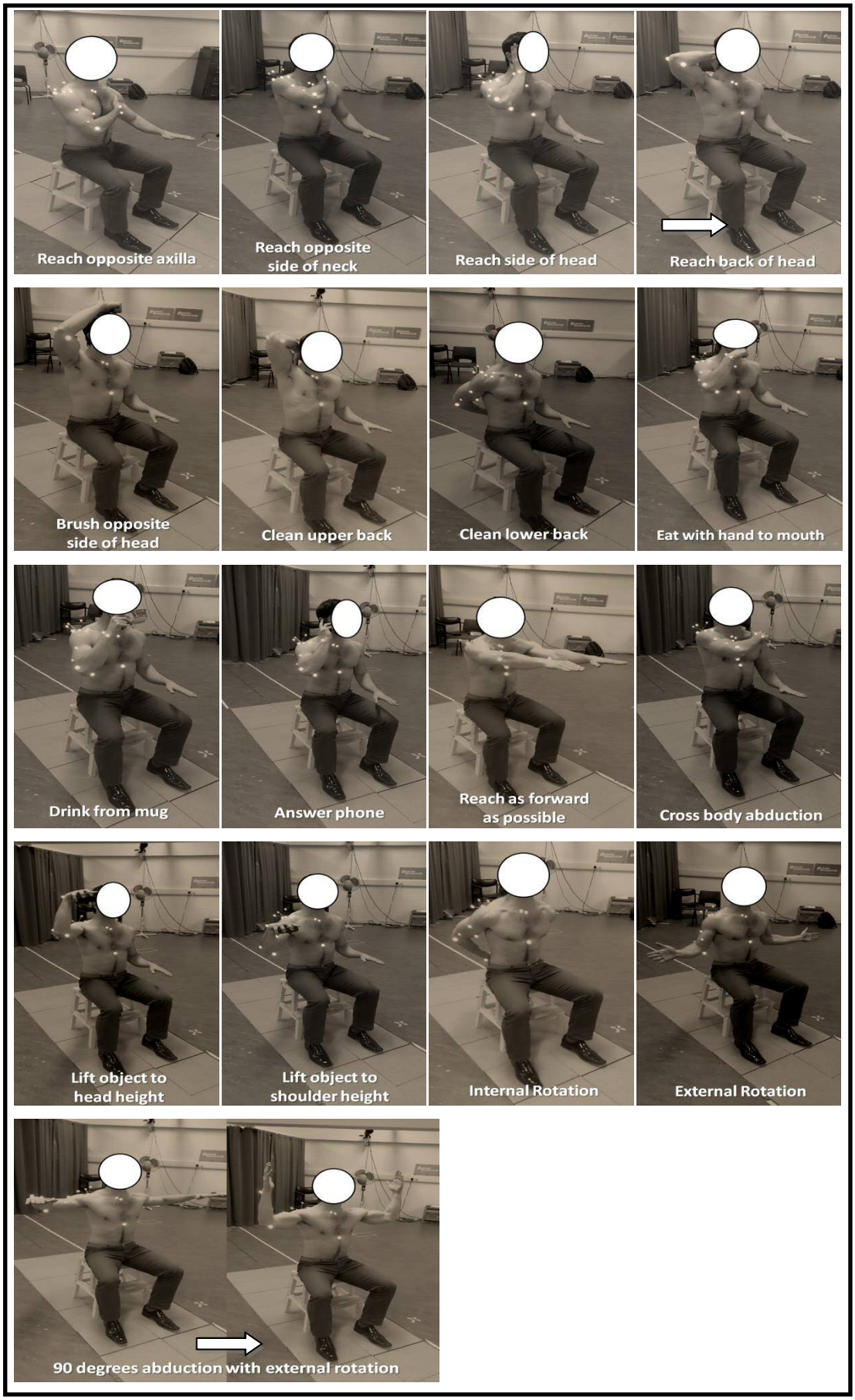


**Figure (5.7)**: Activities of daily living and range of motion tasks.

### *5.6.4. Physiological Range of Motion Measurement*

All the healthy volunteers performed static and dynamic trials starting with arm elevations by the side of the body up to 180° in increments of 20° in the coronal 0° plane (abduction), scapular 30° plane (scaption), and sagittal 90° plane (flexion), see Figure (5.8). Elevations were performed unilaterally with dominant arm, with the thumb pointing upwards for coronal and scapular plane elevation, and with the hand pronated for sagittal plane elevation.

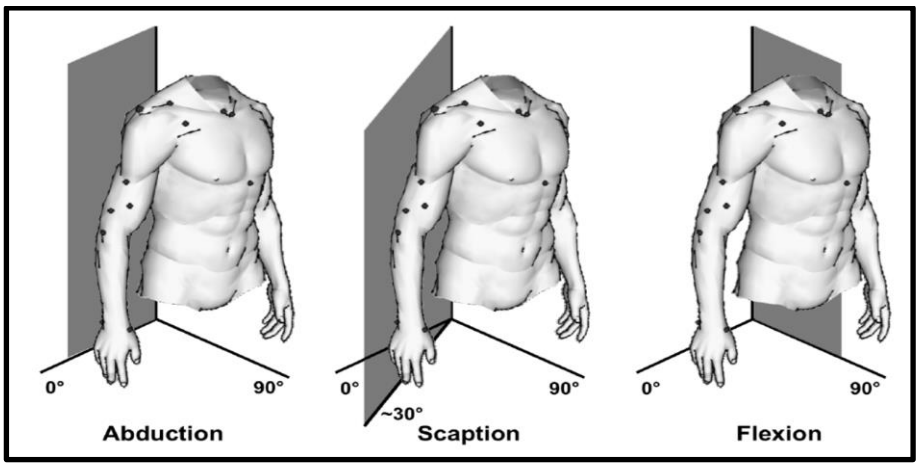


**Figure (5.8)**: Illustration of arm elevation in the coronal 0° plane (abduction), scapular plane 30° (scaption) and sagittal plane 90° (flexion), (Stroud 2011).

An external reference frame fitted with retro-reflective markers was used to guide the arm elevation at 20° intervals in the different planes and assist in post experimental data acquisition. A mirror is placed in front of subjects to aid in identification of the required angle on the frame during static recordings and also to maintain their posture throughout each measurement, see Figure (5.9).

Healthy volunteers were instructed to perform unilateral physiological arm elevation in abduction, scaption and flexion in a seated, upright position (their backs unsupported) with elbows fully extended. Throughout arm abduction and scaption, subjects maintain a supinated arm (the palm of the hands is facing forwards as the arm is being elevated). During flexion elevation measurements, subjects performed the movements with the forearm pronated (palm of hands facing backwards, downwards and forwards as the arm is being elevated). An additional skin marker is attached on the tip of middle finger as an indicator, see Figures (5.10), (5.11) and (5.12).

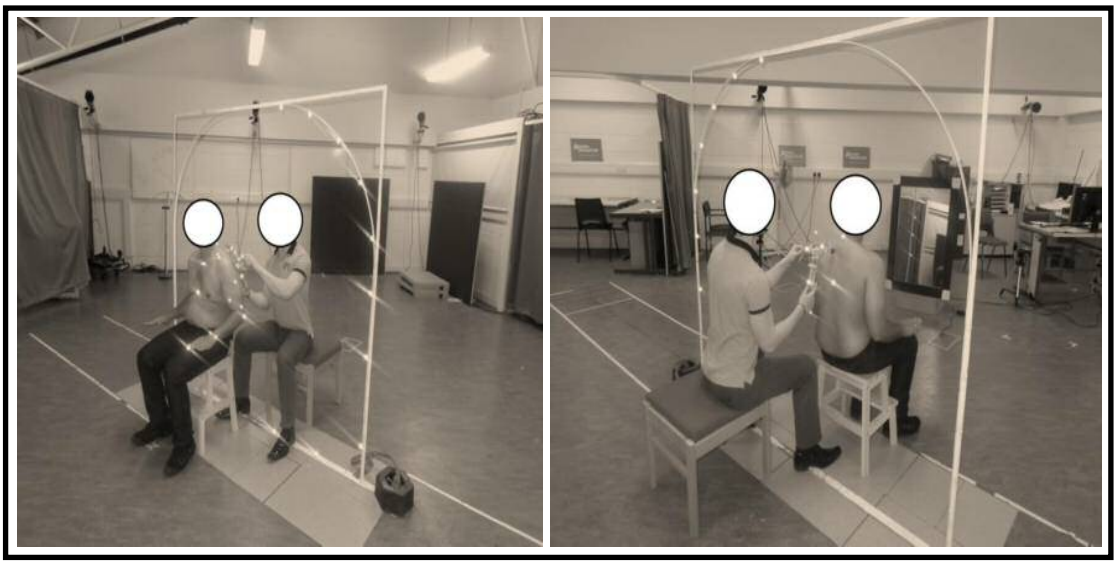

**Figure (5.9)**: Anterior (Left) and posterior (Right) views of participant's positioning and measurement frame during one second recording of neutral position measurement.

Subjects performed each elevation in increments of 20° of the external frame. Static measurements were taken at each increment using a scapula locator with markers attached to represent each of the three scapula bony landmarks. Individual skin mounted markers were then attached to each of the scapula bony landmarks with the subject in a neutral position measurement. Elevations in the coronal, scapular and sagittal planes were then repeated dynamically using skin mounted markers.

Kinematic descriptions of the shoulder complex were recorded for the dominant arms of the five volunteers during static arm elevations in the coronal, scapular, and sagittal planes. Scapula orientation during the static elevations was measured with individual skin mounted markers were attached to each of the scapula bony landmarks, and a scapula locator. The static rotations measured for each articulation were divided into 20° increments of humerothoracic elevation (0° - 20°; 20° - 40°; 40° - 60°; 60° - 80°; 80° - 100°; 100° - 120°; 120° - 140°; 140° - 160° and 160° - 180°). This provides a visual reference to determine what rotations can be measured accurately with the acromion cluster, and during which levels of arm elevation and planes of elevation this is possible.

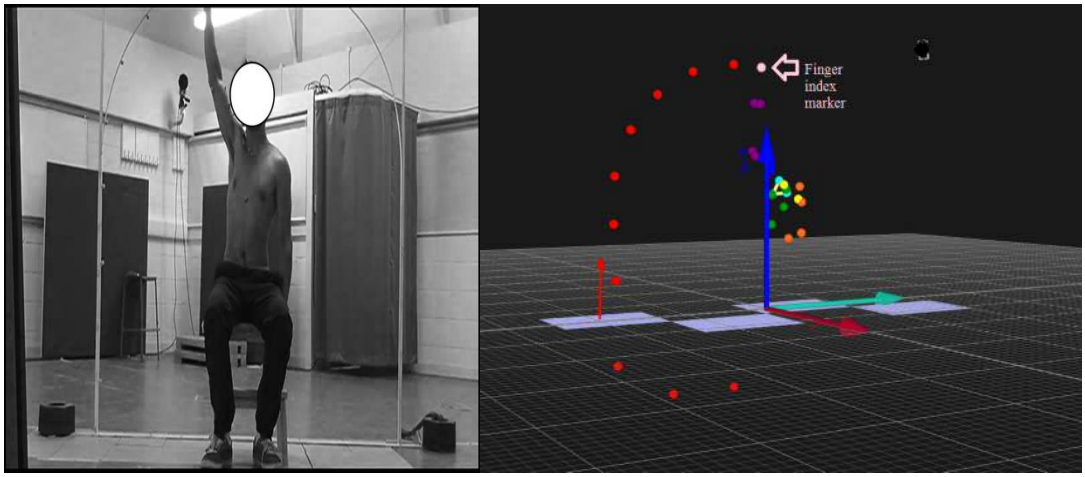


**Figure (5.10)**: A healthy volunteer elevates arm using guidance frame in the coronal plane (0° abduction plane) to 180° humerothoracic elevation; in the real view (Right), and in the Qualysis Track Manager QTM view (Left).

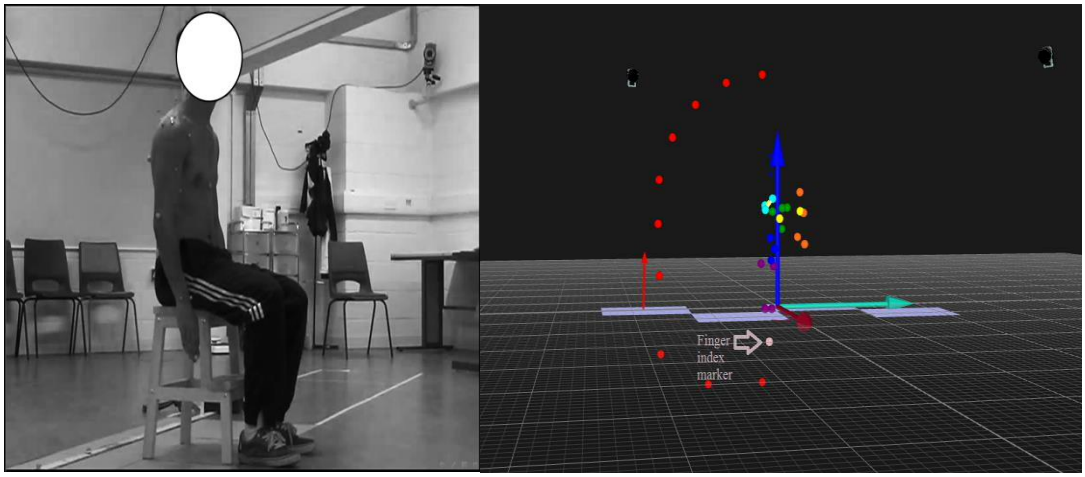


**Figure (5.11)**: A healthy volunteer elevates arm using guidance frame in the sagittal plane (90° flexion plane) to 0° humerothoracic elevation; in the real view (Right), and in the Qualysis Track Manager QTM view (Left).

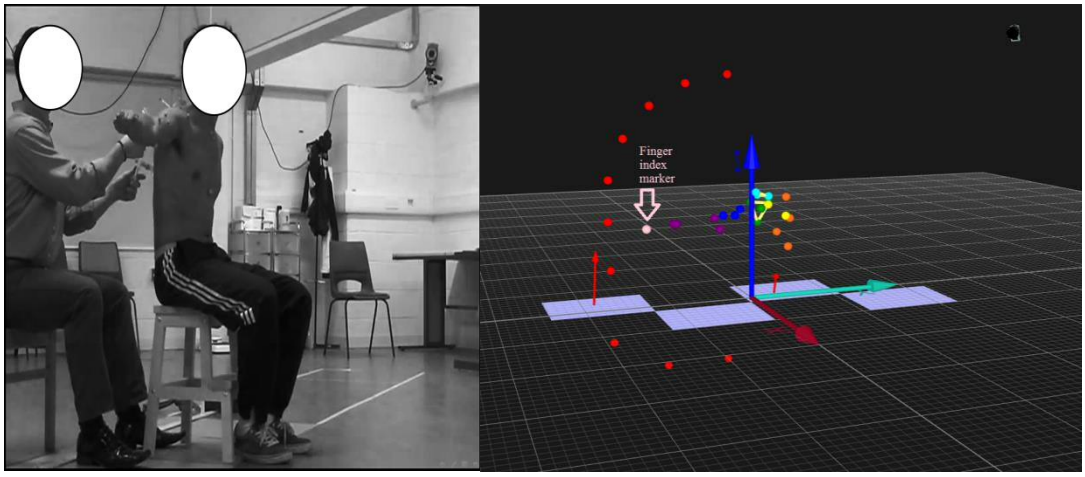


**Figure (5.12)**: A healthy volunteer elevates arm using guidance frame and scapula locator in the scapular plane (30° scaption plane) to 80° humerothoracic elevation; in the real view (Right), and in the Qualysis Track Manager QTM view (Left).

## 5.7 Shoulder complex segments rotations calculations

In the shoulder complex, it can be useful to describe two types of rotations in the shoulder complex: joint rotation and segment rotation. Joint rotation is the rotation of a bone segment with respect to the proximal articulating segment (e.g. SC, AC, ST and GH joints); whereas segment rotation is the rotation of any segment relative to the thorax (humerus relative to the thorax). Many rotation orders are possible such as X-Y-Z in Cardan angles or Y-Z-Y in Euler angles. Rotation orders follow the recommendations of the ISB, which were chosen so that angles remain as close as possible to clinical definitions of joint and segment rotations, (Zatsiorsky 1998).

The fixed body axes established during the anatomical calibration are similarly computed during the movement trials to track the position and pose of the four segments relative to the GCS. A transformation matrix, relating the different anatomical systems, is constructed for every frame of data. Joint rotations are described as the movement of the distal segment relative to the proximal segment using either Euler or Cardan angles. The first rotation is around one of the common axes, and the second and third rotations are expressed around the rotated axes of the moving coordinate system.

Once the position of the markers throughout all movements had been collected in the motion analysis laboratory, the data could then be processed to determine the positions of the local reference systems within the global reference system and hence the angles and ranges of motion for each body segment. The data for each marker was identified, labelled and gap filled (when it is necessary) then been exported from QTM as tab separated variable (tsv) files. Columns represent the X, Y, and Z positions of each marker in the GCS. Rows represent time. For example, a one second measurement at 60 Hz would have 60 rows of data.

In this study, two methods were applied to calculate the three-dimensional kinematics of the shoulder complex:

***(1) Matrix decomposition method*** by using custom Matlab software (Stroud, 2012).

***(2) 6DOF analysis method*** by using the Qualisys tracking manager software.

Through both methods, the kinematics outputs were saved in Excel files. Each column represents a joint or segment rotation in the same order as how is described above. The rows represent the frames. The outputs are subsequently input into a different Excel file with a saved template for further manipulation.

### *5.7.1. Matrix Decomposition Method*

Shoulder complex kinematics was calculated through matrix decomposition following the sequence of rotation summarised in the shown below table (5.2). The method uses elements from the joint transformation matrices to provide a geometric description of the joint and segment rotations. Illustration of the shoulder complex segments rotations are shown in the below figure (5.13).

A custom Matlab software (Mathworks, Natick, MA, United States) was developed by Stroud (2011) and used to generate the anatomical coordinate systems for each joint and segment and to calculate the joint and body segment rotations according to the lSB recommendations, (Wu et al. 2005).

The Matlab software firstly estimated the position of the GH, allowing the Local Coordinate System (LCS) to be set up. Following this, the transformation matrices describing the location and rotation of the LCSare determined, and hence the Euler's angles are calculated.

A schematic flow diagram of the software used to process the data is shown in Figure (5.14). An explanation of the functions and variables used in each of these flow diagrams is available in the appendix.

**Table (5.2)**: Shoulder complex segments rotation calculations as recommended by the ISB.

| Segment Rotation | Transformation Matrix and Joint Rotation Euler Sequence | 1st Rotation | 2nd Rotation | 3rd Rotation |
|---|---|---|---|---|
| **Thorax relative to Global Coordinate System GCS** | **$[T_{ag};T]$**<br>***Z-X-Y*** | **Flexion – Extension**<br>*The thorax rotations around the coincident GCS Z and $z_T$ axes.*<br>**$\alpha_{TG} = -\tan^{-1}(T_{12}/T_{22})$**<br>$T_{12}$: projection of $Y_T$ onto GCS X axis<br>$T_{22}$: projection of $Y_T$ onto GCS Y axis<br>*The angle between $y_T$and GCS Y axis in the sagittal plane.*<br>**Flexion (-) Extension (+)** | **Lateral Rotation**<br>*The thorax rotations around the $x_T$ axis.*<br>**$\beta_{TG} = \mathrm{Sin}^{-1}(T_{32})$**<br>$T_{32}$: projection of $Y_T$ onto GCS z-axis<br>*The angle between $y_T$and GCS Y axis in the frontal plane.*<br>**right lateral flexion (+)**<br>**left lateral flexion (-)** | **Axial Rotation**<br>*The thorax rotations around the $y_T$ axis.*<br>**$\gamma_{TG} = -\tan^{-1}(T_{31}/T_{33})$**<br>$T_{31}$: projection of $X_T$ onto GCS z-axis<br>$T_{33}$: projection of $Z_T$ onto GCS z-axis<br>*The angle between $x_T$and GCS X axis in the transverse plane.*<br>**left axial rotation (+) right axial rotation (-)** |
| **Clavicle relative to Thorax Sternoclavicular (SC) Joint** | **$T_{SC} = [T_{ga};T][T_{ag};C]$**<br>***Y-X-Z*** | **Protraction – Retraction**<br>*The clavicle rotations around the coincident $y_T$ and $y_C$ axes.*<br>**$\alpha_{SC} = \tan^{-1}(T_{13}/T_{33})$**<br>$T_{13}$: projection of $z_C$ onto $x_T$<br>$T_{33}$: projection of $z_C$ onto $z_T$<br>*The angle between $z_C$and$z_T$ axes in the transverse plane.*<br>**retraction (-) protraction (+)** | **Elevation - Depression**<br>*The clavicle rotations around $x_C$ axis.*<br>**$\beta_{SC} = -\mathrm{Sin}^{-1}(T_{23})$**<br>$T_{23}$: projection of $z_C$ onto $y_T$<br>*The angle between $z_C$and$z_T$ axes in the frontal plane.*<br>**elevation (-) depression (+)** | **$\gamma_{SC}$**<br>**backward axial rotation (+)**<br>**forward axial rotation (-)** |
| **Scapula relative to Clavicle Acromioclavicular (AC) Joint** | **$T_{AC} = [T_{ga};C][T_{ga};S]$**<br>***Y-X-Z*** | **Protraction – Retraction**<br>*The scapula rotations around the coincident $y_S$ and $y_C$ axes.*<br>**$\alpha_{AC} = \tan^{-1}(T_{13}/T_{33})$**<br>$T_{13}$: projection of $z_S$ onto $x_C$<br>$T_{33}$: projection of $z_S$ onto $z_C$<br>*The angle between $z_S$and$z_C$ axes in the transverse plane.*<br>**retraction (-) protraction (+)** | **Internal-External Rotation**<br>*The scapula rotations around the $x_S$ axis.*<br>**$\beta_{AC} = -\mathrm{Sin}^{-1}(T_{23})$**<br>$T_{23}$: projection of $z_S$ onto $y_C$<br>*The angle between $z_S$and$z_C$ axes in the frontal plane.*<br>**external rot. (-) internal rot. (+)** | **Anterior-Posterior Tilt**<br>*The scapula rotations around the $z_S$ axis.*<br>**$\gamma_{AC} = \tan^{-1}(T_{21}/T_{22})$**<br>$T_{21}$: projection of $x_S$ onto $y_C$<br>$T_{22}$: projection of $y_S$ onto $y_C$<br>*The angle between $x_S$and$x_C$ axes in the sagittal plane.*<br>**anterior tilt (-) posterior tilt (+)** |

| | | | | |
|---|---|---|---|---|
| **Humerus relative to Scapula**<br>**Glenohumeral (GH) Joint** | $T_{GH} = [T_{ga};S][T_{ag};H]$<br>***Y-X-Y*** | **GH Plane of Elevation**<br>*The humerus rotation around the coincident $y_S$ and $y_H$ axes.*<br>$\alpha_{GH} = \tan^{-1}(T_{12}/T_{32})$<br>$T_{12}$: projection of $y_H$ onto $x_S$<br>$T_{32}$: projection of $y_H$ onto $z_S$<br>*The angle between $x_S$ and $x_H$ axes.*<br>**plane of elevation (-)** | **GH Elevation**<br>*The humerus rotation around $x_H$ axis.*<br>$\beta_{GH} = \cos^{-1}(T_{22})$<br>$T_{22}$: projection of $y_H$ onto $y_S$<br>*The angle between $y_S$ and $y_H$ axes.*<br>**elevation (-)** | **GH Axial Rotations**<br>*The humerus rotation around $y_H$ axis.*<br>$\gamma_{GH} = -\tan^{-1}(T_{21}/T_{23})$<br>$T_{21}$: projection of $z_H$ onto $y_S$<br>$T_{23}$: projection of $z_H$ onto $y_S$<br>*The angle between $z_S$ and $z_H$ axes.*<br>**internal rotation (+)**<br>**external rotation (-)** |
| **Scapula relative to Thorax**<br>**Scapulothoracic (ST) Articulation** | $T_{ST} = [T_{ga};S][T_{ag};T]$<br>***Y-X-Z*** | **Protraction – Retraction**<br>*The scapula rotations around the coincident $x_S$ and $x_T$ axes.*<br>$\alpha_{ST} = \tan^{-1}(T_{13}/T_{33})$<br>$T_{13}$: projection of $z_S$ onto $x_T$<br>$T_{33}$: projection of $z_S$ onto $x_T$<br>*The angle between $z_S$ and $z_T$ axes in the transverse plane.*<br>**retraction (-)**<br>**protraction (+)** | **Internal-External Rotation**<br>*The scapula rotations around $x_S$ axis.*<br>$\beta_{ST} = -\sin^{-1}(T_{23})$<br>$T_{23}$: projection of $z_S$ onto $y_T$<br>*The angle between $z_S$ and $z_T$ axes in the frontal plane.*<br>**External rot. (-)**<br>**internal rot. (+)** | **Anterior-Posterior Tilt**<br>*The scapula rotations around $z_S$ axis.*<br>$\gamma_{ST} = \tan^{-1}(T_{21}/T_{22})$<br>$T_{21}$: projection of $x_S$ onto $y_T$<br>$T_{22}$: projection of $y_S$ onto $y_T$<br>*The angle between $x_S$ and $x_T$ axes in the sagittal plane.*<br>**anterior tilt (-)**<br>**posterior tilt (+)** |
| **Humerus relative to thorax**<br>**Humerothoracic (HT) Rotation** | $T_{HT} = [T_{ga};H][T_{ag};T]$<br>***Y-X-Y*** | **Plane of Elevation**<br>*The humerus rotation around the coincident $y_H$ and $y_T$ axes.*<br>$\alpha_{HT} = \tan^{-1}(T_{12}/T_{32})$<br>$T_{12}$: projection of $y_H$ onto $x_T$<br>$T_{32}$: projection of $y_H$ onto $z_T$<br>*The angle between $x_H$ and $x_T$ axes.*<br>**plane of elevation (-)** | **Elevation**<br>*The humerus rotation around $x_H$ axis.*<br>$\beta_{HT} = -\cos^{-1}(T_{22})$<br>$T_{22}$: projection of $y_H$ onto $y_T$<br>*The angle between $y_H$ and $y_T$ axes in the sagittal plane.*<br>**elevation (-)** | **Axial Rotations**<br>*The humerus rotations around $y_H$ axis.*<br>$\gamma_{HT} = -\tan^{-1}(T_{21}/T_{23})$<br>$T_{21}$: projection of $x_H$ onto $y_T$<br>$T_{23}$: projection of $z_H$ onto $y_T$<br>*The angle between $z_H$ and $z_T$ axes.*<br>**internal rotation (+)**<br>**external rotation (-)** |

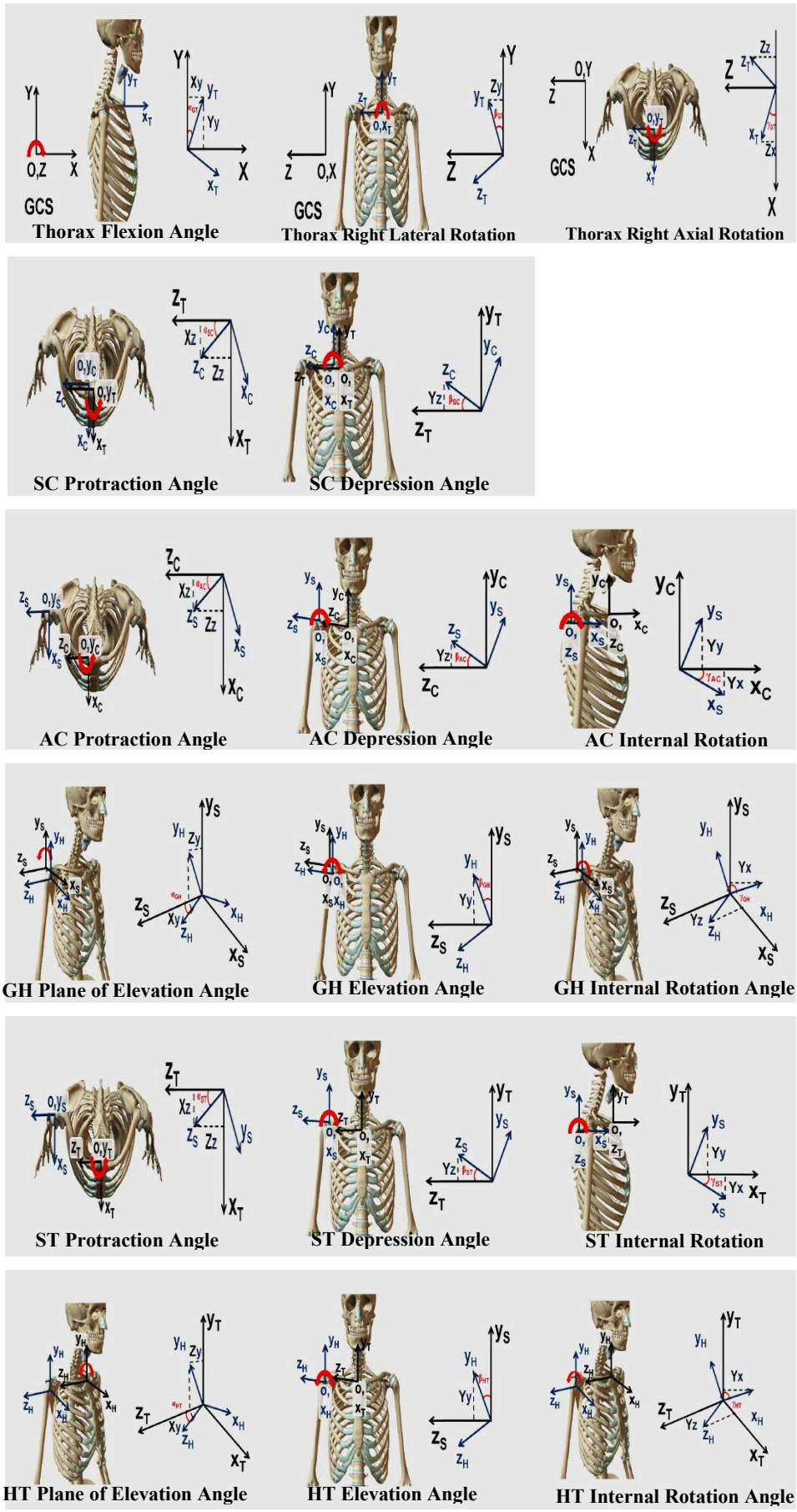


**Figure (5.13)**: Shoulder complex segments rotation calculations as recommended by the ISB, (Stroud 2011).

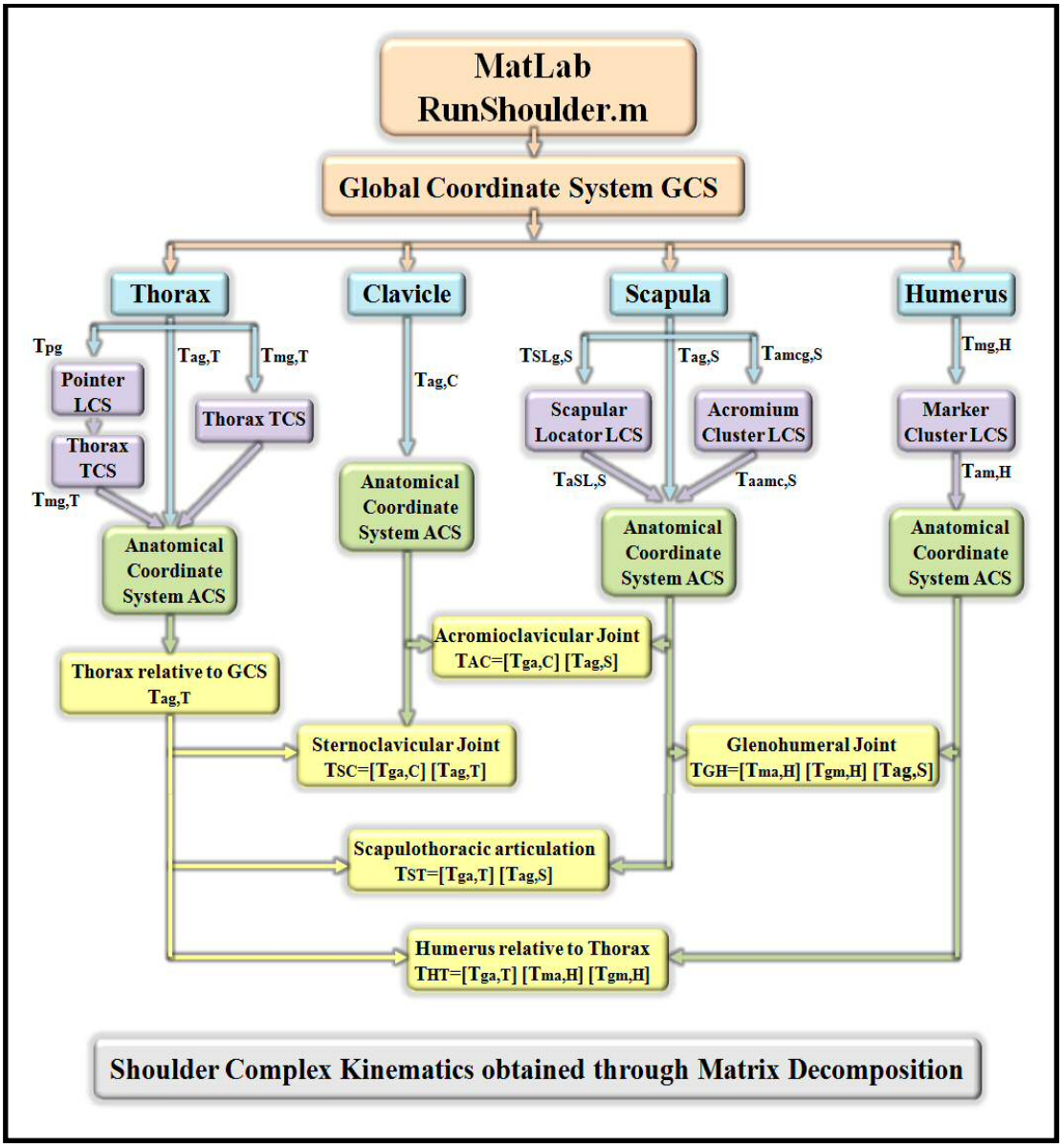


**Figure (5.14)**: A schematic flow diagram of the software used to calculate the kinematics of the shoulder complex using matrix decomposition.

### 5.7.2. Six Degrees of Freedom (6DOF) Analysis

Six degrees of freedom (6DOF) refers to the freedom of movement of a rigid body in three-dimensional space. Specifically, the body can move forward/backward, up/down, left/right (translation in three perpendicular axes) combined with rotation about three perpendicular axes (X, Y and Z), often termed roll, pitch, and yaw respectively. Positive rotation is defined as clockwise rotation when looking in the direction of the axis. The angles are applied to the LCS in the order; roll, pitch and finally yaw. Therefore to find the rotation of a rigid body with given rotation angle from QTM, the rotations are applied in the same order. Also, QTM uses the following default ranges for the angles:-180° ≤ Roll ≤ 180°, -90° ≤ Pitch ≤ 90°, and -180° ≤ Yaw ≤ 180°.In these ranges, roll, pitch and yaw are unambiguous and can describe any orientations of a rigid body, (Qualisys 2011).

QTM uses the rotation matrix internally to describe the rotation of rigid bodies, and when exporting 6DOF to TSV files the rotation matrix is included for all bodies in all frames, together with roll, pitch and yaw angles. Below follows an example to show the definitions of the rotation angles. It starts with a 6DOF body, which is in alignment with the global coordinate system, see Figure (5.15), (Qualisys 2011).

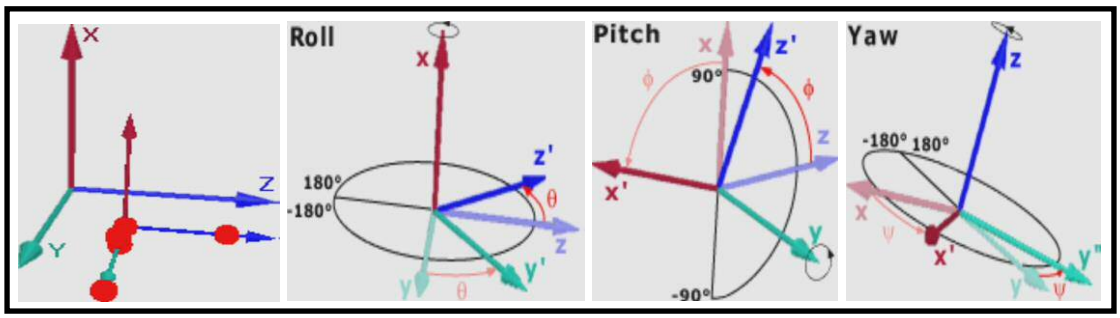


**Figure (5.15)**: The six degrees of freedom: forward/back, up/down, left/right, roll, pitch, and yaw, (Qualisys 2011).

First, the LCS is rotated around the X-axis (roll) with an angle ɵ to the new positions y' and z' of the Y- and Z-axis. After the roll the LCS rotates around the Y-axis (pitch) with the Y-axis in its new position. The X- and Z-axis is rotated with an angle ϕ to the new positions x' and z'. Finally the LCS is rotated around the Z-axis (yaw) with the Z-axis in its final position. The X- and Y-axis is rotated with an angle ɯ to the new positions x' and y', (Qualisys 2011).Any possible movement of a rigid

body, no matter how complex it is, can be expressed in terms of basic six degree of freedom (6DOF) model.

In terms of establishing a six degrees of freedom 6DOF analysis for three-dimensional kinematics of the shoulder complex, four rigid bodies were defined with eleven identified skin markers located on the thorax (C7, T12, IJ and PX), scapula (TS, AI, AA and PC), humerus (DI, BB and BI) and forearm (EL, EM, RS and US). 6 DOF data (roll, pitch, yaw, x, y, z) were calculated according to the ISB recommendations by using the QTM software, (QTM Software, Qualisys, Sweden). Segment coordinate systems were determined for thorax with respect to the laboratory's global coordinate system (GCS), scapula with respect to the thorax, humerus with respect t6o the scapula, humerus with respect to the thorax and humerus with respect to the forearm using Euler angle notation and a sequence of ZXY rotations of the trunk, scapula and humerus, and ZYX rotations of the forearm.The rotation order of the humerus relative to the thorax was ZXY order, rather than the YXY order. As a result, the 6DOF analysis has included five rigid bodies, see Figure (5.16).

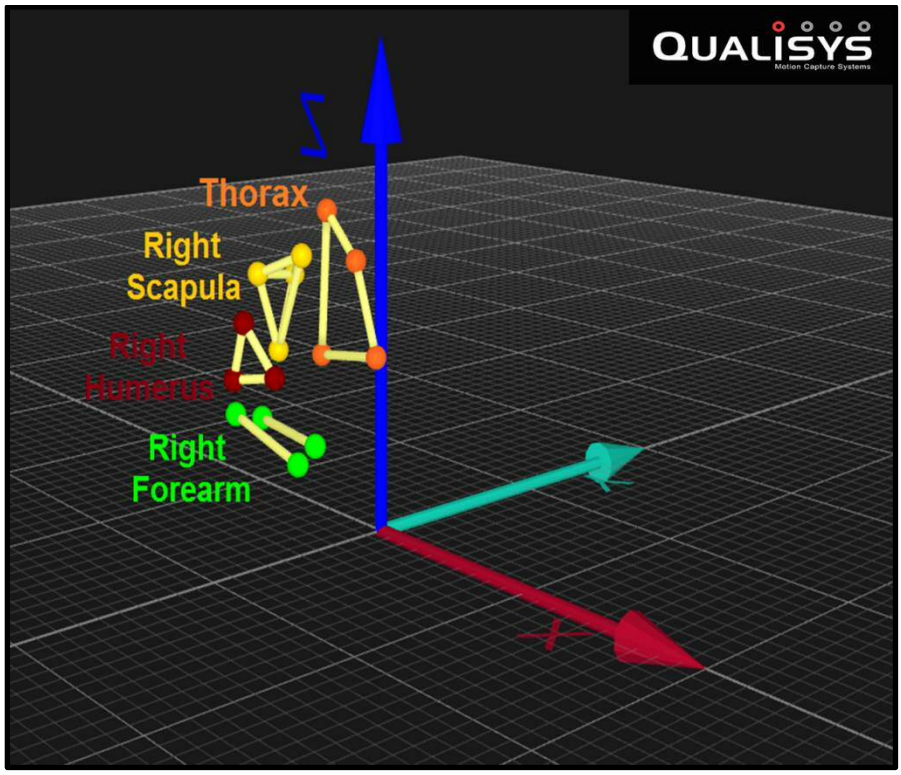


**Figure (5.16)**: A QTM view of a 6DOF model of the thorax, right scapula, humerus and forearm during neutral position.

The analysis for dominant shoulder complex joint angles and segment LCS was applied through the QTM software following the ISB standardisation protocol (Wu et al. 2005). The axes of each segment's LCS are aligned such that the X-axis directs anteriorly, the Y-axis directs superiorly and the Z-axis directs laterally towards the right side. To define an orthogonal LCS to a rigid body segment, the co-ordinates of three non-collinear points within the segment must be known. The coordinate system is thus defined by the three mutually orthogonal unit vectors.The joint angles were determined by the relative motion between two adjacent segments, distal relative to proximal, following the right hand rule with the X-axis as the abduction/adduction axis, the Y-axis as the internal/external rotation axis and the Z-axis as the flexion/extension axis, (Zatsiorsky 1998).

## 5.8 Results

Complete kinematics descriptions of the dominant arm shoulder complex were calculated for the five recruited volunteers using both methods of matrix decomposition and 6DOF analysis. The mean and standard deviation values of the ROM for each joint rotation during the activities of daily living and arm elevation were analysed. To compare the results between the matrix decomposition and 6DOF analysis methods, parametric repeated measures were used since the data were normally distributed. The statistical analyses were employed by using repeated two ways ANOVA and Person's correlation coefficient. P-value was calculated. Descriptive statistics were calculated for each variable. The level of significance was set at $P< 0.05$ for all statistical analyses.

The average joint rotations ROM during the 16 activities of daily living (ADLs) and for dynamic arm elevation in the coronal, scaption and sagittal planes of motion are summarised below in Tables (5.3), (5.4), (5.5) and (5.6) and shown in Figures (5.17) to (5.28). Also, complete kinematics descriptions of each dominant arm shoulder complex were calculated through the matrix decomposition method for static arm elevation with skin mounted markers and scapula locator during abduction, scaption and flexion. The values of ROMs and SD are summarised in the shown below table (5.7).

**Table (5.3)**: Complete shoulder complex 3D kinematics (mean±standard deviation) calculated by matrix decomposition method for 16 activities of daily living.

| **Shoulder Complex Joints Kinematics (°)** | | Reach to opposite axilla | Reach opposite side of neck | Reach side and back of head | Brush opposite side of head | Clean upper back | Clean lower back | Eat with hand to mouth | Drink from mug |
|---|---|---|---|---|---|---|---|---|---|
| Thorax relative to GCS | Flexion Extension | 1.96 ± 0.53 | 1.81 ± 0.68 | 2.44 ± 1.41 | 5.76 ± 3.51 | 18 ± 3.70 | 12.15 ± 3.65 | 4.04 ± 1.46 | 4.21 ± 3.44 |
| | Lateral Bending | 1.24 ± 0.25 | 2.00 ± 0.74 | 2.13 ± 0.74 | 3.40 ± 1.67 | 3.16 ± 0.62 | 6.41 ± 3.29 | 2.6 ± 1.73 | 1.52 ± 0.40 |
| | Axial Rotation | 3.15 ± 2.34 | 2.28 ± 0.93 | 2.51 ± 0.65 | 8.17 ± 3.77 | 9.15 ±3.83 | 7.55 ± 4.36 | 7.38 ± 2.39 | 6.26 ± 2.06 |
| SC Joint | Retraction Protraction | 4.79 ± 3.56 | 7.75 ± 3.50 | 23.8 ± 3.83 | 20.95 ± 7.26 | 48.50 ± 3.79 | 14.54 ± 3.69 | 15.33 ± 4.68 | 14.59 ± 5.97 |
| | Elevation Depression | 8.92 ± 6.26 | 13.66 ± 7.04 | 16.36 ± 4.30 | 18.84 ± 3.71 | 33.92 ± 2.60 | 9.76 ± 2.13 | 6.72 ± 2.24 | 6.82 ± 2.88 |
| AC Joint | Retraction Protraction | 7.40 ± 5.70 | 9.31 ± 4.74 | 10.58 ± 3.07 | 12.80 ± 2.17 | 35.43 ± 12.21 | 10.47 ± 3.44 | 6.27 ± 1.30 | 7.94 ± 1.64 |
| | Medial Lateral Rotation | 3.42 ± 2.03 | 10.10 ± 4.99 | 22.32 ± 1.63 | 15.72 ± 3.39 | 35.47 ± 9.30 | 7.90 ± 2.32 | 4.89 ± 1.78 | 4.65 ± 2.05 |
| | Anterior Posterior Tilt | 10.59 ± 7.40 | 17.19 ± 9.00 | 25.62 ± 6.03 | 23.60 ± 5.12 | 45.18 ± 22.34 | 9.12 ± 1.91 | 8.48 ± 2.78 | 9.65 ± 3.75 |
| GH Joint | Plane of Elevation | 26.49 ± 6.79 | 23.36 ± 7.73 | 53.84 ± 25.71 | 30.79 ± 8.38 | 159.21 ±23.12 | 40.40 ± 10.15 | 20.33 ± 13.88 | 19.52 ± 6.88 |
| | Elevation | 33.28 ± 4.06 | 46.49 ± 10.34 | 59.73 ± 11.54 | 62.70 ± 6.01 | 95.43 ± 14.93 | 36.87 ± 11.09 | 44.88 ± 13.38 | 46.64 ± 11.57 |
| | Axial Rotation | 22.89 ± 13.48 | 13.49 ± 8.23 | 24.42 ±9.53 | 30.78 ±6.06 | 150.46 ±60.38 | 57.56 ± 8.22 | 18.98 ± 12.21 | 20.26 ± 5.26 |
| ST Articulation | Retraction Protraction | 9.58 ±5.02 | 10.59 ± 4.06 | 8.40 ± 1.91 | 17.24 ± 3.14 | 28.39 ± 3.19 | 9.97 ± 3.62 | 13.76 ± 2.74 | 11.64 ± 2.24 |
| | Medial Lateral Rotation | 6.73 ±3.75 | 13.47 ±6.07 | 26.40 ±1.06 | 21.02 ±3.81 | 35.94 ±5.12 | 9.35 ±1.71 | 7.42 ±1.76 | 7.47 ±3.16 |
| | Anterior Posterior Tilt | 3.08 ±1.29 | 4.63 ±2.39 | 8.63 ±2.17 | 6.09 ±2.55 | 13.14 ±1.86 | 4.43 ±1.88 | 3.70 ±0.64 | 4.25 ±1.57 |
| HT Rotation | Plane of Elevation | 61.88 ± 22.69 | 47.79 ± 15.55 | 40.31 ± 9.67 | 39.79 ± 3.23 | 152.75 ±26.77 | 29.79 ± 9.55 | 29.29 ± 14.69 | 30.08 ± 6.72 |
| | Elevation | 28.38 ± 6.93 | 46.45 ± 10.99 | 89.23 ± 6.71 | 69.15 ± 12.67 | 119.22 ± 8.50 | 43.98 ± 2.48 | 44.10 ± 11.71 | 49.43 ± 2.96 |
| | Axial Rotation | 20.48 ± 6.20 | 12.74 ± 5.88 | 34.28 ± 10.38 | 25.38 ± 4.95 | 154.71 ±20.51 | 51.43 ± 16.06 | 18.91 ± 12.36 | 18.53 ± 7.47 |

| **Shoulder Complex Joints Kinematics (°)** | | Answer phone | Reach as far forward as possible | Lift block to shoulder height | Lift block to head height | Cross body abduction | Internal rotation | External rotation | 90º abduction with external rotation |
|---|---|---|---|---|---|---|---|---|---|
| Thorax relative to GCS | Flexion Extension | 6.58 ± 2.55 | 5.99 ± 3.29 | 5.73 ± 1.76 | 10.88 ± 4.42 | 5.03 ± 3.21 | 9.53 ± 4.29 | 15.34 ± 3.83 | 15.96 ± 6.50 |
| | Lateral Bending | 3.56 ± 1.04 | 1.79 ± 0.42 | 3.67 ± 0.62 | 8.88 ± 3.52 | 3.85 ± 1.95 | 6.73 ± 4.05 | 5.31 ± 3.18 | 4.77 ± 3.44 |
| | Axial Rotation | 10.65 ± 4.30 | 2.33 ± 0.99 | 7.59 ± 3.49 | 12.36 ± 6.37 | 22.54 ± 8.54 | 7.56 ± 6.94 | 9.67 ± 4.86 | 8.12 ± 4.29 |
| SC Joint | Retraction Protraction | 23.90 ± 7.12 | 19.49 ± 8.65 | 15.69 ± 4.66 | 23.25 ± 6.78 | 21.69 ± 8.01 | 10.60 ± 3.13 | 27.66 ± 10.80 | 45.68 ± 19.75 |
| | Elevation Depression | 9.89 ± 2.65 | 14.30 ± 8.08 | 15.36 ± 3.92 | 22.96 ± 10.65 | 29.83 ± 8.27 | 10.83 ± 3.65 | 11.29 ± 2.95 | 28.92 ± 16.67 |
| AC Joint | Retraction Protraction | 9.20 ± 1.40 | 10.22 ± 3.20 | 9.50 ± 0.99 | 13.76 ± 6.04 | 15.41 ± 8.38 | 4.36 ± 2.67 | 26.19 ± 2.97 | 28.44 ± 3.59 |
| | Medial Lateral Rotation | 9.15 ± 3.82 | 7.26 ± 1.85 | 12.23 ± 3.01 | 20.10 ± 4.25 | 14.86 ± 6.90 | 6.11 ± 2.22 | 12.06 ± 7.66 | 31.17 ± 9.92 |
| | Anterior Posterior Tilt | 10.80 ± 3.82 | 12.39 ± 7.80 | 18.29 ± 4.25 | 44.31 ± 31.00 | 24.29 ± 7.85 | 8.06 ± 3.28 | 12.99 ± 4.91 | 30.59 ± 6.76 |
| GH Joint | Plane of Elevation | 23.44 ± 9.31 | 14.49 ± 8.27 | 22.92 ± 12.53 | 38.85 ± 26.00 | 29.26 ± 9.49 | 33.01 ± 13.00 | 347.96 ±22.15 | 124.28±28.18 |
| | Elevation | 44.64 ± 10.08 | 77.79 ± 7.91 | 58.57 ± 16.03 | 73.31 ± 6.88 | 74.43 ± 6.71 | 18.95 ± 12.05 | 57.08 ± 20.37 | 63.78 ± 3.64 |
| | Axial Rotation | 25.28 ± 11.83 | 16.42 ± 4.03 | 21.23 ± 7.40 | 28.96 ± 15.99 | 16.06 ± 7.32 | 36.35 ± 12.54 | 366.37 ±29.97 | 128.56 ± 25.5 |
| ST Articulation | Retraction Protraction | 18.55 ± 4.63 | 19.58 ± 4.92 | 12.51 ± 4.02 | 16.17 ± 1.03 | 32.53 ± 9.26 | 8.06 ± 3.09 | 32.98 ± 11.00 | 26.31 ± 11.95 |
| | Medial Lateral Rotation | 12.02 ± 4.59 | 12.76 ± 5.94 | 17.12 ± 5.03 | 29.40 ± 5.60 | 23.23 ± 5.78 | 11.06 ± 5.09 | 15.73 ± 6.94 | 33.32 ± 8.58 |
| | Anterior Posterior Tilt | 4.49 ± 0.94 | 5.81 ± 2.76 | 5.24 ± 0.66 | 6.03 ± 0.70 | 7.14 ± 1.33 | 3.58 ± 1.45 | 6.50 ± 1.98 | 10.51 ± 2.09 |
| HT Rotation | Plane of Elevation | 28.30 ± 15.05 | 34.76 ± 12.46 | 29..08 ± 11.02 | 36.20 ± 20.74 | 69.97 ± 3.59 | 27.78 ± 8.18 | 175.85 ±37.90 | 87.48 ± 15.01 |
| | Elevation | 43.10 ± 11.04 | 73.83 ± 5.26 | 71.96 ± 18.31 | 93.71 ± 15.65 | 59.36 ± 17.68 | 32.75 ± 14.38 | 58.14 ± 27.66 | 87.06 ± 8.35 |
| | Axial Rotation | 25.86 ± 8.22 | 18.33 ± 3.53 | 23.15 ± 5.40 | 26.16 ± 4.25 | 18.73 ± 12.02 | 50.21 ± 20.73 | 122.06 ±45.27 | 107.16 ± 14.3 |

**Table (5.4)**: Complete shoulder complex 3D kinematics (mean±standard deviation) calculated by matrix decomposition method during arm elevation in the abduction, scaption and flexion planes of movement.

| **Shoulder Complex Joints Kinematics (°)** | | Abduction Plane (0°) | Scaption Plane (30°) | Flexion Plane (90°) |
|---|---|---|---|---|
| Thorax relative to GCS | Flexion Extension | 10.16 ± 2.12 | 6.96 ± 2.16 | 9.45 ± 3.90 |
| | Lateral Bending | 2.35 ± 1.30 | 2.13 ± 1.22 | 3.48 ± 1.72 |
| | Axial Rotation | 2.67 ± 0.70 | 2.50 ± 0.73 | 3.54 ± 1.46 |
| SC Joint | Retraction Protraction | 41.54 ± 6.87 | 41.62 ± 6.42 | 41.86 ± 4.31 |
| | Elevation Depression | 25.02 ± 5.28 | 25.31 ± 8.10 | 20.21 ± 4.48 |
| AC Joint | Retraction Protraction | 33.21 ± 10.07 | 43.95 ± 23.21 | 29.98 ± 6.87 |
| | Medial Lateral Rotation | 43.16 ± 3.43 | 40.45 ± 6.95 | 38.49 ± 3.04 |
| | Anterior Posterior Tilt | 39.62 ± 5.52 | 39.81 ± 9.21 | 34.06 ± 4.86 |
| GH Joint | GH Plane of Elevation | 154.31 ± 62.54 | 180.99 ± 35.90 | 43.45 ± 11.82 |
| | GH Elevation | 93.77 ± 12.51 | 91.04 ± 15.14 | 90.67 ± 9.67 |
| | GH Axial Rotation | 183.43 ± 40.33 | 170.26 ± 48.04 | 50.74 ± 9.35 |
| ST Articulation | Retraction Protraction | 17.42 ± 8.77 | 20.63 ± 5.74 | 16.79 ± 5.91 |
| | Medial Lateral Rotation | 45.12 ± 4.09 | 41.49 ± 5.28 | 41.25 ± 4.91 |
| | Anterior Posterior Tilt | 8.88 ± 2.29 | 8.47 ± 2.51 | 9.69 ± 2.18 |
| HT Rotation | Plane of Elevation | 122.68 ± 28.17 | 120.63 ± 20.44 | 74.27 ± 15.47 |
| | Elevation | 135.40 ± 10.17 | 132.89 ± 9.08 | 129.28 ± 8.02 |
| | Axial Rotation | 130.00 ± 25.59 | 133.01 ± 36.32 | 94.80 ± 24.33 |

**Table (5.5)**: Complete shoulder complex 3D kinematics (mean±standard deviation) calculated by 6DOF analysis method for 16 activities of daily living.

| **Shoulder Complex Joints Kinematics (°)** | | Reach to opposite axilla | Reach opposite side of neck | Reach side and back of head | Brush opposite side of head | Clean upper back | Clean lower back | Eat with hand to mouth | Drink from mug |
|---|---|---|---|---|---|---|---|---|---|
| Thorax relative to GCS | Flexion Extension | 2.18 ± 1.34 | 3.40 ± 1.79 | 1.82 ± 0.69 | 4.01 ± 2.98 | 16.87 ± 5.53 | 10.12 ± 2.80 | 3.55 ± 0.47 | 3.93 ± 0.50 |
| | Lateral Bending | 3.65 ± 1.18 | 2.39 ± 2.17 | 2.20 ± 0.45 | 3.422 ± 1.13 | 4.12 ± 1.52 | 6.029 ± 2.80 | 2.40 ± 0.86 | 2.21 ± 1.32 |
| | Axial Rotation | 2.41 ± 1.06 | 2.75 ± 0.55 | 2.64 ± 0.88 | 6.41 ± 1.52 | 6.87 ± 2.41 | 5.78 ± 3.05 | 5.25 ± 0.79 | 4.89 ± 0.53 |
| ST Articulation | Retraction Protraction | 7.46 ± 3.47 | 12.21 ± 4.95 | 9.80 ± 2.25 | 14.54 ± 3.27 | 25.32 ± 3.33 | 7.69 ± 2.28 | 11.78 ± 5.31 | 9.65 ± 2.20 |
| | Medial Lateral Rotation | 8.48 ± 5.71 | 15.72 ± 5.38 | 28.06 ± 3.60 | 23.38 ± 5.35 | 32.27 ± 3.14 | 9.63 ± 5.73 | 6.48 ± 1.81 | 5.74 ± 2.35 |
| | Anterior Posterior Tilt | 3.56 ± 1.61 | 4.62 ± 2.22 | 8.29 ± 3.14 | 7.59 ± 2.69 | 12.75 ± 2.33 | 3.99 ± 1.41 | 3.392 ± 1.71 | 4.89 ± 1.83 |
| GH Joint | GH Plane of Elevation | 29.19 ± 9.11 | 24.18 ± 9.49 | 51.54 ± 23.15 | 40.60 ± 9.03 | 142.82 ±31.78 | 52.31 ± 14.86 | 21.45 ± 10.63 | 19.66 ± 10.92 |
| | GH Elevation | 32.12 ± 11.58 | 47.31± 17.49 | 57.31 ± 14.63 | 61.10 ± 18.92 | 99.49 ± 15.42 | 34.58 ± 17.13 | 39.23 ± 6.95 | 44.68 ± 6.28 |
| | GH Axial Rotation | 30.87 ± 10.09 | 19.86 ± 8.53 | 35.15 ± 12.40 | 42.94 ± 10.62 | 155.93 ±37.35 | 61.27 ± 32.97 | 18.99 ± 8.15 | 25.42 ± 12.38 |
| Elbow Joint | Pronation Supination | 21.44 ± 9.12 | 28.05 ± 10.32 | 24.17 ± 11.70 | 27.56 ± 12.53 | 30.76 ± 16.76 | 26.33 ± 8.86 | 26.35 ± 11.06 | 20.25 ± 8.32 |
| | Flexion Extension | 38.29 ± 16.34 | 49.05 ± 14.17 | 55.22 ± 15.18 | 33.73 ± 15.07 | 47.05 ± 17.63 | 52.91 ± 18.15 | 33.87 ± 11.48 | 30.53 ± 8.29 |
| HT Rotation | Plane of Elevation | 60.54 ± 26.32 | 45.63 ± 13.31 | 36.00 ± 17.86 | 39.73 ± 5.04 | 143.17 ± 24.56 | 27.32 ± 10.87 | 28.44 ± 13.75 | 28.08 ± 9.29 |
| | Elevation | 27.07 ± 8.14 | 55.30 ± 14.36 | 87.87 ± 16.37 | 62.90 ± 35.27 | 108.33 ±21.01 | 48.87 ± 17.41 | 77.12 ± 7.52 | 39.06 ± 8.64 |
| | Axial Rotation | 20.80 ± 7.15 | 12.20 ± 7.27 | 33.45 ± 15.59 | 30.20 ± 6.69 | 160.43 ±27.21 | 66.24 ± 27.46 | 21.60 ± 8.02 | 21.86 ± 7.55 |

| **Shoulder Complex Joints Kinematics (°)** | | Answer phone | Reach as far forward as possible | Lift block to shoulder height | Lift block to head height | Cross body abduction | Internal rotation | External rotation | 90° abduction with external rotation |
|---|---|---|---|---|---|---|---|---|---|
| Thorax relative to GCS | Flexion Extension | 5.17 ± 0.60 | 5.90 ± 0.82 | 5.745 ± 1.45 | 10.17 ± 3.10 | 3.98 ± 1.68 | 7.33 ± 1.09 | 12.89 ± 1.24 | 12.17 ± 0.46 |
| | Lateral Bending | 2.56 ± 0.79 | 2.70 ± 1.30 | 3.14 ± 1.24 | 6.22 ± 3.42 | 5.66 ± 2.12 | 5.58 ± 1.74 | 4.26 ± 0.91 | 2.60 ± 1.17 |
| | Axial Rotation | 9.89 ± 0.79 | 2.00± 0.52 | 6.78 ± 1.49 | 9.31 ± 4.17 | 20.44 ± 0.96 | 8.98± 4.48 | 10.28 ± 1.94 | 9.47± 4.34 |
| ST Articulation | Retraction Protraction | 4.21 ± 2.69 | 20.64 ± 4.53 | 10.51 ± 5.69 | 14.60 ± 6.63 | 27.58 ± 11.09 | 6.07 ± 2.53 | 30.34 ± 1.30 | 22.40 ± 5.83 |
| | Medial Lateral Rotation | 10.82 ± 2.52 | 10.80 ± 4.17 | 17.22 ± 4.22 | 30.91 ± 5.80 | 20.34 ± 5.24 | 12.49 ± 4.77 | 15.80± 6.29 | 30.41 ± 6.98 |
| | Anterior Posterior Tilt | 5.80± 2.11 | 5.83± 1.49 | 4.67 ± 2.16 | 5.84 ± 1.99 | 6.14 ± 2.24 | 3.79 ± 1.53 | 5.39 ± 1.78 | 8.78 ± 3.10 |
| GH Joint | GH Plane of Elevation | 25.59 ± 14.57 | 16.94 ± 9.93 | 28.16 ± 13.20 | 40.29 ± 22.75 | 31.02 ± 11.82 | 36.62 ± 17.60 | 326.12 ± 19.97 | 118.00 ± 37.33 |
| | GH Elevation | 44.05 ± 6.26 | 69.46 ± 16.98 | 63.78 ± 9.78 | 83.76 ± 5.99 | 79.36 ± 27.60 | 23.23± 13.01 | 49.16 ± 5.35 | 54.61 ± 11.56 |
| | GH Axial Rotation | 29.64 ± 11.81 | 19.98 ± 7.22 | 25.20 ± 9.34 | 33.91 ± 17.35 | 20.43 ± 9.22 | 40.04± 10.46 | 327.65 ± 17.71 | 148.60 ± 33.01 |
| Elbow Joint | Pronation Supination | 16.91 ± 7.99 | 65.20 ± 17.58 | 23.13 ± 9.24 | 33.28 ± 9.43 | 28.04 ± 10.52 | 36.37 ± 15.61 | 38.57 ± 17.12 | 30.02 ± 11.76 |
| | Flexion Extension | 46.07 ± 15.42 | 62.67 ± 12.75 | 25.52 ± 7.37 | 35.93 ± 12.69 | 18.65 ± 6.31 | 66.75 ± 28.63 | 26.91± 13.64 | 39.78 ± 8.26 |
| HT Rotation | Plane of Elevation | 25.65 ± 12.13 | 38.15 ± 13.76 | 28.36 ± 14.76 | 37.15 ± 10.99 | 71.46 ± 25.92 | 28.78 ± 7.34 | 143.67 ± 19.84 | 90.24 ± 30.45 |
| | Elevation | 39.23 ± 8.28 | 65.67 ± 21.92 | 70.79 ± 18.43 | 97.95 ± 26.11 | 59.96 ± 19.34 | 39.72 ± 17.75 | 50.43 ± 10.56 | 85.73 ± 15.66 |
| | Axial Rotation | 24.54 ± 8.02 | 19.49 ± 7.70 | 30.35 ± 11.31 | 30.12 ± 10.28 | 19.97 ± 10.81 | 67.365 ± 19.32 | 137.23 ± 18.37 | 112.74 ± 22.93 |

**Table (5.6)**: Complete shoulder complex 3D kinematics (mean±standard deviation) calculated by 6DOF analysis method for dynamic arm elevation during abduction, scaption and flexion.

| **Shoulder Complex Joints Kinematics (°)** | | Abduction Plane (0°) | Scaption Plane (30°) | Flexion Plane (90°) |
|---|---|---|---|---|
| Thorax relative to GCS | Flexion Extension | 12.39 ± 4.54 | 9.32 ± 3.18 | 10.68 ± 1.79 |
| | Lateral Bending | 4.217 ± 1.65 | 3.93 ± 1.40 | 4.99 ± 1.75 |
| | Axial Rotation | 2.76 ± 0.85 | 2.75 ± 1.18 | 3.01 ± 3.52 |
| ST Articulation | Retraction Protraction | 19.06 ± 10.05 | 22.13 ± 5.93 | 18.35 ± 2.46 |
| | Medial Lateral Rotation | 45.28 ± 7.26 | 42.35 ± 9.28 | 41.52 ± 7.43 |
| | Anterior Posterior Tilt | 11.33 ± 4.79 | 10.46 ± 3.46 | 10.29 ± 2.55 |
| GH Joint | GH Plane of Elevation | 168.94 ± 32.87 | 206.85 ± 27.87 | 62.35 ± 33.37 |
| | GH Elevation | 95.10 ± 15.68 | 98.48 ± 16.91 | 97.57 ± 17.03 |
| | GH Axial Rotation | 147.81 ± 23.35 | 138.08 ± 32.13 | 46.84 ± 13.82 |
| Elbow Joint | Medial Lateral Rotation | 15.82 ± 5.81 | 32.47 ± 12.47 | 41.51 ± 13.91 |
| | Anterior Posterior Tilt | 58.99 ± 24.38 | 32.59 ± 8.92 | 31.99 ± 8.79 |
| HT Rotation | Plane of Elevation | 103.03 ± 33.15 | 102.70 ± 22.70 | 60.51 ± 15.94 |
| | Elevation | 121.14 ± 19.25 | 118.96 ± 7.89 | 114.15 ± 10.65 |
| | Axial Rotation | 117.41 ± 20.08 | 122.63 ± 42.78 | 83.27 ± 21.56 |

**Table (5.7)**: Complete shoulder complex 3D kinematics (mean±standard deviation) calculated by matrix decomposition method for static arm elevation with skin mounted markers and scapula locator during abduction, scaption and flexion.

| Shoulder Complex Joints Kinematics (°) | | Abduction | | Scaption | | Flexion* | |
|---|---|---|---|---|---|---|---|
| | | Skin Markers | Scapula Locator | Skin Markers | Scapula Locator | Skin Markers | Scapula Locator |
| Thorax relative to GCS | Flexion Extension | 15.18 ± 3.74 | 14.49 ± 3.08 | 8.92 ± 2.59 | 10.06 ± 4.58 | 14.91 ± 6.24 | 17.41 ± 3.41 |
| | Lateral Bending | 3.39 ± 0.90 | 3.94 ± 2.21 | 1.53 ± 0.58 | 3.54 ± 1.55 | 3.60 ± 1.89 | 3.01 ± 1.03 |
| | Axial Rotation | 4.22 ± 2.55 | 8.49 ± 4.79 | 2.88 ± 0.10 | 6.16 ± 2.14 | 4.709 ± 1.73 | 5.02 ± 2.43 |
| SC Joint | Retraction Protraction | 41.26 ± 8.80 | 37.47 ± 3.90 | 30.02 ± 4.47 | 34.14 ± 4.52 | 34.79 ± 7.17 | 33.24 ±6.08 |
| | Elevation Depression | 22.12 ± 5.27 | 21.37 ± 1.59 | 23.73 ± 0.59 | 25.18 ± 2.81 | 23.42 ± 5.33 | 24.92 ± 3.33 |
| AC Joint | Retraction Protraction | 22.54 ± 12.19 | 24.46 ± 12.50 | 16.36 ± 0.82 | 17.94 ± 4.04 | 120.99 ± 12.82 | 17.10 ± 4.67 |
| | Medial Lateral Rotation | 40.78 ± 3.16 | 38.38 ± 16.66 | 35.81 ± 0.84 | 36.84 ± 14.57 | 51.67 ± 14.41 | 39.38 ± 8.99 |
| | Anterior Posterior Tilt | 38.00 ± 8.82 | 48.04 ± 19.16 | 35.54 ±2.84 | 43.18 ± 18.82 | 44.41 ± 8.89 | 43.31 ± 6.88 |
| GH Joint | GH Plane of Elevation | 167.75 ± 69.25 | 149.15 ± 11.52 | 182.95 ± 6.57 | 143.55 ± 25.10 | 137.88 ± 45.88 | 87.12 ± 29.32 |
| | GH Elevation | 87.37 ± 13.95 | 86.25 ± 16.23 | 74.06 ± 15.94 | 82.58 ± 17.90 | 81.85 ± 11.88 | 76.59 ± 12.73 |
| | GH Axial Rotation | 131.96 ± 65.61 | 157.82 ± 16.64 | 309.54 ± 36.38 | 143.56 ± 73.99 | 85.60 ± 20.69 | 88.42 ± 31.39 |
| ST Articulation | Retraction Protraction | 11.38 ± 3.51 | 18.03 ± 9.92 | 12.64 ± 2.56 | 14.08 ± 6.19 | 104.82 ± 16.53 | 16.29 ± 5.64 |
| | Medial Lateral Rotation | 41.38 ± 4.03 | 41.49 ± 9.04 | 36.05 ± 0.91 | 39.07 ± 9.49 | 77.66 ± 28.60 | 40.42 ± 7.73 |
| | Anterior Posterior Tilt | 6.35 ± 3.53 | 10.57 ± 4.65 | 5.56 ± 1.03 | 8.89 ±1.81 | 23.39 ± 7.85 | 11.62 ± 6.49 |
| HT Rotation | Plane of Elevation | 124.90 ± 20.67 | 133.93 ± 22.76 | 147.00 ± 52.20 | 127.58 ± 35.55 | 77.13 ± 21.14 | 81.49 ± 20.84 |
| | Elevation | 122.13 ± 13.44 | 117.73 ± 7.70 | 111.65 ± 0.86 | 114.87 ± 9.09 | 114.02 ± 9.43 | 112.54 ± 8.63 |
| | Axial Rotation | 137.00 ± 19.42 | 141.39 ± 21.29 | 162.02 ± 33.37 | 135.48 ± 28.29 | 77.98 ± 27.61 | 84.15 ± 20.48 |

*Significant difference between the Kinematic ROM measured for sagittal plane (flexion) elevation with skin markers and scapula locator, P=0.04<0.05.

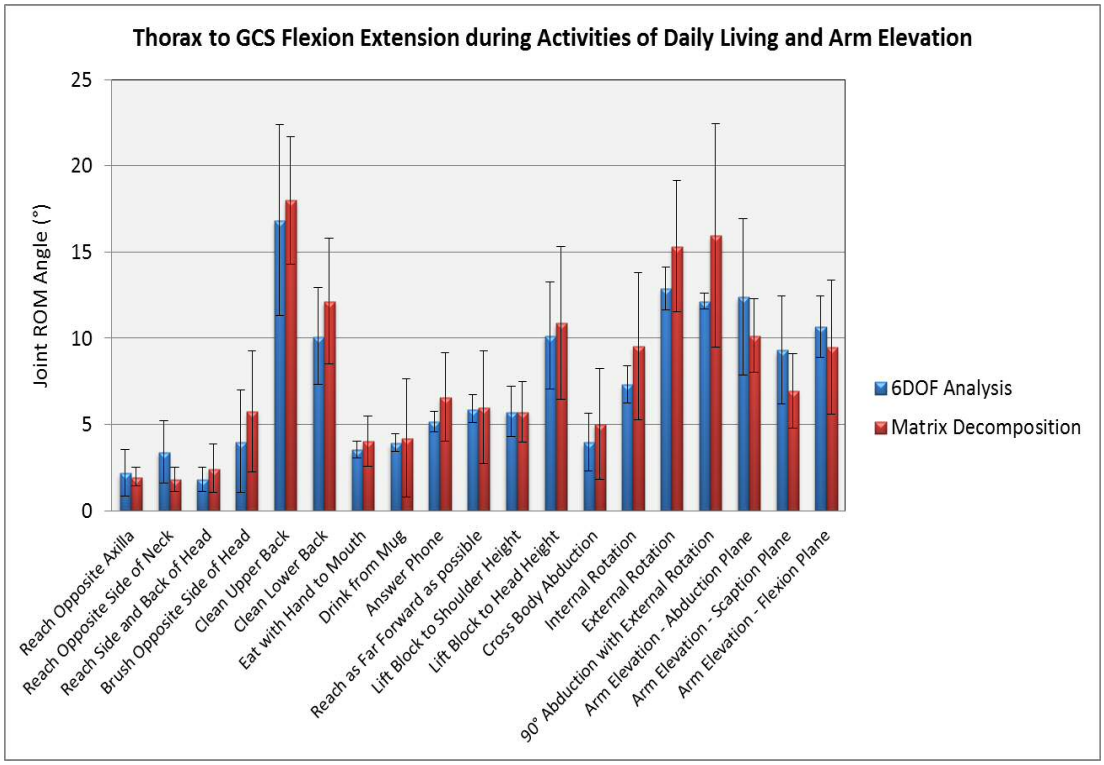


**Figure (5.17)**: Complete shoulder complex 3D kinematics of **Thorax to GCS flexion extension** calculated by matrix decomposition and 6DOF analysis methods during activities of daily living and dynamic arm elevation. Significant difference between the kinematic ROM calculated by matrix decomposition and 6DOF analysis methods.

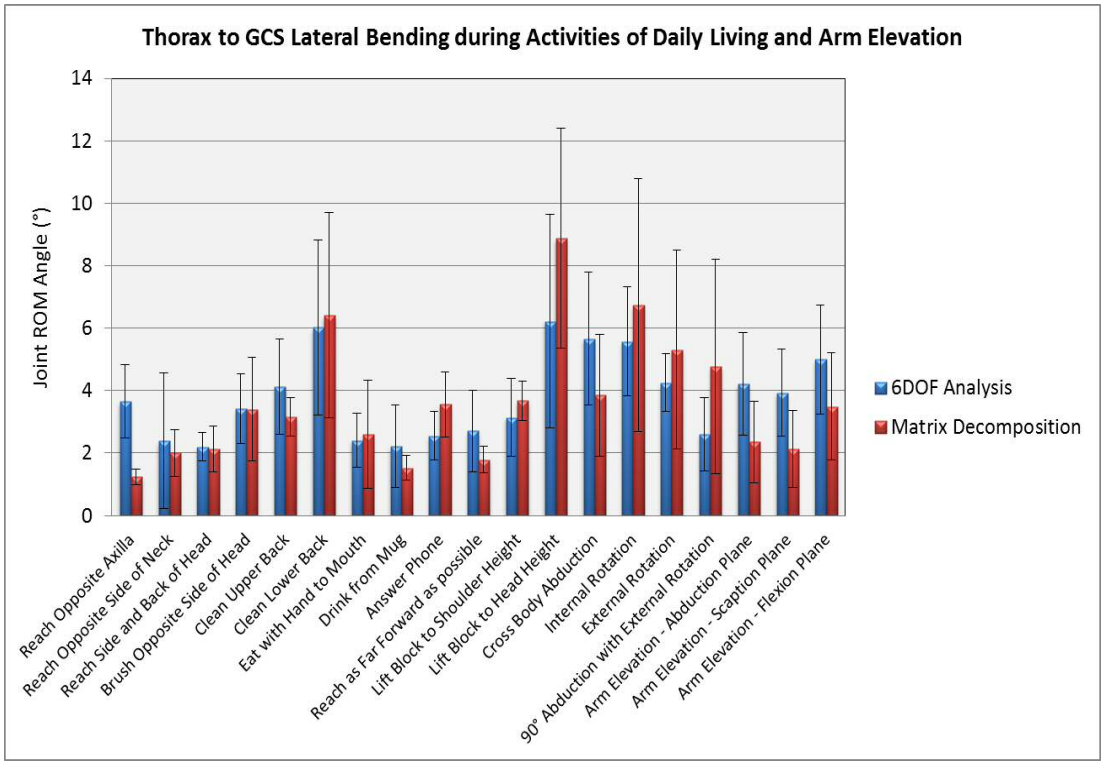


**Figure (5.18)**: Complete shoulder complex 3D kinematics of **Thorax to GCS lateral bending** calculated by matrix decomposition and 6DOF analysis methods during activities of daily living and dynamic arm elevation.

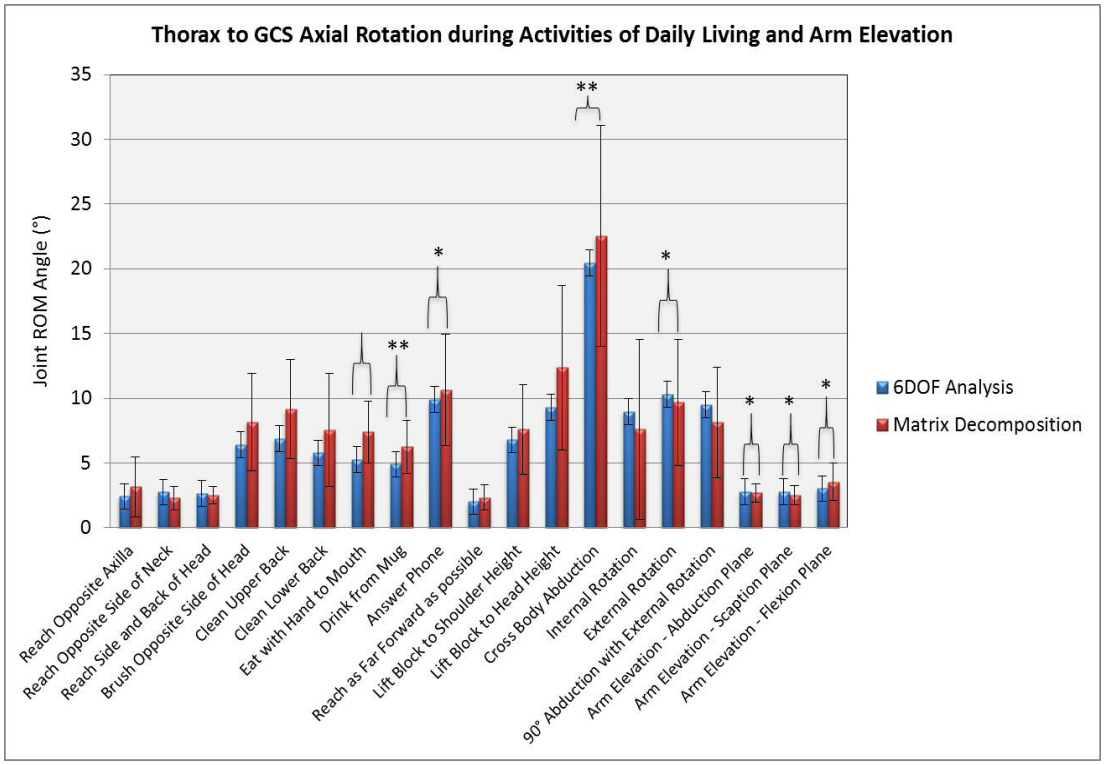


**Figure (5.19)**: Complete shoulder complex 3D kinematics of **Thorax to GCS axial rotation** calculated by matrix decomposition and 6DOF analysis methods during activities of daily living and dynamic arm elevation. Significant difference between the kinematic ROM calculated by matrix decomposition and 6DOF analysis methods, *P<0.05 and ** P<0.001.

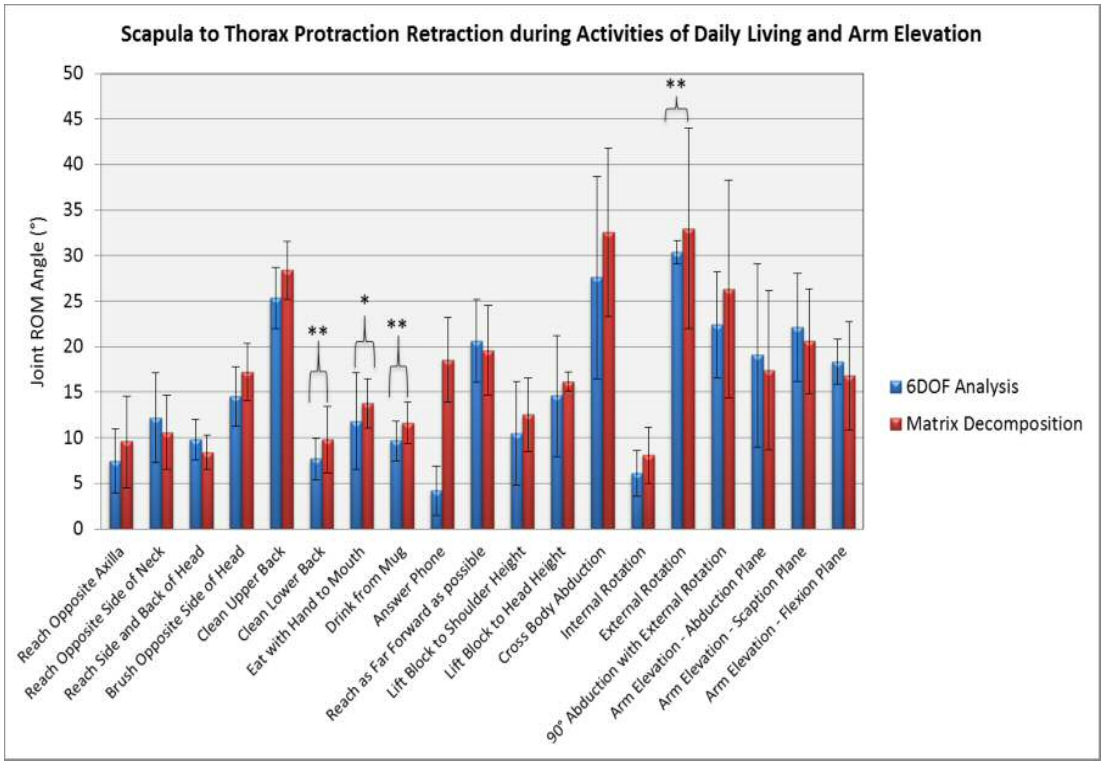


**Figure (5.20)**: Complete shoulder complex 3D kinematics of **Scapula to Thorax protraction retraction** calculated by matrix decomposition and 6DOF analysis methods during activities of daily living and dynamic arm elevation. Significant difference between the kinematic ROM calculated by matrix decomposition and 6DOF analysis methods, *P<0.05 and ** P<0.001.

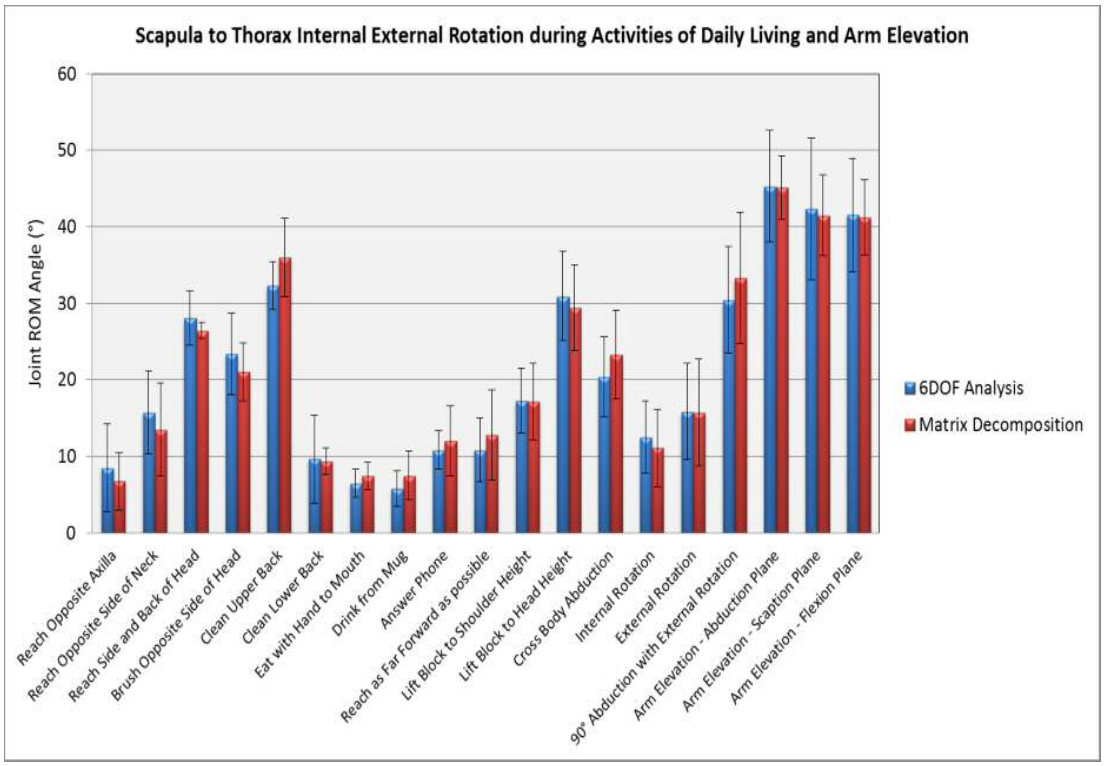


**Figure (5.21)**: Complete shoulder complex 3D kinematics of **Scapula to Thorax internal external rotation** calculated by matrix decomposition and 6DOF analysis methods during activities of daily living and dynamic arm elevation.

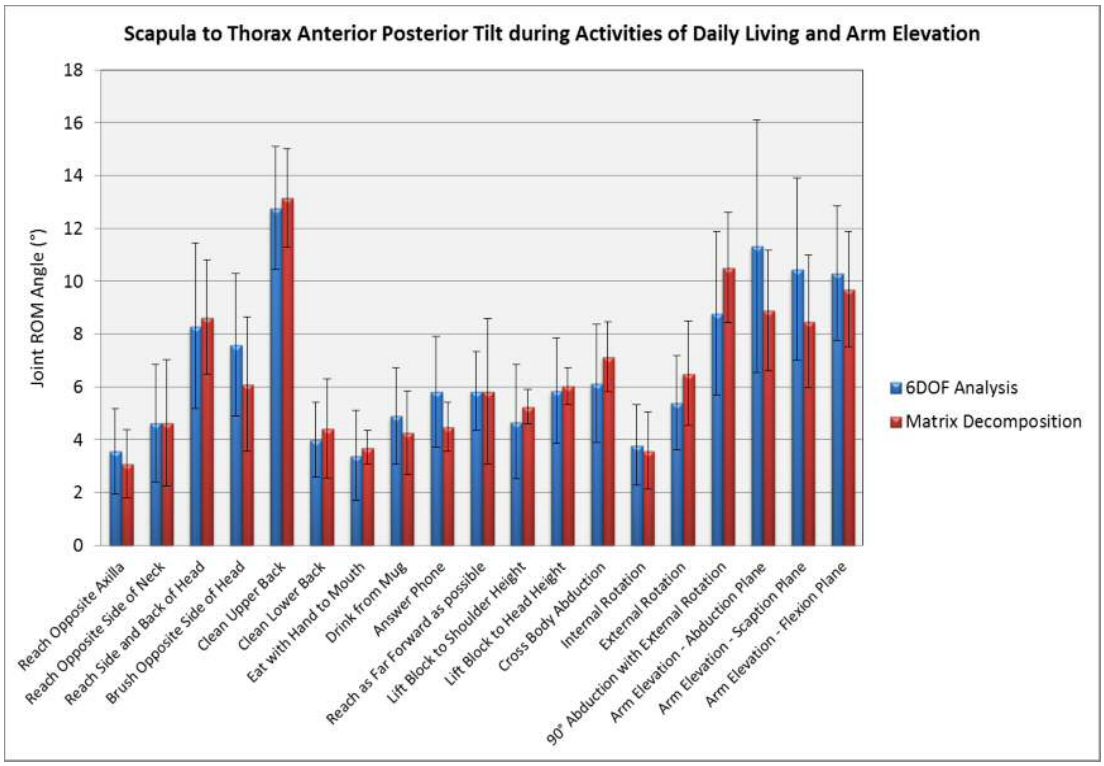


**Figure (5.22)**: Complete shoulder complex 3D kinematics of **Scapula to Thorax anterior posterior tilt** calculated by matrix decomposition and 6DOF analysis methods during activities of daily living and dynamic arm elevation.

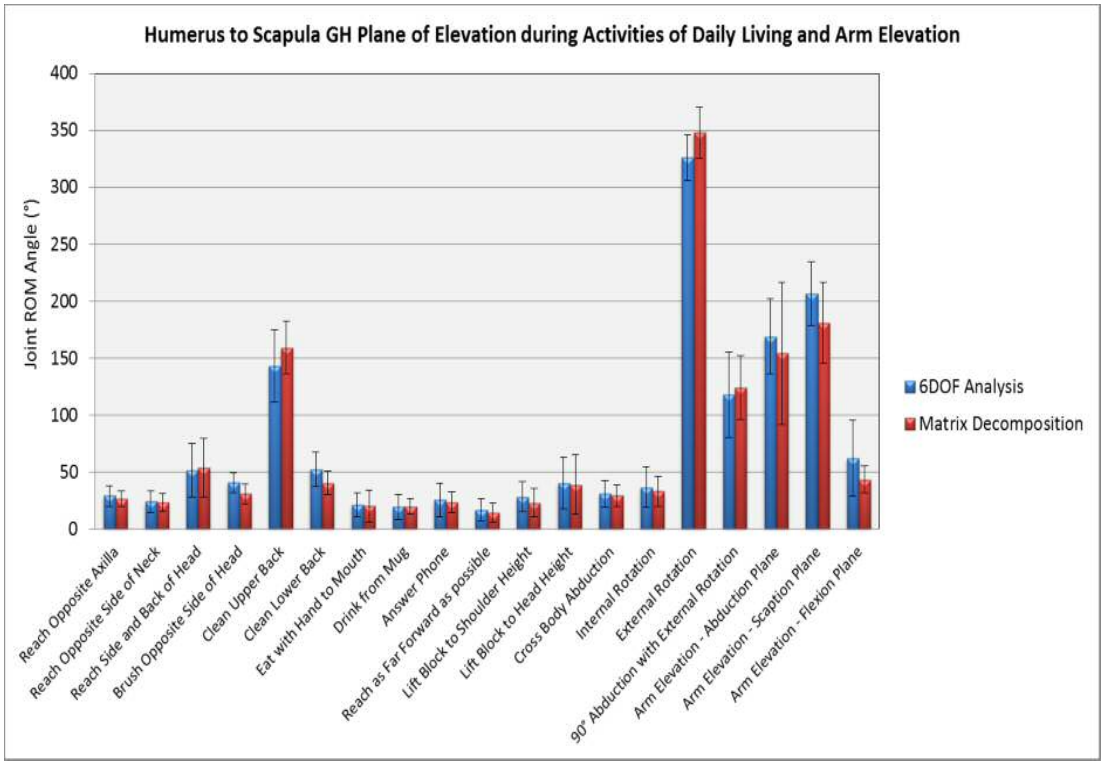


**Figure (5.23)**: Complete shoulder complex 3D kinematics of **Humerus to Scapula GH plane of elevation** calculated by matrix decomposition and 6DOF analysis methods during activities of daily living and dynamic arm elevation.

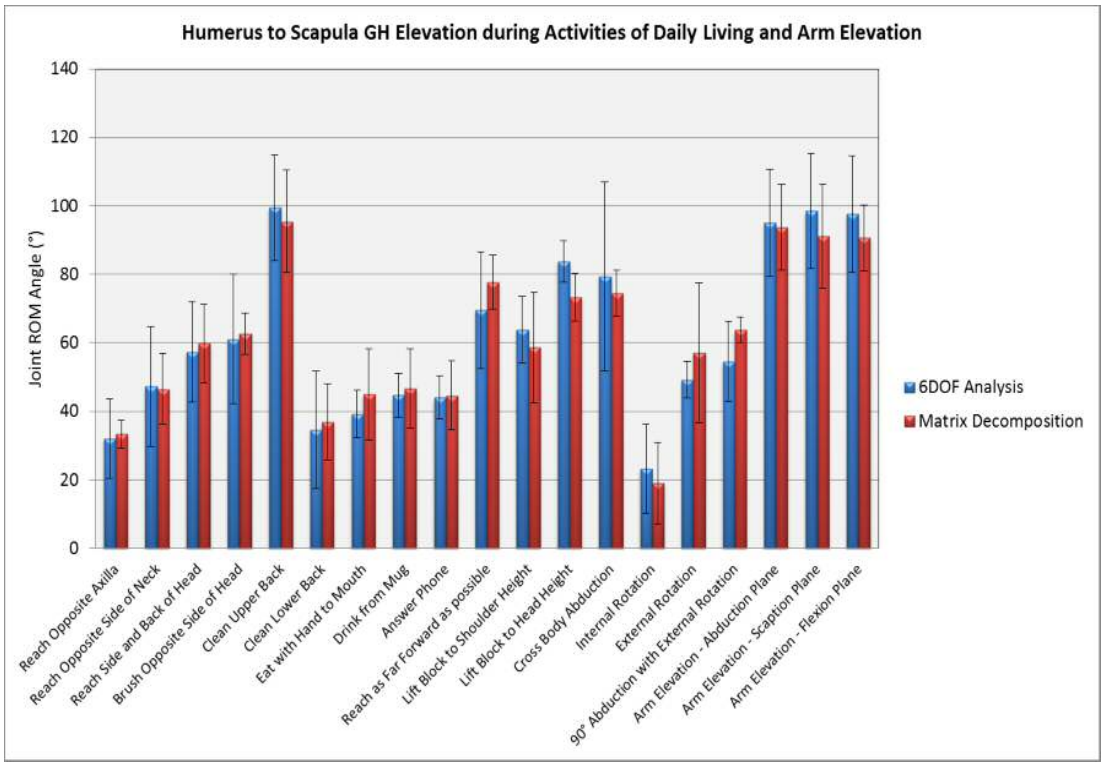


**Figure (5.24)**: Complete shoulder complex 3D kinematics of **Humerus to Scapula GH elevation** calculated by matrix decomposition and 6DOF analysis methods during activities of daily living and dynamic arm elevation.

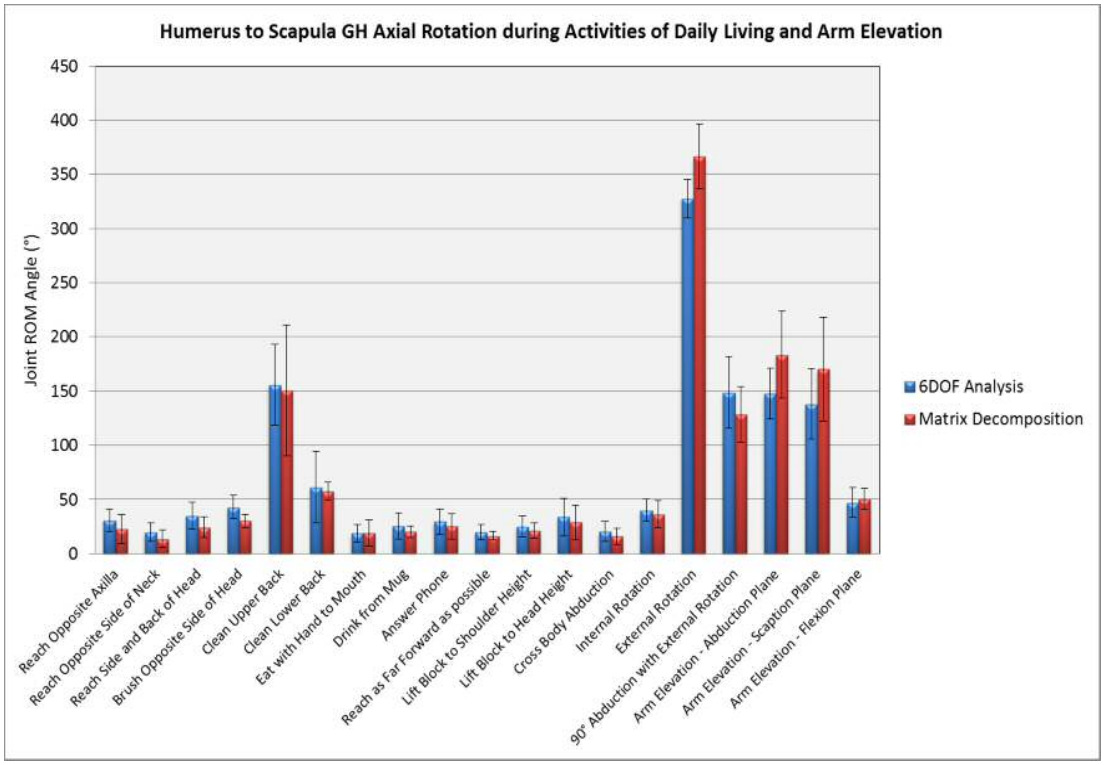


**Figure (5.25)**: Complete shoulder complex 3D kinematics of **Humerus to Scapula GH axial rotation** calculated by matrix decomposition and 6DOF analysis methods during activities of daily living and dynamic arm elevation.

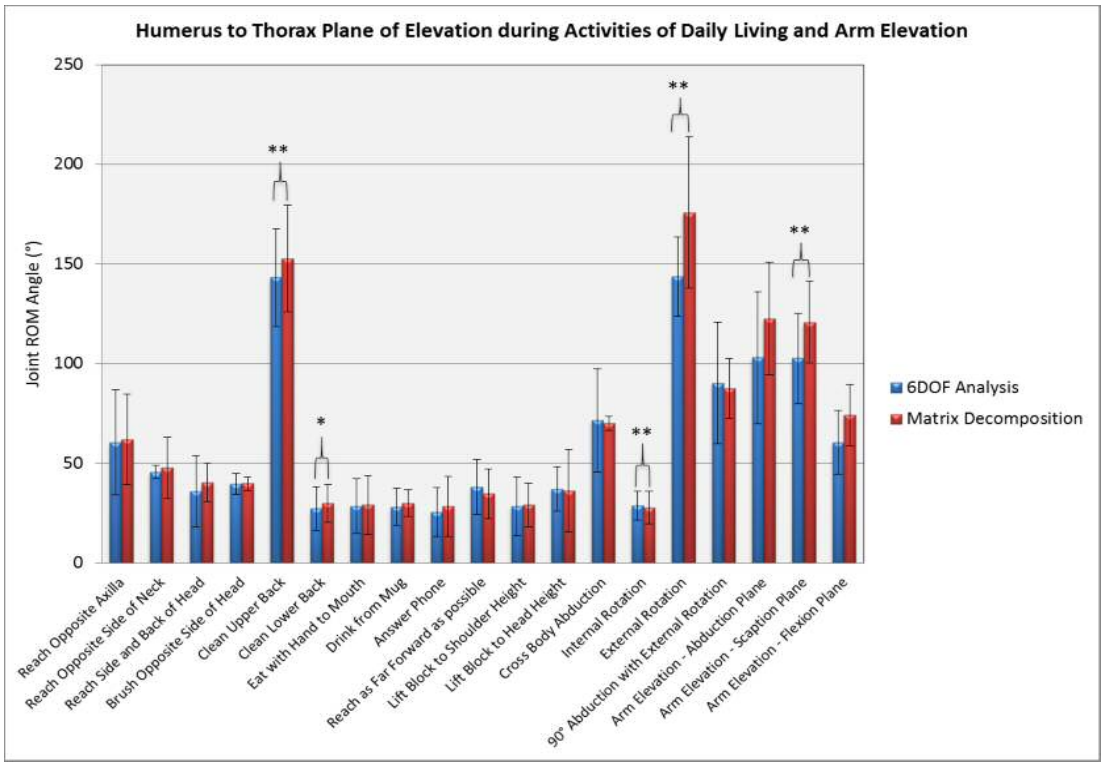


**Figure (5.26)**: Complete shoulder complex 3D kinematics of **Humerus to Thorax plane of elevation** calculated by matrix decomposition and 6DOF analysis methods during activities of daily living and dynamic arm elevation. Significant difference between the kinematic ROM calculated by matrix decomposition and 6DOF analysis methods, *P<0.05 and ** P<0.001.

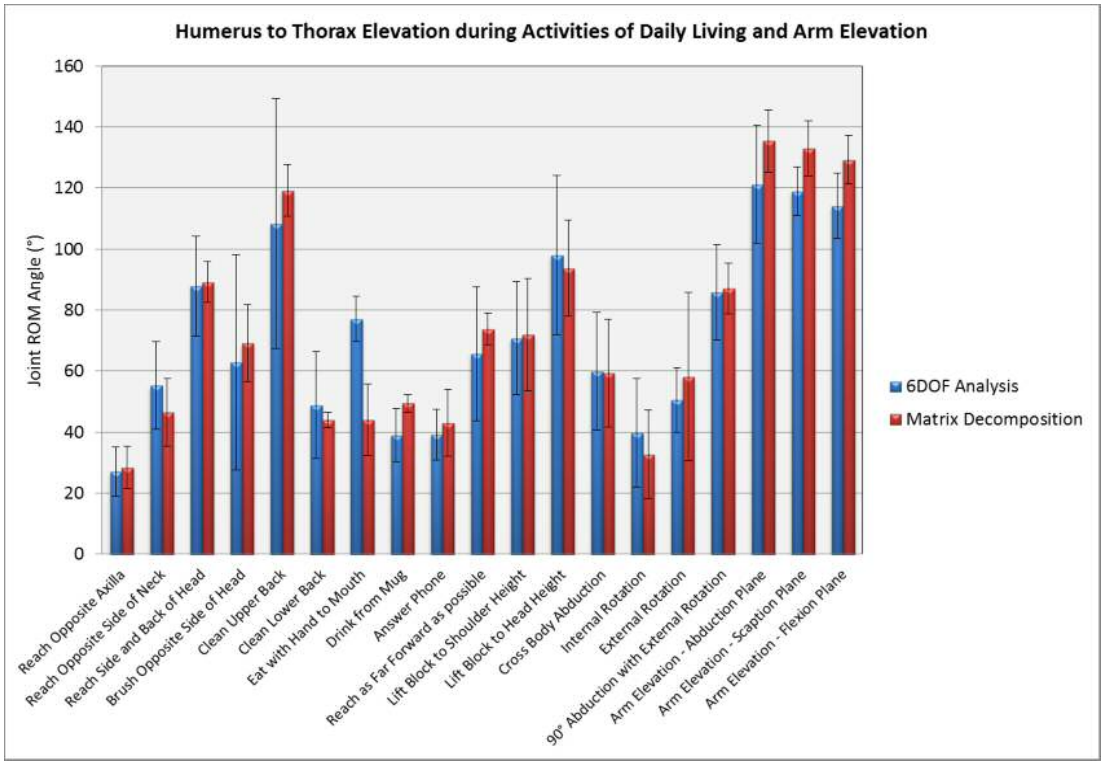


**Figure (5.27)**: Complete shoulder complex 3D kinematics of **Humerus to Thorax elevation** calculated by matrix decomposition and 6DOF analysis methods during activities of daily living and dynamic arm elevation.

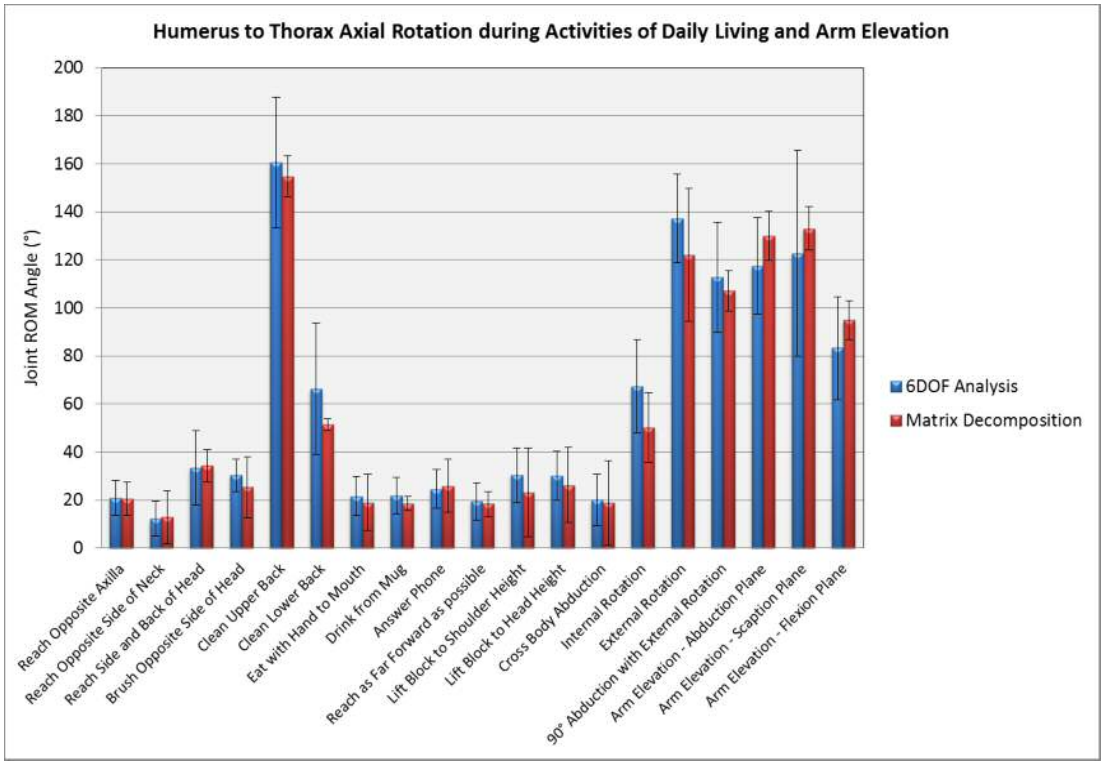


**Figure (5.28)**: Complete shoulder complex 3D kinematics of **Humerus to Thorax axial rotation** calculated by matrix decomposition and 6DOF analysis methods during activities of daily living and dynamic arm elevation.

During the activities of daily living trials, the thorax facilitated certain arm positions for activities that involved internal arm rotation behind the body. Therefore, cleaning the lower back and internal rotation showed the greatest thorax lateral bending ROM (6.41°±3.29 and 6.73°±4.05 respectively). Cleaning the upper back as well as external rotation were the activities with greatest thorax flexion extension ROM (18.00°±3.70 and 15.34°±3.83 respectively). Additionally, cross body abduction was the activity with greatest thorax axial rotation ROM with (22.54°±8.54).

Also, clean upper body required the greatest ROM measured in the SC joint with (48.50°±3.79 and 33.92°±2.60) for protraction retraction and elevation depression respectively. Only two bony landmarks can be discerned on the clavicle: SC and AC. Hence, axial rotation cannot be determined through non-invasive palpation measurements.

In similar manner, clean upper back seemed to be the most challenging activity with the greatest ROM measured in the AC joint with (35.43°±12.21, 35.47°±9.30 and 45.18°±22.34) for scapula protraction retraction, axial rotation and anterior posterior tilt respectively.

External rotation is also considered a highly challenging movement. Furthermore, a large plane of elevation of the GH joint is necessary for the completion of this task with a measured ROM of (347.96°±22.15). Also GH axial rotation showed the greatest movement ROM of (366.37°±29.97). Additionally, lifting a block to head height as well as cross body abduction were the activities with greatest GH elevation with (73.31°±6.88) and (74.43°±6.71) respectively.

As they also seemed to be the most challenging activities, with the greatest ROM measured in other joints, cleaning upper back as well as cross body abduction were the activities with greatest ST axial rotation and retraction protraction with (35.94°±5.12) and (32.53°±9.26) respectively.

Cleaning upper back is also considered a highly challenging movement for the HT plane of elevation, elevation and axial rotation with a measured ROM of

(152.75°±26.77, 119.22°±8.50 and 154.71°±20.51) respectively. Cleaning the upper back requires a high degree of arm elevation and cleaning the lower back requires a large amount of internal rotation.

Smaller *thorax relative to the GCS* rotations were consistently measured when volunteers performed dynamic movement trials as compared to static and scapula locator for abduction, scaption and flexion, see Tables (5.4) and (5.7). Different thorax lateral rotation was measured between static skin and scapula locator measurements during scaption, suggesting that the scapula locator positioning might have an effect on the volunteer adopting a different posture compared to without the scapula locator. So, the smallest average thorax rotations ROM measured by the skin markers were presented for the three planes of elevation; coronal (abduction), scaption and sagittal (flexion) were (10.16°±2.12, 6.96°±2.16 and 9.45°±3.90) for thorax flexion extension, (2.35°±1.30, 2.13°±1.22 and 3.48°±1.72) for thorax lateral bending and (2.67°±0.70, 2.50°±0.73 and 3.54°±1.46) for thorax axial rotation respectively.

*For the SC joint*, it was not possible to directly measure axial rotation of the clavicle, as only two landmarks on the clavicle can be palpated. Therefore, the average retraction protraction measured ROM for dynamic abduction, scaption and flexion were (41.54°±6.78, 41.62°±6.42 and 41.86°±4.31) respectively. While, the average elevation depression measured ROM for dynamic abduction, scaption and flexion were (25.02°±5.28, 25.31°±8.10 and 20.21°±4.48) respectively.

*For the AC joint,* the scapula retraction protraction ROM for dynamic abduction, scaption and flexion were measured as (33.21°±10.07, 43.95°±23.21 and 29.98°±6.87) respectively. The scapula medial lateral rotation ROM for dynamic abduction, scaption and flexion were measured as (43.16°±3.43, 40.45°±6.95 and 38.49°±3.04) respectively. While, the scapula anterior posterior tilt ROM for dynamic abduction, scaption and flexion were measured as (39.62°±5.52, 39.81°±9.21 and 34.06°±4.86) respectively.

*For the ST articulation,* the scapula retraction protraction ROM for dynamic coronal, scaption and sagittal plane elevations were measured as (17.42°±8.77,

20.63°±5.74 and 16.79°±5.91) respectively. The scapula medial lateral rotation ROM for dynamic coronal, scaption and sagittal plane elevations were measured as (45.12°±3.43, 41.49°±5.28 and 41.25°±4.91) respectively. While, the scapula anterior posterior tilt ROM for dynamic coronal, scaption and sagittal plane elevations were measured as (8.88°±2.29, 8.74°±2.51 and 9.69°±2.18) respectively.

*For the GH joint,* the main discrepancy when measuring the plane of elevation of the GH joint during elevation in the coronal and sagittal planes was caused by gimbal lock. This occurs when two of the three rotational axes of the GH joint are aligned with their pivot axes in a single plane. When this occurs it is no longer possible to represent the orientation of the GH joint. This is likely to occur at low and high humeral elevations. Therefore, the average GH plane of elevation ROM for coronal, scaption and sagittal planes were measured as (154.31°±62.54, 180.88°±35.90 and 43.45°±11.82) respectively.

During coronal, scaption and sagittal planes, the GH elevation ROM of (93.77°±12.51, 91.04°±15.14 and 90.67°±9.67) respectively were displayed. While when measuring GH axial rotation, the average ROM of (183.43°±40.33, 170.26°±48.04 and 50.74°±9.35) were observed for dynamic abduction, scaption and flexion elevations respectively.

The HT plane of elevation average ROM for dynamic coronal, scaption and sagittal plane elevations were measured as (122.68°±28.17, 120.63°±20.44 and 74.27°±15.47) respectively. The HT elevation average ROM for dynamic coronal, scaption and sagittal plane elevations were measured as (135.40°±10.17, 132.89°±9.08 and 129.28°±8.02) respectively. While, the HT axial rotation average ROM for dynamic coronal, scaption and sagittal plane elevations were measured as (130.00°±25.59, 133.01°±36.32 and 36.32°±24.33) respectively.

## 5.9 Summary

This chapter investigated the motion requirements for the shoulder complex during activities of daily living and physiological range of motion in healthy volunteers. The quantification of the three-dimensional motions needed for these

tasks should enable clinicians to identify tasks that might be problematic for their patients or provide clinicians with a basis of comparison for evaluating impairments of the effects of interventions.

This chapter presented a brief description of the motion analysis facilities at Cardiff University in terms of camera setup and calibration, marker placement, camera and software operation when taking measurements, subsequent tracking of markers into 3D trajectories and importing this data into bespoke software to calculate the range of motion of the trunk and articulations in the shoulder. The ethical review process, participants and inclusion/exclusion criteria were explained in this chapter.

It also presented a description of the methods developed previously at Cardiff and compared the outputs with those previously obtained in terms of kinematic range of motion using a different approach that calculate the 6 Degree of Freedom ROM developed during these studies. It is important to understand which joints or articulations of the shoulder are most important for performing each movement and how reliably those movements can be measured. However, it can be difficult to choose appropriate activities because the kinematic redundancy of the shoulder complex joints makes it possible to accomplish any task using a variety of movement strategies. In the next chapter, this protocol was developed and applied within manual wheelchair propulsion measurement through using the 6DOF analysis method to describe the kinematics of the trunk and upper limbs with propelling a manual wheelchair during daily mobility and use.

# Chapter 6

## Motion Analysis Protocol for Quantifying Functional Wheelchair Use

People who use a manual wheelchair depend upon their upper limbs to provide a means of locomotion during completion of their activities of daily living. Sonenblum et al. (2012) found that manual wheelchair users were wheeling for only about 10% of the time they spent seated in their wheelchairs per day. Additionally, Cooper et al. (2008) determined that children completed 167 start/stop tasks/1000 m travelled in a day, with an average daily distance of 1600 m.

Due to greater than normal loading on the upper limbs, shoulder pain and injury are commonly associated with manual wheelchair users, (Dubowsky 2008). The act of wheelchair propulsion itself is basically divided into two phase; the push and recovery phases. During the push phase, the path of the hand is confined to the pushrim, however during the recovery the arm is unconfined in its path back towards the wheel contact.Current research is therefore being conducted to capture and analyse most aspects of the movements performed by wheelchair users in order to understand the biomechanical effects of altering the different elements of the wheelchair and also as at route to minimizing upper limb injuries due to overuse during specific tasks or daily activities.

This chapter aimed to demonstrate the motion analysis protocol designed for quantifying the manual wheelchair use of able-bodied volunteers through employing the 6DOF analysis that was applied on the shoulder complex in Chapter Five for designing an upper body model to calculate the three-dimensional kinematics and surface electromyographic (sEMG) analyses during functional tasks of wheelchair mobility.

### 6.1 Instrumentation

The Motion Analysis laboratory at Cardiff University was used for this analysis through an opto-electronic motion capture system, (Oqus Cameras and QTM Software, Qualisys, Sweden). It is equipped with nine Qualisys Pro-Reflex

Oqus Cameras arranged around the periphery of the laboratory's walls. More detailed description was mentioned in section 5.1.

## 6.2 Calibration

Once the cameras are positioned, the system can be calibrated to define a global coordinate system (GSC) for the laboratory. The calibration was performed using a (750 mm) T-shaped wand kit provided by Qualisys (www.qualisys.com) with a 60 seconds capture period prior to the participant's arrival to the laboratory.More detailed description was mentioned in section 5.2.

## 6.3 Subjects

Fifteen healthy male novice individuals, (two left-arm dominant, mean age 32.13 ± 9.17 years, height 178.14 ± 6.74 cm, mass 89.1 ± 16.17 kg and body mass index 28.17 ± 5.54), participated in this research study after giving their written informed consent in accordance with the approval obtained from the Cardiff University Ethics Committee. An informal interview is conducted at the start of the laboratory session. During the interview, the participant’s date of birth, age and arm dominance are documented in the protocol sheet.

Criteria for inclusion were: being able-bodied and having no previous experience with wheelchair propulsion. The exclusion criterion was the presence of any severe medical conditions that could have an influence on parameters measured in this study, based on a physical activity readiness questionnaire (PAR-Q).

## 6.4 Markers Placement

A set of twenty retro-reflective markers were attached to the skin overlying specific bony landmarks of the thorax, right and left upper arms, forearms and hands. These bony landmarks are recommended by the International Society of Biomechanics (ISB), (Wu et al., 2005), to establish body segment and joint coordinate systems. An additional twelve markers were placed on the wheelchair’s backrest and on both right and left wheels to identify a local reference system. The bony landmarks are identified by means of palpation. Markers were attached onto the landmark using double-sided tape. The identified bony landmarks and their anatomical description are shown in Figure (6.1).

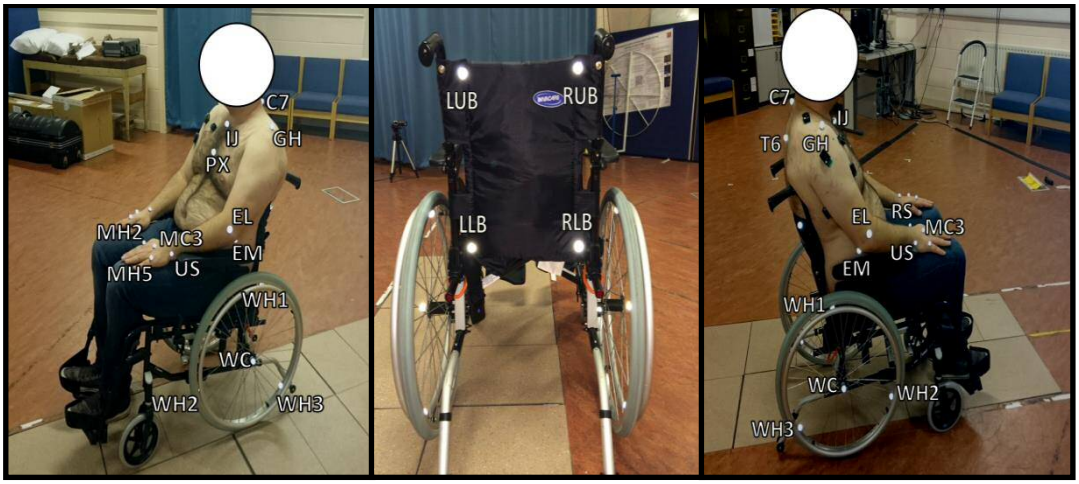


**Figure (6.1):** Trunk, right and left upper limbs and wheelchair markers set placement.

During the bony landmarks identification process, subjects were asked to adopt the neutral position that is sitting down straight on the wheelchair, maintain both arms by the side of the body with elbows flexed at 90° and both hands pronated. The trunk markers included the suprasternal notch (IJ), xiphoid process (PX), spinal processes of (C7) and (T6) vertebrae. According to the volunteers' anthropometries, T6 was used as an alternative bony landmark instead of T8 as the latter may have been inaccessible due to the contact with the wheelchair's backrest of the wheelchair. The upper arm markers included the acromion (GH), humeral medial (EM) and lateral (EL) epicondyles. The forearm markers include the humeral epicondyles and the radial (RS) and ulnar (US) styloids. The hand markers include the 2$^{nd}$ (MH2), 3$^{rd}$ (MC3) and 5$^{th}$ (MH5) metacarpals. An additional four markers were placed on the wheelchair's back rest corners and eight on both right and left wheels (one on each wheel's hub and three markers placed around the inside edge of each wheel rim with 120° interval around the wheel. i.e., at 0°, 120° and 240° positions respectively) to identify a local reference system, see Figure (6.1).

The size (diameter in mm) of the markers used to identity each landmark is provided in the below table. By default, (19.2 mm) diameter markers are used to identify all bony landmarks. For bony landmarks that are prone to "marker swapping" such as RS and US and the hand markers, (9.6 mm) markers were used to minimise this occurrence due to these markers proximity to each other. For the wheelchair's wheel and backrest twelve markers, (19.2 mm) markers were used. See Table (6.1).

**Table (6.1):** Trunk, upper limbs and wheelchair markers set placement with their anatomical description and markers diameters.

| Segment | Bony Landmark | Description of Location | Diameter of Markers |
|---|---|---|---|
| **Thorax** | C7 | Spinous process of the 7th Cervical vertebra | 19.2 mm |
| | T6 | Spinous process of the 6th Thoracic vertebra | 19.2 mm |
| | IJ | Deepest point of IncisureJugularis | 19.2 mm |
| | PX | ProcessusXiphoideus, most caudal point on the sternum | 19.2 mm |
| **Upper Arm** | GH | Glenohumeral joint centre of rotation.Most caudal point on the Acromion | 19.2 mm |
| | EL | Most caudal point on Lateral Epicondyle | 19.2 mm |
| | EM | Most caudal point on Medial Epicondyle | 19.2 mm |
| **Forearm** | RS | Most caudal-lateral point on the Radial Styloid | 9.6 mm |
| | US | Most caudal-medial point on the Ulnar Styloid | 9.6 mm |
| **Hand** | MH2 | The 2nd Hand's Metacarpal | 9.6 mm |
| | MC3 | The 3rd Hand's Metacarpal | 9.6 mm |
| | MH5 | The 5th Hand's Metacarpal | 9.6 mm |
| **Wheelchair's Wheel** | WC | Wheel (hub) centre | 19.2 mm |
| | WH1 | Three markers placed around the inside edge of each wheel rim with 120° interval around the wheel. i.e., at 0°, 120° and 240° positions respectively. | 19.2 mm |
| | WH2 | | 19.2 mm |
| | WH3 | | 19.2 mm |
| **Wheelchair's Backrest** | RUB | Right upper corner | 19.2 mm |
| | LUB | Left upper corner | 19.2 mm |
| | RLB | Right lower corner | 19.2 mm |
| | LLB | Left lower corner | 19.2 mm |

## 6.5 Anthropometric Measurements

Once the participants have signed the consent form, their anthropometric data is collected. The subject's height (cm) is measured with a Seca Ltd. wall mounted measuring tape. Weighing scales are used to measure the participant's mass (kg). Trunk width and circumference, right and left upper arms lengths and diameters, both when the arm is flexed and when it is extended, right and left forearms and hands lengths and diameters are measured with measuring tape (cm) to provide an indication of muscle mass. Arm length is measured as the maximum distance between the acromion marker (GH) and ulnar styloid marker (US) and subject relative-to-ground height, as the maximum height of the (C7) marker. Subject characteristics for each individual and the calculated group averages and standard deviations are given in Table (6.2). Also, the dimensions of the used wheelchair (seat absolute and relative to axle height and depth, backrest height, hand rim and wheel diameters) are measured and are given in Table (6.3) and illustrated in Figure (6.2).

**Table (6.2)**: Measured anthropometric characteristics with their group mean and standard deviation values.

| Subject Anthropometric Characteristics | | Mean | ±STDEV |
|---|---|---|---|
| Age (years) | | 32.133 | 9.172 |
| Height (cm) | | 178.14 | 6.738 |
| Mass (kg) | | 89.1 | 16.169 |
| Body Mass Index | | 28.173 | 5.543 |
| Trunk Width (cm) | | 44.1 | 6.004 |
| Trunk Circumference (cm) | | 98.233 | 9.434 |
| Upper Arm Length (cm) | Right | 32.767 | 2.951 |
| | Left | 32.933 | 3.023 |
| Upper Arm Flexed Circumference (cm) | Right | 34.333 | 4.0473 |
| | Left | 34.6 | 4.342 |
| Upper Arm Extended Circumference (cm) | Right | 30.613 | 3.700 |
| | Left | 31.12 | 3.751 |
| Forearm Length (cm) | Right | 27.2 | 1.192 |
| | Left | 27.333 | 1.305 |
| Forearm Circumference (cm) | Right | 26.913 | 1.733 |
| | Left | 26.52 | 1.869 |
| Fully Extended Arm Length (cm) | Right | 79.167 | 3.871 |
| | Left | 79.7 | 3.590 |
| Hand Length (cm) | Right | 19.2 | 1.177 |
| | Left | 19.5 | 1.210 |
| Wrist Circumference (cm) | Right | 17.88 | 1.456 |
| | Left | 17.72 | 1.367 |

**Table (6.3)**: Standard Specifications of Invacare Action$^2$ NG Self-Propelled Wheelchair.

| | |
|---|---|
| **Maximum User mass (kg)** | 125 |
| **Wheelchair Average mass (kg)** | 16.7 |
| **Overall length (cm)** | 103.5 – 106.5 |
| **Overall width (cm)** | 58.5 – 68.5 |
| **Seat Width (cm)** | 45.5 |
| **Seat Depth (cm)** | 43 |
| **Floor/Seat height (cm)** | 48 |
| **Distance between front and rear wheels (cm)** | 49.5 - 52 |
| **Rear Wheel diameter (cm)** | 61 (24”) solid tyre |
| **Handrim diameter (cm)** | 52 |
| **Castors** | 20 (8”) solid tyre |
| **Parking Brake** | Manual brake with indexed brake shoe |
| **Backrest** | Folding, reclining |
| **Armrests** | Removable, removable and swing-away |
| **Footrest Supports** | Removable and swing-away |
| **Seat Upholstery** | Black nylon on reinforced upholstery |
| **Frame** | Aluminium, epoxy coated |


**Figure (6.2)**: Manufacturer's setting of Invacare Action$^2$ NG Self-Propelled Wheelchair.

## 6.6 Upper body Kinematic Measurements during Wheelchair Mobility

### *6.6.1. Neutral Position Measurement*

During the one second static measurement, recruited subjects sit down straight on the wheelchair and maintain both arms by the side of the body with the elbows flexed to 90°, and both hands pronated. During the recording, the system measures the positions of the individual markers attached to bony landmarks in the global coordinate system (GCS), see Figure (6.3).

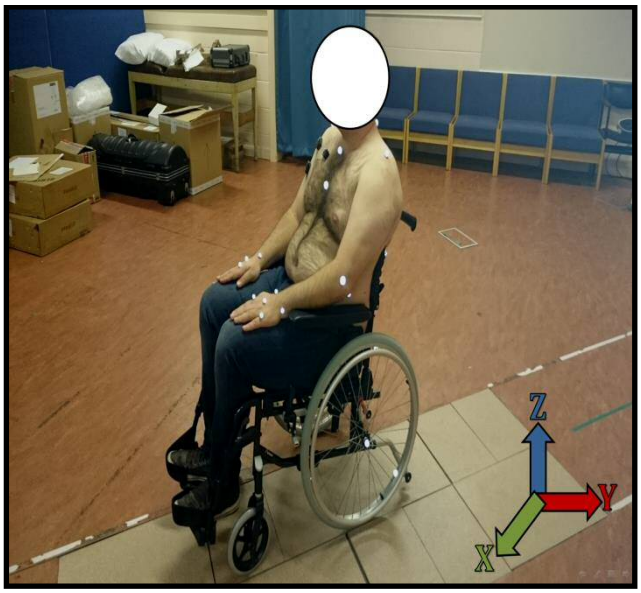


**Figure (6.3)**: Neutral position measurement with markers set on the upper body and the wheelchair.

### 6.6.2. *Dynamic Propulsion Measurement*

All the fifteen recruited subjects were asked to propel an Invacare Action$^2$ NG manual self-propelled wheelchair along a 10 meter linear path in the centre of the motion capture area across the Motion Analysis Lab at Cardiff University, while the motions of their trunk, right and left upper limbs measured using a motion analysis system (Oqus Cameras and QTM Software, Qualisys, Sweden), see Figure (6.4). For three trials conducted per each subject, only consecutive strokes occurring during steady-state propulsion were included in the analysis. The starting up and stopping pushes were excluded. Before the propulsion measurements, subjects are given about (5-10) minutes to get familiar with using the hand-rim wheelchair with their steady self-selected speed and propulsion pattern.


**Figure (6.4)**: Dynamic wheelchair propulsion measurement in the Motion Analysis Lab at Cardiff.

Also, recruited subjects were asked to perform start and stop tasks. They performed the start task inside the motion capture area and asked to propel themselves to the end of this area at the far side of the laboratory. For the stop task, subjects were asked to propel themselves and to stop when they reached the centre of the motion capture area. Three trials were collected for each task, see Figure (6.5).

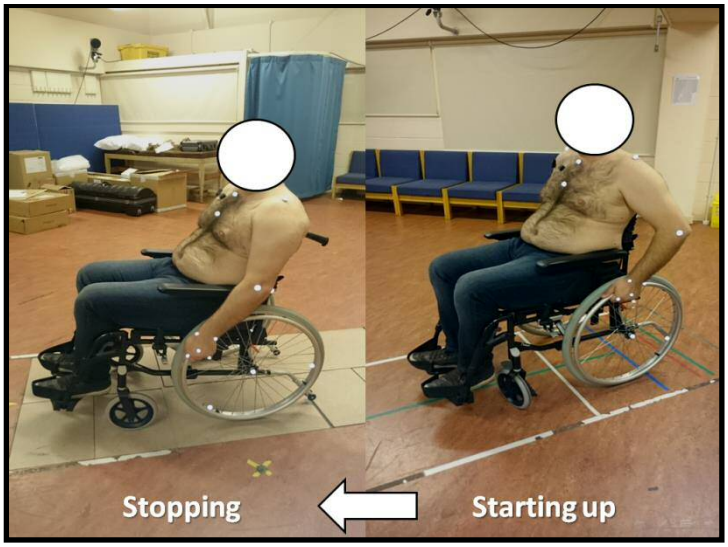


**Figure (6.5)**: Wheelchair starting up (right) and stopping (left) measurements.

### *6.6.3. Physiological Range of Motion ROM Measurement*

Dynamic measurements were performed for the functional range of motion of upper limb joints during performance of manual wheelchair propulsion. Each recruited subject was asked to perform physiological range of motion movements by using their dominant and non-dominant upper limbs starting from their neutral position while sitting on the wheelchairs.Three shoulder joint rotations, one elbow rotation, one forearm rotation and two wrist rotations were quantified simultaneously using three-dimensional measurement system, see Figures(6.6) and (6.7).

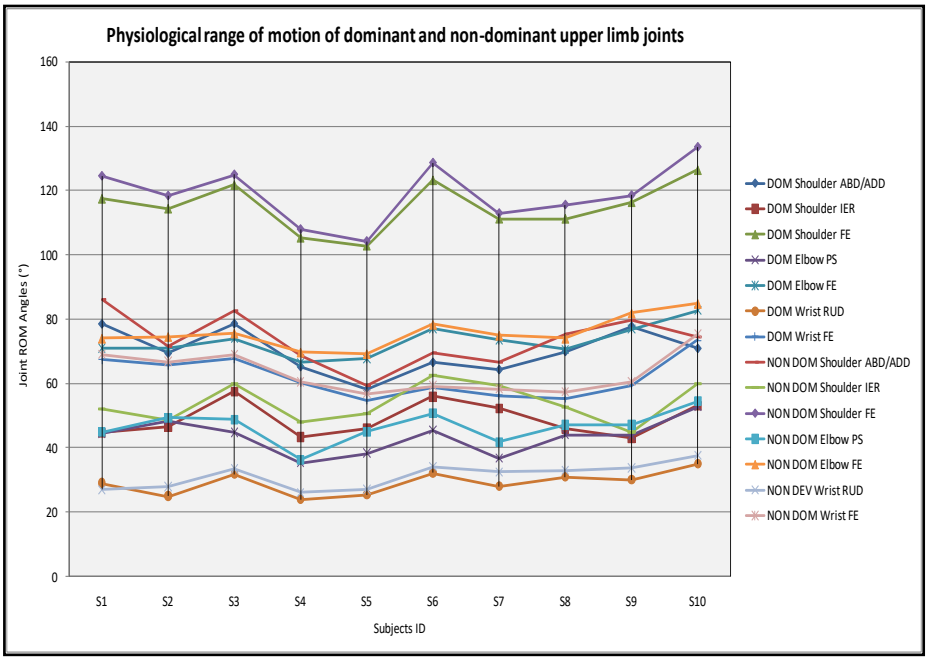


**Figure (6.6)**: Physiological range of motion measurements of dominant and non-dominant upper limbs of ten healthy volunteers. (ABD/ADD): abduction adduction, (IER): internal external rotation, (FE): flexion extension, (PS): pronation supination, and (RUD): ulnar radial deviation.

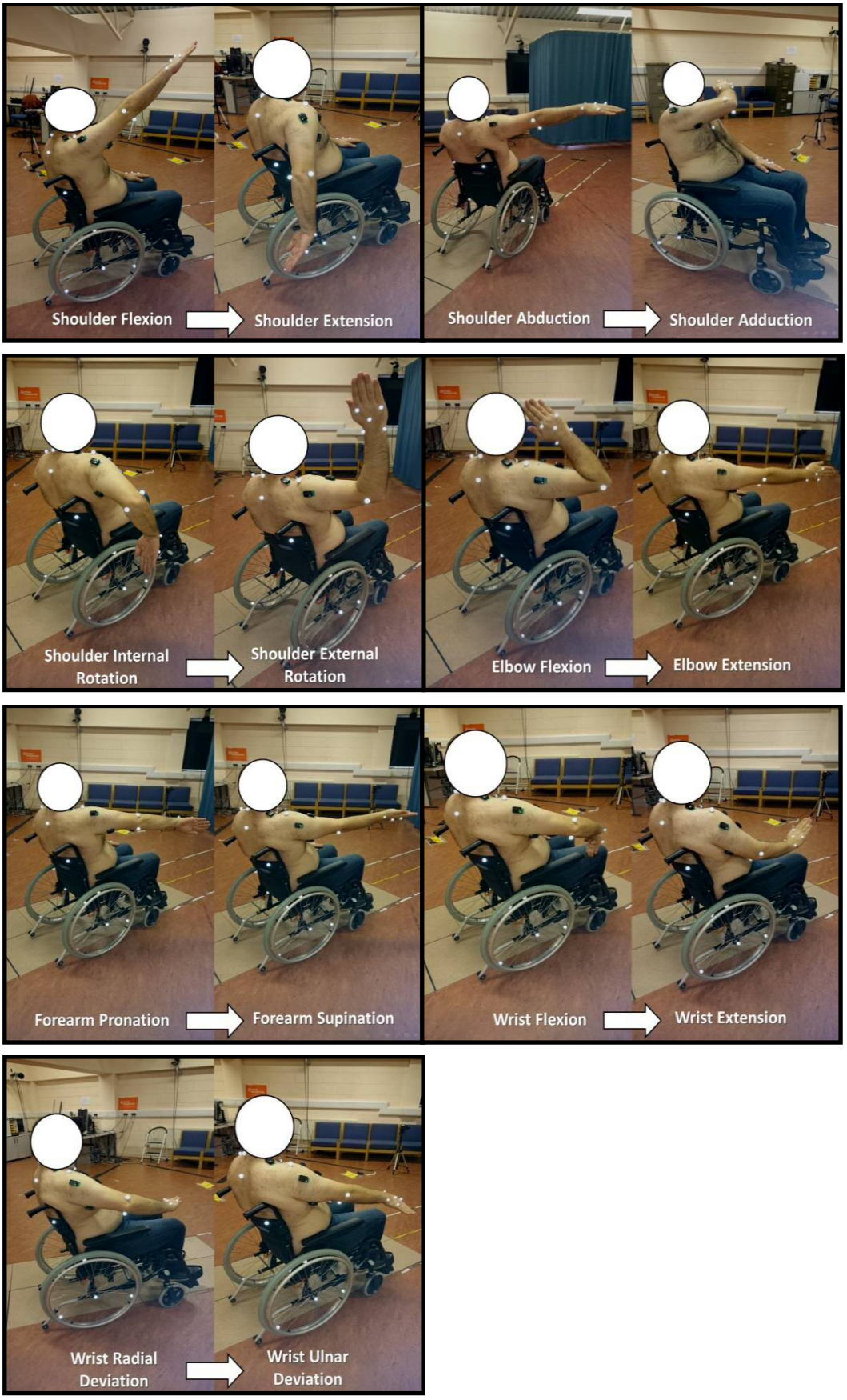


**Figure (6.7)**: Physiological range of motion of upper limb joint measurements.

## 6.7 Six Degrees of Freedom (6DOF) Analysis

In terms of establishing a six degrees of freedom 6DOF analysis for three-dimensional kinematics, each upper limb is modelled as a four segments linked system that consists of trunk, upper arm, forearm and hand. Each segment is considered as a single rigid body. 6DOF data (roll, pitch, yaw, x, y, z) were calculated according to the ISB recommendations by using the QTM software, (QTM Software, Qualisys, Sweden). Joint centres and local coordinate systems for all other segments were defined using International Society of Biomechanics (ISB) recommendations (Wu et al., 2005). Joint angles were defined as the three dimensional motion of the distal segment relative to the proximal segment using Euler angle decomposition on the basis of ISB recommendations. As was described previously in Chapter 4, humerus was defined according to the second option of these recommendations, which uses forearm position to determine the orientation of the humerus about its long axis, (Wu et al., 2005).

Following the ISB recommendations, the axes of each segment's coordinate system are aligned such that the X-axis directs anteriorly, the Y-axis directs superiorly and the Z-axis directs laterally towards the right side. A LCS was determined for each segment. Segment coordinate systems were determined for trunk and right and left upper limbsusing Euler angle notation and a sequence of ZXY rotations of the trunk, upper arm and hand, and ZYX rotations of the forearm.Although it is recognized that the shoulder complex motion involves the intricate linkages between the humerus, scapula and thorax, kinematic distinction between these rigid bodies were not considered per this study, and instead, only the gross motion of the humerus (upper arm) relative to the thorax (trunk) was considered in terms of humero-thoracic rotation. The rotation order of the humerus relative to the thorax was ZXY order, rather than the YXY order. As, in the latter order, gimbal lock occurs when the elevation of the upper arm will tend to zero degree. Also, both the axial rotation and the plane of elevation change greatly giving rise to extreme values, (Doorenbosch et al. 2003).

Therefore, motions of the thorax relative to the global coordinate system were described as: lateral flexion, axial rotation, and flexion–extension for the

trunk.Shoulder (humero-thoracic) angles were described as: plane of elevation, elevation, and axial rotation. Elbow angles were defined as motion of the forearm with respect to the upper arm and described as: flexion, carrying angle, and pronation–supination, in which 0° corresponds to full extension and a neutral forearm. Wrist angles were defined motion was defined as motion of the hand with respect to the radius and described as: flexion– extension, ulnar–radial deviation, and pronation–supination.

Additionally, the wheelchair backrest was modelled as a one rigid body segment using four markers, and both wheels were modelled as two rigid bodies using four markers per each. Wheelchair movements were determined with respect to the laboratory's global coordinate system. As the wheelchair is considered as a segment, it clearly cannot internally or externally rotate nor can it abduct or adduct at any time in the cycle, since it is secured on its axle in a fixed manner which does not allow movement in these directions. However, the wheelchair can flex or extend (produced by rotating about the hub axle) relative to the user's upper limb segment during propulsion.As a result, the 6DOF analysis has included 11 rigid bodies, see Figure (6.8).

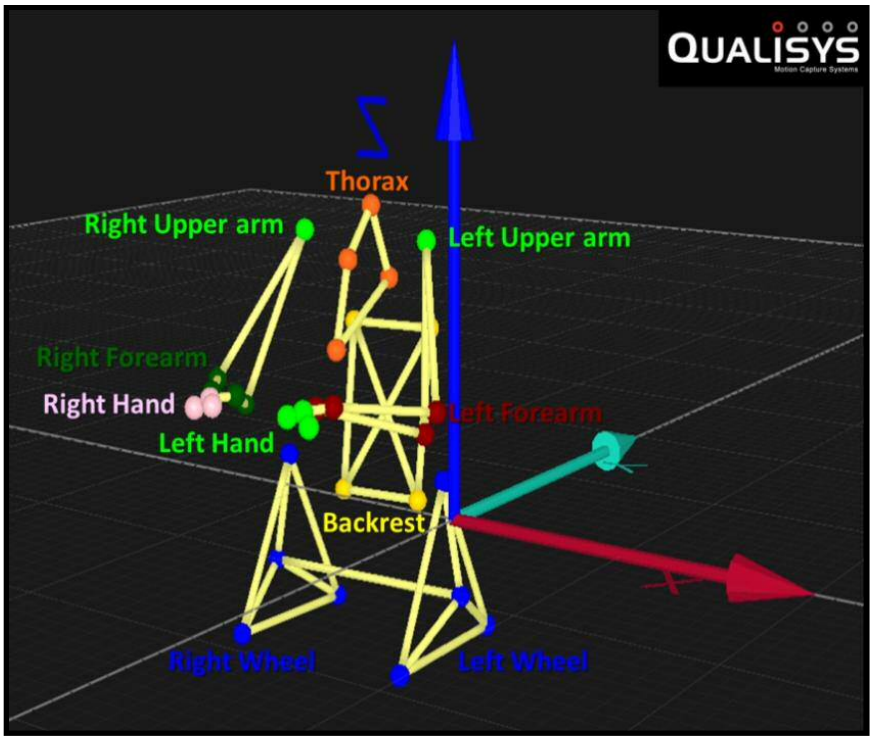


**Figure (6.8)**: A QTM view of a 6DOF model of the trunk, right and left upper limbs and the wheelchair (backrest and wheels) during neutral position.

## 6.8 Kinematic and Spatiotemporal Data Processing

6 DOF calculations were established for the markers arrays described above using the ISB convention. For each subject, the wheelchair stroke cycles were analysed to compute the mean group parameters of interest. Peak joint angles (maximum and minimum) were identified and used to compute the ranges of motion (ROMs).

For everyday manual wheelchair propulsion, the stroking motion is a bilateral cyclic motion. The stroke cycle starts at the instant the hand contacts the wheelchair handrim, and ends at the instant immediately before the next hand contact on the same wheel. The instant the hand loses contact with the rim (hand release) divides a stroke cycle into two phases – contact and recovery phases. Stroke cycle parameters include average velocity, distance travelled, stroke time, stroke frequency (cadence), push and release times and percentages, and contact, release, and push angles. One hundred percent stroke cycle is defined by both the contact and recovery phases, with 0% stroke cycle representing the initial contact at the beginning of the contact phase. The top dead centre is the highest point of the wheel regardless of the wheelchair orientation, see Figure (6.9), Chow et al. 2011).

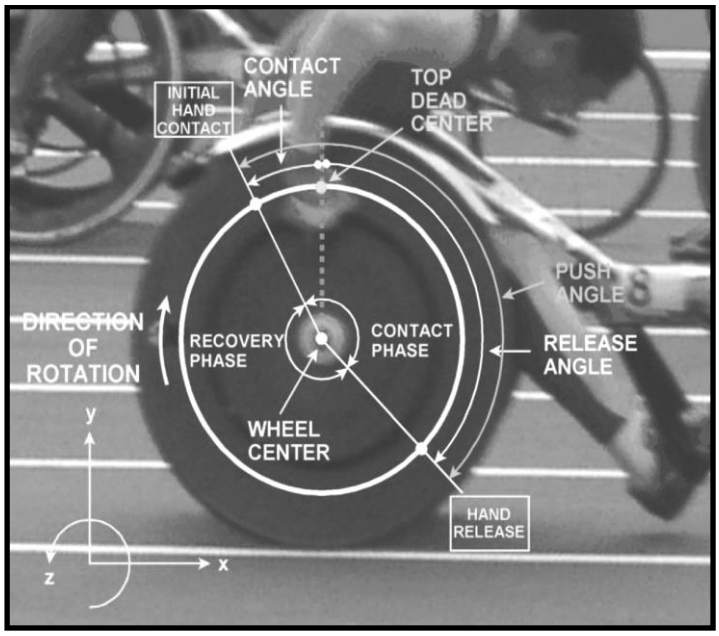


**Figure (6.9):** Critical instants and phases of a stroke cycle. The contact and release angles indicate the locations of hand relative to the wheel centre at the instants of hand contact and release, respectively, Chow et al. (2011).

Contact and release angles were calculated by coupling the markers trajectory between the wheel axle hub (WC) and the 3rd metacarpophalangeal joint centre

(MC3). The contact angle is the angle between the line which connects the initial hand-rim contact point (at the third MCP joint centre) of the propulsion cycle to the wheel axle hub (centre) and the horizontal line. While the release angle is the angle between the line which connects the final hand-rim contact point (at the third MCP joint centre) of the propulsion cycle to the wheel axle hub and the horizontal line.Then, the propulsion angle is the angle where the wheel moved during hand contact with the handrim, was determined by subtracting the wheel angle at the end of the contact phase (contact angle) from the wheel angle at the start of contact phase (release angle), (Kwarciak et al., 2009), see Figure (6.10).

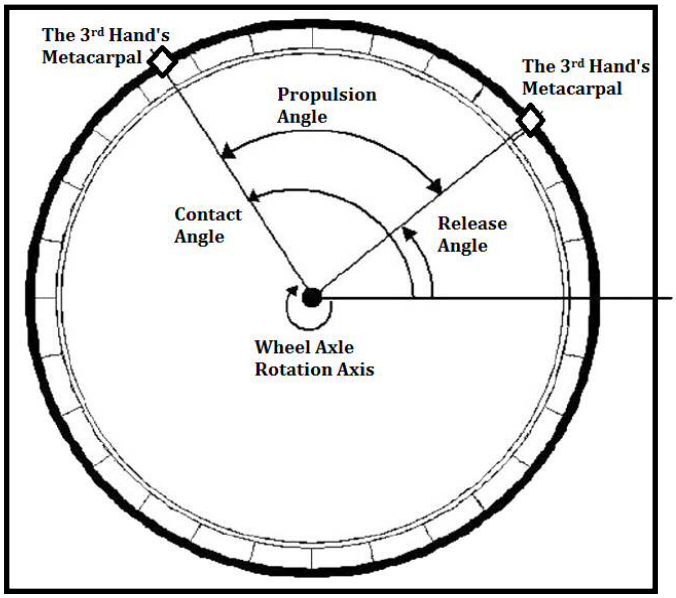


**Figure (6.10)**: Contact, release and propulsion angles, (Kwarciak et al., 2009).

## 6.9 Shoulder Muscle Recruitment during Wheelchair Mobility

The shoulder complex consists of several joints that function optimally when there are precise recruitment and coordination of the muscles attaching to these joints (Veeger and van der Helm, 2007). The muscles around this complex are largely responsible for maintaining the upper limb dynamic stability and provide adequate kinematic functioning. Since shoulder muscles function may guide the prescription of training and prevention of shoulder complex disorders, many studies have evaluated muscle function using surface electromyography (EMG).

De Luca (1997), in his classic study, showed that the number of active motor units has an important contribution to the EMG amplitude signal, although there is

no direct relationship between EMG amplitude and force. Biomechanical studies have linked manual wheelchair propulsion with a prevalence of upper limb musculoskeletal disorders. Upper limbs of wheelchair users are subject to unnatural loading conditions and repetitive use. Over time, the shoulder complex and especially the rotator cuff (shoulder) musculature of manual wheelchair users (MWU) deteriorate, which leads to a painful condition that is difficult to treat surgically, (Qi et al. 2014).

As previously explained, the push and recovery phases initiation was identified by the contact of the subject's hand on the hand-rim. When the hand initially made contact with the hand-rim, the push phase had begun, and as soon as the hand-rim was released the recovery phase had begun. Several studies have documented the muscle activation patterns during wheelchair propulsion using surface, (Requejo et al. 2008, Rodgers et al. 1994 and Yang et al. 2006) and indwelling (Mulroy et al. 1996 and Lighthall-Haubert et al. 2009) electromyographic (EMG) techniques.

Two muscle synergies have been identified during wheelchair propulsion, (Mulroy et al., 1996). The push phase synergy is dominated by anterior deltoid, pectoralis major, and biceps brachii. These muscles decelerate the back swing of the arm in the late recovery phase and then contribute to shoulder flexion in the push phase, and to prepare the hand, by increasing the hand speed, for impact on the pushrim, (Mulroy et al., 2004).

After the follow-through part of the push phase, the shoulder motions reversed direction in the recovery phase. The recovery muscle synergy is dominated by the middle deltoid, posterior deltoid and upper trapezius contracted eccentrically first to restrain shoulder flexion and then contracted concentrically to return the arm to its starting position during the recovery phase, (Mulroy et al., 1996). After the hand has made contact with the rim, the pull phase starts with an initial elbow flexion, accompanied by activity of the biceps brachii muscle. Anterior deltoid shows high activity at the beginning of hand contact, whereas pectoralis major displays a more constant activity of longer duration. These two muscles are considered to be the prime movers in wheelchair propulsion (Mulroy et al., 1996).

It has been reported that at the elbow joint, biceps brachii was activated in the late recovery phase and continued its action over a period when elbow flexion torque would contribute to the propulsion (Lighthall-Haubert et al., 2009). The peak muscular activity of the biceps brachii muscle was found at hand contact. Muscular activity of triceps brachii increased progressively during the push phase, reaching maximal values at hand release (Chow et al., 2011). In addition, synergy was shown between pectoralis major, anterior deltoid and latissimus dorsi. Muscular activity of these muscles increased from the end of the recovery phase and reached a maximum during the push phase. Posterior and middle deltoids together with upper trapezius were highly active during recovery, which illustrates their prime mover function, see Figure (6.11) and Table (6.4).

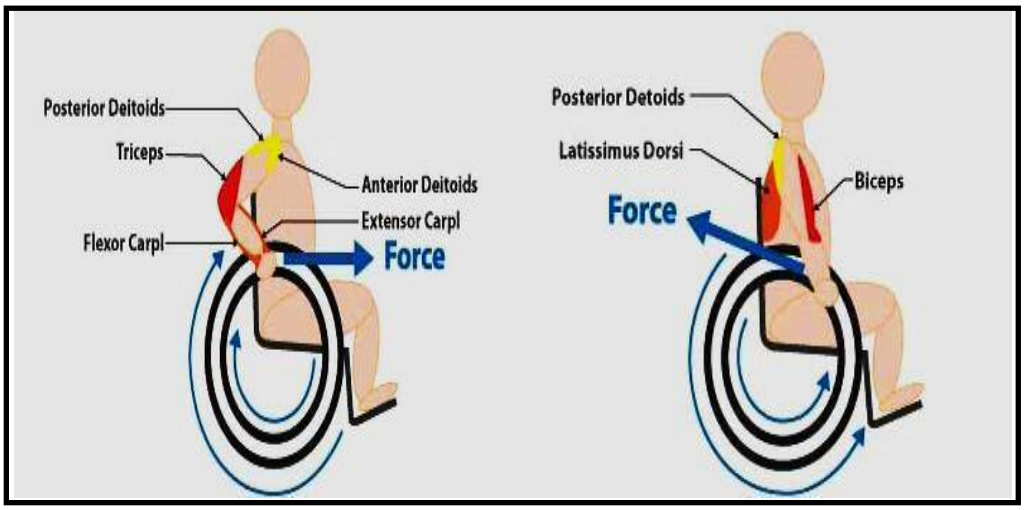


**Figure (6.11):** Shoulder activated muscles during the pushing phase (left) and the recovery phase (right) of the wheelchair propulsion.

**Table (6.4):** Muscle movements in the shoulder complex during manual wheelchair propulsion.

| Activated Muscle | Action during Manual Wheelchair Propulsion |
|---|---|
| **Anterior Deltoid** | Flexion and abduction at the shoulder joint. |
| **Posterior Deltoid** | Extension and abduction at the shoulder joint. |
| **Trapezius** | Elevate, retract, depress and rotate the scapula upward. Elevate the clavicle. |
| **Pectoralis Major** | Flexion, adduction and medial rotation at the shoulder joint. |
| **Biceps Brachii** | Flexes the elbow, supinates the forearm and flexes the shoulder. |
| **Triceps Brachii** | Extends the elbow. |

## 6.10 Surface Electromyography sEMG

Being a non-invasive and painless measure, surface electromyography (sEMG) has been applied in motion analysis to assess superficial muscle function, with application in sports, ergonomics, occupational and rehabilitation medicine. It allows for investigation of both muscle activation and muscle physiological characteristics, (Merlo et al. 2010). Surface EMG electrodes were positioned along the midline of the muscle belly in the direction of the muscle fibers because this will reduce the likeliness of the electrode detecting crosstalk from the adjacent muscle fibers. , In this location the EMG signal with the greatest amplitude is detected, see Figure (6.12).

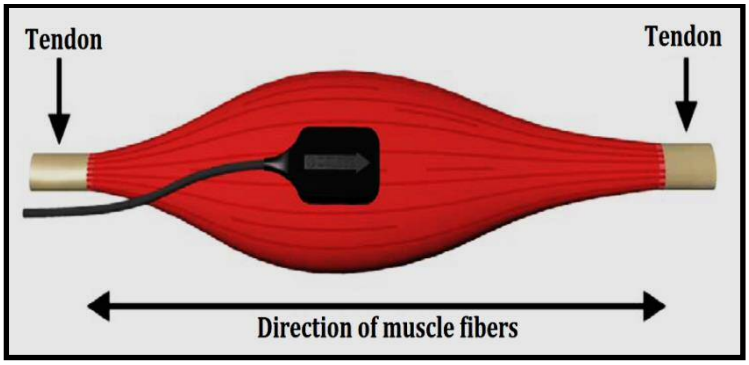


**Figure (6.12)**: The preferred position of surface EMG electrode in the midline of the muscle belly between the nearest innervation zone and the myotendonous junction.

### *6.10.1. sEMG Instrumentation*

Surface electromyography activity of upper extremity muscles was recorded using parallel-bar EMG Sensors (double differential sensor, 1mm in diameter and separated by 10 mm, Bagnoli$^{TM}$, Delsys Inc., Boston, MA, USA), see Figure (6.13), (Delsys). Volunteers were prepared for the placement of these sEMG electrodes by shaving the skin hair of each electrode site, cleaning it carefully with an alcohol wipe and lightly abrading it.

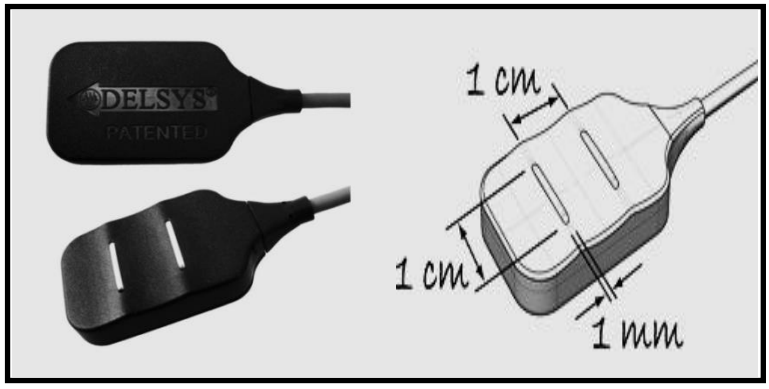


**Figure (6.13)**: Delsys surface EMG electrode used in this particular study, (Delsys).

Delsys Trigno wireless EMG system was used to measure the sEMG signals detected on six shoulder muscles of each healthy volunteer's dominant arm, which were recruited for their well-known contribution to manual wheelchair propulsion, see Figure (6.15), (Delsys). These muscles were: anterior deltoid, posterior deltoid, sternal head of the pectoralis major, biceps brachii, triceps brachii and the upper part of the trapezius, (Louis and Gorce 2010).


**Figure (6.14)**: DelsysTrigno wireless EMG system, (Delsys).

### *6.10.2. sEMG Electrode Placement*

Surface electrodes placement was confirmed by testing elevation (anterior, and posterior deltoid), external rotation (upper trapezius and posterior deltoid), internal rotation (pectoralis major) and arm flexion (biceps brachii and triceps brachii), see Figure (6.15). The electrodes placement locations are selected based on (Perotto, 2011) that involving muscles position and their EMG electrodes location as summarised per the following Table (6.5) and shown in Figure (6.16).

Along with this, the EMG voltage plot was used to distinguish between the push and recovery phases of wheelchair propulsion. The EMG analysis was mainly used to determine which muscles are activated to initiate the two phases of propulsion and which are the prime movers during these phases, see Figure (6.17).

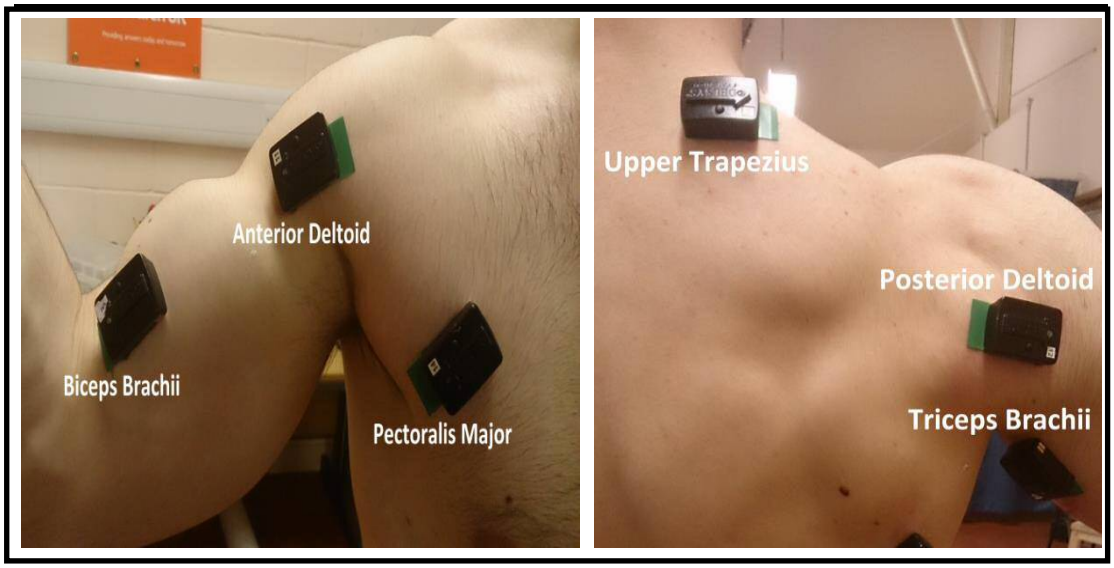


**Figure (6.15)**: DelsysTrigno wireless surface EMG electrodes placed over six dominant shoulder muscles.

**Table (6.5):** Shoulder muscles position, their sEMG electrodes location and required test maneuver.

| Shoulder Muscle | Position | sEMG Electrode Location (x) | Test Maneuver |
|---|---|---|---|
| **Triceps Brachii** | Patient prone with arm abducted | Three finger breadths proximal to the medial epicondyle (EM) of humerus | Extension of elbow |
| **Anterior Deltoid** | Patient supine with arm at side | Three finger breadths below the anterior margin of the acromion (GH) | Forward elevation of the arm |
| **Posterior Deltoid** | Patient prone with arm abducted to 90° and elbow flexed over the edge of plinth | Two finger breadths below the posterior margin of the acromion (GH) | To elevate the arm off the plinth |
| **Biceps Brachii** | The patient supine with the arm extended | Into the bulk of the muscle in mid-arm | To flex or to supinate the forearm |
| **Pectoralis Major** | Patient supine | Insert needle electrode into anterior axillary fold | Horizontal adduction of the arm |
| **Upper Trapezius** | Patient prone | At angle of the neck and shoulder | Shrug shoulder |

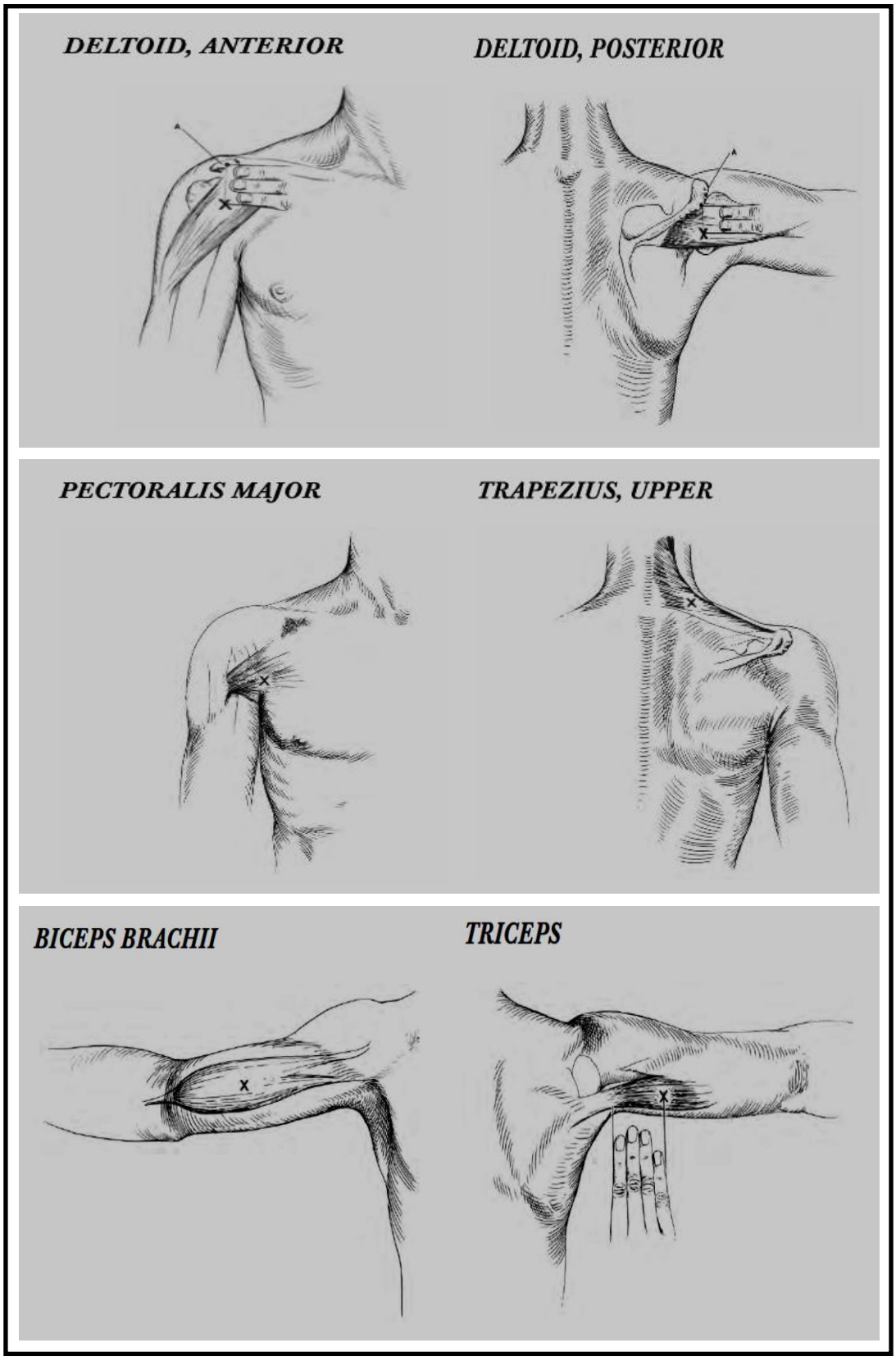


**Figure (6.16):** Shoulder muscles position and their sEMG electrodes location, Perotto 2011.

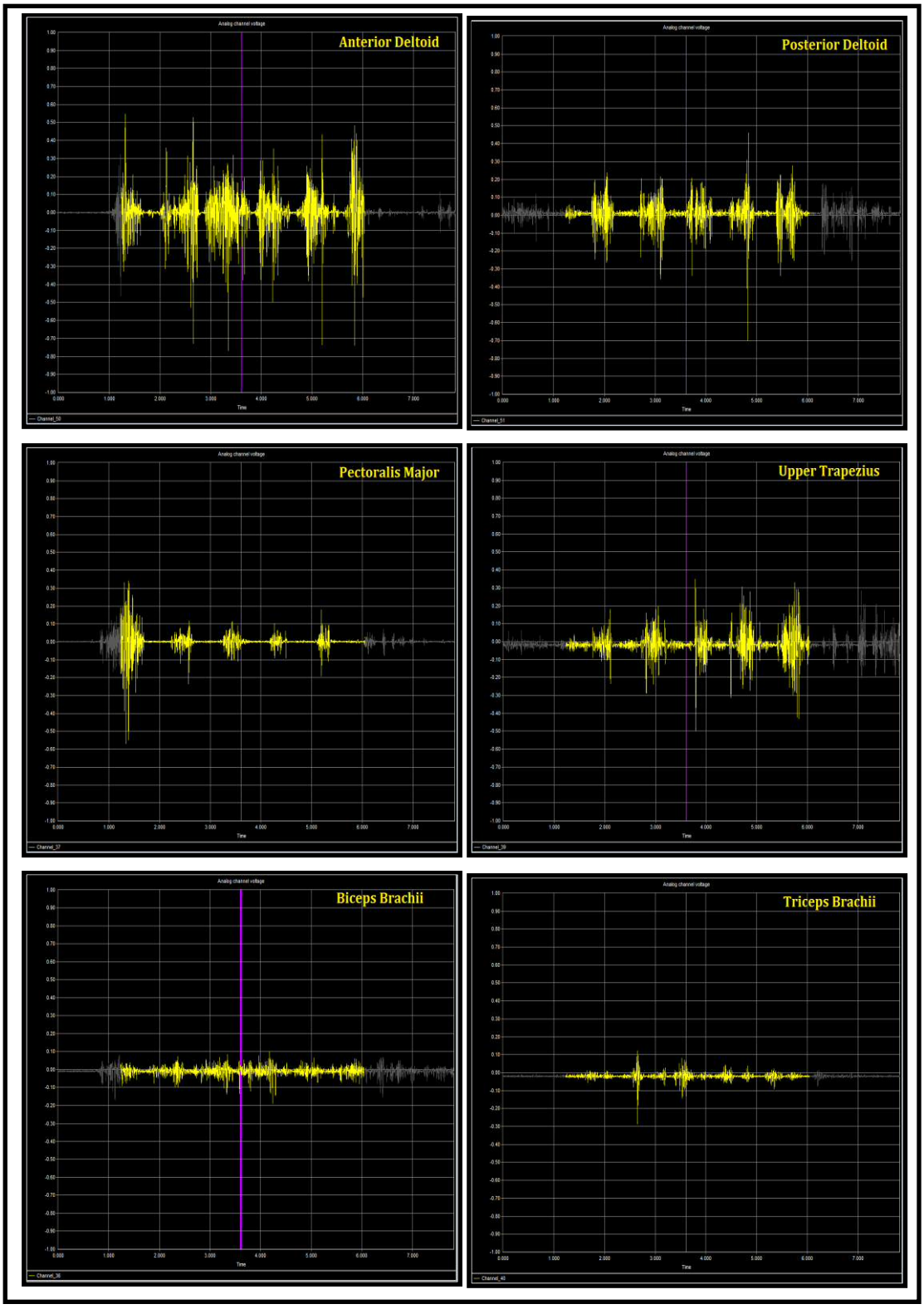


**Figure (6.17)**: Recorded EMG signals of six shoulder muscles during five active consecutive propulsion cycles of manual wheelchair propulsion.

## 6.11 Normalisation of EMG Signal

A comparison of electromyographic (EMG) activity of the muscles between and within subjects, and during separate occasions of testing, requires normalisation. Normalisation of EMG signals is usually performed by dividing the EMG signals during a task by a reference EMG value obtained from the same muscle. By normalising to a reference EMG value collected using the same electrode configuration, factors that affect the EMG signals during the task and the reference contraction are the same. Therefore, one can validly obtain a relative measure of the activation compared to the reference value, (Halaki and Ginn 2012). The most common way for generating the reference level used for normalising shoulder EMG data is with a maximum voluntary contraction (MVC).

### *6.11.1. Maximum Voluntary Contraction (MVC)*

The most common method of normalising EMG signals from a given muscle uses to the EMG recorded from the same muscle during a maximal voluntary contraction (MVC) as the reference value (Soderberg et al. 1991). The process of normalisation using MVC is that a reference test is identified which produces a maximum contraction in the muscle of interest. Prior to the collection of propulsion data, a set of muscle tests in a seated position were performed by each subject for inducing a maximum voluntary contraction (MVC) in each muscle in terms of normalising the EMG activity of the shoulder muscles reliably. These tests were described by Boettcher et al. (2008), who examined the activity of 12 shoulder muscles during functional tasks and identified a set of four tests known as (Shoulder Normalization Tests) to maximally and reliably activate all the shoulder muscles tested. Therefore, this study suggests that these tests be adopted as the standard tests for generating a maximum voluntary contraction MVC for normalization in future EMG research at the shoulder.

These four tests are illustrated as follows, see Figure (6.18):

***Task 1:*** The ‘‘***empty can***’’ test position with the shoulder abducted to 90° in the plane of the scapula, internal humeral rotation, and elbow extended. The arm is abducted as resistance is applied at the wrist.

***Task 2:*** The "***internal rotation 90°***" test position with the shoulder abducted to 90° in the plane of the scapula, neutral humeral rotation, and elbow flexed 90°. The arm is internally rotated as resistance is applied at the wrist.

***Task 3:*** The ''***flexion 125°***'' test position with the shoulder flexed to 125° as resistance is applied proximal to the elbow and at the inferior angle of the scapula, attempting to de rotate the scapula with the subject sitting in an erect posture with no back support.

***Task 4:*** The ''***palm press***'' test position with the shoulders flexed to 90° bilaterally, the heel of the hands together, elbows flexed 20°, and then the arms horizontally adducted.

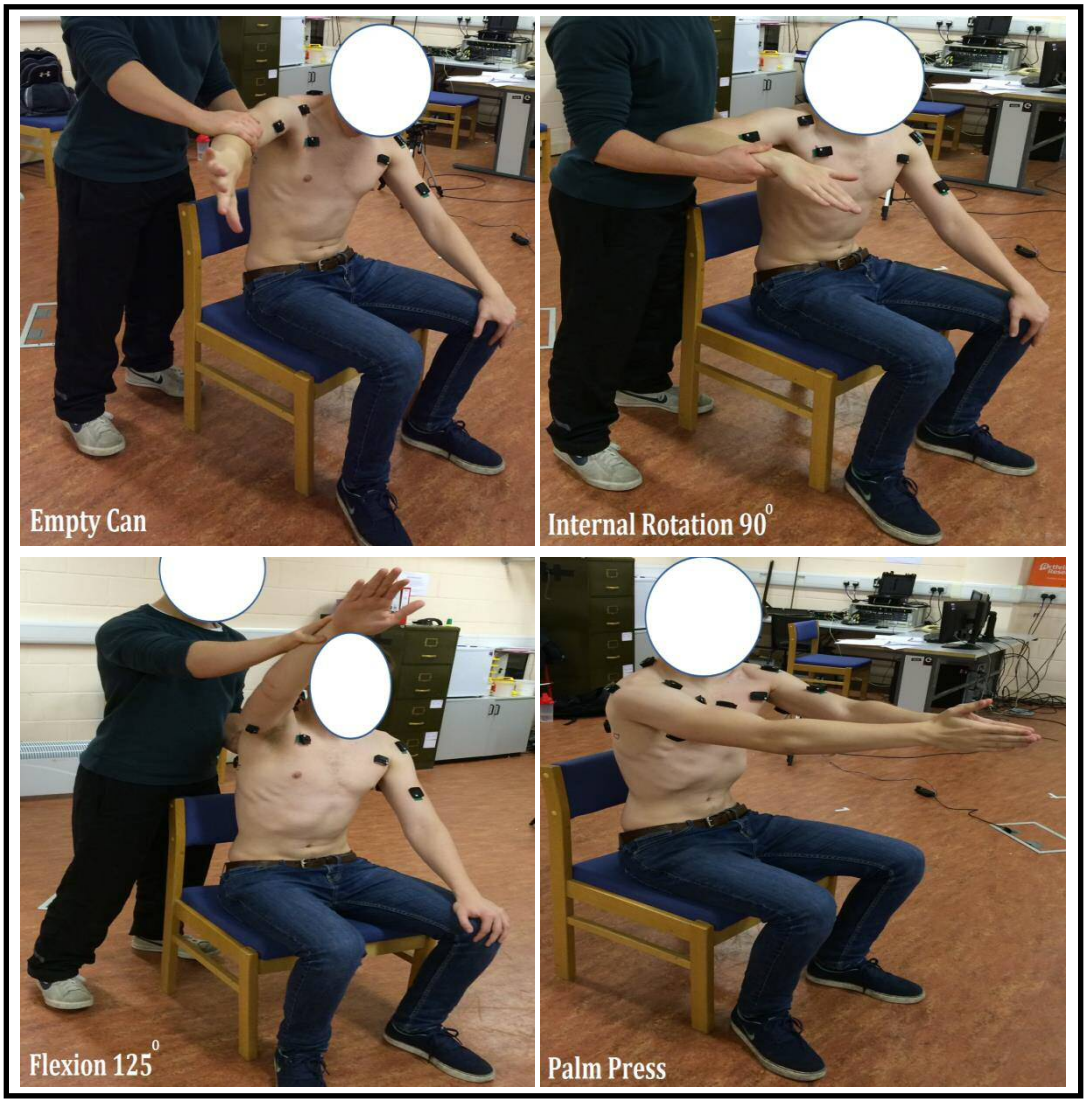


**Figure (6.18)**: Shoulder muscles normalization test; empty can, internal rotation 90°, flexion 125° and palm press, Boettcher et al. (2008).

These four MVC tasks were performed together, separated by at least 30 seconds between each one. Based on the repeatability between test measures, two repetitions of the tests were performed separated, by at least three minutes to reduce any possible fatigue effects. The maximum values obtained from the processed signals during all repetitions of the test were used as the reference value for normalizing the EMG data, processed in a similar manner from the muscles of interest.

Boettcher et al. (2008) have shown that multiple tests can produce maximum recording from any given muscle and that no specific test produces maximum recording from a given muscle in all individuals tested. This indicates that the use of a separate single MVC test to identify maximum activity in a given muscle is not valid and that sets of tests are required in order to ensure maximum activity in a given muscle is recorded from all subjects.

Provided that maximum neural activation is achieved in all muscles and individuals tested, using MVCs is a highly reliable method to normalise EMG data and can be used to compare activity between muscles, between tasks and between individuals. To achieve the maximum neural activation in all muscles and individuals, sets of MVC tests that produce maximum activation in each muscle need to be identified.

The collected EMG data were normalised to the MVC taken on the day of those particular trials. This was to make the normalised data more reliable because the MVC was recorded with exactly the same electrode configuration, positions and conditions as was used in the propulsion trials.

## 6.12 EMG Raw Data Processing

The recorded EMG signals were amplified and sampled at a frequency of (1080 Hz). Raw EMG data for each activated muscle were identified according to its EMG channel throughout the MVC test and every dynamic wheelchair propulsion trial, then been exported to Matlab (Mathworks, Natick, MA, United States) for signal analysis and post-acquisition processing. The signals were pre-amplified,

high-pass filtered by a Butterworth fourth order filter at (20 Hz), full wave rectified, and low pass filtered with a fourth order Butterworth filter at (500 Hz). Muscle activation was described as the linear envelope of the signal. This type of treatment eliminates ambient noise through the high-pass filter, and smoothens the curve through full-wave rectification and the low pass filter, thus creating the linear envelope (Boettcher et al., 2008).

As mentioned by Rose (2014), the high pass filter was used to remove the low frequency signals associated with soft tissue artefacts caused by skin movement due to muscle contraction. The low pass filter was used to remove the high frequency signals associated with interruption caused by the electrodes being subject to a force that may be applied by the observer's resistance at the participant's scapula, elbow and wrist during performing the MVC tasks. Both the high and low pass filters were utilized in a band pass filter. Once the signal processing had been applied, the processed EMG data were normalised to the MVC tasks performed so as to be presented as a percentage of the maximum contraction that was established in the MVC four tasks against time.

Once the analysis process had been implemented, the outputs were subsequently input into a different Excel files as processed EMG data (voltage against time) and normalised EMG data as a percentage of the maximum contraction (%MVC against time) that was established in the MVC test to define each muscle activity.

## 6.13 Statistical Analysis

The mean and standard deviation values of the trunk and dominant and non-dominant upper limb joint kinematics, as well as the mean and standard deviation values of the dominant shoulder muscle normalised activities were analysed. To compare the results between the different wheelchair configurations, parametric repeated measures were used since the data were normally distributed. The statistical analyses were employed by using repeated two ways ANOVA and Person's correlation (r) coefficient. P-value was calculated. Descriptive statistics were

calculated for each variable. The level of significance was set at $P < 0.05$ for all statistical analyses.

Moreover, the data were tested for normality through using the Shapiro-Wilk expanded tests with using the Q-Q plots for the normal distribution comparison. When P-value was more than the chosen level of significance (i.e. 0.05), then an evidence that the data tested were from a normally distributed population. While when the P-value was less than 0.05 then the null hypothesis that the data are normally distributed is rejected.

## 6.14 Summary

This chapter is an extension of the previous Chapter Five that aimed to introduce the general procedure that was followed to quantify functionality of the trunk and upper limbs in able-bodied individuals with propelling a manual wheelchair during daily mobility and use. The motion analysis facilities at Cardiff University were employed to investigate three-dimensional kinematics across a range of daily living activities, including manual wheelchair starting up, propulsion and stopping. The 6DOF analysis method was applied to quantify the kinematics of the trunk and upper limbs in terms of range of motion angles. Spatiotemporal parameters such as contact and release angles, as well as stroke cadence, time and velocity were used to assess variations across wheelchair diverse configurations as well as performance outcomes. Also, this chapter presented the general procedure that was followed to measure the surface electromyographic activity (sEMG) of the shoulder muscles which have a dominant role during the wheelchair mobility. It provided a detailed illustration about the instrumentation, surface electrodes placement and maximum voluntary contraction tasks used to investigate the activation patterns of the recruited muscles during manual wheelchair daily mobility and use. The ethical review process, participants and inclusion/exclusion criteria were explained in this chapter.

# Chapter 7

## Impact of Wheelchair Configurations on Upper Body Biomechanics

The use of a manual wheelchair suitable for a user's individual characteristics and needs can improve their independence, sense of participation and quality of life. Many aspects relating to wheelchair configuration affect user actions in a manual wheelchair; determining the overall mobility performance. Changes in the wheelchair configuration can affect propulsion forces, the range of motion (ROM) of the upper limb joints and system stability. Ultimately, all these aspects determine how easy or difficult it is to propel a wheelchair in everyday mobility, (Medola et al, 2014).

System stability and mobility performance are two inter-related variables: improving one has an impact on the other. Accordingly, healthcare professionals have to find the best balance between stability and performance when prescribing a wheelchair. Consequently, understanding how the changes in wheelchair configuration impact a user's work and system stability is important for minimizing the demand on the upper limbs during manual propulsion and optimizing the user's mobility, (Medola et al. 2014).

Apart from the user's postural and pressure management goals, the manual wheelchair should be configured to optimise stability and manoeuvrability for everyday function. Stability is necessary to ensure the user safety and security in chair use. A very stable wheelchair would minimise risk of the user tipping out of the wheelchair rearward, forward or laterally during propulsion and activities. However such a wheelchair configuration would have a long wheelbase, reduced manoeuvrability and be difficult when trying to raise the front castors for climbing gutters or descending a slope or kerb. Manoeuvrability affects access to tight spaces and the ease of propulsion. Manoeuvrability and stability in the wheelchair can be altered by adjustment of the rear axle and the front castor positions in relation to the centre of mass of the wheelchair and user. A very manoeuvrable wheelchair would fit into tight spaces and be very responsive to the user in rolling, turning and performing a wheelstand, (NSW Spinal Seating Service 2011).

This chapter is an extension of Chapter Six that aimed to present focused a development of the wheelchair-user interaction through investigating the impact of wheelchair diverse configuration on the upper body biomechanics. From a biomechanical perspective, the most important factors affecting manual wheelchair mobility are the position of the wheels and seat height relative to the user. Therefore, this chapter employed the methods described in the previous Chapter six to address these features and how they influence the upper body biomechanics with propelling a manual wheelchair during daily mobility and use.

Variation was focused on the two most important wheelchair settings in terms of the biomechanics of manual propulsion; seat height and anterior-posterior axle position of the rear wheel. The vertical distance between the rear wheels and the seat greatly influences the biomechanics of manual propulsion. Having a lower seat benefits manual propulsion because it results in increased push angle. However, it results in increased upper limbs' ROM, such as shoulder abduction, internal rotation and elevation to move through the pushing, which is potentially harmful if physiological limits are exceeded (van der Woude et al. 1989). On the other hand, when the user is too high above the wheels (i.e. in a higher seat), he/she can only push the handrims over a short distance (small push angle), and to maintain the desired speed, the user has to increase push frequency which may lead to muscular fatigue (Boninger et al. 2000).

The anterior–posterior position of the rear wheels influences two important aspects of wheelchair mobility: stability and manual propulsion. While positioning the wheels rearward improves stability, it limits the user's ability to reach the handrims in this rearward position, thus reducing the push angle and increasing the angle of shoulder extension and wrist radial deviation when grasping the handrim. An axle located behind the shoulder position would require a greater angle of shoulder extension to reach the rear wheel and place the wrist in a greater radial deviated position. Alternatively, moving the wheels forward improves propulsion biomechanics but reduces stability. The optimal position of the rear wheels is a client-dependent decision, based on the user's perception of stability and ease of chair propulsion, (Medola et al. 2014).

## 7.1 Experimental Work

The relationship between manual propulsion biomechanics and wheelchair configurations was investigated in this chapter using the same protocol was applied before while the wheelchair was being setup according the manufacturer's specification, (Invacare, 2011).

Ten healthy male able-bodied novice individuals, (eight right-arm dominant, mean age mean age 38.00 ± 3.97 years, and body mass index 30.79 ± 4.41), with no previous experience with manual wheelchair propulsion performed, were performed the same activities defined by the previous protocol separately with four wheelchair configurations resulting from two different seat heights and two different anterior-posterior axle positions. Trunk and both upper limbs joints kinematics and dominant shoulder muscles recruitment were analysed for these wheel configurations to investigate its impact on upper limbs biomechanics during functional tasks of manual wheelchair propulsion.

These configurations were set by adjusting the following:

(1) The horizontal axle position of both rear wheels by (3 cm) and (6 cm) backward displacements from the original position set by the manufacturer.

(2) The vertical distance between the wheelchair seat and the floor distance set by the manufacturer by (45 cm) and (50 cm) heights.

These two adjustment sets were also made at the motion analysis laboratory of Cardiff University according to the set up instructions mentioned by the product adjustments manual. The existing adjustment holes on the used wheelchair frame were incremented from the manufacturer’s wheel hub by (1 cm) between each other, (Invacare, 2011), see Figure (7.1).

Providing wheelchair users with adjustable seat height and axle position and then fitting the user to the wheelchair can improve propulsion biomechanics and likely reduce the risk of injury, (Boninger et. al, 1999).

Most of the ten recruited volunteers were of large body mass index. Therefore, as the rear wheels are moved more forward (anteriorly), the distance between the centre of gravity and the rear wheel axle will be shorter and the centre of

gravity will get closer to the rear wheel axle. If the rear wheels are too far forward for balance skills of the user then the chair will be at risk of tipping over backwards. This can be considered as a health and safety concern for any person, especially with non-experienced users. Therefore, only posterior displacements were recommended per this study.


**Figure (7.1)**: The manufacturer and displacements of (Right) the wheelchair rear wheel axle and (Left) seat to floor position, (Invacare, 2011).

The following steps were performed to make the required rear wheel axle position adjustments, see Figure (7.2), (Invacare 2009):

(1) Locate the wheelchair on the back for easier access to the underside of the wheelchair.

(2) Press in the detent pin on the centre of the wheel and slowly pull the wheel off of the frame to release the Quick Release axles.

(3) Use the Allen key and the flat jaw pliers simultaneously to secure the mounting screws, remove the five mounting screws securing each side of the axle mount.

(4) Move the axle mount the required number of slots (3 cm between each) to maintain the desired position.

(5) Re-attach the mounting screws to fix the axle mount in its new position. Then re-attach the wheel by holding the detent pin down, and inserting the wheel back into the axle mount.

(6) Repeat the above five steps for the other side rear wheel. Note that both rear wheels should be set at the same position.

The seat-to-floor distance is adjusted by raising or lowering the quick-release axle spacer on the wheelchair frame. Raising the spacer lowers the seat, and vice versa. In order to obtain the desired seat to floor height, it will be necessary to perform changing the rear wheel height positioning.

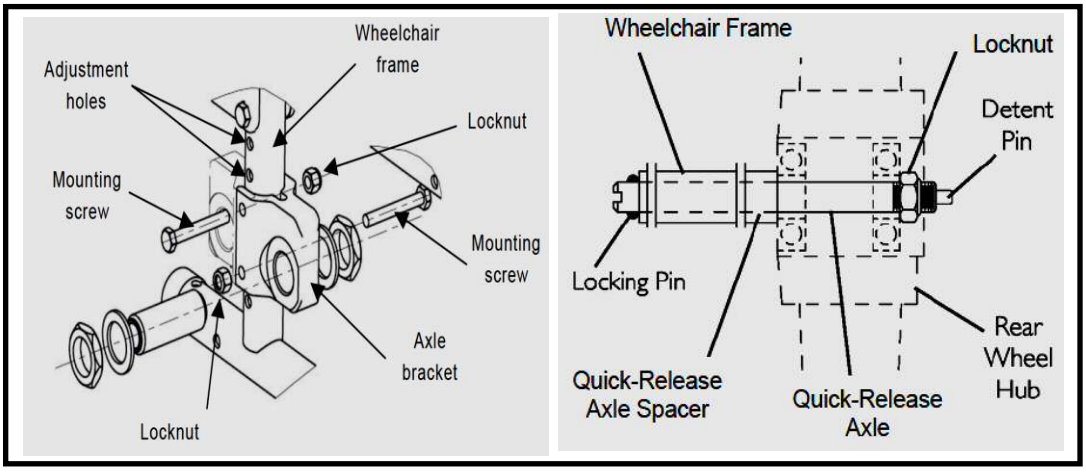


**Figure (7.2)**: Schematic diagram of the wheel axle and axle mount adjustment, (Invacare, 2009).

Adjusting seat-to-floor distance affects the front castor angle. Therefore, there should be also adjustment to compensate the castor angle, see Figure (7.3). The following steps were performed to make the required castor stem angle:

(1) Loosen the two mounting screws that secure the castor assembly to the wheelchair frame. It is not necessary to remove the mounting screws.

(2) Rotate the castor assembly to the desired angle. Both castors should be set at thesame angle.

(3) Tighten the mounting screws that secure the castor to the wheelchair frame.

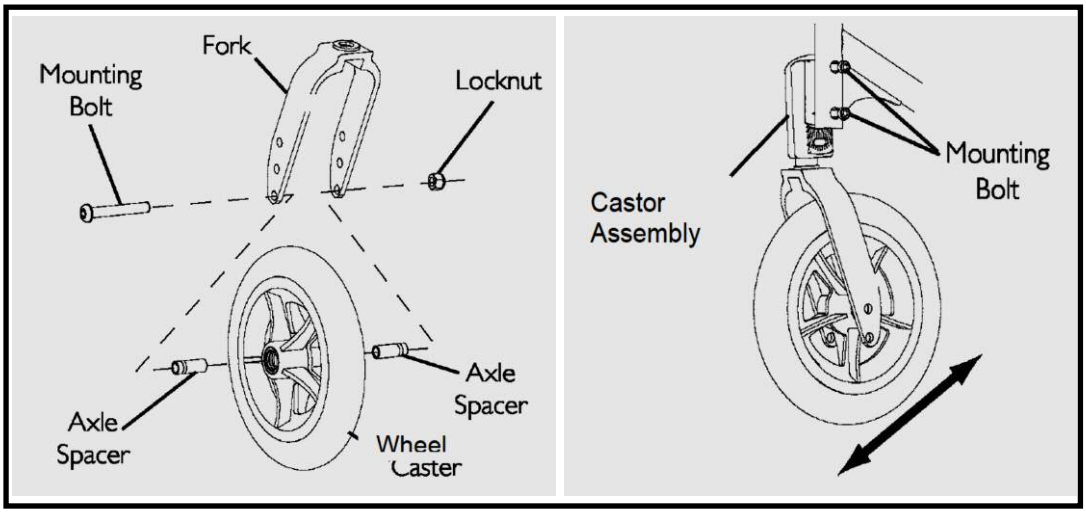


**Figure (7.3)**: Schematic diagram of the castor stem angle adjustment, (Invacare, 2009).

When correctly adjusted the castor stem should be perpendicular to the ground, i.e. castor stem angle = 90°, the following steps were performed to make the required seat to floor position (distance between the rear of the seat upholstery and the ground) adjustments, see Figure (7.2), (Invacare 2009):

(1) Locate the wheelchair on the back for easier access to the underside of the wheelchair.

(2) Press in the detent pin on the centre of the wheel and slowly pull the wheel off of the frame to release the Quick Release axles.

(3) Use the Allen key and the flat jaw pliers simultaneously to remove the locknut and secure the mounting screws that secure the axle bracket to the wheelchair frame.

(4) Align the axle bracket with one of the six adjustment holes on the wheelchair frame to maintain the desired position.

(5) Secure the axle bracket to the wheelchair frame, at the desired height, with the locknut and mounting screw. Then re-attach the wheel by holding the detent pin down, and inserting the wheel back into the axle mount.

(6) Repeat the above five steps for the other side rear wheel. Note that both rear wheels should be set at the same position.

## 7.2 Results

All the selected kinematic, sEMG and spatiotemporal parameters data were averaged from three trials for each manual wheelchair mobility task (starting up, propulsion and stopping) performed by each recruited volunteer then averaged again for the ten volunteers for each wheelchair configuration. See Tables (7.1) to (7.16).

### *7.2.1. Trunk and Upper Limb Kinematics*

Under the wheelchair manufacturer's configurations, it was found that the average and standard deviation values to be within the range of (8.988° ± 2.365°) for trunk flexion/extension, (7.007° ± 1.502°) for trunk lateral bending and (5.540° ± 1.398°) for trunk axial rotation. Gagnon et al. (2015) reported trunk flexion/extension motion to be within the range of (5.88° ± 2.12°).

Dominant shoulder abduction/adduction, internal/external rotation and flexion/extension were evaluated within the range of (17.448° ± 3.875°), (28.254° ± 6.218°) and (48.299° ± 7.330°) respectively.

Non-dominant shoulder abduction/adduction, internal/external rotation and flexion/extension were evaluated within the range of (18.780° ± 3.481°), (30.590° ± 6.219°) and (49.349° ± 6.124°) respectively. Boninger et al. (1998) reported shoulder motion at speed of (1.3 m/sec) to be within the range of (75°) for flexion/extension, (26°) for abduction/adduction and (37°) for internal/external rotation. While Soltau et al. (2015) reported shoulder motion to be within the range of (72.6°) for flexion/extension, (67.9°) for abduction/adduction and (22.8°) for internal/external rotation.

Dominant elbow pronation/supination and flexion/extension were evaluated within the range of (19.886° ± 5.580°) and (42.189° ± 4.790°) respectively. Non-dominant elbow pronation/supination and flexion/extension were evaluated within the range of (20.907° ± 2.912°) and (42.449° ± 4.776°) respectively. Soltau et al. (2015) reported elbow motion to be within the range of (45.7°) for flexion/extension and (28.8°) for pronation/supination (forearm rotation).

Dominant wrist radial/ulnar deviation and flexion/extension were evaluated within the range of (33.347° ± 5.584°) and (51.090° ± 5.828°) respectively. Non-dominant wrist radial/ulnar deviation and flexion/extension were evaluated within the range of (33.641° ± 4.527°) and (52.432° ± 5.276°) respectively. Boninger et al. (2004) reported wrist motion at low speed (0.9 m/sec) to be within the range of (50.3°) for flexion/extension and (44.6°) for radial/ulnar deviation. Also, Crespo-Ruis et al. (2011) reported wrist motion in their study about wheelchair basketball to be within the range of (27.18°) for flexion/extension and (21.46°) for radial/ulnar deviation.

### *7.2.2. Functional Tasks of Manual Wheelchair Mobility*

During the starting up task, both shoulder and wrist joints showed the largest ROM of flexion–extension, (44.897° ± 16.194°) and (55.877° ± 8.328°) respectively. While the trunk axial rotation and lateral bending showed the smallest ROM of (4.154° ± 1.336°) and (5.293° ± 1.646°) respectively.

Additionally, during the stopping task, both shoulder and wrist joints showed the largest ROM of flexion–extension, (25.005° ± 5.230°) and (33.825° ± 4.772°)

respectively. While the trunk axial rotation and lateral bending displayed the smallest ROM of (3.213° ± 1.143°) and (3.738° ± 0.600°) respectively.

**Table (7.1)**: Kinematic ROM angles of trunk and upper limb joints with the manufacturer's rear wheel axle position and (3 cm) and (6 cm) backward displacements during ***manual wheelchair propulsion***. All the joint ROM angles are presented as group mean and standard deviation values in degrees.

| Upper Body Rigid Segment Kinematics | | Joint ROM Angles (°) at Rear Wheel Axle Position | | |
|---|---|---|---|---|
| | | Manufacturer's position (0 cm) | 3 cm Backward Displacement | 6 cm Backward Displacement |
| Trunk | Flexion / Extension | 5.847 ± 1.057 | 6.329 ± 1.567 | 6.768 ± 1.0457 |
| | Lateral Bending | 5.146 ± 1.202 | 5.356 ± 1.406 | 5.453 ± 1.514 |
| | Axial Rotation | 4.379 ± 1.444 | 4.568 ± 1.171 | 4.733 ± 1.459 |
| Dominant Shoulder | Adduction / Abduction | 19.060 ± 6.494 | 20.083 ± 6.296 | 22.027 ± 7.875 |
| | Internal / External Rotation | 15.254 ± 5.569 | 17.049 ± 6.242 | 17.592 ± 5.907 |
| | Flexion / Extension | 30.586 ± 6.312 | 34.811 ± 6.975 | 36.332 ± 7.086 |
| Dominant Elbow | Pronation / Supination | 18.876 ± 6.828 | 19.521 ± 6.187 | 21.371 ± 6.583 |
| | Flexion / Extension | 26.690 ± 7.657 | 29.339 ± 7.221 | 30.005 ± 8.375 |
| Dominant Wrist | Radial / Ulnar Deviation | 35.535 ± 8.229 | 37.812 ± 9.649 | 41.404 ± 11.676* |
| | Flexion / Extension | 48.759 ± 9.837 | 50.116 ± 10.248 | 53.591 ± 9.652* |
| Non-dominant Shoulder | Adduction / Abduction | 17.333 ± 6.910 | 21.860 ± 7.025 | 24.133 ± 6.616 |
| | Internal / External Rotation | 16.270 ± 3.997 | 17.300 ± 4.853* | 18.086 ± 5.873* |
| | Flexion / Extension | 28.724 ± 6.236 | 39.215 ± 8.795 | 40.396 ± 7.977 |
| Non-dominant Elbow | Pronation / Supination | 16.699 ± 5.335 | 19.054 ± 6.534 | 19.483 ± 5.628* |
| | Flexion / Extension | 30.916 ± 7.156 | 31.180 ± 6.644 | 33.633 ± 7.324 |
| Non-dominant Wrist | Radial / Ulnar Deviation | 27.393 ± 7.920 | 31.3661 ± 4.511 | 39.953 ± 7.337 |
| | Flexion / Extension | 42.458 ± 9.651 | 45.579 ± 8.789 | 47.493 ± 7.098 |

*Significant difference between the manufacturer's wheel axle position and (3 cm) and (6 cm) backward displacements.

**Table (7.2)**: Kinematic ROM angles of trunk and upper limb joints with the manufacturer's rear wheel axle position and (3 cm) and (6 cm) backward displacements during ***manual wheelchair starting up***. All the joint ROM angles are presented as group mean and standard deviation values in degrees.

| Upper Body Rigid Segment Kinematics | | Joint ROM Angles (°) at Rear Wheel Axle Position | | |
|---|---|---|---|---|
| | | Manufacturer's position (0 cm) | 3 cm Backward Displacement | 6 cm Backward Displacement |
| Trunk | Flexion / Extension | 7.504 ± 1.397 | 8.018 ± 1.563 | 8.057 ± 1.685 |
| | Lateral Bending | 5.905 ± 1.232 | 6.136 ± 1.234 | 6.345 ±1.647* |
| | Axial Rotation | 7.012 ± 1.909 | 7.143 ± 1.452* | 7.279 ± 1.571 |
| Dominant Shoulder | Adduction / Abduction | 24.627 ± 4.274 | 25.897 ± 4.759 | 28.228 ± 7.081 |
| | Internal / External Rotation | 17.314 ± 6.388 | 18.724 ± 7.472 | 20.533 ± 5.724 |
| | Flexion / Extension | 40.021 ± 8.348 | 43.029 ± 7.096 | 46.945 ± 10.606 |
| Dominant Elbow | Pronation / Supination | 21.520 ± 6.501 | 24.153 ± 7.766 | 25.679 ± 6.926 |
| | Flexion / Extension | 34.366 ± 7.376 | 35.977 ± 7.185 | 40.137 ± 9.297 |
| Dominant Wrist | Radial / Ulnar Deviation | 36.884 ± 8.162 | 39.310 ± 6.798* | 47.065 ± 8.203* |
| | Flexion / Extension | 55.877 ± 8.328 | 56.813 ± 11.844 | 57.036 ± 11.066* |
| Non-dominant Shoulder | Adduction / Abduction | 29.123 ± 7.353 | 29.223 ± 6.734 | 30.534 ± 8.104 |
| | Internal / External Rotation | 18.499 ± 3.423 | 19.449 ± 4.516 | 19.566 ± 5.622 |
| | Flexion / Extension | 43.331 ± 6.889 | 44.404 ± 4.925 | 44.858 ± 7.072 |
| Non-dominant Elbow | Pronation / Supination | 21.997 ± 5.563 | 25.544 ± 5.147 | 26.238 ± 5.641 |
| | Flexion / Extension | 32.945 ± 6.410 | 38.262 ± 6.811 | 46.347 ± 7.070 |
| Non-dominant Wrist | Radial / Ulnar Deviation | 33.791 ± 7.529 | 40.237 ± 7.716 | 48.428 ± 9.528 |
| | Flexion / Extension | 50.449 ± 10.580 | 55.197 ± 9.499 | 57.868 ± 10.327 |

*Significant difference between the manufacturer's wheel axle position and (3 cm) and (6 cm) backward displacements.

**Table (7.3)**: Kinematic ROM angles of trunk and upper limb joints with the manufacturer's rear wheel axle position and (3 cm) and (6 cm) backward displacements during ***manual wheelchair stopping***. All the joint ROM angles are presented as group mean and standard deviation values in degrees.

| Upper Body Rigid Segment Kinematics | | Joint ROM Angles (°) at Rear Wheel Axle Position | | |
|---|---|---|---|---|
| | | Manufacturer's position (0 cm) | 3 cm Backward Displacement | 6 cm Backward Displacement |
| Trunk | Flexion / Extension | 4.938 ± 0.958 | 5.628 ± 1.143 | 5.980 ± 0.575 |
| | Lateral Bending | 3.738 ± 0.600 | 3.983 ± 0.738 | 4.362 ± 1.310 |
| | Axial Rotation | 3.213 ± 1.143 | 3.985 ± 0.622 | 4.578 ± 1.089 |
| Dominant Shoulder | Adduction / Abduction | 16.148 ± 4.939 | 16.371 ± 4.919 | 17.502 ± 5.813 |
| | Internal / External Rotation | 12.508 ± 3.179 | 13.036 ± 4.350 | 13.950 ± 3.873 |
| | Flexion / Extension | 23.824 ± 4.224 | 26.444 ± 6.009 | 26.633 ± 5.704 |
| Dominant Elbow | Pronation / Supination | 14.318 ± 4.795 | 14.761 ± 4.935* | 15.493 ± 4.703 |
| | Flexion / Extension | 18.094 ± 4.976 | 20.325 ± 5.310 | 23.921 ± 6.009 |
| Dominant Wrist | Radial / Ulnar Deviation | 20.225 ± 3.184 | 23.844 ± 3.115* | 29.816 ± 4.792* |
| | Flexion / Extension | 30.369 ± 6.335 | 31.214 ± 6.134 | 40.950 ± 8.383* |
| Non-dominant Shoulder | Adduction / Abduction | 13.725 ± 3.235 | 18.686 ± 5.682 | 18.894 ± 4.628 |
| | Internal / External Rotation | 14.471 ± 4.587 | 15.234 ± 4.519 | 16.675 ± 4.194 |
| | Flexion / Extension | 21.350 ± 5.667 | 29.130 ± 4.476 | 29.391 ± 4.676 |
| Non-dominant Elbow | Pronation / Supination | 14.523 ± 1.799 | 15.347 ± 5.172 | 16.517 ± 2.955 |
| | Flexion / Extension | 22.390 ± 5.075 | 23.406 ± 4.811 | 31.095 ± 4.770 |
| Non-dominant Wrist | Radial / Ulnar Deviation | 22.699 ± 5.249 | 26.983 ± 4.845 | 27.575 ± 6.393* |
| | Flexion / Extension | 30.986 ± 4.968 | 36.440 ± 6.260 | 40.685 ± 6.429* |

*Significant difference between the manufacturer's wheel axle position and (3 cm) and (6 cm) backward displacements.

**Table (7.4)**: Kinematic ROM angles of trunk and upper limb joints with the manufacturer's wheelchair seat height and (45 cm) and (50 cm) seat heights during ***manual wheelchair propulsion***. All the joint ROM angles are presented as group mean and standard deviation values in degrees.

| Upper Body Rigid Segment Kinematics | | Joint ROM Angles (°) at Wheelchair Seat Height | | |
|---|---|---|---|---|
| | | Manufacturer's Height (48 cm) | 45 cm Seat Height | 50 cm Seat Height |
| Trunk | Flexion / Extension | 9.155 ± 2.290 | 8.445 ± 1.455 | 9.337 ± 2.14 |
| | Lateral Bending | 6.985 ± 1.699 | 6.543 ± 1.367 | 7.121 ± 1.587 |
| | Axial Rotation | 4.859 ± 1.154 | 4.584 ± 0.881 | 5.108 ± 1.537 |
| Dominant Shoulder | Adduction / Abduction | 27.083 ± 10.6 | 26.896 ± 7.828 | 28.053 ± 8.252 |
| | Internal / External Rotation | 20.263 ± 6.058 | 19.120 ± 5.821 | 20.710 ± 6.809 |
| | Flexion / Extension | 44.177 ± 10.730 | 41.217 ± 11.391 | 45.565 ± 11.697 |
| Dominant Elbow | Pronation / Supination | 17.379 ± 5.107 | 15.129 ± 4.803 | 19.656 ± 7.500* |
| | Flexion / Extension | 38.0713 ± 8.303 | 35.232 ± 7.577 | 39.380 ± 8.530 |
| Dominant Wrist | Radial / Ulnar Deviation | 28.296 ± 6.445 | 26.294 ± 6.332 | 30.871 ± 7.705 |
| | Flexion / Extension | 48.355 ± 9.320 | 44.796 ± 12.359 | 49.588 ± 9.395 |
| Non-dominant Shoulder | Adduction / Abduction | 29.743 ± 7.125 | 27.413 ± 7.050* | 29.859 ± 6.750 |
| | Internal / External Rotation | 19.529 ± 4.820 | 19.312 ± 4.082 | 20.949 ± 5.767 |
| | Flexion / Extension | 44.852 ± 7.577 | 42.952 ± 7.342 | 45.976 ± 8.171 |
| Non-dominant Elbow | Pronation / Supination | 19.503 ± 4.904 | 18.762 ± 6.300 | 20.709 ± 9.835 |
| | Flexion / Extension | 41.679 ± 7.228 | 38.679 ± 9.164 | 45.268 ± 11.502 |
| Non-dominant Wrist | Radial / Ulnar Deviation | 29.510 ± 7.528 | 26.859 ± 5.856 | 33.155 ± 8.759 |
| | Flexion / Extension | 50.404 ± 13.125 | 46.935 ± 12.591 | 50.575 ± 11.583 |

*Significant difference between the manufacturer's wheelchair seat height and (45 cm) and (50 cm) seat heights.

**Table (7.5)**: Kinematic ROM angles of trunk and upper limb joints with the manufacturer's wheelchair seat height and (45 cm) and (50 cm) seat heights during ***manual wheelchair starting up***. All the joint ROM angles are presented as group mean and standard deviation values in degrees.

| Upper Body Rigid Segment Kinematics | | Joint ROM Angles (°) at Wheelchair Seat Height | | |
|---|---|---|---|---|
| | | Manufacturer's Height (48 cm) | 45 cm Seat Height | 50 cm Seat Height |
| Trunk | Flexion / Extension | 7.689 ± 3.019 | 7.007 ± 1.954 | 9.646 ± 3.911 |
| | Lateral Bending | 5.293 ± 1.646 | 5.258 ± 1.751* | 7.181 ± 2.194 |
| | Axial Rotation | 4.154 ± 1.336 | 3.703 ± 1.008 | 4.953 ± 1.182* |
| Dominant Shoulder | Adduction / Abduction | 27.890 ± 9.926 | 22.241 ± 5.199 | 28.877 ± 10.733 |
| | Internal / External Rotation | 20.123 ± 7.011 | 15.825 ± 5.548 | 20.780 ± 8.603 |
| | Flexion / Extension | 44.897 ± 16.194 | 40.320 ± 11.085 | 45.602 ± 15.753 |
| Dominant Elbow | Pronation / Supination | 17.880 ± 6.421 | 15.230 ± 5.0154* | 19.972 ± 6.263* |
| | Flexion / Extension | 40.232 ± 13.122 | 37.080 ± 13.224 | 45.603 ± 15.519 |
| Dominant Wrist | Radial / Ulnar Deviation | 30.888 ± 8.493 | 28.710 ± 6.089 | 32.461 ± 6.383* |
| | Flexion / Extension | 48.410 ± 14.792 | 48.302 ± 9.238 | 53.011 ± 6.167 |
| Non-dominant Shoulder | Adduction / Abduction | 29.364 ± 8.379 | 26.959 ± 5.875 | 30.326 ± 10.894 |
| | Internal / External Rotation | 19.080 ± 7.882 | 18.936 ± 7.108 | 19.774 ± 9.015 |
| | Flexion / Extension | 44.010 ± 14.560 | 42.952 ± 15.798 | 47.463 ± 14.676 |
| Non-dominant Elbow | Pronation / Supination | 18.436 ± 7.392 | 17.286 ± 6.064* | 21.216 ± 7.101 |
| | Flexion / Extension | 43.322 ± 11.968 | 40.459 ± 10.409 | 47.937 ± 8.876 |
| Non-dominant Wrist | Radial / Ulnar Deviation | 33.346 ± 6.221 | 28.888 ± 4.656* | 36.044 ± 7.346 |
| | Flexion / Extension | 53.661 ± 15.409 | 47.572 ± 6.318 | 57.806 ± 10.483 |

*Significant difference between the manufacturer's wheelchair seat height and (45 cm) and (50 cm) seat heights.

**Table (7.6)**: Kinematic ROM angles of trunk and upper limb joints with the manufacturer's wheelchair seat height and (45 cm) and (50 cm) seat heights during ***manual wheelchair stopping***. All the joint ROM angles are presented as group mean and standard deviation values in degrees.

| Upper Body Rigid Segment Kinematics | | Joint ROM Angles (°) at Wheelchair Seat Height | | |
|---|---|---|---|---|
| | | Manufacturer's Height (48 cm) | 45 cm Seat Height | 50 cm Seat Height |
| Trunk | Flexion / Extension | 5.749 ± 1.526 | 5.730 ± 1.435 | 7.191 ± 1.606 |
| | Lateral Bending | 4.644 ± 1.187 | 4.273 ± 1.476 | 5.614 ± 1.503 |
| | Axial Rotation | 3.608 ± 0.915 | 3.416 ± 1.188 | 3.858 ± 1.111 |
| Dominant Shoulder | Adduction / Abduction | 15.877 ± 6.170 | 14.198 ± 5.612 | 16.193 ± 5.246 |
| | Internal / External Rotation | 10.880 ± 5.085 | 10.757 ± 2.841 | 11.046 ± 3.423 |
| | Flexion / Extension | 25.005 ± 5.230 | 24.078 ± 6.102 | 26.589 ± 6.851 |
| Dominant Elbow | Pronation / Supination | 8.759 ± 2.726 | 8.425 ± 2.929* | 12.654 ± 3.688 |
| | Flexion / Extension | 23.397 ± 6.933 | 22.243 ± 7.720 | 31.736 ± 7.2840 |
| Dominant Wrist | Radial / Ulnar Deviation | 15.862 ± 4.514 | 14.524 ± 4.743 | 21.893 ± 5.268 |
| | Flexion / Extension | 33.825 ± 4.772 | 28.494 ± 6.390 | 36.816 ± 6.374 |
| Non-dominant Shoulder | Adduction / Abduction | 20.163 ± 6.828 | 14.141 ± 5.183 | 20.495 ± 6.567* |
| | Internal / External Rotation | 13.833 ± 5.027 | 9.596 ± 3.826 | 12.790 ± 5.356* |
| | Flexion / Extension | 26.414 ± 5.012 | 20.452 ± 6.397 | 28.049 ± 6.684 |
| Non-dominant Elbow | Pronation / Supination | 10.522 ± 3.459 | 9.896 ± 2.978* | 13.899 ± 3.747 |
| | Flexion / Extension | 26.319 ± 7.687 | 25.968 ± 6.054 | 34.039 ± 5.675 |
| Non-dominant Wrist | Radial / Ulnar Deviation | 16.639 ± 5.907 | 19.061 ± 5.742 | 20.398 ± 4.645 |
| | Flexion / Extension | 32.567 ± 8.213 | 31.279 ± 6.956 | 35.477 ± 8.089 |

*Significant difference between the manufacturer's wheelchair seat height and (45 cm) and (50 cm) seat heights.

The Figures (7.4), (7.5) and (7.6) illustrate the trunk and dominant and non-dominant upper limb joint kinematics during manual wheelchair propulsion, starting up and stopping functional tasks at three rear wheel axle positions respectively, while the Figures (7.7), (7.8) and (7.9) illustrate the trunk and dominant and non-dominant upper limb joint kinematics during manual wheelchair propulsion, starting up and stopping functional tasks at the three wheelchair seat heights respectively.

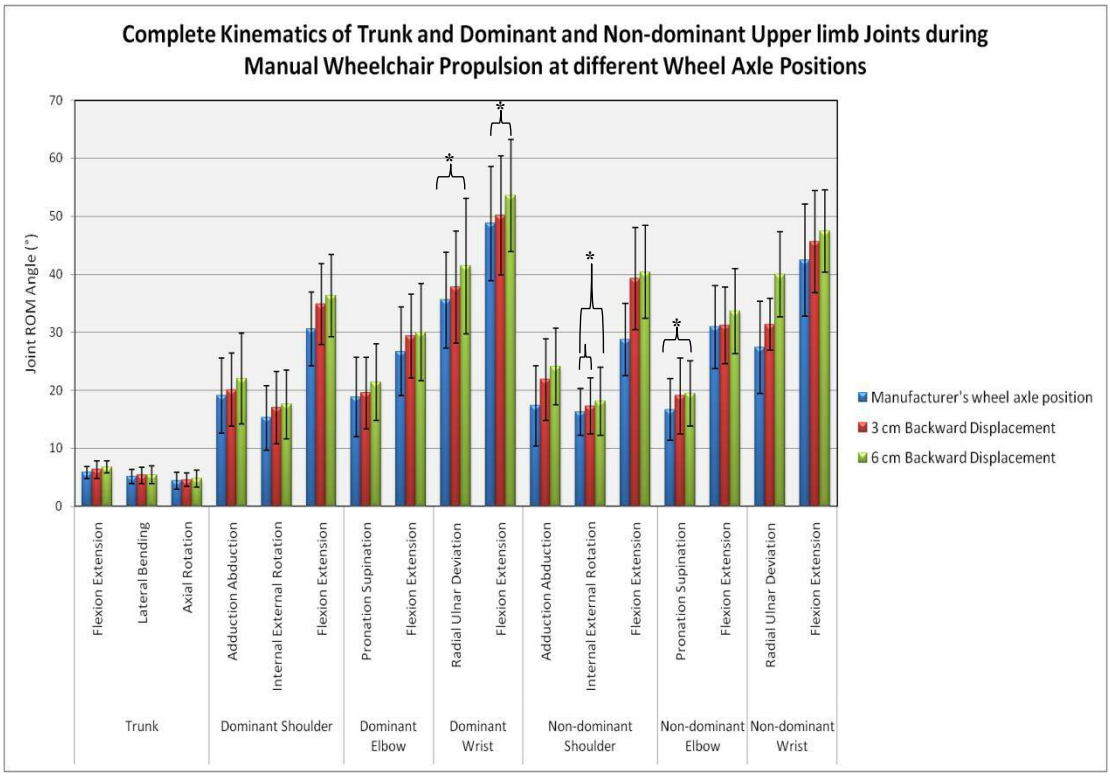


**Figure (7.4):** Kinematic ROM angles of trunk and dominant and non-dominant upper limb joints during *manual wheelchair propulsion* at three wheel axle positions. All the joint ROM angles are presented as group average values,*P<0.05.

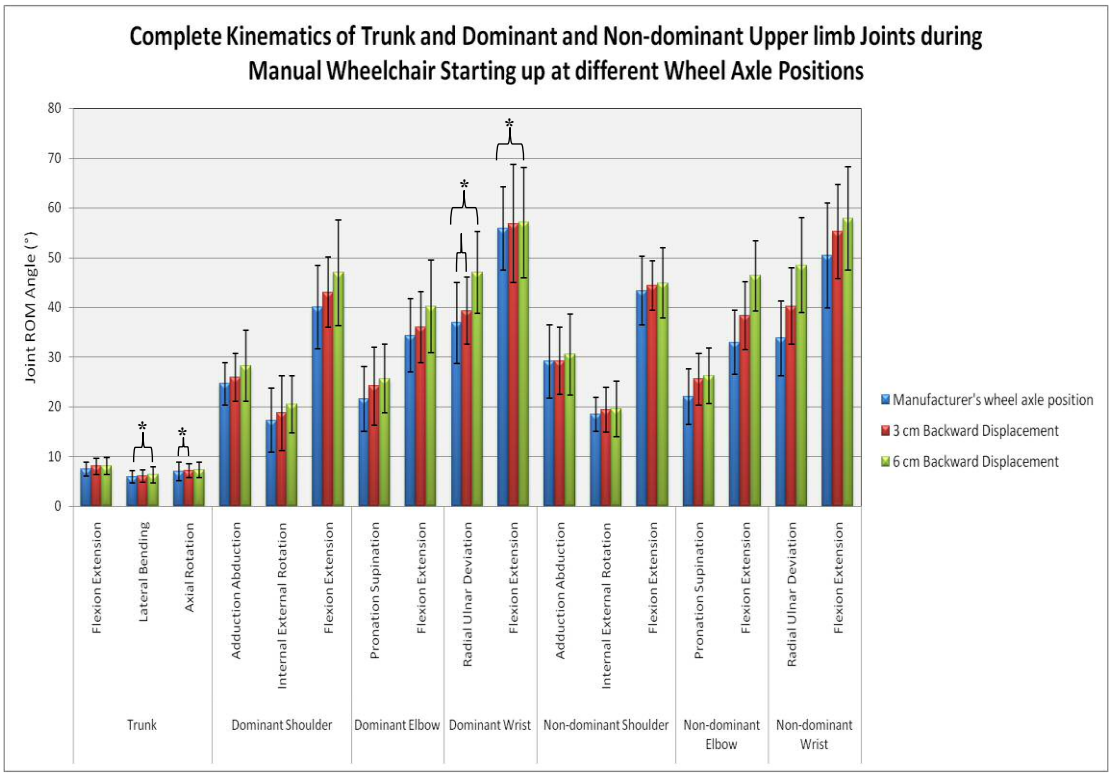


**Figure (7.5):** Kinematic ROM angles of trunk and dominant and non-dominant upper limb joints during *manual wheelchair starting up* at three wheel axle positions. All the joint ROM angles are presented as group average values, *P<0.05.

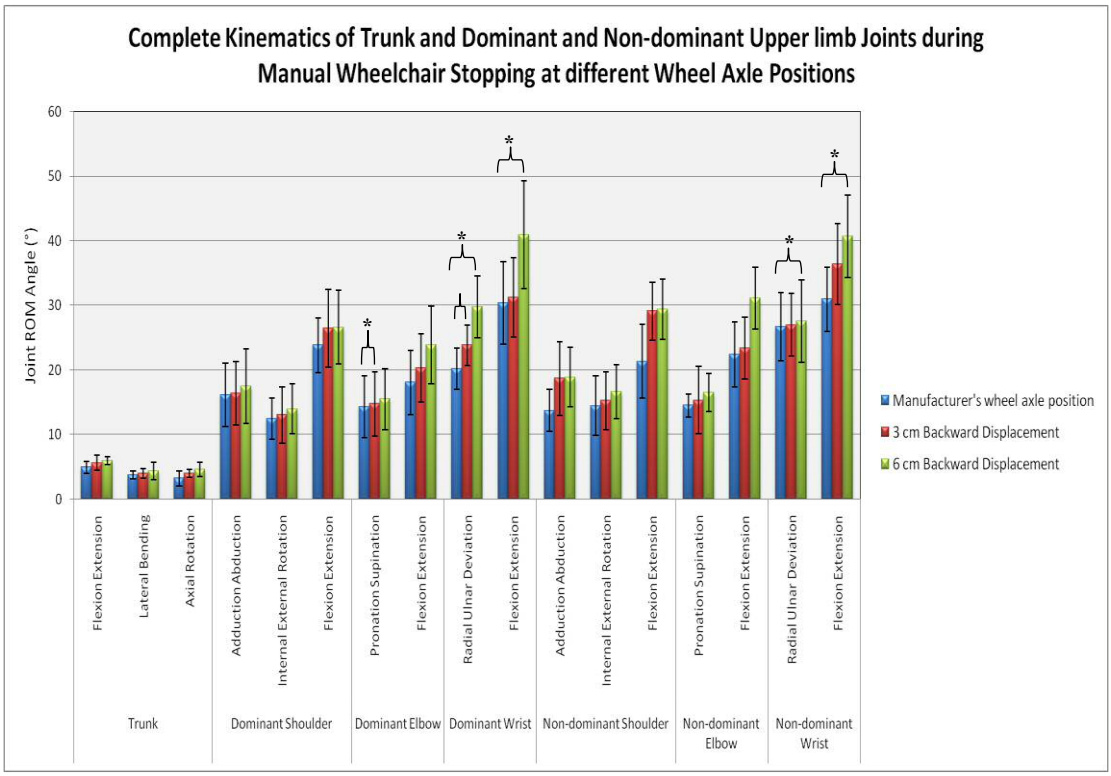


**Figure (7.6):** Kinematic ROM angles of trunk and dominant and non-dominant upper limb joints during *manual wheelchair stopping* at three wheel axle positions. All the joint ROM angles are presented as group average values, *P<0.05.

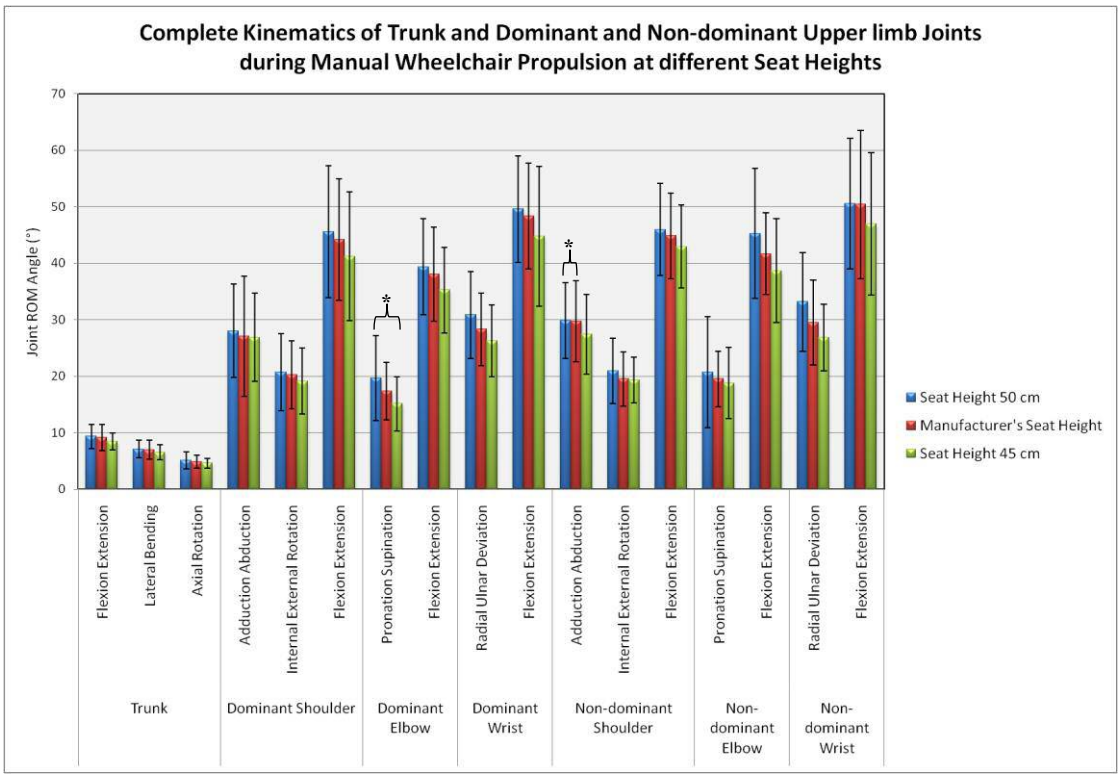


**Figure (7.7):** Kinematic ROM angles of trunk and dominant and non-dominant upper limb joints during *manual wheelchair propulsion* at three wheelchair seat heights. All the joint ROM angles are presented as group average values,*P<0.05.

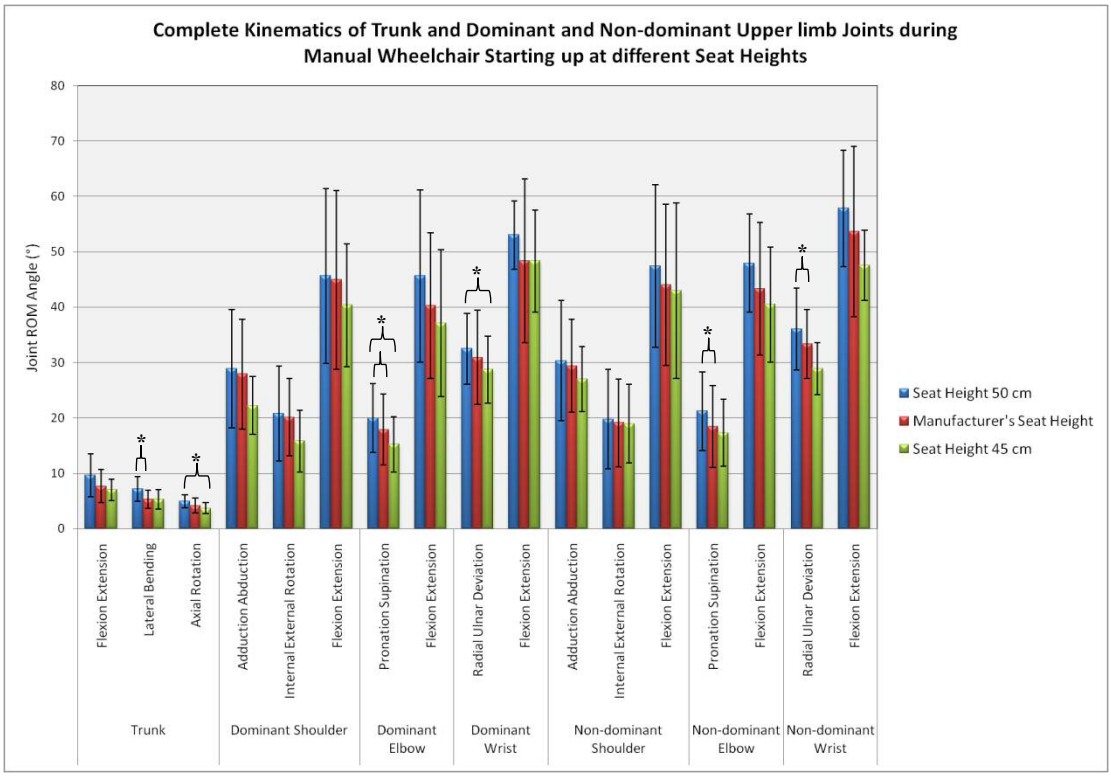


**Figure (7.8):** Kinematic ROM angles of trunk and dominant and non-dominant upper limb joints during *manual wheelchair starting up* at three wheelchair seat heights. All the joint ROM angles are presented as group average values, *P<0.05.

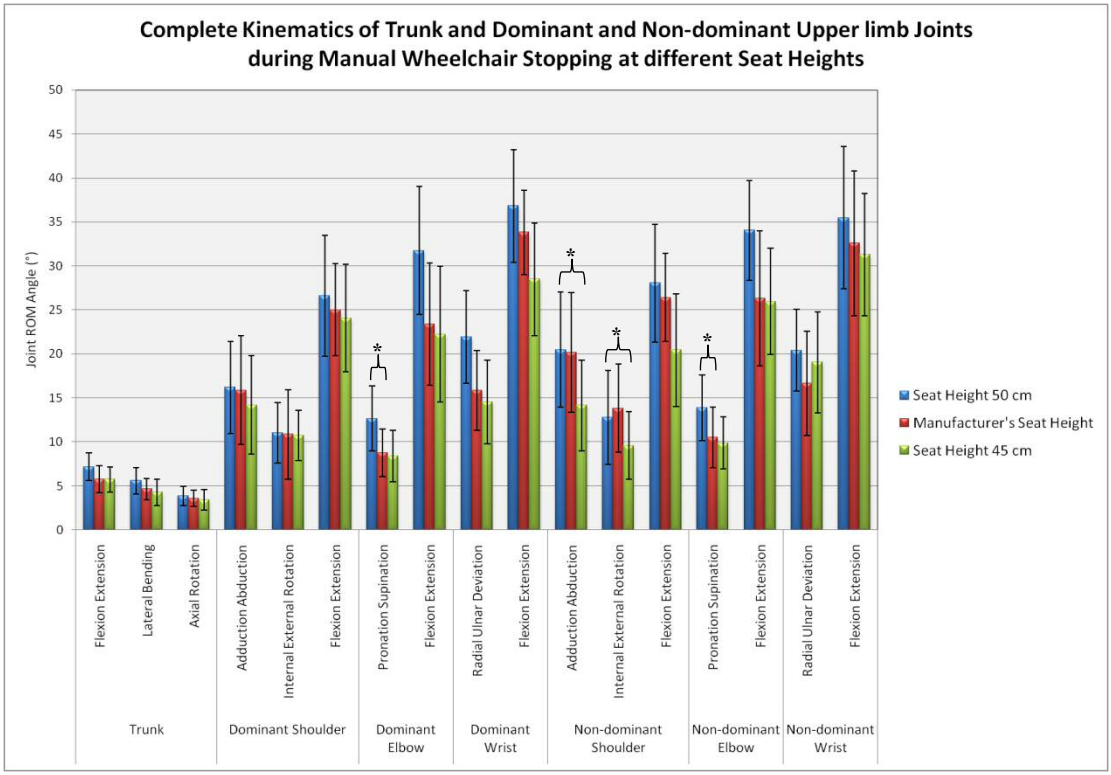


**Figure (7.9):** Kinematic ROM angles of trunk and dominant and non-dominant upper limb joints during *manual wheelchair stopping* at three wheelchair seat heights. All the joint ROM angles are presented as group average values, *P<0.05.

### *7.2.3. Shoulder Muscles EMG Activity*

Under the wheelchair manufacturer's configurations, EMG results showed that the posterior deltoid had the highest peak muscle activity (34.434 ± 4.799) during the propulsion trials as relative to the other dominant shoulder muscles. The other average muscles activities were evaluated as (23.15 ± 4.206) for upper trapezius, (17.203 ± 2.174) for pectoralis major, (16.331 ± 2.011) for triceps brachii, (12.628 ± 2.053) for anterior deltoid and (11.085 ± 1.746) for the biceps brachii as the lowest peak EMG muscle activity. All these peak values were normalised and expressed in percentage of MVC activity (%MVC).

Meanwhile, posterior deltoid displayed the largest shoulder muscle activity during the starting up and stopping tasks, (14.205 ± 3.034) and (10.793 ± 1.682) respectively, while the biceps brachii displayed the lowest muscle activity during the starting up and stopping tasks, (4.637 ± 1.094) and (2.988 ± 0.462) respectively.

**Table (7.7):** Muscle activation in terms of normalised ***peak EMG*** of dominant shoulder muscles expressed in percentage MVC with the manufacturer's rear wheel axle position and (3 cm) and (6 cm) backward displacements during ***manual wheelchair propulsion***. All the muscles normalised EMG %MVC are presented as group mean and standard deviation values.

| Dominant Shoulder Muscle | Normalised peak EMG %MVC at Rear Wheel Axle Positions | | |
|---|---|---|---|
| | Manufacturer's Rear Axle Position | 3 cm Backward Displacement | 6 cm Backward Displacement |
| **Anterior Deltoid** | 12.625 ± 2.529 | 12.537 ± 1.716 | 12.124 ± 1.795 |
| **Posterior Deltoid** | 32.930 ± 5.670 | 33.239 ± 5.559 | 33.943 ± 5.428 |
| **Biceps Brachii** | 11.493 ± 0.807 | 11.214 ± 2.070 | 11.029 ± 2.510 |
| **Pectoralis Major** | 17.588 ± 2.929 | 17.166 ± 2.174 | 16.288 ± 1.914 |
| **Upper Trapezius** | 22.794 ± 4.494 | 22.906 ± 3.673 | 23.050 ± 3.792 |
| **Triceps Brachii** | 15.970 ± 1.713 | 16.085 ± 2.333 | 16.231 ± 1.795 |

**Table (7.8):** Muscle activation in terms of normalised ***average EMG*** of dominant shoulder muscles expressed in percentage MVC with the manufacturer's rear wheel axle position and (3 cm) and (6 cm) backward displacements during ***manual wheelchair propulsion***.All the muscles normalised EMG %MVC are presented as group mean and standard deviation values.

| Dominant Shoulder Muscle | Normalised average EMG %MVC at Rear Wheel Axle Positions | | |
|---|---|---|---|
| | Manufacturer's Position | 3 cm Backward Displacement | 6 cm Backward Displacement |
| **Anterior Deltoid** | 3.570 ± 0.259 | 3.456 ± 0.426 | 3.143 ± 0.531 |
| **Posterior Deltoid** | 11.425 ± 1.33 | 11.846 ± 1.738 | 12.298 ± 2.074 |
| **Biceps Brachii** | 3.263 ± 0.101 | 4.116 ± 0.390 | 4.305 ± 0.630 |
| **Pectoralis Major** | 6.886 ± 0.514 | 6.189 ± 0.272 | 5.203 ± 0.793 |
| **Upper Trapezius** | 6.985 ± 1.366 | 7.242 ± 1.415 | 7.424 ± 1.240 |
| **Triceps Brachii** | 5.392 ± 0.954 | 4.4951 ± 0.947 | 4.258 ± 0.410 |

**Table (7.9):** Muscle activation in terms of normalised ***average EMG*** of dominant shoulder muscles expressed in percentage MVC with the manufacturer's rear wheel axle position and (3 cm) and (6 cm) backward displacements during ***manual wheelchair starting up***. All the muscles normalised EMG %MVC are presented as group mean and standard deviation values.

| Dominant Shoulder Muscle | Normalised average EMG %MVC at Rear Wheel Axle Positions | | |
|---|---|---|---|
| | Manufacturer's Position | 3 cm Backward Displacement | 6 cm Backward Displacement |
| **Anterior Deltoid** | 4.465 ± 1.111 | 4.351 ± 0.849 | 4.275 ± 0.724 |
| **Posterior Deltoid** | 13.848 ± 3.847 | 14.699 ± 4.226 | 15.221 ± 4.126 |
| **Biceps Brachii** | 3.955 ± 0.897 | 4.280 ± 0.513 | 5.382 ± 1.161 |
| **Pectoralis Major** | 7.325 ± 1.356 | 7.044 ± 1.414 | 6.958 ± 1.607 |
| **Upper Trapezius** | 7.008 ± 1.814 | 7.338 ± 1.621 | 7.804 ± 1.751 |
| **Triceps Brachii** | 5.470 ± 1.082 | 5.170 ± 1.363 | 4.694 ± 0.795 |

**Table (7.10):** Muscle activation in terms of normalised ***average EMG*** of dominant shoulder muscles expressed in percentage MVC with the manufacturer's rear wheel axle position and (3 cm) and (6 cm) backward displacements during ***manual wheelchair stopping***. All the muscles normalised EMG %MVC are presented as group mean and standard deviation values.

| Dominant Shoulder Muscle | Normalised average EMG %MVC at Rear Wheel Axle Positions | | |
|---|---|---|---|
| | Manufacturer's Position | 3 cm Backward Displacement | 6 cm Backward Displacement |
| **Anterior Deltoid** | 4.555 ± 0.849 | 4.142 ± 0.768 | 3.961 ± 0.612 |
| **Posterior Deltoid** | 10.793 ± 1.682 | 11.606 ± 1.956 | 11.914 ± 1.610 |
| **Biceps Brachii** | 2.988 ± 0.462 | 3.092 ± 0.446 | 4.136 ± 0.616 |
| **Pectoralis Major** | 6.227 ± 1.104 | 5.973 ± 1.626 | 5.146 ± 1.740 |
| **Upper Trapezius** | 4.920 ± 0.955 | 5.141 ± 1.092 | 5.530 ± 1.139 |
| **Triceps Brachii** | 3.233 ± 0.457 | 3.195 ± 0.580 | 2.958 ± 0.392 |

**Table (7.11):** Muscle activation in terms of normalised ***peak EMG*** of dominant shoulder muscles expressed in percentage MVC with the manufacturer's wheelchair seat height and (45 cm) and (50 cm) seat heights during ***manual wheelchair propulsion***. All the muscles normalised EMG %MVC are presented as group mean and standard deviation values.

| Dominant Shoulder Muscle | Normalised peak EMG %MVC at Wheelchair Seat Heights | | |
|---|---|---|---|
| | Manufacturer's Height | 45 cm Seat Height | 50 cm Seat Height |
| **Anterior Deltoid** | 13.300 ± 1.887 | 13.681 ±3.383 | 12.882 ± 2.459 |
| **Posterior Deltoid** | 33.275 ± 4.849 | 33.275 ± 4.849 | 33.890 ± 5.485 |
| **Biceps Brachii** | 11.816 ± 1.615 | 11.816 ± 1.615 | 10.854 ± 1.959 |
| **Pectoralis Major** | 18.286 ± 4.079 | 18.286 ± 4.079 | 17.247 ± 2.367 |
| **Upper Trapezius** | 25.098 ± 4.788 | 25.098 ± 4.788 | 26.117 ± 4.767 |
| **Triceps Brachii** | 16.695 ± 2.404 | 16.695 ± 2.404 | 18.411 ± 2.320 |

**Table (7.12):** Muscle activation in terms of normalised ***average EMG*** of dominant shoulder muscles expressed in percentage MVC with the manufacturer's wheelchair seat height and (45 cm) and (50 cm) seat heights during ***manual wheelchair propulsion***. All the muscles normalised EMG %MVC are presented as group mean and standard deviation values.

| Dominant Shoulder Muscle | Normalised average EMG %MVC at Wheelchair Seat Heights | | |
|---|---|---|---|
| | Manufacturer's Height | 45 cm Seat Height | 50 cm Seat Height |
| **Anterior Deltoid** | 4.481 ± 1.148 | 3.791 ± 0.727 | 4.872 ± 1.036 |
| **Posterior Deltoid** | 12.654 ± 2.834 | 11.455 ± 2.331 | 12.865 ± 2.117 |
| **Biceps Brachii** | 3.852 ± 0.837 | 4.195 ± 0.623 | 3.479± 0.356 |
| **Pectoralis Major** | 6.332 ± 1.743 | 6.798 ± 1.300 | 5.254 ± 0.814 |
| **Upper Trapezius** | 6.511 ± 1.995 | 5.782 ± 1.782 | 7.030 ± 1.307 |
| **Triceps Brachii** | 5.444 ± 1.436 | 5.573 ±1.067 | 4.279 ± 1.141 |

**Table (7.13):** Muscle activation in terms of normalised ***average EMG*** of dominant shoulder muscles expressed in percentage MVC with the manufacturer's wheelchair seat height and (45 cm) and (50 cm) seat heights during ***manual wheelchair starting up***. All the muscles normalised EMG %MVC are presented as group mean and standard deviation values.

| Dominant Shoulder Muscle | Normalised average EMG %MVC at Wheelchair Seat Heights | | |
|---|---|---|---|
| | Manufacturer's Height | 45 cm Seat Height | 50 cm Seat Height |
| **Anterior Deltoid** | 5.609 ± 1.102 | 5.800 ± 1.265 | 5.282 ± 0.904 |
| **Posterior Deltoid** | 14.205 ± 3.034 | 12.969 ± 2.798 | 14.539 ± 2.378 |
| **Biceps Brachii** | 4.637 ± 1.094 | 4.793± 0.686 | 4.373 ± 0.799 |
| **Pectoralis Major** | 6.574 ± 1.397 | 6.956 ± 1.602 | 6.159 ± 1.610 |
| **Upper Trapezius** | 6.774 ± 1.424 | 6.596 ± 1.831 | 7.049 ± 1.342 |
| **Triceps Brachii** | 5.377 ± 0.864 | 5.099 ± 1.154 | 5.526 ± 0.663 |

**Table (7.14):** Muscle activation in terms of normalised ***average EMG*** of dominant shoulder muscles expressed in percentage MVC with the manufacturer's wheelchair seat height and (45 cm) and (50 cm) seat heights during ***manual wheelchair stopping***. All the muscles normalised EMG %MVC are presented as group mean and standard deviation values.

| Dominant Shoulder Muscle | Normalised average EMG %MVC at Wheelchair Seat Heights | | |
|---|---|---|---|
| | Manufacturer's Height | 45 cm Seat Height | 50 cm Seat Height |
| **Anterior Deltoid** | 3.723 ± 0.876 | 3.283 ± 0.760 | 3.994 ± 0.978 |
| **Posterior Deltoid** | 10.838 ± 1.930 | 10.472 ± 1.821 | 11.748 ± 1.552 |
| **Biceps Brachii** | 3.723 ± 0.876 | 3.283 ± 0.760 | 3.994 ± 0.978 |
| **Pectoralis Major** | 4.169 ± 0.766 | 4.317 ± 0.957 | 4.133 ± 1.038 |
| **Upper Trapezius** | 4.338 ± 1.088 | 4.238 ± 0.842 | 4.536 ± 1.027 |
| **Triceps Brachii** | 3.828 ± 0.703 | 4.054 ± 0.795 | 3.323 ± 0.777 |

The Figures (7.10), (7.11), (7.12) and (7.13) illustrate the dominant shoulder muscles EMG activity during manual wheelchair propulsion, starting up and stopping functional tasks at the three rear wheel axle positions respectively, while the Figures (7.14), (7.15), (7.16) and (7.17) illustrate the dominant shoulder muscles EMG activity during manual wheelchair propulsion, starting up and stopping functional tasks at the three wheelchair seat heights respectively.

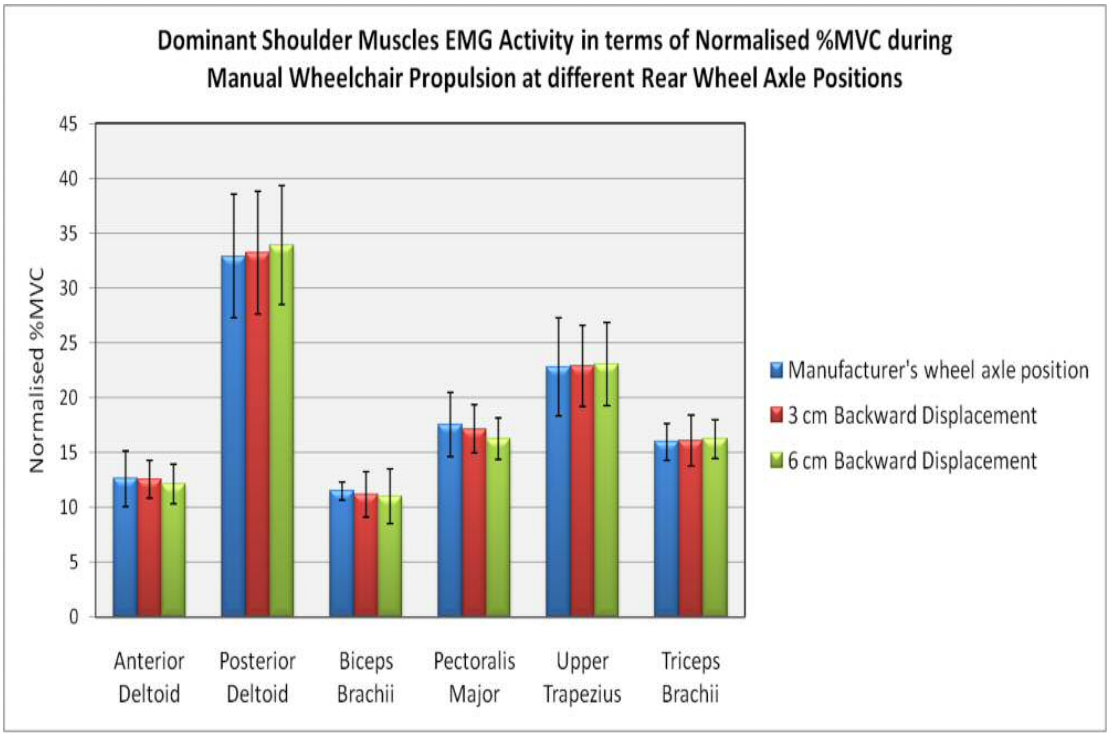


**Figure (7.10):** Dominant shoulder muscles peak EMG activity in terms of normalised MVC percentage during *manual wheelchair propulsion* at three wheel axle positions. All the muscles normalized EMG %MVC are presented as group average values.

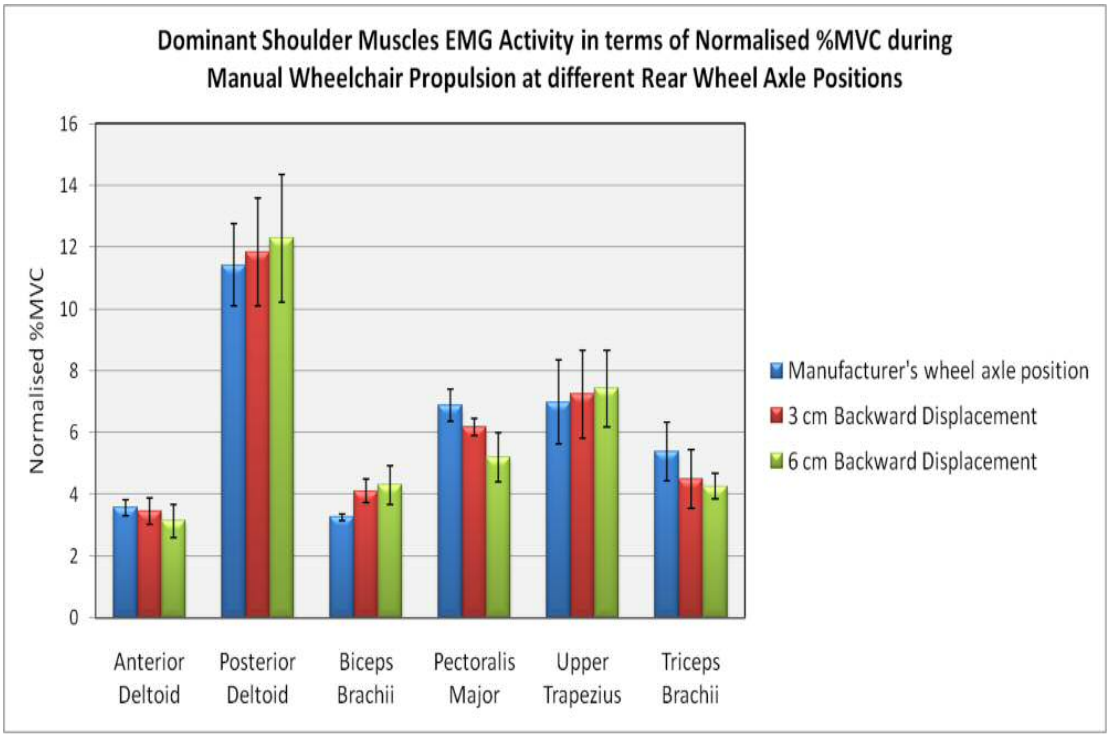


**Figure (7.11):** Dominant shoulder muscles averageEMG activity in terms of normalised MVC percentage during *manual wheelchair propulsion* at three wheel axle positions. All the muscles normalized EMG %MVC are presented as group average values.

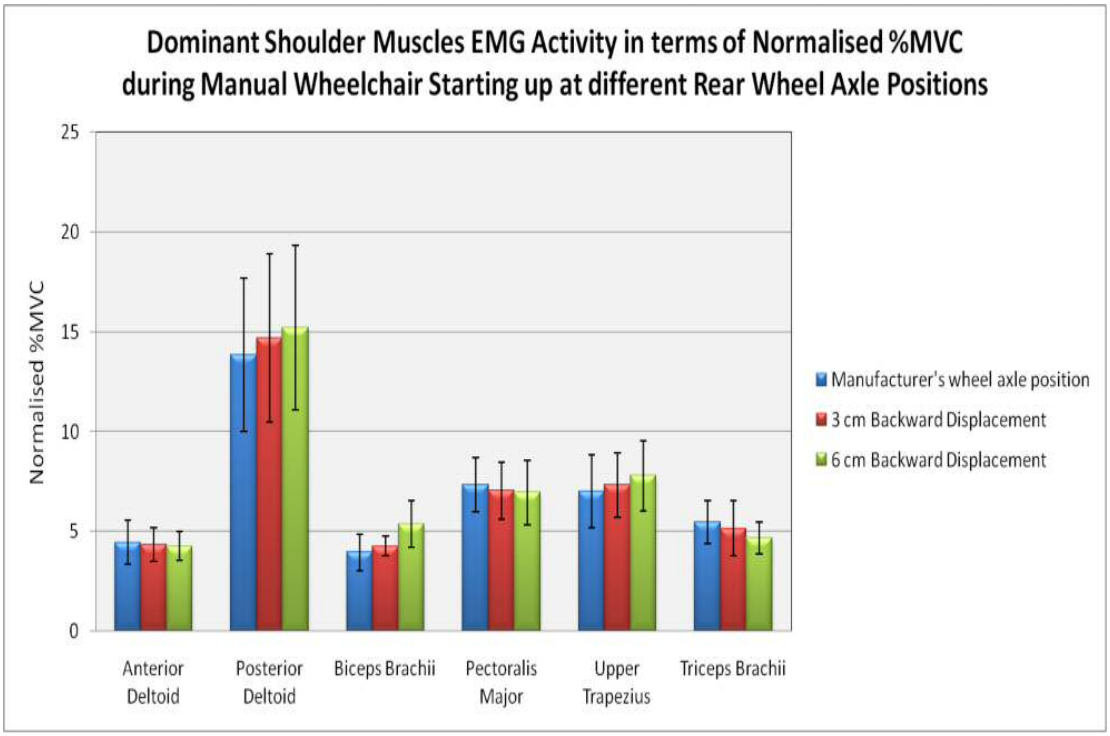


**Figure (7.12):** Dominant shoulder muscles average EMG activity in terms of normalised MVC percentage during *manual wheelchair starting up* at three wheel axle positions. All the muscles normalized EMG %MVC are presented as group average values.

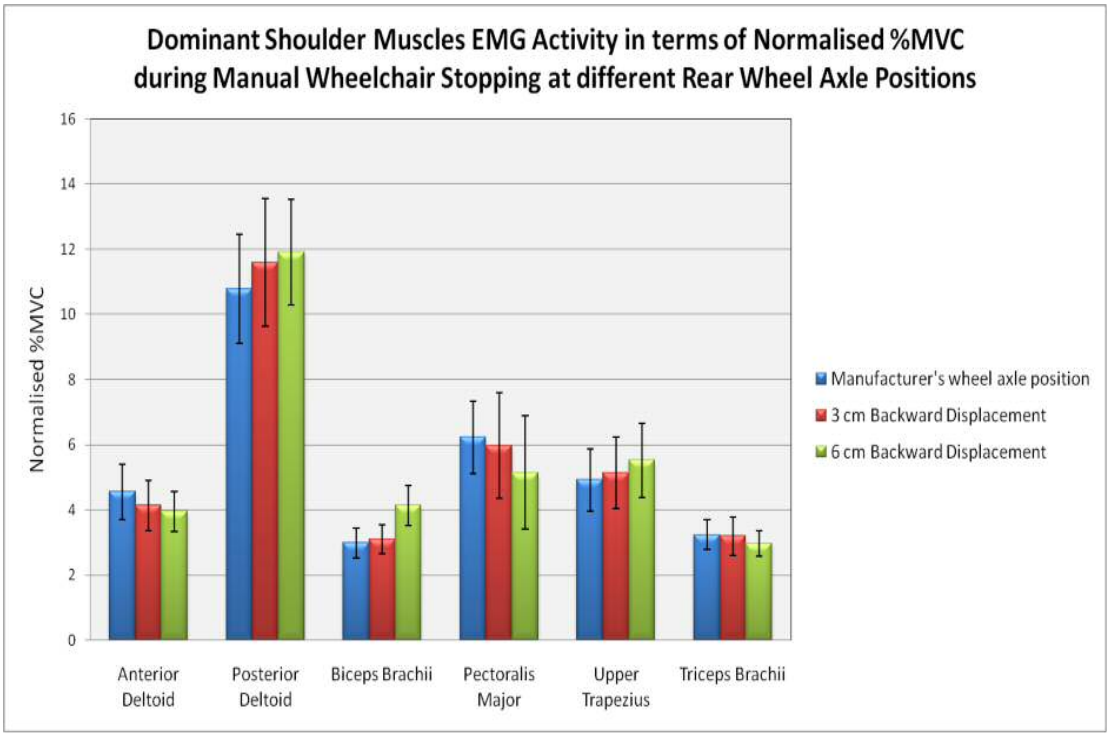


**Figure (7.13):** Dominant shoulder muscles average EMG activity in terms of normalised MVC percentage during *manual wheelchair stopping* at three wheel axle positions. All the muscles normalized EMG %MVC are presented as group average values.

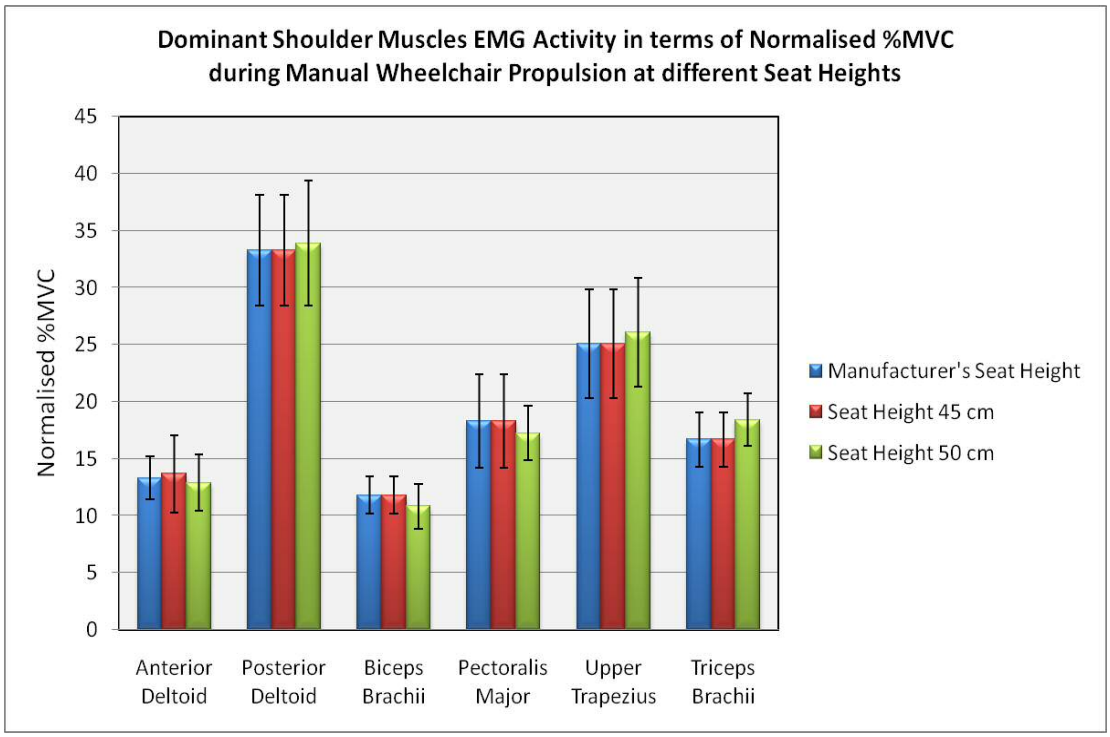


**Figure (7.14):** Dominant shoulder muscles peak EMG activity in terms of normalised MVC percentage during *manual wheelchair propulsion* at three wheelchair seat heights. All the normalized EMG %MVC are presented as group average values.

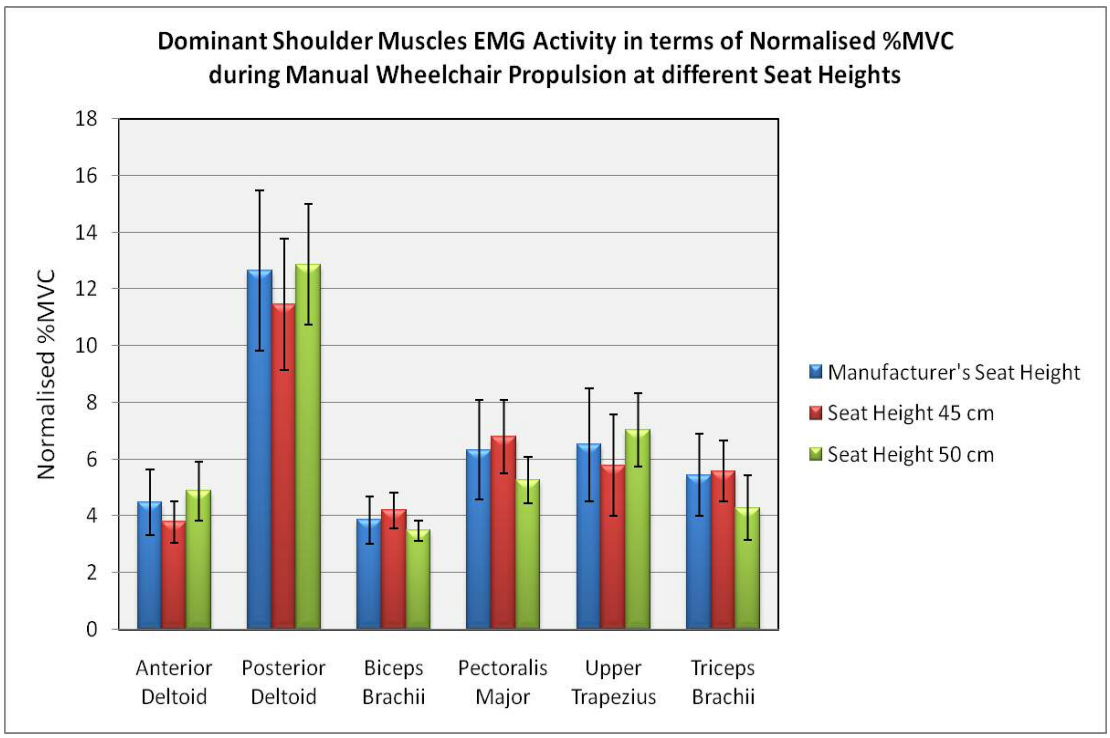


**Figure (7.15):** Dominant shoulder muscles average EMG activity in terms of normalised MVC percentage during *manual wheelchair propulsion* at three wheelchair seat heights. All the normalized EMG %MVC are presented as group average values.

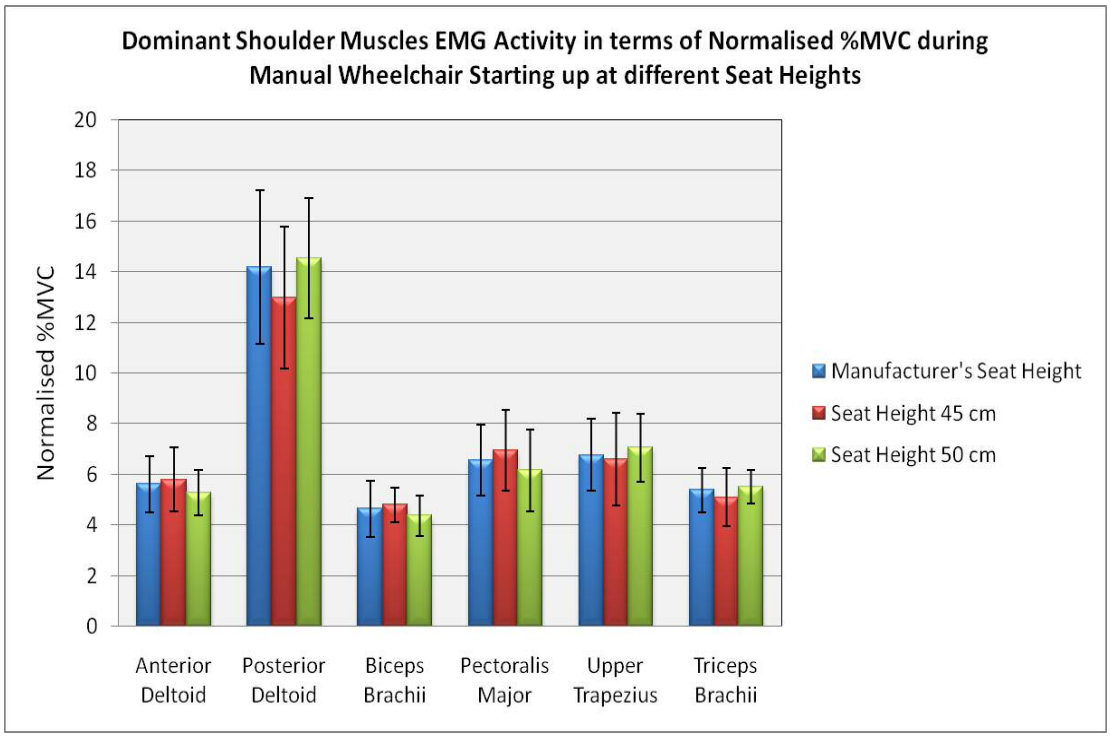


**Figure (7.16):** Dominant shoulder muscles average EMG activity in terms of normalised MVC percentage during *manual wheelchair starting up* at three wheelchair seat heights. All the normalized EMG %MVC are presented as group average values.

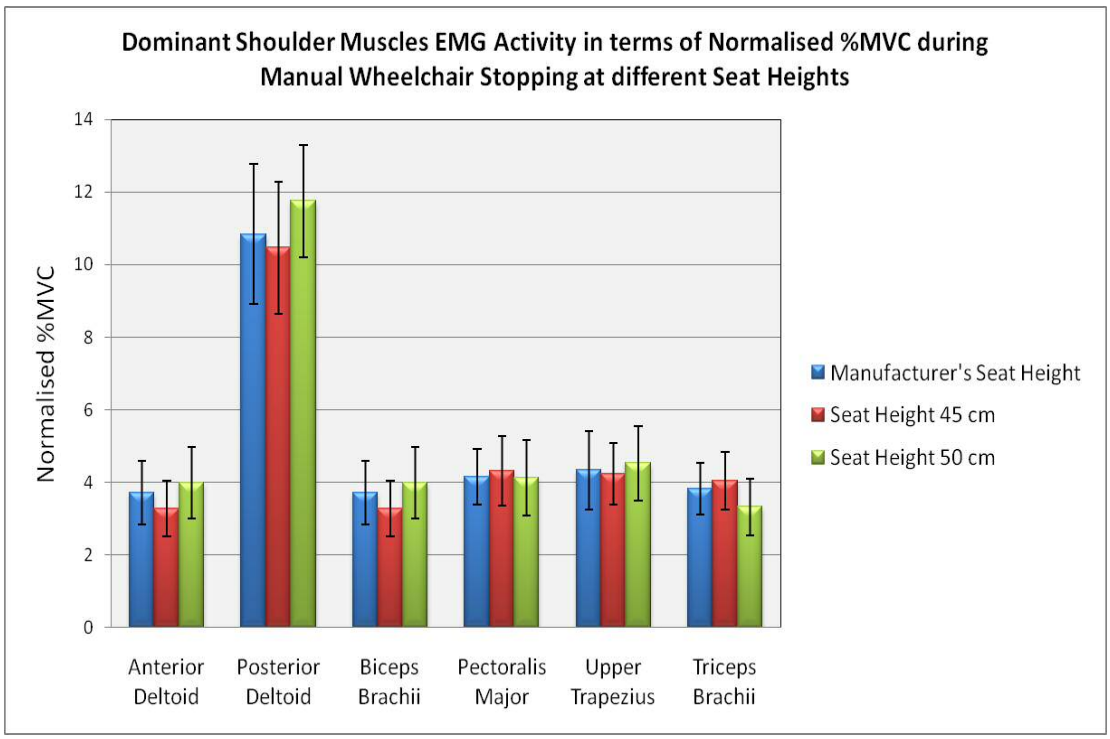


**Figure (7.17):** Dominant shoulder muscles average EMG activity in terms of normalised MVC percentage during manual wheelchair stopping at three wheelchair seat heights. All the normalized EMG %MVC are presented as group average values.

### *7.2.4. Spatiotemporal Parameters of Manual Wheelchair Propulsion*

The calculated averaged contact, release and push angles of dominant and non-dominant upper limbs during manual wheelchair propulsion while adjusting both wheelchair configurations (wheelchair's seat height and rear wheel axle position) are illustrated per the below Tables (7.15) and (7.16). Group average data of each spatiotemporal parameter along with standard deviation for both dominant and non-dominant upper limbs were calculated.

**Table (7.15)**: Spatiotemporal parameters of dominant and non-dominant upper limbs with the manufacturer's rear wheel axle position and (3 cm) and (6 cm) backward displacements. All parameters are presented as group mean and standard deviation values in its specific units.

| Spatiotemporal Parameter | | Rear Wheel Axle Position | | |
|---|---|---|---|---|
| | | Manufacturer's Position | 3 cm Backward Displacement | 6 cm Backward Displacement |
| **Propulsion Velocity (km/hr)** | | 3.21 ± 0.577 | 3.313 ± 0.496 | 3.412 ± 0.467 |
| **Propulsion Cycle (sec)** | | 4.966 ± 0.389 | 4.62 ± 0.694 | 4.445 ± 0.776 |
| **Stroke Time (sec)** | **Dominant Upper limb** | 0.993 ± 0.168 | 0.982 ± 0.225 | 0.929 ± 0.137 |
| | **Non-dominant Upper limb** | 0.992 ± 0.168 | 0.980 ± 0.223 | 0.929 ± 0.136 |
| **Push Percentage (%)** | **Dominant Upper limb** | 0.437 ± 0.024 | 0.432 ± 0.021 | 0.429 ± 0.034 |
| | **Non-dominant Upper limb** | 0.443 ± 0.015 | 0.447 ± 0.021 | 0.436 ± 0.030 |
| **Release Percentage (%)** | **Dominant Upper limb** | 0.563 ± 0.024 | 0.568 ± 0.021 | 0.571 ± 0.034 |
| | **Non-dominant Upper limb** | 0.558 ± 0.015 | 0.552 ± 0.021 | 0.565 ± 0.030 |
| **Cadence (stroke/sec)** | | 1.035 ± 0.173 | 1.104 ± 0.414 | 1.107 ± 0.162 |
| **Contact Angle (°)** | **Dominant Upper limb** | 99.34 ± 6.157 | 98.36 ± 7.129* | 95.89 ± 13.448 |
| | **Non-dominant Upper limb** | 104.8 ± 7.467 | 100.6 ± 10.337* | 98.89 ± 12.280 |
| **Release Angle (°)** | **Dominant Upper limb** | 31.34 ± 6.472 | 32.37 ± 5.736* | 35.57 ± 6.684 |
| | **Non-dominant Upper limb** | 33.33 ± 7.290 | 31.65 ± 5.805* | 35.78 ± 6.075 |
| **Push Angle (°)** | **Dominant Upper limb** | 67.63 ± 8.052 | 66.24 ± 9.328* | 60.11 ± 14.025 |
| | **Non-dominant Upper limb** | 71.09 ± 7.540 | 69.15 ± 10.354* | 63.08 ± 14.052 |

*Significant difference between the manufacturer's wheel axle position and (3 cm) and (6 cm) backward displacements.

**Table (7.16)**: Spatiotemporal parameters of dominant and non-dominant upper limbs with the manufacturer's wheelchair seat height and (45 cm) and (50 cm) seat heights. All parameters are presented as group mean and standard deviation values in its specific units.

| Spatiotemporal Parameter | | Wheelchair Seat Height | | |
|---|---|---|---|---|
| | | Manufacturer's Height | 45 cm Seat Height | 50 cm Seat Height |
| Propulsion Velocity (km/hr) | | 3.452 ± 0.703 | 3.452 ± 0.487 | 3.512 ± 0.671 |
| Propulsion Cycle (sec) | | 3.951 ± 0.980 | 4.61 ± 0.933 | 3.746 ± 0.667 |
| Stroke Time (sec) | Dominant Upper limb | 0.795 ± 0.198 | 0.922 ± 0.187 | 0.749 ± 0.134 |
| | Non-dominant Upper limb | 0.796 ± 0.199 | 0.921 ± 0.186 | 0.749 ± 0.133 |
| Push Percentage (%) | Dominant Upper limb | 0.417 ± 0.034 | 0.435 ± 0.025 | 0.4 ± 0.024* |
| | Non-dominant Upper limb | 0.427 ± 0.040 | 0.439 ± 0.022 | 0.403 ± 0.032* |
| Release Percentage (%) | Dominant Upper limb | 0.583 ± 0.034 | 0.565 ± 0.025 | 0.6 ± 0.024* |
| | Non-dominant Upper limb | 0.573 ± 0.040 | 0.562 ± 0.022 | 0.597 ± 0.032* |
| Cadence (stroke/sec) | | 1.327 ± 0.265 | 1.13 ± 0.233 | 1.373 ± 0.229* |
| Contact Angle (°) | Dominant Upper limb | 92.18 ± 7.424 | 97.98 ± 7.586 | 89.83 ± 8.525 |
| | Non-dominant Upper limb | 94.2 ± 8.315 | 100.9 ± 11.452 | 90.93 ± 7.912 |
| Release Angle (°) | Dominant Upper limb | 36.99 ± 3.431 | 34.02 ± 6.118 | 35.93 ± 4.477 |
| | Non-dominant Upper limb | 36.33 ± 2.340 | 34.26 ± 4.909 | 34.89 ± 3.947 |
| Push Angle (°) | Dominant Upper limb | 55.19 ± 8.419 | 63.51 ± 10.545 | 53.9 ± 8.004 |
| | Non-dominant Upper limb | 57.87 ± 7.415 | 66.11 ± 12.036 | 56.04 ± 8.082 |

*Significant difference between the manufacturer's wheelchair seat height and (45 cm) and (50 cm) seat heights.

The Figures (7.18) and (7.19) illustrates the propulsion angles of dominant and non-dominant upper limb during manual wheelchair propulsion at three rear wheel axle positions and three wheelchair seat heights respectively.

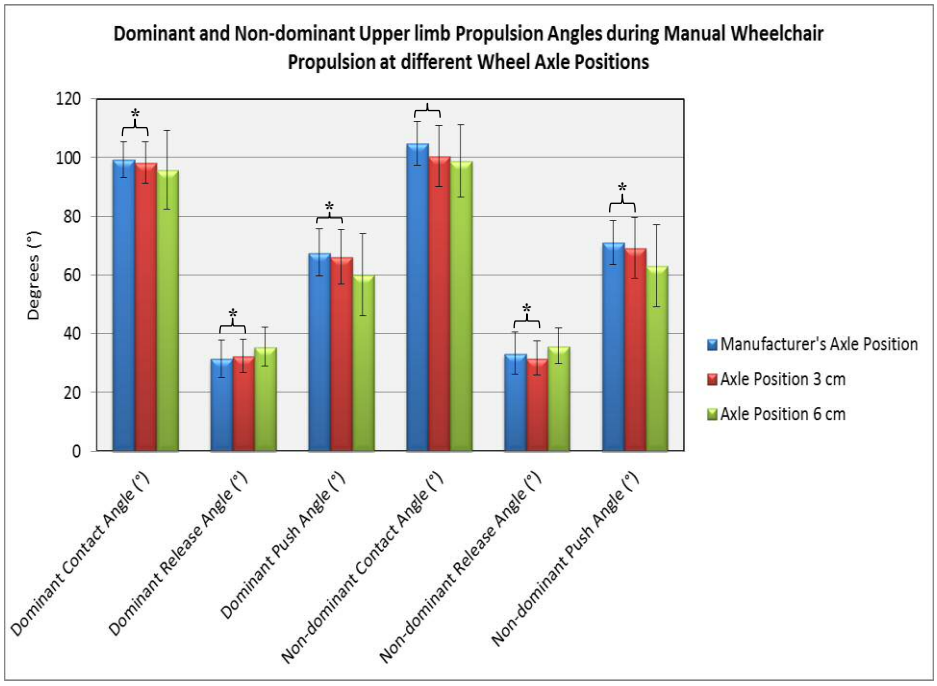


**Figure (7.18):** Propulsion angles of dominant and non-dominant upper limb during manual wheelchair propulsion at three wheel axle positions. All the propulsion angles are presented as group average values.

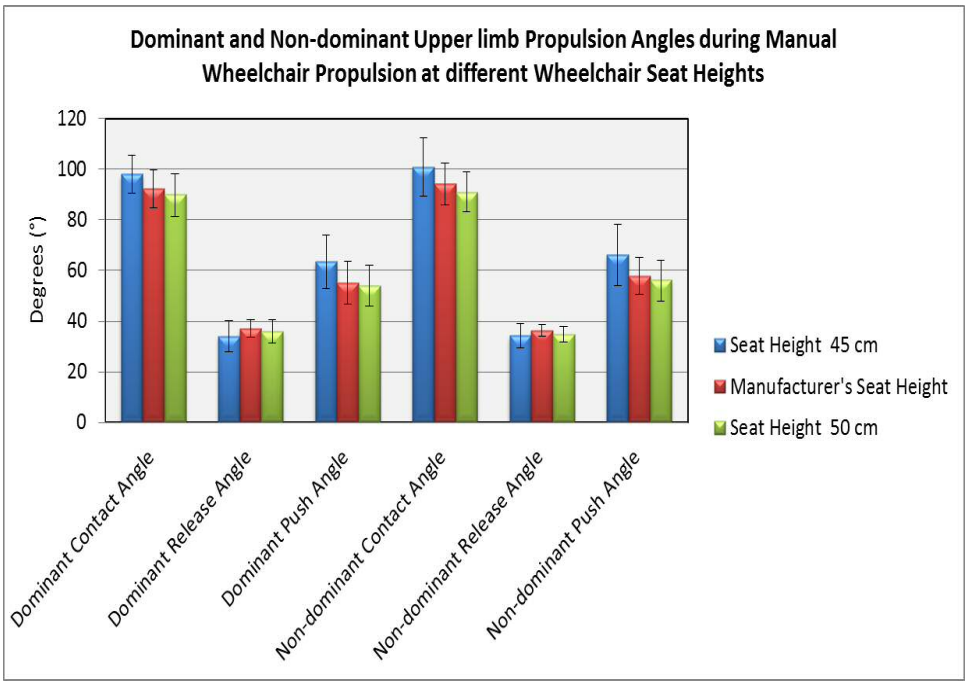


**Figure (7.19):** Propulsion angles of dominant and non-dominant upper limb during manual wheelchair propulsion at three wheelchair seat heights. All the propulsion angles are presented as group average values.

### *7.2.5. Impact of Users' Anthropometrics on Biomechanical Outcomes*

Biomechanics of the upper body were analysed according to the anthropometrics of fifteen recruited healthy male novice individuals; (mean age 32.13 ± 9.17 years, height 178.14 ± 6.74 cm, mass 89.1 ± 16.17 kg and body mass index 28.17 ± 5.54), as using the hand-rim wheelchair with their steady self-selected speed and propulsion pattern. A series of anthropometric measurements were taken from the fifteen recruited volunteers, see Section (6.5).Mean and standard deviation values were calculated for these characteristics, as well as for all biomechanical outcome measures,

Pearson coefficient (*r*) was calculated to understand whether there is a correlation between the measured anthropometric characteristics of the recruited volunteers and the biomechanical outcomes, in terms of their upper body kinematics and shoulder muscles EMG activity and spatiotemporal parameters, calculated at their dominant side, during performing manual wheelchair propulsion, see Tables (7.17), (7.18) and (7.19).The *r* value obtained for each outcome measure was interpreted according to the guidelines proposed by Altman (1991): poor agreement (r≤0.20), fair (r=0.21-0.40), moderate (r=0.41-0.60), good (r=0.61-0.80) and very good (r≥0.81).

**Table (7.17)**: Calculated Pearson's Coefficient between anthropometric characteristics and shoulder muscles EMG activity.

| Anthropometric Characteristics N=15 | Shoulder Muscles Peak EMG Activity | | | | | |
|---|---|---|---|---|---|---|
| | Anterior Deltoid | Posterior Deltoid | Biceps Brachii | Pectoralis Major | Upper Trapezius | Triceps Brachii |
| **Body Weight** | -0.29£ | -0.13£ | 0.61£ | 0.28£ | 0.17£ | -0.15£ |
| **Body Height** | -0.25£ | 0.18$ | -0.35£ | 0.2$ | 0.16$ | -0.16$ |
| **Trunk Width** | -0.23£ | - | -0.32£ | 0.25£ | -0.14£ | - |
| **Trunk Circumference** | -0.26$ | - | - | 0.48$ | 0.22$ | - |
| **Trunk Length** | 0.13$ | - | -0.32$ | - | 0.17$ | - |
| **Upper Limb Length** | 0.18$ | 0.23£ | -0.13$ | - | - | 0.12$ |
| **Upper arm Length** | 0.21£ | 0.22£ | -0.1$ | - | - | 0.16$ |
| **Upper arm Circumference** | -0.22£ | 0.24£ | 0.56£ | - | - | 0.44£ |
| **Flexed Upper arm Circumference** | -0.35£ | 0.24£ | 0.64£ | - | - | 0.52£ |

$: $p < 0.001$; £: $p < 0.01$; *: $p < 0.05$ and without superscript: $p < 0.5$.

**Table (7.18)**: Calculated Pearson's Coefficient between anthropometric characteristics and trunk and upper limb joints kinematics.

| Anthropometric Characteristics N=15 | Trunk Kinematics | | | Shoulder Kinematics | | | Elbow Kinematics | | Wrist Kinematics | |
|---|---|---|---|---|---|---|---|---|---|---|
| | FE | LB | AR | AA | IER | FE | PS | FE | RUD | FE |
| **Body Weight** | -0.23£ | -0.16£ | -0.1£ | 0.52£ | -0.1£ | 0.1£ | -0.4* | 0.23£ | -0.23* | -0.1£ |
| **Body Height** | -0.54$ | -0.48$ | -0.41$ | 0.52£ | 0.14$ | 0.24$ | -0.35£ | 0.27£ | 0.67$ | 0.27$ |
| **Trunk Width** | 0.12$ | -0.12$ | 0.13$ | - | - | - | - | - | - | - |
| **Trunk Circumference** | -0.37$ | -0.26$ | -0.16$ | - | - | - | - | - | - | - |
| **Trunk Length** | -0.54$ | -0.48$ | -0.41$ | - | - | - | - | - | - | - |
| **Upper Limb Length** | - | - | - | -0.1$ | 0.1$ | 0.21£ | - | - | - | - |
| **Upper arm Length** | - | - | - | -0.1£ | 0.21£ | 0.34£ | - | - | - | - |
| **Upper arm Circumference** | - | - | - | 0.4£ | 0.3* | -0.1£ | - | - | - | - |
| **Flexed Upper arm Circumference** | - | - | - | 0.4£ | -0.28£ | -0.26£ | - | - | - | - |
| **Forearm Length** | - | - | - | - | - | - | -0.33* | -0.7£ | - | - |
| **Forearm Circumference** | - | - | - | - | - | - | 0.2* | 0.3$ | - | - |
| **Hand Length** | - | - | - | - | - | - | - | - | 0.58$ | 0.54£ |
| **Wrist Circumference** | - | - | - | - | - | - | - | - | 0.43£ | 0.47$ |

$: $p < 0.001$; £: $p < 0.01$; *: $p < 0.05$ and without superscript: $p < 0.5$. FE: flexion-extension, LB: lateral bending, AR: axial rotation, AA: abduction-adduction, IER: internal-external rotation, PS: pronation-supination, and RUD: radial-ulnar deviation.

**Table (7.19)**: Calculated Pearson's Coefficient between anthropometric characteristics and spatiotemporal parameters of manual wheelchair propulsion.

| Anthropometric Characteristics N=15 | Propulsion Velocity (km/hr) | Propulsion Cycle (sec) | Stroke Time (sec) | Push% | Release% | Cadence (stroke/sec) | Contact Angle | Release Angle | Push Angle |
|---|---|---|---|---|---|---|---|---|---|
| **Body Weight** | 0.11£ | -0.58£ | -0.57£ | -0.14£ | 0.13£ | 0.6£ | -0.4£ | 0.65* | -0.72£ |
| **Body Height** | -0.2$ | 0.35$ | 0.35$ | 0.33$ | -0.33$ | -0.3$ | -0.7$ | 0.7$ | 0.35$ |
| **Trunk Width** | -0.04£ | -0.61£ | -0.61£ | 0.13£ | -0.14£ | 0.61£ | -0.4£ | 0.81£ | -0.79* |
| **Trunk Circumference** | 0.23$ | -0.57$ | 0.56$ | 0.01$ | -0.01$ | 0.61$ | -0.4$ | 0.42$ | 0.61* |
| **Trunk Length** | -0.20$ | 0.36$ | 0.35$ | 0.33$ | -0.33$ | -0.3$ | -0.6£ | 0.7£ | 0.35* |
| **Upper Limb Length** | -0.38$ | 0.44$ | 0.44$ | 0.5$ | -0.5$ | 0.36$ | 0.01£ | -0.4£ | 0.26£ |
| **Upper arm Length** | -0.25$ | 0.5$ | 0.5$ | 0.33$ | -0.32$ | -0.5$ | 0.21$ | -0.5 | 0.44£ |
| **Upper arm Circumference** | -0.19$ | -0.15$ | -0.14$ | -0.01$ | -0.01$ | 0.24$ | -0.3$ | 0.4* | -0.44£ |
| **Flexed Upper arm Circumference** | -0.08$ | -0.29$ | -0.29$ | 0.02$ | -0.03$ | 0.39$ | -0.4$ | 0.4 | -0.53£ |
| **Forearm Length** | -0.46$ | 0.12$ | 0.13$ | 0.44$ | -0.45$ | -0.04$ | -0.02$ | 0.2* | -0.11£ |
| **Forearm Circumference** | 0.03$ | -0.14$ | -0.14$ | 0.05$ | -0.06$ | 0.26$ | -0.5$ | -0.4* | -0.27£ |
| **Hand Length** | -0.17$ | 0.2$ | 0.2$ | 0.5$ | -0.51$ | 0.1$ | -0.1$ | -0.3£ | 0.1£ |
| **Wrist Circumference** | 0.21$ | -0.47$ | -0.46$ | 0.13$ | -0.13$ | 0.52$ | -0.3$ | 0.47£ | -0.54£ |

$: $p < 0.001$; £: $p < 0.01$; *: $p < 0.05$ and without superscript: $p < 0.5$.

No studies have reported a thorough correlation between the anthropometric characteristics of the recruited volunteers and the biomechanical outcomes, in terms of their upper body kinematics and shoulder muscles EMG activity and spatiotemporal parameters, calculated during their performing manual wheelchair propulsion.

This study demonstrates such a significant correlation to quantify the association of upper body parts with the biomechanical behaviour during the repetitive usage of the upper limb of manual wheelchair users. Anthropometric measurements whenever be considered for designing, can help in achieving comfortability, reduce musculoskeletal disorders and improve performance of the users. This information could potentially help clinical professionals and researchers to better optimise wheelchair prescription by knowing whether a user propelling more efficiently with a specific dimensions of upper body part or using a type of wheelchair over another to evaluate the effect of interventions such as adjusting wheelchair configuration.

## 7.3 Summary

This chapter is an extension of Chapter Six that aimed to present focused a development of the wheelchair-user interaction through investigating the impact of wheelchair diverse configuration on the upper body biomechanics. From a biomechanical perspective, the most important factors affecting manual wheelchair mobility are the position of the wheels and seat height relative to the user. Therefore, this chapter employed the methods described in the previous chapter six to address these features and how they influence the upper body biomechanics with propelling a manual wheelchair during daily mobility and use. This chapter presented a detailed calculation of three-dimensional kinematics of the trunk and upper limb joints, shoulder muscles EMG activity and spatiotemporal patterns during three displacements of rear wheel axle position and seat height including the manufacturer's set. These calculations were performed across a range of daily living activities, including manual wheelchair starting up, propulsion and stopping. The obtained results had implications for the design of wheelchair to improve the user performance and limit the risk of injury. It was found that changes in the users'

relative position to the rear wheels and seat height affected important aspects of the user-wheelchair interaction in terms of the trunk and upper limbs range of motion (ROM), muscles activities and handrim propulsion patterns. Also, this chapter introduced a thorough correlation between the anthropometric characteristics of the recruited volunteers and the biomechanical outcomes, in terms of their upper body kinematics and shoulder muscles EMG activity and spatiotemporal parameters, calculated during their performing manual wheelchair propulsion. A brief description of the results obtained per the established protocol was displayed.

# Chapter 8

# Discussion, Conclusions and Future Research

This chapter attempts to provide an overall discussion of the work conducted throughout this study and reported in this thesis. It also highlights the major findings and provides a set of conclusions drawn from the work undertaken in this study and leads directions for future studies.

## 8.1 Overall Discussion

The shoulder joint complex presents a challenge regarding its complexity. It composed of three bones; clavicle, scapula and humerus, and the thorax that linked by three anatomical joints; sternoclavicular (SC), acromioclavicular (AC) and glenohumeral (GH), and a functional scapulothoracic (ST) joint and a wide variety of muscle-ligamentous structures. Such complexity produces several Degrees of Freedom (DOF) and greater amplitude of motions than any other joints of the human body. In this way, it performs the three pairs of basic motions (flexion/extension, abduction/adduction and internal/external rotation), and the sum of the three groups results in circumduction that make it possible to perform a wide range of activities of daily living. For manual wheelchair users, the role of the shoulder complex essentially becomes that of the hip joint in able-bodied individuals and provides locomotion by means of manual wheelchair propulsion. Forces applied to the wheelchair resulted in reactive loads acting on upper limb that may over time lead to pain and/or injury.

The global elevation range of motion (ROM) of the shoulder complex is mainly the result of a coordinated motion between the movements of the GH and ST joints. ST motion includes both rotation and translation and involves simultaneous rotations of the clavicle at SC and AC joints. The efficiency of the upper limb biomechanical function is based on the coordinated and combined movements of the different shoulder joints; therefore, any clinical modification of one element of the shoulder complex will affect the global function of its kinematic chain, requiring the development of appropriate methods of investigating the shoulder joint complex.

Basically, this study aimed to simultaneously analyse the biomechanics of upper body in able-bodied individuals during performing different functional activities of daily living and manual wheelchair mobility. Better understanding of the upper body biomechanics during these activities will optimise the manual wheelchair users' everyday mobility that will improve their independence and quality of life, and also contribute to clinical knowledge, aiding who work with such field when prescribing, designing and selecting a device to provide the proper comfort and functionality for the user and prevent upper body musculoskeletal disorders.

The development of three-dimensional motion analysis techniques has allowed for precise and simultaneous kinematic measurements of the trunk and upper limb joints. To standardise the description of movements, the International Society of Biomechanics (ISB) has defined the frames of reference for each bony segment from specific anatomic points and rotations according to Euler angles formalism. A marker based on motion capture analysis protocol was developed in Cardiff University that can track dynamic movements of the shoulder complex using a non-invasive motion analysis technique. More recently, new, more flexible approaches to the six degrees of freedom (6DOF) calculations have become available, as an integrated feature in the software that is used to collect the motion capture data (Qualisys Track Manager, QTM, Qualisys, Sweden). Although this allows greater flexibility in the calculations, a thorough understanding of the establishment of anatomical coordinate systems, in line with the ISB recommendations, is still required in order to ensure that the resulting joint range of motion outputs are sensible.

### *8.1.1. Shoulder Complex Functionality*

This study aspect investigated the motion requirements for the shoulder complex during activities of daily living and physiological range of motion in healthy volunteers. The quantification of the three-dimensional motions needed for these tasks should enable clinicians to identify tasks that might be problematic for their patients or provide clinicians with a basis of comparison for evaluating impairments of the effects of interventions. Five healthy volunteers were performed twelve functional tasks of daily living during hygiene, feeding and reaching activities and four physiological ROM by their dominant arms.

The presented range of motion (ROM) results for the thorax, SC, AC, GH, ST and HT articulations were compared to those reported in the literature by Magermans et al. (2005), Lovern (2010) and Stroud (2011). Where comparison was possible, most ROM results presented per this study were within 10° or less to those reported per other literatures. That is probably caused by the different sample size of recruited volunteers besides the different marker set configuration and tracking capabilities used per the studies.

Functional tasks related to hygiene, feeding and reaching were investigated due to their importance in everyday independent living and also because of the physical challenges in doing them. The objective of this study aspect was to determine the extent of the shoulder complex's full physiological ROM that is required to perform functional activities of daily living.

In conclusion, it was found that most of upper limb activities of daily living can be performed without the capacity for full physiological range of motion of the individual articulations of the shoulder complex. The most demanding tasks based on the level of GH elevation required to perform them were: cleaning the upper back, reaching the side and back of the head; brushing the opposite side of the head and lifting a block to the shoulder height.

Although the majority of the shoulder complex motion occurs at the GH joint and the ST articulation, motion at the SC and AC joints are required for full arm elevation. The strong clavicle fixation to the scapula through the coracoclavicular ligament means that clavicle rotation occurs with scapula movement. The clavicle movements relative to the thorax (SC joint) were described using two rotations: elevation/depression about an axis pointing forward, and protraction-retraction about an axis aligned on the thorax vertical axis.

The scapula movements relative to the trunk (AC joint) were described by three rotations: protraction/retraction, about the vertical trunk axis, the internal rotation taking the scapula medial border away from the thorax; medial/lateral rotation, about an antero-posterior axis perpendicular to the scapula plane, the lateral rotation taking the scapula inferior angle away from the spinous processes line; and

anterior/posterior tilt, about an axis along the scapula spine, the anterior tilt taking the scapula inferior angle away from the thorax.

Scapula motion aids in arm position by maintaining a better congruence between the humerus and the glenoid of the scapula, thus reducing the risk of GH dislocation. The results showed that retraction, lateral rotation and posterior tilting of the scapula occur during arm elevation in the three axes.

Physiological ROM recordings are useful measurements to determine the extent to which the individual joints in the shoulder contribute to overall arm elevation. It is widely accepted that the motion of the ST articulation facilitates arm elevation by placing the glenoid cavity in the correct position to maintain congruency between the humerus and the scapula. Therefore the humerus and the scapula couple their movements, in what researchers describe as the scapulohumerual rhythm. This complex relationship, between GH elevation and scapula lateral rotation, has been investigated by numerous research groups with various ratios being reported ranging from 1.25:1to 2.5:1, (Stroud 2011).

The same recruited volunteers performed static and dynamic trials starting with arm elevations by the side of the body up to 180° in increments of 20° in the coronal 0° plane (abduction), scapular 30° plane (scaption), and sagittal 90° plane (flexion). Elevations were performed unilaterally with dominant arm, with the thumb pointing upwards for coronal and scapular plane elevation, and with the hand pronated for sagittal plane elevation.

Arm elevation trials were measured statically and dynamically with mounted skin markers and scapula locator to assess differences that may arise from muscle stabilisation as well as control of the joint during dynamic and static trials. No significant differences were indicated between the shoulder complex segment rotations ROM during static arm elevations in the coronal and scapular planes measured with individual skin mounted markers were attached to each of the scapula bony landmarks, and a scapula locator, ($P>0.05$). While there was a significant difference between the ROMs measured with the individual skin markers and the

scapula locator during the static arm elevation in the sagittal plane, i.e. flexion, ($P=0.04<0.05$), see Table (5.7).

For the GH joint, the main discrepancy when measuring the plane of elevation of the GH joint during elevation in the coronal and sagittal planes was caused by gimbal lock. This occurs when two of the three rotational axes of the GH joint are aligned with their pivot axes in a single plane. When this occurs it is no longer possible to represent the orientation of the GH joint. This is likely to occur at low and high humeral elevations. Arm elevation relative to the trunk (HT elevation) referred to the angle between the humerus and the thorax, regardless of the plane of elevation imposed by the task. The error seems acceptable for arm elevation < 120º.

To summarise, the complete upper limb elevation is principally the combination of the GH and ST joint movements (rotations and translations). ST motion involves a coordinated mobility of the AC and SC joints. For both clinical settings and research, assessment of the shoulder complex should not only be limited to GH movements but also must include the associated scapula-clavicle and trunk movements.

Basically, upper body motion is highly variable and complex, often challenging all degrees of freedom (DOFs) in the kinematic chain during functional activities of daily living. Such variability and complexity makes movement standardisation for the purpose of kinematic assessment difficult. This kinematic analysis technique has some limitations. One of the main practical difficulties is associated with using retro-reflective markers is the movement of skin causing relative displacement between the markers and the underlying bone. This can be particularly troublesome for movement of the scapula. In addition the placement of the markers can be unreliable through detecting the anatomical landmarks with the palpitation method proving to be slightly objective. Also there was a problem of body interposition obscuring markers from the field of view of the cameras; where interpolation of the gaps cannot always be reliable. The scapula is particularly difficult to assess because it is flat and surrounded by muscles, not readily visible during a clinical examination. This problem was particularly noticeable for tasks involving reaching across the body, such as touching the opposite side of the neck or

the opposite axilla or crossing body abduction or during arm elevation beyond 120° angulation.

Another difficulty is determining the GH rotation centre because it cannot be palpated and must be calculated. There are also limitations that depend on the Euler angles convention due to mathematical singularities, particularly for large arm movements. However, the main limitation is soft tissue artefact (movement occurring between the skin and underlying bone) related to the use of sensors fixed on the skin.

### *8.1.2 Biomechanics of Functional Wheelchair Use*

Manual wheelchair users depend on their trunk and upper limbs for mobility during their activities of daily living. As a result of greater than normal usage and load, shoulder and wrist pain and pathology are common among manual wheelchair users. This study aspect provides a biomechanical analysis of the manual wheelchair mobility in control subjects during their functional activities of daily living. A protocol for 3D kinematic bilateral measurements of the trunk and upper limb joints was applied using a six degrees of freedom (6 DOF) analysis and sEMG data were recorded to understand the effect of wheelchair configurations on the shoulder muscles recruitment and calculated as % Maximum Voluntary Contraction (%MVC). A population of ten healthy subjects was characterised for different wheelchair configurations, set by adjusting the horizontal axle position of both rear wheels by (3 cm) and (6 cm) posteriorly from the original position that was set by the manufacturer (Invacare, 2011) and by adjusting the seat-to-floor distance by (45 cm) and (50 cm) from the manufacturer's wheelchair seat position(Invacare, 2011). These measurements were taken in the Cardiff University Motion Analysis Laboratory.

Three-dimensional trunk and dominant upper limb joints kinematics during manual wheelchair propulsion has been evaluated. Peak joint angles (maximum and minimum) were identified and used to compute the ranges of motion (ROMs).

The trunk, while not an actual joint, also had its motion analysed. In the sagittal plane, the thorax was in a state of flexion (or forward bend) throughout the

propulsion cycle. Additionally, the trunk was consistently rotated in the transverse plane and laterally bent in the coronal plane to the subject's non-dominant side. This may suggest that the subject is working harder with his dominant side and incorporating his trunk to assist. Subjects with high level of SCI have less trunk control. In this study, able-bodied participants showed better trunk control as they usually lean their trunk forward during the pushing which generates body momentum to assist the pushing. That may diminish the co-contraction of shoulder muscles during the early stage of recovery.

It was found that the adjusted wheelchair configurations that provide greater trunk motion promoted a contact position with increased trunk flexion; however, it should also be noted this study recruited able-bodied individuals. This propulsion approach has the advantage of utilising gravitational forces to counter-balance the trunk extension reaction forces generated by the hand pushing on the wheel, but limits the propulsion angle as contact occurs further around the wheel.

The shoulder joint experienced its largest range of motion in the sagittal plane. While, both elbow joints were in a constant state of flexion and forearm pronation during both phases of propulsion cycle. Both wrist joints were always in a state of extension during both phases of propulsion cycle. Also, they were in its largest extension rotation and ulnar deviation at almost the same instant.

Mulroy at al. (1996) identified two synergies of shoulder muscle function during wheelchair propulsion. The push phase synergy was dominated by muscles with shoulder flexion (anterior deltoid, pectoralis major), external rotation (supraspinatus, infraspinatus) and scapular protraction (serratus anterior) functions.

In this study, peak and average sEMG values were evaluated to test the activity of pectoralis major, anterior deltoid muscles in the push phase synergy muscle group and posterior deltoid and upper trapezius in the recovery phase synergy muscle group. The peak EMG activity evaluated in this study was lower than the activities reported by other studies (Mulroy et al. 1996) due to the differences of participant populations between the studies. It was concluded by Schantz et al. (1999) that the biceps brachii and triceps brachii, anterior deltoid and

pectoralis major muscles could be anticipated to propel the wheelchair forward, whereas the posterior deltoid and trapezius muscles could be expected to play a role, especially during the recovery phase. However, individual differences exist.

This high activation on average for the muscles predominantly involved with the recovery phase could be associated with the increase in the shoulder ROM required for the volunteer to reach their starting position on the hand rim. Also, the decreased activation on average for the muscles predominantly involved with the push phase could be associated with the increased upper limbs kinematics and the muscles pre-stretch potentiation.

Moreover, the findings of this study indicates that the general order of muscles activation is of, first, the biceps brachii, thereafter the pectoralis major and anterior deltoid, and then the triceps brachii muscles during the push phase of propulsion, and this is in agreement with other studies, (Mulroy et al. 1996).

The subjects recruited per this study were able-bodied and non-experienced in manual wheelchair propulsion. Therefore, for transferring the obtained findings to the population of persons with a spinal cord injury, one has to keep in mind that due to the potential loss of muscle function, the relative muscle activity might be higher as reported in this study. Mainly for persons with a high lesion the muscle activity needed for manual wheelchair propulsion is distributed over fewer muscles, which could increase the actual stress on these remaining muscles and could result in higher loading on the shoulder joint.

Manual wheelchair mobility functional tasks, such as starting up and stopping may be more challenging than propulsion and it is important to understand the trunk and upper limb joints demands during these functional tasks for improved rehabilitation and treatment planning. Therefore, kinematics of trunk and upper limb joints and shoulder muscles activity were quantified during these functional tasks.

Overall, the start task demands the largest ROM in the sagittal plane of all upper limb joints, (shoulder, elbow and wrist) as it is also the plane in which the greatest amount of movement occurs during manual wheelchair use.

Upper limb joints ROM, were significantly smaller in all three planes of motion, during the stopping task, while propelling and starting a wheelchair utilize similar motion demands and magnitudes of the shoulder, elbow, and wrist joints, while stopping a wheelchair is significantly different. Similarly, activity of shoulder muscles predominantly involved with both pushing and recovery phases of propulsion were smaller during stopping than propulsion and starting up tasks.

Overall, propulsion, starting, and stopping tasks during manual wheelchair mobility were significantly different. Starting a wheelchair appears to be the most demanding task (largest ROM) on the trunk and upper limb joints, while stopping appears to be the least demanding task. That was expected due to the nature of beginning movement of the wheel and overcoming inertia. Once the wheel is in motion, as during propulsion, less ROM is needed to keep the wheelchair moving.

Propulsion, starting, and stopping tasks proved to be different biomechanically, which suggests that clinicians should consider all functional tasks when developing rehabilitation protocols and planning long-term mobility strategies.

Knowing the repetitiveness of upper limb movements for wheelchair propulsion that occur on a daily basis could be important for understanding and preventing pain and injury. This study estimated spatiotemporal parameters of wheelchair propulsion including stroke number, propulsion velocity, push and release time, and propulsion angles based on hand push rim coupling movement collected via motion analysis system among manual wheelchair users.

The release phase was associated with a longer push phase than usual as more time spent in the push phase relative to the release phase. These two findings may imply to less loads per unit of time during the push phase, which may reduce the risk of upper limb injuries. A shorter release phase than usual may lead to increased efforts in accelerating/decelerating movements during the recovery phase due to the inexperience of the recruited participants.

Also, the increased push phase time with no change of total propulsion cycle time corresponds to the increase of hand contact angle range on the pushrim. It was accomplished by decreasing the hand release angle without changing the initial hand

contact angle on the pushrim. Increasing the push phase time in the recruited participants was resulted by the delay of hand release on the pushrim. During the late part of the push phase, the hand continues propelling the wheel and moving down along with the pushrim until the hand cannot reach further and has to let go of the wheel. In order to continue propelling the pushrim, the upper trunk leans forward during the push phase so the hand can reach down.

It was found that increasing the backward displacement of the rear wheel axle position led to an increased propulsion time and decreased velocity and cadence performed by the recruited volunteers. This will be requiring the user a greater shoulder extension to reach back the handrim and, consequently, pushing the wheels in a smaller propulsion arc. Further, the pushing percentage of the propulsion cycle and push angles were decreased while release percentage of the propulsion cycle and release angles were increased as the horizontal axle displacement was moved from the manufacturer's position to (3 cm) and (6 cm) respectively as a result to the decreased pushing muscles and increased recovery muscles activities. This is recommended, as it has the potential to reduce the number of strokes needed to maintain a given speed. This results in a lower number of repetitive motions performed by the upper limbs. However, this condition increases the resultant force experienced at the shoulders during propulsion, which contributes to joint damage and injuries.

In a similar manner, it was found that that raising the wheelchair's seat height led to an increased propulsion time and decreased velocity and cadence performed by the recruited volunteers. Further, the pushing percentage of the propulsion cycle and push angles were decreased while release percentage of the propulsion cycle and release angles were increased as the wheelchair seat-to-floor distance was moved from the manufacturer's seat height to (45 cm) and (50 cm) respectively as a result to the decreased pushing muscles and increased recovery muscles activities.

As a result, more muscle activities are required to slow down the arm or to change the direction of hand movement during the recovery phase. More muscle activities could lead to increased upper limb joints stress which may diminish the risk of pain and/or injury.

For the shoulder muscles EMG activity, the highest correlation was observed between the upper arm and flexed upper arm circumferences with the biceps and triceps brachii activities. In a similar manner, a moderate and positive correlation was exhibited between the trunk circumference and the activity of the pectoralis major muscle. These results might indicate the relative contribution of muscular size to the muscle activation as it reflects the amount of contractile protein within the skeletal muscle. Therefore, shoulder muscles activity had higher correlations with the anthropometric circumference dimensions than length dimensions compared to other biomechanical outcomes. Furthermore, there were poor relationships between the other shoulder muscles activity and upper limb segments anthropometrics.

Additionally, there was a moderately negative correlation between the trunk kinematics in both frontal (lateral bending) and transverse (axial rotation) planes of movement with both body height and trunk length. During manual wheelchair propulsion, most users do exhibit paradoxical movement of the trunk and arms in which the trunk moves backwards at the beginning of the stroke while the arms push forward. Therefore, higher trunk lengths will lend to poorer propulsion kinematics and would be a style of that of an individual having less wheelchair propulsion experience. Also, higher body heights may be explained in part by the fact that some participants were classified as being overweight with associated abdominal obesity that limited their ability to increase forward trunk flexion to accommodate for the wheelchair pushing.

Furthermore, there were poor relationships between the other joints kinematics and upper limb segments anthropometrics. However, hand length had good and positive correlation to the wrist kinematics in the frontal plane of movement. Higher hand lengths will lend to increase the wrist radial ulnar deviation ROM which is required for the volunteers to reach their starting position on the hand rim.

The highest correlations were exhibited between the upper body anthropometrics and the spatiotemporal parameters of the manual wheelchair propulsion. Good and negative correlation coefficients were observed between the

body mass index and the time of propulsion cycle and stroke. Higher body mass index of the participant will lead to decreased time of the propulsion, as well as increased cadence (fewer number of strokes), make it harder to push the wheelchair. Additionally, trunk width was negative highly correlated with the propulsion timing exhibited a similar indication.

Similarly, body height exhibited a positive and a negative good correlation with the contact and release angles of propulsion respectively. Higher body heights may be explained in part by the fact that some participants were classified as being overweight. Besides, both contact and release angles are initially associated with stroke time and cadence. Therefore, higher body heights will tend to decrease the contact and release angles that will lead to decreased time of the propulsion, as well as increased cadence (fewer number of strokes), make it harder to push the wheelchair. Also, trunk length was positively and negatively highly correlated with the release and contact angles of propulsion respectively exhibited a similar indication.

Additionally, upper arm length observed a positively good correlation with the propulsion cycle and strokes timings. Therefore, higher upper arm lengths will lend to increased time of propulsion cycle and stroke, make it easier for the participant to push the wheelchair.

Upper limb and hand lengths exhibited positive and negative good correlation with the pushing and release phases of the propulsion cycle respectively. Therefore, higher hand lengths will tend to increased pushing percentage and decreased release percentage of the propulsion cycle as that is required for the volunteers to reach their starting position on the hand rim.

Furthermore, there were poor relationships between the spatiotemporal parameters and other upper limb round anthropometrics (circumferences). However, wrist circumference observed negative moderate correlation with the pushing angle exhibited a similar indication.

It has been reported that experienced manual wheelchair users adapt their stroke techniques and patterns accompanied by the employment of wheelchairs. The longer they use the wheelchair as their major means of locomotion and mobility, the smoother and more consistent their body segment movements and muscle activities are during wheelchair propulsion. Differences in biomechanical results were expected with pathological individuals due to physiological differences, such as disability and body composition plus experience of wheelchair use. Therefore, it may be seemed difficult to compare the results of trunk and upper limb kinematics between studies, and the differences between studies may come from the differences of pushing speeds, stroke patterns, participants and definition of coordinate system among studies. Meanwhile, it also may be inappropriate to relate the results of this study to wheelchair propulsion in the elderly users since most likely they propel their wheelchairs with their hands and legs. In addition, muscle strength and joint flexibility (range of motion) declines as people age, which can affect the analyses.

## 8.2 Conclusions

Upper limb function can be impaired by a variety of injuries to the neuromuscular or musculoskeletal systems, including spinal cord injury or stroke. Such impairments can greatly affect one's ability to perform activities of daily living (ADLs). Quantifying three-dimensional kinematics of the upper body during functional tasks could be a valuable method for assessing the upper limb function and provide an important step towards understanding movement disorders of the upper limbs and evaluating the effect of rehabilitation interventions.

As the number of manual wheelchair users is developing around the world, it becomes very essential to increase the understanding of the biomechanics of upper body to enhance the performance and decrease the risk of injury.

In the context of manual wheelchair propulsion, biomechanics of upper body involves the study of how a manual wheelchair user imparts power to the wheels to achieve mobility. In general, the primary goal of biomechanical analysis of manual wheelchair propulsion is to generate knowledge that can be used to improve performance and/or prevent injuries. Either directly or indirectly, the knowledge

accumulated is likely to have implications to the quality of life of manual wheelchair users.

This study showed an interrelationship between diverse wheelchair configurations of adjustable wheelchair rear wheel axle position and seat height and upper body kinematic behaviour, muscles recruitment and spatiotemporal patterns during manual wheelchair mobility.

It was observed that changing rear wheel axle position posteriorly and raising the seat-to-floor distance (i.e. raising the seat height position) are correlated with higher upper body kinematics and release phase muscle activities and lower pushing patterns and push muscle activities during functional wheelchair mobility and so could be linked with higher risk of musculoskeletal disorders. Also, it was observed that the rear wear axle position was the factor that most influence the kinematics of the trunk and upper limbs during manual wheelchair mobility, as it determines the user's reach to the wheels. While, the effect of adjusting wheelchair seat height was more influential on the shoulder muscles activity.

The increased joints ROM and muscles activity are required for the users to reach their starting position with the pushrim to perform the propulsion properly. Also, the reduced pushing patterns will tend the user to increase the pushing frequency. All that may lead to increased risk of muscular fatigue and upper limb joints wear.

Meanwhile, this study exhibited correlation between the anthropometric characteristics of upper body joints and their biomechanical behaviour during the manual wheelchair propulsion.

When it comes to mobility, manual wheelchairs should provide a balance between efficiency, stability and preservation of upper limbs function. Appropriate wheelchair configuration should ensure the user's trunk and upper limb joints ROM fall within the normal range. Wheelchair configurations that cause joints to use maximum joint ROM considered inappropriate as the excessive movement may cause overuse injury due to joint impingement and tissue undue stress. Therefore, the

optimisation of the wheelchair configuration, based on functional characteristics of the user, appears beneficial.

It is hoped that this knowledge will help both manufacturers and clinicians when designing and prescribing wheelchairs that are more proper to the users' functional features, needs and expectations, accordingly profiting users' independence and quality of life.

## 8.3 Future Research

There is a large scope for possible future research on the upper body biomechanics during manual wheelchair propulsion. This study provided an initial analysis of the upper body biomechanics during manual wheelchair propulsion in able-bodied non-experienced individuals with a relatively small sample size (n=10), single gender (male), and narrow age range. Recruit more experienced users matched with age, gender, spinal cord injury level and body size for each group can improve the researchso that more realistic analysis of wheelchair propulsion can be generated.

Additionally, the propulsion activities were examined at a self-selected speed and pattern per the current study. Results of previous investigations suggest that people who use manual wheelchairs modify their hand pattern with changes in propulsion speed (Boninger et al. 2002 and Slowik et al. 2015) and grade of incline (Richter 2007). Thus, for future work should examine upper limb demand during these other propulsion conditions.

Regarding the kinematic analysis, a simplification of the shoulder joint, which has been modelled as a universal joint, was considered in this analytical study. Further studies may consider including the clavicle and scapula motions to achieve a more comprehensive analysis of the upper limb.

Following the successful evaluation of manual wheelchair propulsion over ground under laboratory conditions, this should be expanded on and parlayed for use across other terrain surfaces, such as carpet, grass and aggregate concrete, which are

encountered during daily living, through investigating the impact of rolling resistance on manual wheelchair biomechanics.

The current study investigated two wheelchair configurations; rear wheel axle position and wheelchair seat height. Further investigations should explore the influence of adjusting more configurations, such as wheelchair camber, on upper body biomechanics and propulsion patterns during functional wheelchair activities.

Further research using SmartWheels is required to collect the kinetic data (three-dimensional components of force and moment components) about the point of action and investigate bilateral differences and effects due to hand dominance. These investigations will also provide a foundation for investigating contact forces in manual wheelchair users and their potential risk to injury.

Last, it is important to explore the impact of physical activity on manual wheelchair locomotion and mobility. Future research should entail a method of accurately estimating the energy expenditure in wheelchair user through incorporating measures of physiological signals such heart rate, oxygen uptake ($VO_2$) and carbon dioxide production ($VCO_2$).This can be used as a clinical tool to assess the efficacy of health behaviour change in wheelchair users during performing their activities of daily living.

# References

Alm, M., Saraste, H. and Norrbrink, C. (2008). Shoulder pain in persons with thoracic spinal cord injury: prevalence and characteristics. Journal of Rehabilitation Medicine; 40(4): 277–283.

Altman, D.G. (1991). Practical Statistics for Medical Research, Chapman and Hall, London, UK.

Bednarczyk, J.H. and Sanderson, D.J.(1995). Limitations of kinematics in the assessment of wheelchair propulsion in adults and children with spinal cord injury. Physical Therapy; 75(4):281-289.

Beekrman, C.E., Miller-Porter, L. and Schoneberger, M., (1999). Energy cost of propulsion in standard and ultralight wheelchairs in people with spinal cord injuries. Physical Therapy; 79:146-158.

Boettcher, C.E., Ginn, K.A. and Cathers, I. (2008). Standard MVC Tests for Normalizing Shoulder Muscle EMG. Journal of Orthopaedic Research; 26(12):1591-1597.

Boninger, M.L., Cooper, R.A., Shimada, S.D. and Rudy, T.E. (1998). Shoulder and elbow motion during two speeds of wheelchair propulsion: a description using a local coordinate system. Spinal Cord; 36:418-426.

Boninger, M.L., Cooper, R.A., Baldwin, M.A., Shimada, S.D. and Koontz, A. (1999). Wheelchair pushrim kinetics: body weight and median nerve function. Archives of Physical Medicine and Rehabilitation; 80:910–915.

Boninger, M.L., Baldwin, M., Cooper, R.A., Koontz, A. and Chan, L. (2000). Manual wheelchair pushrim biomechanics and axle position. Archives of Physical Medicine and Rehabilitation; 81:608-613.

Boninger, M.L., Souza, A.L., Cooper, R.A., Fitzgerald, S.G., Koontz, A.M. and Fay, B.T. (2002). Propulsion patterns and pushrim biomechanics in manual wheelchair propulsion. Archives of Physical Medicine and Rehabilitation; 83:718-723.

Boninger, M.L., Impink, B.G., Cooper, R.A. and Koontz, A. (2004). Relation between median and ulnar nerve function and wrist kinematics during wheelchair propulsion. Archives of Physical Medicine and Rehabilitation; 85:1141-1145.

Bowling, R. W. and Rockar, P. (1985). The elbow complex. In J. Gould, G. J. Davies (Eds.). Orthopaedics and Sports Physical Therapy. St. Louis: Mosby, pp. 476–496.

Brose, S.W., Boninger, M.L., Fullerton, B., McCann, T., Collinger, J.L., Impinil, B.G. and Dyson-Hudson, T.A. (2008). Shoulder ultrasound abnormailities, physical examination findings and pain in manual wheelchair users with spinal cord injury. Archives of Physical Medicine and Rehabilitation; 89:2086-2093.

Brubaker, C.E., McLaurin, C.A. and McClay, I.S. (1986). Effects of side slope on wheelchair performance. Journal of Rehabilitation Research and Development, 23:55–58.

Cailliet, R. (2004). The Illustrated Guide to Functional Anatomy of the Musculoskeletal System. AMA Press. ISBN 1-57947-408X. USA.

Campbell, A.C., Lloyd, D.G., Alderson, J.A. and Elliott, B.C. (2009). MRI development and validation of two new predictive methods of glenohumeral joint center location identification and comparison with established techniques. Journal of Biomechanics; 42(10):1527-1532.

Cappozzo, A., Leo, T., and Pedotti, A. (1975). A general computing method for the analysis of human locomotion. Journal of Biomechanics; 8:307-320.

Cappozzo, A., Figura, F., Leo, T., and Marchetti, M. (1978). Movements and mechanical energy changes of the upper part of the human body during walking. In

Biomechanics VI-A, edited by E. Asmussen and K. Jørgensen; 272-279. University Park Press, Baltimore, MD, USA.

Cerquiglini, S., Figura, F., and Marchetti, M. (1981). Biomechanics of wheelchair propulsion. Biomechanics VIII A. Proceedings of the 7th International Congress of Biomechanics, Warsaw, Poland. University Park Press, Baltimore, MD, USA.

Cherubini M, Melchiorri G. (2012). Descriptive study about congruence in wheelchair prescription. European journal of physical and rehabilitation medicine; 48(2):217-222.

Chow, J.W. and Levy, C.E. (2011). Wheelchair propulsion biomechanics and wheelers' quality of life: an exploratory review, Disability and Rehabilitation: Assistive Technology, September 2011; 6(5):365-377.

Collinger, J.L., Boninger, M.L., Koontz, A.M., Price, R., Sisto, S.A., Tolerico, M.L., and Cooper, R.A. (2008). Shoulder biomechanics during the push phase of wheelchair propulsion: A multisite study of persons with paraplegia. Archives of Physical Medicine and Rehabilitation; 89:667-676.

Cooney, W.P., Lucca, M.J., Chao, E.Y.S. and Linscheid, R.L.(1981). The kinesiology of the thumb trapeziometacarpal joint. Journal of Bone and Joint Surgery63A (9):1371–1381.

Cooper R.A., Robertson, R.N., Van Sickle, D.P., Boninger, M.L. and Shimada, S.D. (1997). Methods for determining three-dimensional wheelchair pushrim forces and moments: a technical note. Journal of Rehabilitation Research and Development; 34(2):162-70.

Cooper, R.A., Boninger, M.L., Shimada, S.D. and Lawrence, B.M. (1999). Glenohumeral joint kinematics and kinetics for three coordinate system representations during wheelchair propulsion. American Journal of Physical Medicine and Rehabilitation; 78(5):435-446.

Cooper R.A., Wolf, E. and Fitzgerald, S.G. (2003). Seat and footrest shocks and vibrations in manual wheelchairs with and without suspension. Archives of Physical Medicine and Rehabilitation; 84: 96–102.

Cooper R.A., Tolerico M., Kaminski B.A., Spaeth D., Ding D. and Cooper R. (2008). Quantifying wheelchair activity of children: a pilot study. Archives of Physical Medicine and Rehabilitation; 87:977–983.

Cooper, R.A. (2009). SMART$^{Wheel}$: From Concept to Clinical Practice. Prosthetics and Orthotics International. September 2009; 33(3):198–209.

Cowan, R.E., Nash, M.S., Collinger, J.L., Koontz, A.M., and Boninger, M.L. (2009). Impact of surface type, wheelchair weight, and axle position on wheelchair propulsion by novice older adults. Archives of Physical Medicine and Rehabilitation; 90(7):1076-1083.

Crespo-Ruis, B., Del Ama-Espinosa, A. and Gil-Agudo, A. (2011). Relation between kinematic analysis of wheelchair propulsion and wheelchair functional basketball classification. Adapted Physical Activity Quarterly; 28:157-172.

Curtis, K. A., Drysdale, G. A., Lanza, R. D., Kolber, M., Vitolo, R. S., and West, R. (1999). Shoulder pain in wheelchair users with tetraplegia and paraplegia. Archives of Physical Medicine and Rehabilitation; 80:453- 457.

de Beer, J.F., Lam, F., Bhatia, D.N., Mostofi, S.B. and van Rooyen, K. (2007). Biomechanical considerations of the normal and rotator cuff deficient shoulders and the reverse shoulder prosthesis. Orthopaedics and Trauma; (21):40-46.

de Groot, J.H., Valstar, E.R. and Arwert, H.J. (1998). Velocity effects on the scapulohumeral rhythm. Clinical Biomechanics; 13:593–602.

De Luca C. (1997). The Use of Surface Electromyography in Biomechanics. Journal of Applied Biomechanics; 13:135-163.

Dellabiancia, F., Porcellini, G. and Merolla, G. (2013). Instruments and techniques for the analysis of wheelchair propulsion and upper extremity movement in patients with spinal cord injuries: current concept review. Muscles Ligaments Tendons Journal. Jul-Sep; 3(3):150-156.

Delsys, 2012. *Technical Note 101: EMG Sensor Placement* [online], available at: https://www.delsys.com/KnowledgeCenter/Tutorials_Technical%20Notes.html [Accessed: 14/10/2015].

Delsys, 2012. *Technical Note 103: EMG Signal Analysis* [online], available at: https://www.delsys.com/KnowledgeCenter/Tutorials_Technical%20Notes.html [Accessed: 14/10/2015].

Desroches, G., Chèze, L., and Dumas, R. (2010). Expression of joint moment in the joint coordinate system. Journal of Biomechanical Engineering, 132(11):114503.

DiGiovine, C., Koontz, A., and Boninger, M.L. (2006). Advances in Manual Wheelchair Technology. Topics in Spinal Cord Injury Rehabilitation: Spring 2006, 11(4):1-14.

Doorenbosch, C., A., Harlaar, J. and Veeger, D., H. (2003). The globe system: An unambiguous description of shoulder positions in daily life movements. Journal of Rehabilitation Research and Development; 40:147–155.

Dubowsky, S.R., Rasmussen, J., Sisto, S.A., and Langrana, N.A. (2008). Comparison of Kinematics, Kinetics, and EMG throughout Wheelchair Propulsion in Able-Bodied and Persons with Paraplegia: An Integrative Approach. Journal of Biomechanical Engineering; 131(2):021015.

Ferran, N.A. (2010). Measurement of anterior glenohumeral translation in patients with multidirectional instability (MDI) and healthy controls using optoelectronic motion analysis techniques. MSc dissertation in Orthopaedic Engineering. Cardiff University, UK.

Finley, M., Rasch, E., Keyser, R., and Rodgers, M. (2004). The biomechanics of wheelchair propulsion in individuals with and without upper-limb impairment. Journal of Rehabilitation Research and Development; 41:395-402.

Freixes, O., Fernández, S.A., Gatti, Crespo, M.J., Olmos, L.E., and Rubel, I.F. (2010).Wheelchair axle position effect on start-up propulsion performance of persons with tetraplegia. Journal of Rehabilitation Research and Development; 47(7):661-668.

Gagnon, D., Babineau, A., Champagne, A., Desroches, G., Aissaoui, R. (2015). Trunk and shoulder kinematic and kinetic and electromyographic adaptations to slope increase during motorized treadmill propulsion among manual wheelchair users with a spinal cord injury. BioMed Research International, volume 2015, article ID 636319.

Gorce, P. and Louis, N. (2012).Wheelchair propulsion kinematics in beginners and expert users: influence of wheelchair settings. Clinical Biomechanics; 27(1):7-15.

Grood, E.S., and W. J. Suntay. (1983). "A Joint Coordinate System for the Clinical Description of Three-Dimensional Motions: Application to the Knee." Trans. A.S.M.E. 105:136-144.

Guo, LY, Su, FC, Wu, HW and An, KN. (2003). Mechanical energy and power flow of the upper extremity in manual wheelchair propulsion. Clinical Biomechanics; 18(2): 106–114.

Halaki, M. and Ginn, K.A. (2012). Normalization of EMG Signals: To Normalize or Not to Normalize and What to Normalize to? In book: Computational Intelligence in Electromyography Analysis - A Perspective on Current Applications and Future Challenges, Chapter: 7, Publisher: Rijeka, InTech, Editors: G. R. Naik, pp.175-194.

Hamill, J., Knutzen, K. M., and Derrick, T. R. (2015). Biomechanical Basis of Human Movement. Fourth Edition. Wolters Kluwer, pp. 131-171.

Hughes, C.J., Weimar, W.H., Sheth, P.N., and Brubaker, C.E. (1992). Biomechanics of wheelchair propulsion as a function of seat position and user-to-chair interface. Archives of Physical Medicine and Rehabilitation; 73(3):263-269.

Hurd, W.J., Morrow, M.M., Kaufman, K.R.andAn, K.N. (2008). Biomechanic evaluation of upper-extremity symmetry during manual wheelchair propulsion over varied terrain. Archives of Physical Medicine and Rehabilitation; 89(10):1996-2002.

Invacare, 2009. *Invacare Action 2 NG Maintenance and Adjustment,* Invacare France Operations.

Invacare, 2011. *Invacare Action 2 NG Range User Guide.* [online], available at: http://www.altonaids.co.uk/uploads/34594action_2_manual.pdf
[Accessed: 29/11/2015]

Jensen, S.L., Olsen, B.S., Tyrdal, S., Sojbjerg, J.O. and Sneppen, O. (2005). Elbow joint laxity after experimental radial head excision and lateral collateral ligament rupture efficacy of prosthetic replacement and ligament repair. Journal of shoulder elbow surgery; 14:78.

Johnson, G. R., Stuart, P.R. and Mitchell, S. (1993). A method for the measurements of three-dimensional scapular movement. Clinical Biomechanics; 8:269–273.

Jones, L., Holt, C.A., Bowers, A. (2006). Movement of the shoulder complex: the development of a measurement technique based on proposed ISB standards. The Ninth International Symposium on 3D analysis of human movement, Valenciennes, France, 28-30 June 2006.

Karduna, A., McClure, P., Michener, L., and Sennett B. (2001). Dynamic measurements of three dimensional scapular kinematics: a validation study. Journal of Biomechanical Engineering; 123(2):184–190.

Koontz, A.M., Cooper, R.A., Boninger, M.L., Souza, A.L., and Fay, B.T. (2002). Shoulder kinematics and kinetics during two speeds of wheelchair propulsion. Journal of Rehabilitation Research and Development; 39(6):635-650.

Koontz, A.M., Cooper, R.A., Boninger, M.L., Yang, Y., Impink, B.G., and van der Woude, L.H.V. (2005).A kinetic analysis of manual wheelchair propulsion during start-up on select indoor and outdoor surfaces. Journal of Rehabilitation Research and Development; 42(4):447-458.

Kulig, K., Rao, S.S., Mulroy, S.J., Newsam, C.J., Gronley, J.K., Bontrager, E.L., and Perry, J. (1998). Shoulder joint kinetics during the push phase of wheelchair propulsion. Clinical Orthopaedics and Related Research; 354:132-143.

Kulig, K., Newsam, C.J. and Mulroy, S.J. (2001). The effect of level of spinal cord injury on shoulder joint kinetic during manual wheelchair propulsion. Clinical Biomechanics; 16:744-751.

Kwarciak, A.M., Sisto, S.A., Yarossi, M., Price, R., Komaroff, E., and Boninger, M.L. (2009). Redefining the manual wheelchair stroke cycle: Identification and impact of non-propulsive pushrim contact. Archives of Physical Medicine and Rehabilitation; 90:20-26.

Lighthall-Haubert, L., Requejo, P.S., Mulroy, S.J., Newsam, C.J., Bontrager, E., Gronley, J.K. and Perry, J. (2009). Comparison of shoulder muscle electromyographic activity during standard manual wheelchair and push-rim activated power assisted wheelchair propulsion in persons with complete tetraplegia. Archives of Physical Medicine and Rehabilitation; 90:1904–1915.

Liu, H.Y., Pearlman, J. and Cooper, R. (2010). Evaluation of aluminium ultralight rigid wheelchairs versus other ultralight wheelchairs using ANSI/RESNA standards. Journal of Rehabilitation Research and Development; 47:441–455.

Lloyd, D.G., Alderaan, J. and Elliot, B.C. (2000).An upper limb kinematic model for the examination of Cricket bowling: a case study of Muttiah Muralitharan. Journal of Sports Sciences; 18(12):975-982.

Louis, N. and Gorce, P. (2010). Surface electromyography activity of upper limb muscle during wheelchair propulsion: Influence of wheelchair configuration. Clinical Biomechanics; 25:879–885.

Lovern, B. (2010). Functional Analysis of the Shoulder Complex in Healthy and Pathological Subjects using Three-Dimensional Motion Analysis Techniques. PhD thesis, Cardiff University, UK.

Magermans, D.J., Chadwick, E.K., Veeger, H.E.and van der Helm, F.C. (2005). Requirements for upper extremity motions during activities of daily living. Clinical Biomechanics; 20(6):591-9.

Mathworks, United States, 2016. *Signal Processing Toolbox Documentation* [online], available at: http://uk.mathworks.com/help/signal/index.html [Accessed: 29/02/2016].

Medina, G.I., Jesus, C.L., Ferreira, D.M., Pacheco, E.M., Beraldo, G.L., de Franca Urquiza, F. and Cliquet, A. (2015). Is sport practice a risk factor for shoulder injuries in tetraplegic individuals? Spinal Cord; 53(6):461-466.

Medola, F. O., Elui, V. M., Santana, Cda. S., and Fortulan, C. A. (2014). Aspects of manual wheelchair configuration affecting mobility: a review. Journal of Physical Therapy Science; 26(2):313-318.

Merlo, A. and Campanini, I. (2010). Technical Aspects of Surface Electromyography for Clinicians. The Open Rehabilitation Journal; 3:98-109.

Meskers, C.G.M., van der Helm, F.C.T., Rozendal, L.A. and Rozing, P.M. (1998). In vivo estimation of the glenohumeral joint rotation center from scapular bony landmarks by linear regression. Journal of Biomechanics; 31(1):93–96.

Microsoft, United States, 2016. Excel Spreadsheet Software. Available at: https://www.microsoft.com/en-gb/

Moon Y., Jayaraman C., Hsu I. M., Rice I. M., Hsiao-Wecksler E. T. and Sosnoff J. J. (2013). Variability of peak shoulder force during wheelchair propulsion in manual wheelchair users with and without shoulder pain. Clinical Biomechanics; 28:967–972.

Morrow, M.M.B., Hurd, W,J., Kaufman, K.R., and An, K.N. (2009). Upper-limb joint kinetics expression during wheelchair propulsion. Review article. Journal of Rehabilitation Research and Development; 46(7):939-944.

Mulroy, S.J., Gronley, JK, Newsam, C.J., and Perry, J. (1996). Electromyographic activity of shoulder muscles during wheelchair propulsion by paraplegic persons. Archives of Physical Medicine and Rehabilitation; 77(2):187-193.

Mulroy, S.J., Farrokhi, S., Newsam, C.J., and Perry, J. (2004). Effects of spinal cord injury level on the activity of shoulder muscles during wheelchair propulsion: An electromyographic study. Archives of Physical Medicine and Rehabilitation; 85:925-934.

Mulroy, S.J., Newsam, C.J., Gutierrez, D.D., Requejo, P., Gronley, J.K., Haubert, L.L., and Perry, J. (2005). Effect of fore-aft seat position on shoulder demands during wheelchair propulsion: part 1. A kinetic analysis. Journal of Spinal Cord Medicine; 28: 214-221.

Newsam, C.J., Rao, S. S., Mulroy, S.J., Gronley, J.K., Bontrager, E.L., and Perry, J. (1999). Three dimensional upper extremity motion during manual wheelchair propulsion in men with different levels of SCI. Gait & Posture; 10(3):223-232.

NSW Spinal Seating Service 2011, spinal seating module, agency for clinical innovation [online], available at: https://www.aci.health.nsw.gov.au/networks/spinal-cord-injury/spinal-seating/module-9 [Accessed: 11/12/2016].

Perdios, A., Sawatzky, B.J. and Sheel, A.W. (2007). Effects of camber on wheeling efficiency in the experienced and inexperienced wheelchair user. Journal of Rehabilitation Research and Development; 44(3): 459–466.

Perotto, A.O. (2011). Anatomical Guide for the Electromyographer. Fifth edition published by Charles C. Thomas, Springfield, USA.

Qi, L., Wakeling, J., Grange, S. and Ferguson-Pell, M. (2014). Patterns of Shoulder Muscle Coordination Vary Between Wheelchair Propulsion Techniques. IEEE Transactions on Neural Systems and Rehabilitation Engineering, Vol.22. No.3.

Qualysis Track Manager QTM user manual:[online], available at: http://www.qualisys.com/fy.chalmers.se/~f7xiz/TIF081C/QTM-usermanual.pdf. [Accessed: 18/11/2014].

Rao, S.S., Bontrager, E.L., Gronley, J.K., Newsam. C.J. and Perry, J. (1996).Three-Dimensional Kinematics of Wheelchair Propulsion. IEEE Transactions on Rehabilitation Engineering; 4:152-159.

Requejo, P.S., Lee, S.L., Mulroy, S.J., Lighthall-Haubert, L., Bontrager, E.L., Gronley, J.K. and Perry, J. (2008). Shoulder Muscular Demand During Lever-Activated Vs Pushrim Wheelchair Propulsion in Persons With Spinal Cord Injury. Journal of Spinal Cord Medicine; 31(5): 568–577.

Richter, W.M. (2001). The effect of seat position on manual wheelchair propulsion biomechanics: a quasi-static model-based approach. Medical Engineering & Physics; 23: 707–712.

Richter, W.M., Rodriguez, R., Woods, K.R., Karpinski, A.P. and Axelson, P.W. (2006). Reduced finger and wrist flexor activity during propulsion with a new flexible handrim. Archives of Physical Medicine and Rehabilitation; 87:1643–1647.

Richter, W.M., Rodriguez, R., Woods, K.R. and Axelson, P.W. (2007). Stroke pattern and handrim biomechanics for level and uphill wheelchair propulsion at self-selected speeds. Archives of Physical Medicine and Rehabilitation; 88:81–87.

Rodgers, M.M., Gayle, G.W., Figoni, S.F., Kobayashi, M., Lieh, J. and Glaser, R.M.(1994). Biomechanics of wheelchair propulsion during fatigue. Archives of Physical Medicine and Rehabilitation; 75(1):85-93.

Rose, W. (2014). Mathematics and Signal Processing for Biomechanics [online], available at: https://www.udel.edu/biology/rosewc/kaap686/notes/EMG%20analysis.pdf [Accessed: 29/02/2016].

Samuelsson, O.T., Kersti, A.M., Tropp, H., Nylander, E. and Gerdle, B. (2004). The effect of rear-wheel position on seating ergonomics and mobility efficiency in wheelchair users with spinal cord injuries: A pilot study. Journal of Rehabilitation Research and Development; 41(1):65-74.

Sanderson, David J., and H. J. Sommer III. (1985). Kinematic Features of Wheelchair Propulsion. Journal of Biomechanics; 18: 423-429.

Schantz, P., Bjorkman, P., Sandberg, M. and Andersson, E. (1999). Movement and muscles activity pattern in wheelchair ambulation by persons with para- and tetraplegia. Scandinavian Journal of Rehabilitation Medicine; 31:67-76.

Schenkman, M. and De Cartaya, V.R. (1987). Kinesiology of the Shoulder Complex. Journal of Orthopaedic and Sports Physical Therapy; 8:438-450.

Schmeler, M., and Buning, M. (1999). Manual Wheelchairs: Set-Up and Propulsion Biomechanics. [online], available at: http://www.wheelchairnet.org/WCN_WCU/SlideLectures/MS/5WCBiomech.pdf. [Accessed: 30/06/2016].

Schmidt, R., Disselhorst-Klug, C., Silny, J. and Rau, G. (1999). A Marker-based measurement procedure for unconstrained wrist and elbow motions. Journal of Biomechanics; 32(6):615-621.

Shimada, Sean D., Rick N. Robertson, Michael L. Bonninger, and Roray A. Cooper. (1998). Kinematic Characterization of Wheelchair Propulsion. Journal of Rehabilitation Research and Development; 35:210-218.

Soderberg, G. L. (1986). Kinesiology: Application to Pathological Motion. Baltimore: Williams & Wilkins, pp. 109–128.

Soderberg, G.L., Cook, T.M., Rider, S.C. and Stephenitc, B.L. (1991) Electromyographic activity of selected leg musculature in subjects with normal and chronically sprained ankles performing on a BAPS board. Physical Therapy; 71(7):514-22.

Slowik, J.S., Requejo, P.S, Mulroy, S.J. and Neptune, R.R. (2015). The influence of speed and grade on wheelchair propulsion hand pattern. Clinical Biomechanics; 30: 927–932.

Soltau, S., Slowik, J., Requejo, P., Mulroy, S., and Neptune, R. (2015). An investigation of bilateral symmetry during manual wheelchair propulsion. Frontiers in Bioengineering and Biotechnology, Volume 3, Article 86.

Sonenblum, S.E., Sprigle, S. and Lopez, R.A. (2012). Manual Wheelchair Use: Bouts of Mobility in Everyday Life. Rehabilitation Research and Practice, Volume 2012, Article ID 753165.

Stroud, L.A. (2011). In vivo Measurement and Objective Classification of Healthy, Injured and Pathological Subjects Using Three-dimensional Motion Analysis Techniques. PhD Thesis, Cardiff University, UK.

Terry, G.C. and Chopp, T.M. (2000). Functional anatomy of the shoulder. Journal of Athletic Training; 35:248–255.

Tsai, C.Y., Lin, C.J., Y.C., Huang, Lin, P.C. and Su, F.C. (2012). The effects of rear-wheel camber on the kinematics of upper extremity during wheelchair propulsion. BioMedical Engineering Online; 11:87.

Tubiana R., and Chamagne, P. (1988). Functional anatomy of the hand. Medical Problems of Performing Artists; 3:83–87.

Vanlandewijck,Y., Theisen, D., and Daly, D. (2001). Wheelchair Propulsion Biomechanics; Implications for Wheelchair Sports. Sports Med; 31(5): 339-367.

van der Woude, L.H., Veeger, D.J. and Rozendal, R.H. (1989). Seat height in handrim wheelchair propulsion. Journal of Rehabilitation Research and Development; 26: 31–50.

van der Helm, F.C.T. and Pronk, G.M. (1995). Three dimensional recording and description of motions of the shoulder mechanism. Journal of Biomechanical Engineering; 177:27–40.

van der Helm, F.C.T., (1996). A standardized protocol for motions recordings of the shoulder. In: Veeger, H.E.J., Van der Helm, F.C.T. and Rozing, P.M. (Eds.), Proceedings of the First Conference of the International Shoulder Group. Shaker Publishing, Maastricht, pp. 1–7.

van der Woude L.H., Veeger H.E., Dallmeijer A.J., Janssen T.W. and Rozendaal, L.A. (2001). Biomechanics and physiology in active manual wheelchair propulsion. Medical Engineering and Physics; 23(10):713-33.

van der Woude, L.H., Formanoy, M. and de Groot., S.(2003). Hand rim configuration: effects on physical strain and technique in unimpaired subjects. Medical Engineering and Physics; 25:765–774.

van der Woude, L.H., Bouw, A. and Van Wegen, J. (2009). Seat height: effects on submaximal hand rim wheelchair performance during spinal cord injury rehabilitation. Journal of Rehabilitation Medicine; 41:143–149.

van der Woude L.H., de Groot S., Janssen T.W. (2006). Manual wheelchairs: research and innovation in rehabilitation, sports, daily life and health. Medical Engineering and Physics; 28:905–915.

van Drongelen, S., van der Woude, L. H., Janssen, T. W., Angenot, E. L., Chadwick, E. K., and Veeger, DJ. H. (2005). Mechanical load on the upper extremity during wheelchair activities. Archives of Physical Medicine and Rehabilitation; 86, 1214-1220.

van Drongelen, S., van der Woude, L.H.V., Janssen, T.W.J., Angenot, E.L.D., Chadwick, E.K.J., and Veeger, H.E.J. (2006). Glenohumeral joint loading in tetraplegia during weight relief lifting: a simulation study. Clinical Biomechanics; 21(2):128–137.

Veeger, D., van der Woude, L.H. and Rozendal, R.H. (1989). The effect of rear wheel camber in manual wheelchair propulsion. Journal of Rehabilitation Research and Development; 26(2): 37–46.

Veeger, D., van der Woude L.H., Rozendal R.H. and Sargeant, T.J. (1989). Seat height in handrim wheelchair propulsion: a follow-up study. Journal of Rehabilitation Sciences; 26(4): 31–50.

Veeger, H.E., van der Woude, L.H. and Rozendal, R.H. (1992). Effect of handrim velocity on mechanical efficiency in wheelchair propulsion. Medicine and Science in Sports and Exercise; 24(1):100-107.

Veeger, H.E. and Rozendal, L.H.V. (1992). Load on the upper extremity in manual wheelchair propulsion. Journal of Electromyography and Kinesiology; 1:270-280.

Veeger, D., van der Linden, M.L. and Valent, L. (1996). The effect of wheelchair handrim tube diameter on propulsion efficiency and force application (tube diameter and efficiency in wheelchairs). IEEE Transactions on Rehabilitation Engineering; 4: 123–132.

Veeger, D., Rozendaal, L.A. and van der Woude, L.H. (2003). The push force pattern in manual wheelchair propulsion as a balance between cost and effect. Journal of Biomechanics; 36(2): 239–247.

Vegter, R., Lamoth, C.J., de Groot, S., Veeger, D., H.E.J. and der Woude, L.H.V. (2013). Variability in bimanual wheelchair propulsion: consistency of two instrumented wheels during handrim wheelchair propulsion on a motor driven treadmill. Journal of Neuro Engineering and Rehabilitation; 10:9.

Wang, X., (1996). Construction of arm kinematic linkage from external surface markers. In: Proceeding of the Fourth International Symposium on 3D Analysis of Human Movement, 1–3 July, 1996, Grenoble, France.

Wang, Yong Tai, Helga Deutsch, Martin Mose, Brad Hedrick, and Tim Millikan. (1995). Three-Dimensional Kinematics of Wheelchair Propulsion Across Racing Speeds. Adapted Physical Activity. Quarterly; 12: 78-89.

Wilson, A.B., Jr. (1986). Wheelchairs: A prescription guide. Charlottesville, VA, USA: Rehabilitation Press.

World Report on Disability and Rehabilitation. World Health Organization WHO, 2011, [online], available at: www.who.int/disabilities/world_report/2011/report.pdf. [Accessed on 03/07/2016].

Wu, G., van der Helm, F. C. T., Veeger, H. E. J., Makhsous, M., Van Roy, P., Anglin,C., and Buchholz, B. (2005). ISB recommendation on definitions of joint coordinate systems of various joints for reporting of human joint motion- Part II: Shoulder, elbow, wrist, and hand. Journal of Biomechanics, 38, 981-992.

Yang, Y.S., Koontz, A.M., Triolo, R.J., Mercer, J.L. and Boninger, M.L. (2006). Surface electromyography activity of trunk muscles during wheelchair propulsion. Clinical Biomechanics; 21:1032–1041.

Yang Y.S., Koontz, A.M., Yeh, S.J., Chang, J.J. (2012). Effect of backrest height on wheelchair propulsion biomechanics for level and uphill conditions. Archives of Physical Medicine and Rehabilitation; 93:654-659.

Zatsiorsky, V. (1998). Kinematics of human Motion. Champaign, IL, USA: Human Kinetics.

Zuckerman, J. D., and Matsea III, F. A. (1989). Biomechanics of the shoulder. In M. Nordin and V. H. Frankel (Eds). Biomechanics of the Musculoskeletal System. Philadelphia: Lea and Febiger, 225–248.

# Appendix A

## Volunteer Consent Form and Study Sheets

Dr Andrea Longman/Dr Helen Hodgson
Research Coordinator
Cardiff School of Bioscience
Cardiff University

### VOLUNTEER CONSENT FORM

**Assessment of joint function in healthy volunteers using three dimensional motion analysis techniques**

**Study Number:**

**Volunteer Identification Number for this trial:**

You DO NOT have to sign this document. Please DO NOT sign this document unless you fully understand it. If there is ANYTHING which you do not understand please do not hesitate to ask for a full explanation.

To confirm agreement with each of the statements below, please initial the box and amend as necessary:

1. I confirm that I have read and understand the information sheet dated 21/02/2013 (Version 7) for the above study and have had the opportunity to ask questions. ☐

2. I understand that my participation in the study is voluntary and that I am free to withdraw time, without giving any reason, and without my medical care or legal rights being affected. ☐

3. You may/may not contact me in the future to take part in other research projects or surveys. ☐

4. I do/do not agree for you to share anonymised information with external collaborators. ☐

5. I agree to take part in the above study. ☐

Version 7 21/02/2013

Name of Participant: _____

Signature: _____ Date: _____

I confirm that I have fully explained the experimental protocol and purpose of the study

Name of Researcher: _____

Signature: _____ Date: _____

Name of person taking consent: _____

(If different from researcher)

Signature: _____ Date: _____

*1 copy for the participant; 1 copy for the researcher*

Version 7 21/02/2013

# Shoulder Complex Functions
## Healthy Volunteers Study Sheet

**Date of Session:** _____

**Full Name:** _____

**Date of Birth:** _____ **M/F:** _____ **Dominant Side (Rt/Lt):** _____

**Address:** _____

**Telephone Number:** _____

**Anthropometric Measurements**

| | | |
|---|---|---|
| Height (cm) | | |
| Weight (kg) | | |
| Body Mass Index | | |
| Trunk Length (cm) | | |
| Trunk Width (cm) | | |
| Trunk Circumference (cm) | | |
| Upper Arm Length (cm) | Right | |
| | Left | |
| Upper Arm Flexed Circumference (cm) | Right | |
| | Left | |
| Upper Arm Extended Diameter (cm) | Right | |
| | Left | |
| Forearm Length (cm) | Right | |
| | Left | |
| Forearm Circumference (cm) | Right | |
| | Left | |
| Fully Extended Arm Length (cm) | Right | |
| | Left | |
| Hand Length | Right | |
| | Left | |
| Wrist Circumference (cm) | Right | |
| | Left | |

| Neutral Position Measurement | Filename | |
|---|---|---|
| with Skin fixed Markers | xx01 | |
| with Scapula Locator | xx02 | |

| Circumduction Measurement | Filename | |
|---|---|---|
| | xx03 | |

**Activities of Daily Living Measurements**

| Activity / Arm movement | Filename | |
|---|---|---|
| Reach opposite axilla | xx11 | |
| Reach opposite side of neck | xx12 | |
| Reach side and back of head | xx13 | |
| Brush opposite side of head | xx14 | |
| Clean upper back | xx15 | |
| Clean lower back | xx16 | |
| Eat with hand to mouth | xx17 | |
| Drink from mug | xx18 | |
| Answer phone | xx19 | |
| Reach as far forward as possible | xx20 | |
| Lift block to shoulder height | xx21 | |
| Lift block to head height | xx22 | |
| Cross body abduction | xx23 | |
| Internal rotation | xx24 | |
| External rotation | xx25 | |
| 90° abduction, external rotation | xx26 | |

**Physiological ROM Measurements**

| Skin Fixed Markers | | | | | | | | |
|---|---|---|---|---|---|---|---|---|
| *0° Plane of Elevation* (Abduction) | | | *Scapular Plane of Elevation* (Scaption) | | | *90° Plane of Elevation* (Flexion) | | |
| Arm Elevation | Filename | | Arm Elevation | Filename | | Arm Elevation | Filename | |
| 0° | xx31 | | 0° | xx51 | | 0° | xx71 | |
| 20° | xx32 | | 20° | xx52 | | 20° | xx72 | |
| 40° | xx33 | | 40° | xx53 | | 40° | xx73 | |
| 60° | xx34 | | 60° | xx54 | | 60° | xx74 | |
| 80° | xx35 | | 80° | xx55 | | 80° | xx75 | |
| 100° | xx36 | | 100° | xx56 | | 100° | xx76 | |
| 120° | xx37 | | 120° | xx57 | | 120° | xx77 | |
| 140° | xx38 | | 140° | xx58 | | 140° | xx78 | |
| 160° | xx39 | | 160° | xx59 | | 160° | xx79 | |
| 180° | xx40 | | 180° | xx60 | | 180° | xx80 | |
| Dynamic | xx41 | | Dynamic | xx61 | | Dynamic | xx81 | |
| Dynamic | xx42 | | Dynamic | xx62 | | Dynamic | xx82 | |

| Scapula Locator | | | | | | | | |
|---|---|---|---|---|---|---|---|---|
| *0° Plane of Elevation* (Abduction) | | | *Scapular Plane of Elevation* (Scaption) | | | *90° Plane of Elevation* (Flexion) | | |
| Arm Elevation | Filename | | Arm Elevation | Filename | | Arm Elevation | Filename | |
| 0° | xx91 | | 0° | xx111 | | 0° | xx131 | |
| 20° | xx92 | | 20° | xx112 | | 20° | xx132 | |
| 40° | xx93 | | 40° | xx113 | | 40° | xx133 | |
| 60° | xx94 | | 60° | xx114 | | 60° | xx134 | |
| 80° | xx95 | | 80° | xx115 | | 80° | xx135 | |
| 100° | xx96 | | 100° | xx116 | | 100° | xx136 | |
| 120° | xx97 | | 120° | xx117 | | 120° | xx137 | |
| 140° | xx98 | | 140° | xx118 | | 140° | xx138 | |
| 160° | xx99 | | 160° | xx119 | | 160° | xx139 | |
| 180° | xx100 | | 180° | xx120 | | 180° | xx140 | |
| Dynamic | xx101 | | Dynamic | xx121 | | Dynamic | xx141 | |
| Dynamic | xx102 | | Dynamic | xx122 | | Dynamic | xx142 | |

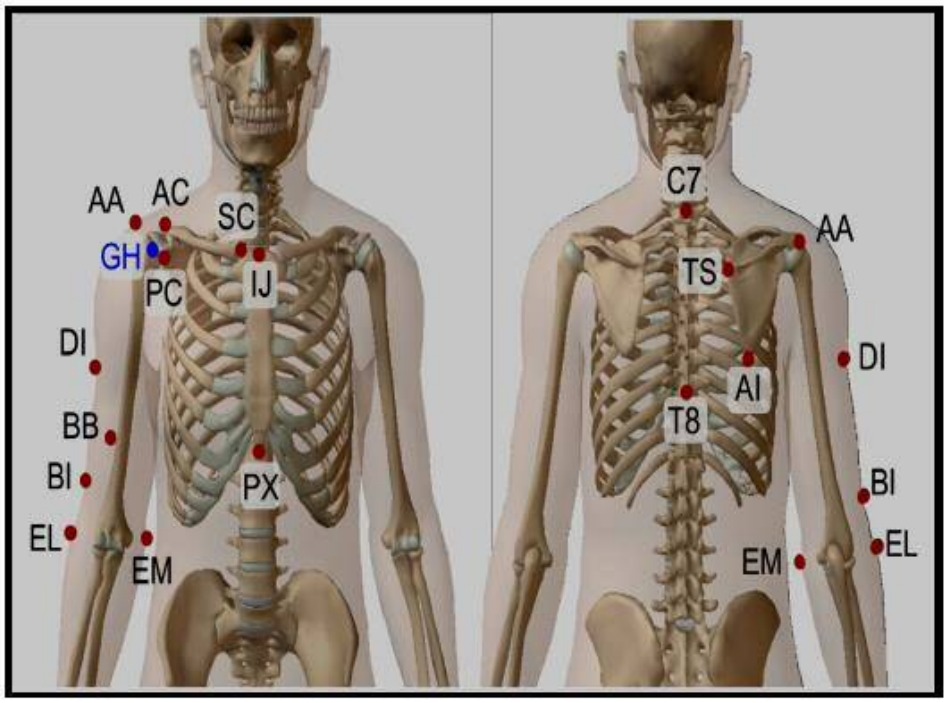


**Researcher on the computer:** _____

**Researcher palpating landmarks:** _____

# Manual Wheelchair Propulsion
## Healthy Volunteers Study Sheet

**Date of Session:** _____

**Full Name:** _____

**Date of Birth:** _____ **M/F:** _____ **Dominant Side (Rt/Lt):** _____

**Address:** _____

**Telephone Number:** _____

**Anthropometric Measurements**

| | | |
|---|---|---|
| Height (cm) | | |
| Weight (kg) | | |
| Body Mass Index | | |
| Trunk Length (cm) | | |
| Trunk Width (cm) | | |
| Trunk Circumference (cm) | | |
| Upper Arm Length (cm) | Right | |
| | Left | |
| Upper Arm Flexed Circumference (cm) | Right | |
| | Left | |
| Upper Arm Extended Diameter (cm) | Right | |
| | Left | |
| Forearm Length (cm) | Right | |
| | Left | |
| Forearm Circumference (cm) | Right | |
| | Left | |
| Fully Extended Arm Length (cm) | Right | |
| | Left | |
| Hand Length | Right | |
| | Left | |
| Wrist Circumference (cm) | Right | |
| | Left | |

| Neutral Position Measurement | |
|---|---|

**Physiological ROM Measurements**

| | |
|---|---|
| Shoulder Flexion/Extension | |
| Shoulder Abduction/Adduction | |
| Shoulder Internal/External Rotation | |
| Elbow Flexion/Extension | |
| Elbow Pronation/Supination | |
| Wrist Flexion/Extension | |
| Wrist Ulnar/Radial Deviation | |
| Wrist Pronation/Supination | |

**Wheelchair Mobility Tasks**

| | | |
|---|---|---|
| Manual Propulsion | Trial 1 | |
| | Trial 2 | |
| | Trial 3 | |
| | Trial 4 | |
| | Trial 5 | |
| Starting Up | Trial 1 | |
| | Trial 2 | |
| | Trial 3 | |
| Stopping | Trial 1 | |
| | Trial 2 | |
| | Trial 3 | |

**Researcher on the computer:** _____

**Researcher palpating landmarks:** _____

## Physical Activity Readiness Questionnaire (PAR-Q)

***PAR-Q*** has been designed to identify the small number of adults for whom physical activity might be inappropriate or those who should have medical advice concerning the type of activity most suitable for them. For most people, physical activity should not pose any problems or hazard.

**Full Name:** _____ **Date of Birth:** _____

**Address:** _____ **Telephone Number**: _____

Common sense is your best guide in answering these few questions. Please read the carefully and check **YES** or **NO** opposite the question if it applies to you. If yes, please explain.

| | ***Question*** | ***YES*** | ***NO*** |
|---|---|---|---|
| **1** | *Has your doctor ever said you have heart trouble? If yes, please state:* | | |
| **2** | *Do you frequently have pains in your heart and chest? If yes, please state:* | | |
| **3** | *Do you often feel faint or have spells of severe dizziness? If yes, please state:* | | |
| **4** | *Has a doctor ever said your blood pressure was too high? If yes, please state:* | | |
| **5** | *Has your doctor ever told you that you have a bone or joint problem(s), such as arthritis that has been aggravated by exercise, or might be made worse with exercise? If yes, please state:* | | |
| **6** | *Is there a good physical reason, not mentioned here, why you should not follow an activity program even if you wanted to? If yes, please state:* | | |
| **7** | *Are you or have you been pregnant in the last 6 months?* | | |
| **8** | *Do you suffer from any problems of the lower back, i.e., chronic pain, or numbness? If yes, please state:* | | |
| **9** | *Are you currently taking any medications? If YES, please specify.* | | |
| **10** | *Do you currently have a disability or a communicable disease? If yes, please state:* | | |

If you answered **NO** to all questions above, it gives a general indication that you may participate in physical and aerobic fitness activities. The fact that you answered **NO** to the above questions, is no guarantee that you will have a normal response to exercise. If you answered **YES** to any of the above questions, then you may need written permission from a physician before participating in physical and aerobic fitness activities.

| _____ | _____ | _____ |
|---|---|---|
| ***Participant's Name*** | ***Signature*** | ***Date*** |
| _____ | _____ | _____ |
| ***Researcher's Name*** | ***Signature*** | ***Date*** |

# Appendix (B)

***Experimental Motion Analysis Protocol of Manual Wheelchair Propulsion***

The experimental protocol of this study was highly structured as a step-by-step instructional procedure for performing bilateral kinematic and unilateral sEMG analysis simultaneously, healthy individuals during manual wheelchair mobility, see Figure (B.1). All of the healthy volunteers recruited per this study were non-experienced wheelchair users with no current shoulder pain or previous history of any injury related to the upper limbs.

It is highly important to know the multi aspects of this exhaustive protocol which requires a comprehensive analysis and systematic evaluation of the motion of all upper body segments, and therefore tends to be more time consuming and laborious under laboratory conditions.

Prior to testing, a Health and Safety induction (including risk assessment of the lab) was carried out and ethical approval had to be obtained from the Ethical Review Committee of Cardiff School of Engineering. The healthy volunteers were then acquired, informed of the protocol via email and given their own pre-arranged time and date for testing.

Before volunteers' arrival, all of the hypoallergenic adhesive tape was applied on to the retro-reflective markers and surface EMG electrodes. These electrodes should be put on charge at least 2 hours before starting the protocol so that they had sufficient power to complete the testing. The static calibration was performed using the L-Frame and the T-Wand (as explained earlier), so that the calibrated volume of measurement is defined by QTM. All of this work was done so that the volunteer's time in the lab could be utilised.

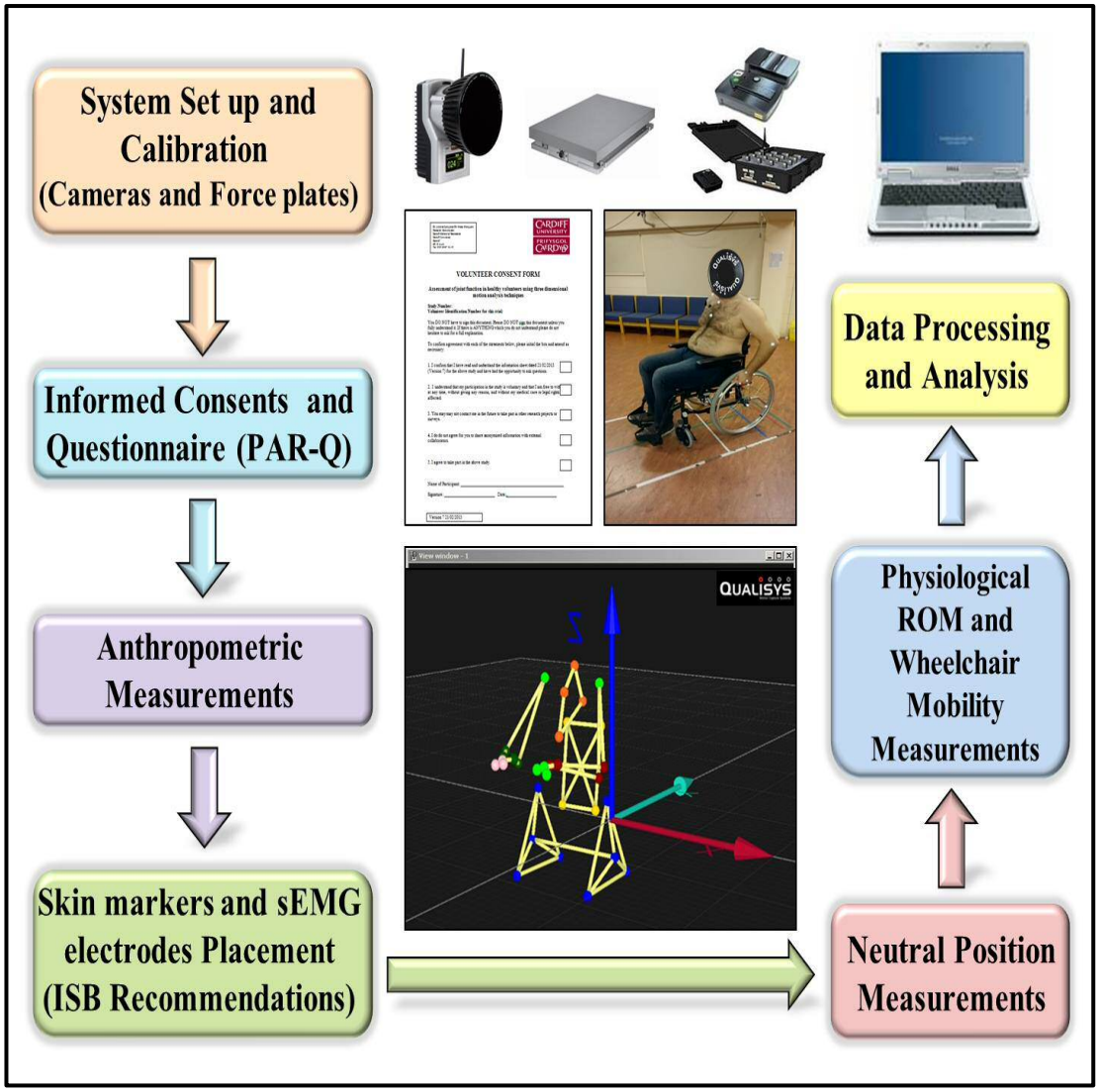


**Figure (B.1):** Experimental protocol of human motion analysis for manual wheelchair mobility performed at Cardiff University.

Once they arrived, the volunteer was informed of the protocol involved with the study. They were then instructed to read through the patient consent forms and the patient information sheets in order to give them a clear idea of what the analysis consisted of. All of the volunteers were also notified that at any point they felt uncomfortable or unwilling to continue, they could ask for the trial to be ended and leave without reason.

The below table shows the time required to perform this experimental protocol for single participant including the adjustment of single wheelchair configuration under laboratory condition.

| Task Order No. | Task Description | Estimated Duration (minutes) |
|---|---|---|
| **1** | Perform the required anthropometric measurements on the volunteer once they have completed filling in the consent and patient information forms. | 5 |
| **2** | Ask the volunteer to remove their shirt and perform with them, a brief upper body stretching routine. Prepare the sites for the surface EMG electrodes on the volunteer by shaving the skin, if necessary. Then sanitizer and abrasive cream will be used to clean the site. Electrode gel is then used to ensure good conduction between the skin surrounding the muscles of interest and the electrodes. (Note: Sanitary Gloves should be worn during this process and any razors used disposed of in the Biological Waste bin). | 15 |
| **3** | Attach the surface electrodes onto the volunteer muscle sites, making sure that the arrow on the surface of the electrode is in the direction of the muscle fibers. | 15 |
| **4** | Turn each of the electrodes on and ensure that the data recording process on the computer is running. Ask the volunteer to take a seat. Begin recording the data from the electrodes and perform the shoulder standardisation tests to induce the Maximum Voluntary Contraction (MVC) for each of the muscle groups of interest. Once the desired test position has been reached and the observer is ready, there will be a 1 second latency period (preparing for maximum effort and adjusting to resistance), a 3 second maximum effort and a 1 second recovery/return to neutral position. | 25 |
| **5** | Attach the 20 reflective markers onto the volunteer's skin bony landmarks using the ISB (International Society of Biomechanics) recommendations. | 20 |
| **6** | Perform static position calibration with the wheelchair facing in the direction of travel down the track, and the volunteer's hands on their knees, to define the marker trajectory locations in the local coordinate system. | 10 |
| **7** | Allow each volunteer 5-10 minutes to use the wheelchair inside the lab so they can familiarise themselves with it and determine their own steady self-speed, stroke pace and propulsion technique. | 10 |
| **8** | Ask the volunteer to position themselves aligned at the end of the track. Then ask them to propel themselves along the track at a self-selected speed and a self-selected stroke rate. (Note: Make sure that the markers on the wheel rim are aligned in the static calibration position before the volunteer performs the task). Repeat this dynamic task 5 times. | 15 |
| **9** | Now, record the Starting strokes. Ask the volunteer to position himself or herself about one third of the way down the track. Again aligning the wheels in the static calibration position, ask the volunteer to propel down to the end of the track. Repeat this dynamic task 5 times. | 15 |
| **10** | Finally, record the Stopping stroke/movement. Ask the volunteer to get into position at the start of the track. After aligning the wheels as before, ask the volunteer to propel down the track and stop roughly two thirds of the way down the track. Repeat this dynamic task 5 times. | 15 |

| | | |
|---|---|---|
| **11** | First, put the wheelchair on its back side for easy accessibility to the underside of the wheelchair. To release the *Quick Release* axles, press in the detent pin on the centre of the wheel and slowly pull the wheel off of the frame, Invacare 2009). | <5 |
| **12** | Using the Allen Key (5/32" Long Arm) and the Flat Jaw Pliers simultaneously to secure the mounting screws, remove the 5 mounting screws securing each side of the axle mount. | 10 |
| **13** | Move the axle mount by the required number of slots on the wheelchair frame (3 cm between each) to achieve the desired position. | <5 |
| **14** | Re-attach the mounting screws to fix the axle mount in its new position. Then reattach the wheel by holding the detent pin down, and inserting the wheel back into the axle mount. | 10 |
| **15** | Repeat this for the other wheel. | 20 |
| **16** | Loosen the two mounting screws that secure the castor assembly to the wheelchair frame. It is not necessary to remove the mounting screws. | <5 |
| **17** | Rotate the castor assembly to the desired angle. Both castors should be set at the same angle. | <5 |
| **18** | Tighten the mounting screws that secure the castor assembly to the wheelchair frame. | <5 |
| **19** | Repeat this for the other castor. | 5 |
| ***Total Estimated Time in minutes*** | | **200** |

During the testing, at any point where a reflective marker fell off of the volunteer or the wheelchair, the static calibration had to be performed again. This was to eliminate the errors associated with the markers not being put back in their original position. When this occurred, the marker location was noted and was re-applied. Following testing, the data file needed to be modified. The 3D marker trajectories were to be identified, labelled and any gaps filled, when necessary, with their respective bony landmarks and location on the wheelchair. Each sEMG electrode and their associated data had a dedicated channel number (64 channels in total), which meant the correct channels needed to be isolated to access the data for the muscles of interest. This allowed the muscles that were active, to be identified throughout the push and recovery phases of the wheelchair propulsion cycle. Also, the capture period was trimmed down to an appropriate range as to remove the first accelerating and the last decelerating strokes.

The analysis from the QTM software was then performed using rigid body analysis and 6 DOF calculations. Also, the EMG signal were processed, filtered and the signal normalised to the MVC represent the EMG signals for each of the muscles analysed.

Moreover, the spatio-temporal parameters of the manual wheelchair propulsion were determined from the propulsion cycle of each volunteer based on when the push and recovery phases began. The push and recovery phase initiation was determined by the contact of the volunteer's hand on the hand-rim. When the hand initially made contact with the hand-rim, the push phase had begun, and as soon as the hand-rim was released the recovery phase had begun. Along with this, the EMG voltage plot was used to distinguish between the push and recovery phases. The EMG analysis was mainly used to see which muscles are activated to initiate the two phases and which are the prime movers during the phases. After the first trials were performed using the standard wheelchair manufacturer's specifications (Invacare, 2011), the next set of trials were performed by the same volunteers as before, with changes as horizontal displacement in the rear wheel axle position and as vertical displacement in the wheelchair's seat-to-floor distance. These adjustments were made using the instructions mentioned in Invacare (2009). The trials were performed with all of the volunteers with one wheelchair configuration and then they were called back again to perform with the other configurations.

As explained above, each volunteer had about 90 measures over his experimental motion analysis were sessions performed inside the lab. Therefore, the amount of work required to collect, process and analyse these data under laboratory condition is a challenging as it takes a long time and potential. It was justified that the time duration required for achieving the objectives of this study by around 18 months, from the participant's recruitment till the statistical analysis, plus 12 months prior to that for exploring the different approaches and testing different protocols used previously at Cardiff University and elsewhere. Then there was a period of six months for designing this protocol, processing pipeline and full operating procedure from when the volunteer enters the lab to when we have the final data set from them. All that cannot be easily appreciated by people who are outside the experimental field of biomechanics of human motion analysis.

# Appendix C

## Upper Body Anthropometric Measurements

Anthropometric measurement provides the data used in the indirect appraisal of body composition. Girths and skin folds can be entered into a number of equations to estimate the body density, total body fat and the overlying subcutaneous fat. Moreover, trunk and limb girths provide estimates of relative muscle mass.

There are many advantages beyond using anthropometric measurement as it is a non-invasive technique that is relatively easy to carry out with a modest amount of training. Also, most techniques utilize inexpensive equipment that is generally portable.

**Measuring upper limb lengths**

Length of limb segments can be measured either directly between two skeletal landmarks or as vertical distance between a constant flat surface (as the floor) and a skeletal landmark. This latter is preferred as projected lengths, which through subtraction gives a number of derived segment lengths.

The use of tape measurement is the most valid tool for measuring limb length (long measurement). Upper limb length discrepancy affects the cosmetic appearance, while lower limb length discrepancy affects both cosmetic appearance and function. Tape measurement is also used for round measurement or the contour of the:

- Muscle to detect atrophy or hypertrophy.

- Joint to determine swelling.

- Chest to determine its mobility.

***(1) Whole upper limb length***

Measurement is taken from most superior lateral point of acromion process (acromial landmark) to the lower and lateral border of styloid process of radius (radial landmark). The arm is positioned in the anatomical position, relaxed at the side of the subject.

***(2) Segmental measurement***

- *Upper arm length:* With arm flexed at 90º, so that ulnar surface of forearm and hand are horizontal and palms facing medially with fingers extended, measurement is taken from acromial landmark to the posterior surface of olecranon process of ulna.

- *Forearm length:* It is the distance from the head of radius (upper radial landmark) to the most distal point of the styloid process of radius (or styloin).

- *Hand length:* With hand extended and the palm rested in the direction of the longitudinal axis of forearm, measurement is taken from styloid process at base of thumb to the tip of middle finger.

***(3) Upper limb Round (girth or circumference) measurement***

This length is looped around the part to be measured and held so that the printed notches on the scale are next to each other (the stub end is pulled superior to the easing end). As the tension applied to the tape varies, skin surfaces should not be compressed or an observable space between the skin and the tape left. Tapes with spring easing are not recommended. Measurements should be recorded to the nearest 0.1 cm.

- *Upper arm girth:* It is also known as arm circumference, upper arm circumference, biceps circumference or relaxed arm girth. The tape is applied around the mid-upper arm.

- *Forearm girth:* This measurement is the maximal girth of the forearm. It is taken around the upper third of forearm.

- *Wrist girth:* It is the perimeter of the wrist taken distal to the styloid process of the radius and ulna.

- *Trunk girth:* The chest should be bare and the subject stands in a natural erect posture. Measurements are taken from under the axilla and around the chest, passing by the xyphoid process either just below the axillary fold or at the level of the nipple or at the xyphoid process itself.

For all measurements the measuring band should always be held as straight as possible and should not be bended around body segments. The shown below figures (C.1-9) illustrate description of the upper body segments measurements.

**Figure (C.1)**: Trunk Width - Measure from middle of the collarbone to rotation axis of the shoulder/upper arm.(Modified from Karlsruhe institute of technology, Body Human Motion Database 2016).

**Figure (C.2)**: Thorax Length - Measure from middle of the collarbone to central projection of last rip (not directly to the last rip, to an imaginary line from the last rip below the collarbone).(Modified from Karlsruhe institute of technology, Body Human Motion Database 2016).

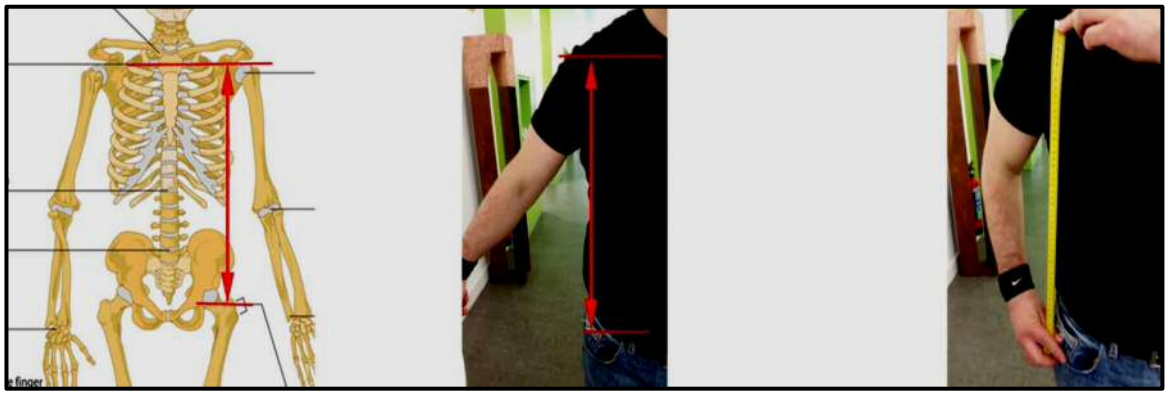

**Figure (C.3)**: Trunk Length - Measure from hip bone to rotation axis of the shoulder/upper arm.(Modified from Karlsruhe institute of technology, Body Human Motion Database 2016).

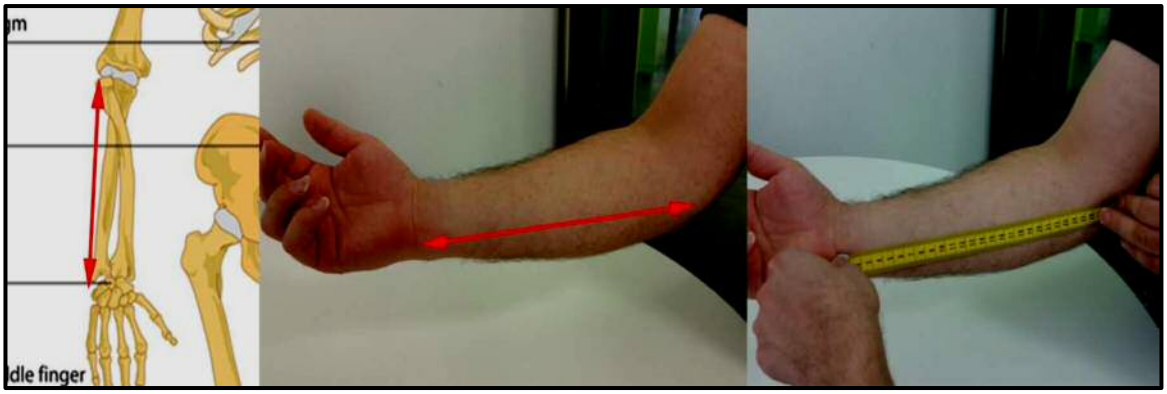

**Figure (C.4)**: Forearm Length - Measure from elbow (line between elbow and bend) to hand wrist joint.(Modified from Karlsruhe institute of technology, Body Human Motion Database 2016).

**Figure (C.5)**: Elbow Width - Measure the elbow width, the measuring tape has to be hold straight.(Modified from Karlsruhe institute of technology, Body Human Motion Database 2016).

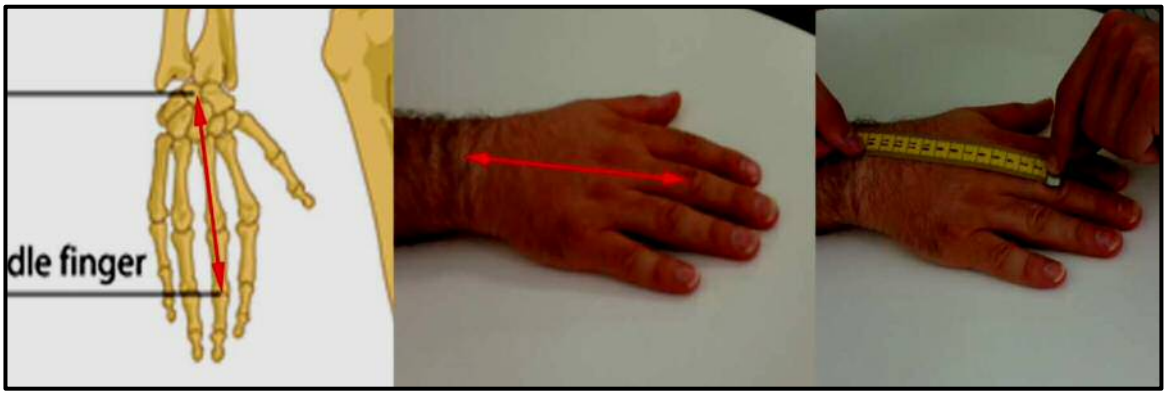


**Figure (C.6)**: Hand Length - Measure from hand wrist to second knuckle of the middle finger.(Modified from Karlsruhe institute of technology, Body Human Motion Database 2016).

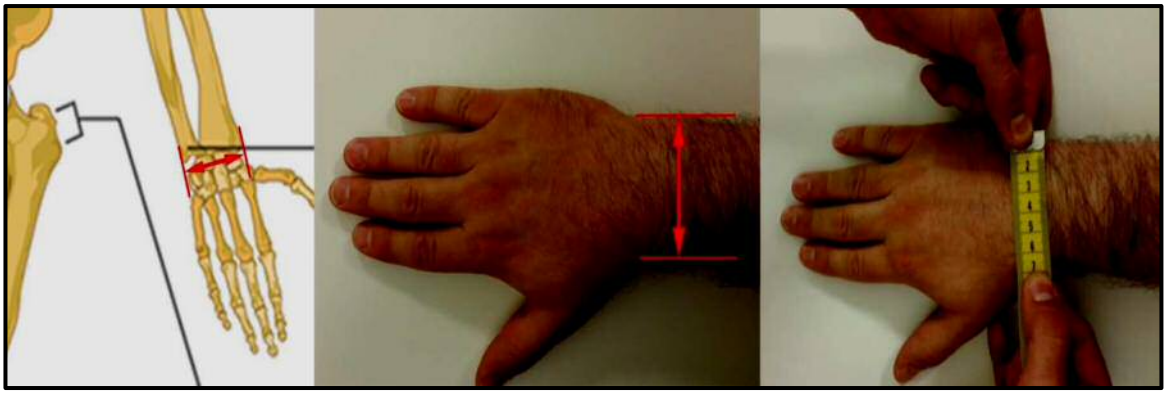

**Figure (C.7)**: Wrist Width - Measure the wrist width, the measuring tape has to be hold straight.(Modified from Karlsruhe institute of technology, Body Human Motion Database 2016).

**Figure (C.8)**: Upper Arm Length - Measure from rotation axis of shoulder to rotation axis of elbow (line between elbow and bend).(Modified from Karlsruhe institute of technology, Body Human Motion Database 2016).

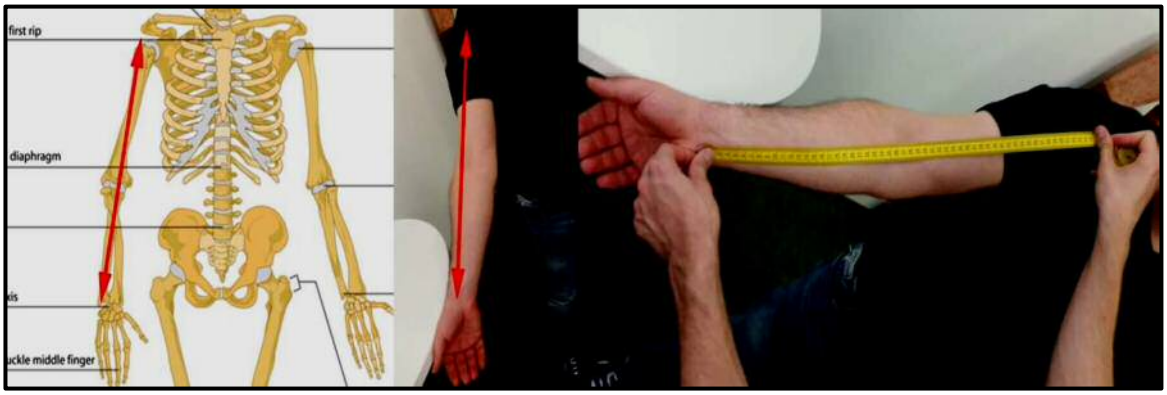


**Figure (C.9)**: Total Arm - Measure from rotation axis of shoulder to hand wrist.(Modified from Karlsruhe institute of technology, Body Human Motion Database 2016).

# Appendix D

## Manual Wheelchair Measuring Guide

Wheelchair measurements are critical for everyday wheelchair users to have a comfortable and functional piece of equipment which will meet all their needs and provide for the best possible results. This guide is by no means etched in stone and often there are circumstances which require ignoring the basic rules of thumb for measuring a wheelchair however this guide is applicable to 90% of the wheelchair user population, see Figure (3.11).

**(1)** ***Seat Depth***: It is determined by measuring from the backside to the inside of the knee, then subtract approximately two inches. Some prefer more leg overhang to make room for their hand when lifting their leg. The longer the seat depth of the wheelchair, the more stable the user will be and their weight will be distributed over a larger area which in turn will reduce sitting discomfort.

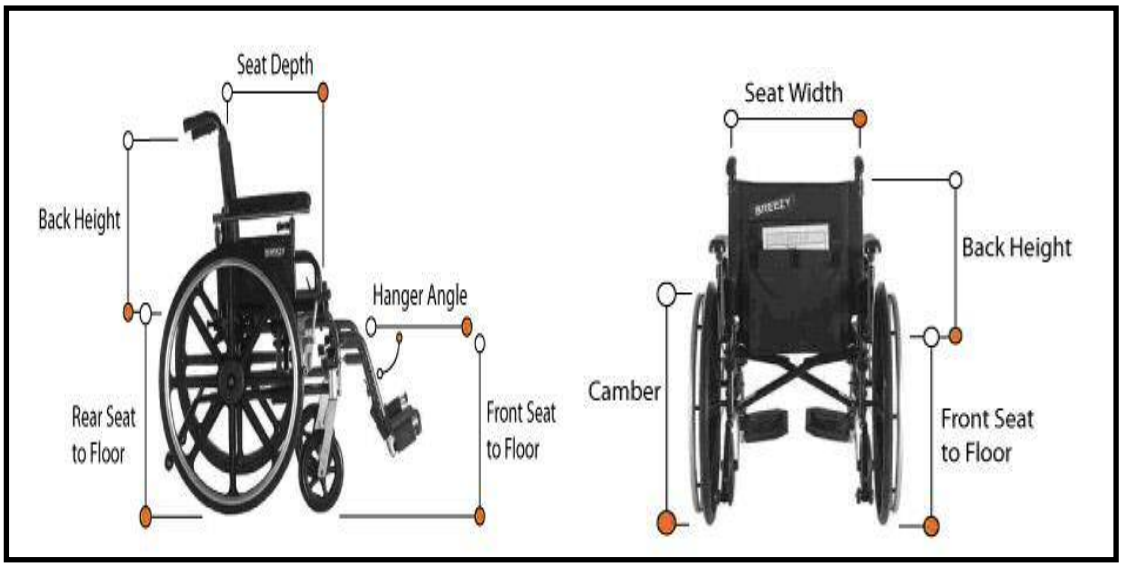


**Figure (D.1)**: Manual wheelchair measurements, (www.medicalsupplydepot.com).

**(2)** ***Backrest Height***: It is determined by measuring from the bottom of the seat base to the top of the wheelchair back. Backrest height depends on the degree of user disability and level of support required. Users who require more back support should opt for a higher back height but if they propel their wheelchair with their arms too high a back height will impede the range of motion in their shoulders which will reduce the efficiency of their pushing their chair.

**(3)*Rear Seat to Floor***: It is determined by measuring from the rear edge of the seat straight down to the ground. This determines the rearward slope angle (known as "dump" or "squeeze") of the wheelchair seat. By having a lower rear seat height to front seat height gives the chair 'seat bucket' meaning a sloping seat towards the rear. Seat height is more about function than comfort. Ideally the seat height will put the users at a height that will allow them to perform everyday tasks.

**(4) *Hanger Angle***: It determines how far the toes extend away from the body, measured from the horizontal. A tighter angle allows the wheelchair to turn around in less space. The preferred angle will depend on the knee's ability to bend.

**(5) *Seat Width***: Seat width is usually the first measurement determined when fitting a person for a wheelchair. It is determined by measuring from the outside to the outside of the seat frame tubes across the width of the seat. This should be measured across the widest point of the body from knee to hip, and then add approximately an inch to ensure room to move. Consider that bulkier clothing (such as a winter coat) will require additional width to maintain equivalent space.

**(6) *Wheel Camber***: This is the degree of angle on the rear wheels. Higher camber improves stability and agility, but also limits ability to pass through narrow spaces. A typical daily wheelchair use three degrees of camber. However, camber also increases the overall width of the wheelchair. As a rough guide, 2 degrees of camber increases the overall width by 1 inch.

**(7) *Front Seat to Floor***: It is determined by measuring from the front edge of the seat straight down to the ground.

**(8) *Footrest Width***: It is determined by measuring from the inside of each legrest tubing the distance or desired distance between legrests.

**(9) *Centre of Gravity***: It is determined by measuring from the front of the backrest post to the centre of the rear wheel axle. The larger the measurement, the more 'tippy' the wheelchair will be. The more 'tippy' the chair, the easier to turn on the spot and quicker to maneuver but better balance is required as more likely for the chair to tip backwards especially if not using anti-tipping aids.

**(10)** ***Seat to Footrest Length***: As with seat width and depth, footrest length determination begins with the user's seat height. It is determined by measuring from the edge of the seat to the top rear of the footrest. It is also known as "knee to heel length" that can be measured from the back of the user's knee to the bottom of the sole of the shoe.

**(11)** ***Backrest Angle***: It is determined by measuring the angle of the backrest post to the ground. 90 degrees will be perpendicular to the ground, to approximate the angle from the backrest post to the seat, subtract two degrees from measurement for every 0.5 inch of dump.

# Appendix E

## Summary of the Most Relevant Studies with Biomechanics of Manual Wheelchair Propulsion

| *Reference* | *Research Questions and Context* | *Methods* | *Impact* |
|---|---|---|---|
| **Beekman et al. 1999** | To compare wheelchair propulsion in ultralight and standard wheelchairs in people with different levels of spinal cord injury. | (n=74) subjects with spinal cord injury resulting in motor loss (n=30 with tetraplegia and n=44 with paraplegia). Standard and ultralight wheelchair around an outdoor track at self-selected speeds. Data collected at four predetermined intervals. Speed, distance travelled, and oxygen cost ($VO_2$ mL/kg/m) compared by wheelchair, group, and over time. | Ultralight wheelchair improved efficiency of propulsion: speed and distance travelled were greater for both subject groups. Paraplegic subjects propelled faster and farther with less $VO_2$. Tetraplegic subjects (especially at the C6), are limited in their ability to propel a wheelchair. |
| **Boninger, Cooper, Knootz 2000** | To determine the effect of rear axle position relative to the shoulder on pushrim biomechanics. | (n=40) subjects with paraplegia who use manual wheelchairs for mobility propelled their own wheelchairs on a dynamometer at two different steady-state speeds, from a dead stop to maximum speed. Bilateral biomechanics data obtained using a force- and moment-sensing pushrim and a motion analysis system. | Specific biomechanical parameters known to correlate with median nerve injuries found to be related to axle position relative to shoulder. Providing wheelchair users with adjustable axle position and fitting the user to the wheelchair can improve propulsion biomechanics and likely reduce the risk of injury. |
| **Boninger, Cooper, Knootz 2002** | To classify stroke patterns of manual wheelchair users and to determine if different patterns of propulsion lead to different biomechanics. | (n=38) subjects with paraplegia who use manual wheelchairs for mobility propelled their own wheelchair on a dynamometer at two different steady state speeds.<br>Bilateral biomechanical data were obtained by using a force and moment sensing pushrim and a motion analysis system. | Semicircular propulsion motion displayed characteristics consistent with reduced repetition and more efficient propulsion. Clinicians should consider training individuals in this propulsion style which may reduce trauma to the upper extremities. |

| | | | |
|---|---|---|---|
| **Collinger et al. 2008** | To present a descriptive analysis and comparison of shoulder kinetics and kinematics during wheelchair propulsion at multiple speeds (self-selected and steady-state target speeds) for a large group of manual wheelchair users with paraplegia while also investigating the effect of pain and subject demographics on propulsion. | Multi-site study (3 labs). (n=61) subjects with paraplegia who use a manual wheelchair for mobility, propelled their own wheelchairs on a dynamometer at 3 speeds (self-selected, 0.9 m/s, 1.8 m/s) while kinetic/kinematic data were recorded. | Significant increases in shoulder joint loading with increased propulsion velocity.<br>Body weight was primary demographic variable affecting shoulder forces, whereas pain did not affect biomechanics.<br>Peak shoulder joint loading occurs with the arm extended and internally rotated, which may leave the shoulder at risk for injury. |
| **Collinger et al. 2010** | To investigate acute ultrasound changes of biceps and supraspinatus tendon appearance after an intense wheelchair propulsion task, and how these changes relate to demographic and biomechanical risk factors. | (n=60) manual wheelchair users were recruited (18 and 65 years), at least 1 year post-injury with no progressive disabilities. Quantitative ultrasound (QUS) measures of biceps and supraspinatus tendon appearance, stroke frequency, resultant force, tendinopathy score, and duration of wheelchair use. | Subjects with tendinopathy or a longer duration of wheelchair use were more likely to have a darker, diffuse tendon appearance immediately after propulsion. Supraspinatus tendon appearance after propulsion was only significantly predicted by baseline QUS measures. |
| **Cowan et al. 2009** | To investigate the influence of the position of the rear wheels' axle and the use of accessories on the activity of upper limb muscles during manual wheelchair propulsion. | EMG signals of the biceps, triceps, anterior deltoids and pectoralis major were collected for (n=11) able-bodied subjects in a wheelchair propulsion protocol with four different wheelchair configurations (differing in axle position and the use of accessories) on sprint and slalom courses. | With accessories, moving the axle forward led to decreased activity of all muscles in sprint (significant differences in triceps, anterior deltoids and biceps) and slalom (significant difference in anterior deltoids and biceps). However, without accessories, no difference was found related to axle position. Changes in configuration influence manual wheelchair propulsion ergonomics. Reducing biomechanical loads may benefit mobility, independence and social participation. |

| | | | |
|---|---|---|---|
| **Desroches et al. 2008** | To determine the relationship between the resultant force at the pushrim and the net shoulder joint moments during manual wheelchair propulsion in elderly persons. | Kinematic and kinetic data collected during manual wheelchair propulsion at a speed between 0.96 m/sec and 1.01m/sec for 10 seconds and at a power output around 22.4W on a wheelchair ergometer. Net shoulder joint moments computed using an inverse dynamic model. Mechanical use of the forces at pushrim and mechanical fraction of effective force measured during propulsion. | Suggest that because the resultant force at the pushrim has a greater tangential component and a greater proportion of the maximal voluntary force, most of the net moments around the shoulder are higher. Thus the optimal propelling techniques, from a mechanical point of view (i.e, tangential), may not be advantageous for manual wheelchair users. |
| **Desroches et al. 2010** | To estimate upper limb joints loads during manual wheelchair propulsion. | (n=9) spinal cord injured subjects with reflective markers propelled a wheelchair with an instrumented wheel. Inverse dynamics were interpreted using joint coordinate systems, 3D joint power and the 3D angle between the joint moment and joint angular velocity vectors at the three upper limb joints. | Wrist and elbow joints are mainly in a stabilization configuration (angle close to 90º) with a combination of extension and ulnar deviation moments and an adduction moment respectively. The shoulder is in a propulsion configuration, but close to stabilization (angle hardly below 60º) with a combination of flexion and internal rotation moments. |
| **Dubowsky et al. 2008** | To simultaneously quantify and compare the push rim forces, upper-limb kinematics, and shoulder EMG during wheelchair propulsion between able-bodied participants and individuals with paraplegia. It was hypothesize that an integrated, simultaneous data collection and interpretation will allow for the comparison of differences in wheelchair propulsion between able-bodied individuals and persons with paraplegia. | (n=5) subjects with paraplegia and (n=6) able-bodied subjects with reflective markers and surface electrodes on the right upper arm, with force-sensing pushrim (SmartWheel's) attached to the subject's wheelchair. Kinematics, EMG, and kinetics data collection for ten push strokes. Wheelchair secured on a dynamometer. | Individuals with paraplegia use a greater percentage of their posterior deltoids, biceps, and triceps in relation to maximal voluntary contraction. Muscles act as joint stabilizers, and recruitment determines magnitude and direction of the resultant joint force. Differences in muscle forces are responsible for increasing shoulder joint forces, which *may* in turn cause shoulder pain or pathology. |

| | | | |
|---|---|---|---|
| **Finley et al. 2004** | The biomechanics of wheelchair propulsion in individuals with and without upper limb impairment | Instrumented wheelchair ergometer and 3D motion analysis system to collect joint kinematic and temporal data, as well as hand rim and joint kinetics, in (n=47) manual wheelchair users (15 with upper-limb impairment and 32 without upper-limb impairment). | The group with upper-limb impairment propelled with a higher stroke frequency and reduced hand-rim contact time, and smaller peak joint angles and joint excursion of the wrist, elbow, and shoulder during the contact phase. They propelled with reduced power output, hand-rim propulsive and resultant forces, moments and joint compressive forces. These kinematic/kinetic strategies might be a mechanism to allow MWCUs with upper-limb impairment to remain independent.<br>Reduced joint excursion and magnitude of forces may protect them from the development of secondary upper-limb pathologies. |
| **Freixes et al. 2010** | To assess the changes in speed, acceleration, stroke frequency, and shoulder range of motion (ROM) associated with different wheelchair axle positions in people with chronic cervical (C6) tetraplegia. | Measure the speed, acceleration, stroke frequency, and shoulder ROM in four different axle positions in eight subjects with C6 SCI. | The up and forward axle position results were in an increase of speed and acceleration, with a higher stroke frequency and a decreased shoulder ROM. In addition, The down and backward axle position results in the lowest speed and acceleration, with a lower stroke frequency and an increased shoulder ROM. The up and forward axle position was the most conducive to stroke compared with other positions were analysed. |
| **Gil-Aqudo et al. 2011** | To compare the forces and moments of the whole upper limb, analysing forces and moments at the shoulder, elbow and wrist joints simultaneously during manual wheelchair propulsion of persons with different levels of spinal cord injury (SCI) on a treadmill. | (n=51) people were grouped by their level of SCI: C6, C7 tetraplegia, high paraplegia and low paraplegia. An inverse dynamic model was defined to compute net joint forces and moments from segment kinematics, the forces acting on the pushrim, and subject anthropometrics. Right side, upper limb kinematic data were collected with four camcorders. Kinetic data were recorded by replacing the wheels with SmartWheels. | Increased superior joint forces in the shoulder, elbow and wrist, an increased adduction moment in the shoulder and the constancy of the moments of force of the wrist. This pattern may increase the risk of developing upper limb overuse injuries in tetraplegic subjects. |

| | | | |
|---|---|---|---|
| **Gorce and Louis 2010** | To record upper limb muscle recruitment patterns using surface electromyography during wheelchair propulsion. Recordings were made for various wheelchair configurations to understand the effect of wheelchair configuration on muscle recruitment. | (n=10) paraplegic and (n=10) able-bodied subjects propelled a test wheelchair on a roller ergometer system at a comfortable speed. (12) Wheelchair configurations were tested. Upper limb surface electromyography and kinematics were recorded for each configuration. Based on the hand position relative to the handrim, the propulsion cycle was divided into three phases to explain the activation patterns. | Compared to the able-bodied subjects, the paraplegic subjects presented higher activation. During early push, activation of nearly all muscles was affected by the axle position, where as seat height only affected BB and PM activation. During late push, the AD was affected by axle position and the BB by seat height. During recovery, the TZ was affected by axle position, the PD by seat height and the BB by both. This study provides indications on how muscle recruitment is affected by wheelchair configuration. |
| **Gorce and Louis 2012** | To examine the influence of the wheelchair settings on upper limb kinematics during wheelchair propulsion. | (n=10) experts and (n=10) beginners' subjects propelled an experimental wheelchair on a roller ergometer system at a comfortable speed. (12) wheelchair configurations were tested. Kinematics were recorded for each configuration. Based on the hand position relatively to the handrim, the main kinematic parameters of wheelchair propulsion were investigated on the whole propulsion cycle and a key event such as handrim contact and release. | Compared to the beginner subjects, all the experts' subjects generally present higher joint amplitude and propulsion speeds. Seat height and antero-posterior axle position influence usage of the hand-rim, timing parameters and configurations of upper limb joints. Low and backward seat position allow a greater efficiency. Too low and backward seat position, increasing joints positions and amplitudes, could increase the risk of upper limb injuries in relation with manual wheelchair propulsion. |
| **Guo et al. 2003** | To investigate the characteristics of mechanical energy and power flow of the upper limb during wheelchair propulsion. | (n=12) healthy male adults were recruited for this study. 3D kinematic and kinetic data of the upper extremity were collected during wheelchair propulsion using a Hi-Res Expert Vision system and an instrumented wheel, respectively. | Joint power plays an important role in energy transfer as well as the energy generated and absorbed by muscles spanning the joints during wheelchair propulsion. Energy and power flow information during wheelchair propulsion allows gaining a better understanding of the coordination of the movement by the musculoskeletal system. |

| | | | |
|---|---|---|---|
| **Guo et al. 2013** | To examine the effect of handrim size (54 cm, 43 cm, and 32 cm) on mechanical energy and power flow during wheelchair propulsion. | (n=12) healthy male adults were recruited for this study. 3D kinematic and kinetic data of the upper extremity were collected during wheelchair propulsion using a Hi-Res Expert Vision system and an instrumented wheel, respectively. | The kinetic, potential and total mechanical energy of the upper extremity increased as the handrim size increased. The joint translational power and the rotational power of the proximal joint increased with increasing handrim size. The increased kinetic, potential and total mechanical energy were due to the increased linear velocity and the elevated positions of the upper extremity segments. The shoulder and trunk flexors increased the magnitude of their concentric contractions during propulsion with the large handrim as increased output power is required. |
| **Hubert et al. 2009** | To compare spatio-temporal propulsion characteristics and shoulder muscle electromyographic activity in persons with cervical spinal cord injury propelling a standard pushrim wheelchair and a commercially available pushrim-activated power assisted wheelchair (PAPAW) design on a stationary ergometer. | (n=14) participants propelled a standard pushrim WC and PAPAW during 3 propulsion conditions: self-selected free and fast and simulated 4% or 8% graded resistance propulsion. | For participants with complete tetraplegia, push phase shoulder muscle activity was decreased in the PAPAW compared with standard pushrim WC, indicating a reduction in demands when propelling a PAPAW. |

| | | | |
|---|---|---|---|
| **Hughes et al. 1992** | To investigate the biomechanics of lever and hand-rim propulsion and the effects of seat position on propulsion mechanics. | (n=9) able-bodied and (n=6) paraplegic spinal cord injured persons participated and performed hand-rim and lever propulsion on a wheelchair test simulator at a speed and load of 3km/hr and 7.5 watts/side, respectively. Direct measurement techniques were used to monitor and quantify 3D motion measures of the trunk, shoulder, elbow, and wrist. Hub torque and stroke arc measurements were determined. The major components of the system included the following: seating frame, dynamometer and visual feedback system, motion sensors, and data-acquisition software. | Hand-rim propulsion required less elbow motion, greater shoulder extension, less shoulder rotation and less arm abduction than lever propulsion. Both methods of propulsion required a substantial amount of internal rotation at the shoulder. Seat position changes had a greater effect on joint motion ranges when hand-rim propulsion was performed. The findings provide additional information for development of a model for the optimization of wheelchair propulsion. |
| **Kulig et al. 1998** | To quantify the forces and moments at the shoulder joint during free, level wheelchair propulsion and to document changes imposed by increased speed, inclined terrain, and 15 minutes of continuous propulsion. | A six-camera VICON motion analysis system, a strain gauge instrumented wheel, and a wheelchair ergometer. (n=17) men with low level paraplegia participated in this study. Shoulder joint forces and moments were calculated using a 3D model applying the inverse dynamics approach. | At the end of 15 minutes of continuous free propulsion, there were no significant changes compared with short duration free propulsion. The increased joint loads documented during fast and inclined propulsion could lead to compression of subacromial structures against the overlying acromion. |
| **Kulig et al. 2001** | The effects of spinal cord injury level on shoulder kinetics during manual wheelchair propulsion were studied. | (n=69) male subjects were divided into four groups: low level paraplegia (n=17), high level paraplegia (n=19), C7 tetraplegia (n=16) and C6 tetraplegia (n=17). Measurements were recorded using a six-camera VICON motion analysis system, a strain gauge instrumented wheel, and wheelchair ergometer. Shoulder joint forces and moments were calculated using the inverse dynamics approach. | Increased vertical force at the shoulder joint, coupled with reduced shoulder depressor strength, may contribute to shoulder problems in subjects with tetraplegia. Wheelchair design modifications, combined with strength and endurance retention, should be considered to prevent shoulder pain development. |

| | | | |
|---|---|---|---|
| **Mercer, Boninger, Knootz, Cooper 2006** | To examine the relationship between shoulder forces and moments experienced during wheelchair propulsion and shoulder pathology. | Kinetic and kinematic data was recorded from (n=33) subjects with paraplegia as they propelled their wheelchairs at two speeds (0.9 and 1.8 m/s). Shoulder joint forces and moments were calculated using inverse dynamic methods and shoulder pathology was evaluated using a physical exam and magnetic resonance imaging scan. | Specific joint forces and moments were related to measures of shoulder pathology. This may indicate a need to reduce the overall force required to propel a wheelchair in order to preserve upper limb integrity. |
| **Morrow et al. 2010** | To investigate shoulder joint kinetics over a range of daily activity and mobility tasks associated with manual wheelchair propulsion to characterize demands placed on the shoulder during the daily activity of manual wheelchair users. | (n=12) individuals who were experienced manual wheelchair users. Upper extremity kinematics and handrim wheelchair kinetics were measured over level propulsion, ramp propulsion, start and stop over level terrain, and a weight relief maneuver. Shoulder intersegmental forces and moments were calculated from inverse dynamics for all conditions. | Weight relief resulted in significantly higher forces and ramp propulsion resulted in significantly higher moments than the other conditions. Surprisingly, the start condition resulted in large intersegmental moments about the shoulder equivalent with that of the ramp propulsion, while the demand imparted by the stop condition was shown to be equivalent to level propulsion across all forces and moments. |
| **Mulroy et al. 1996** | Phasing and intensity of shoulder muscle activity during wheelchair propulsion were documented to identify muscles at risk for fatigue and overuse. | EMG activity of 12 muscles was recorded with wire electrodes in (n=17) paraplegic men during propulsion on a stationary ergometer. Push and recovery phases of the propulsion cycle were determined with an instrumented pushrim. EMG intensities, onset and cessation of EMG were compared between muscles. | Muscles most vulnerable for fatigue were pectoralis major, supraspinatus, and recovery muscles. Endurance training was recommended. |

| | | | |
|---|---|---|---|
| **Mulroy et al. 2004** | To determine the influence of spinal cord injury (SCI) level on shoulder muscle function during wheelchair propulsion. | (n=69) men, different SCI level Fine-wire electromyographic activity of 11 muscles was recorded during wheelchair propulsion. Timing of muscle activity onset, cessation, and duration, and time of peak intensity for each functional group were compared Median electromyographic intensity was also compared. | For subjects with tetraplegia, pectoralis major activity was significantly prolonged compared with subjects with paraplegia. Subscapularis activity shifted from a recovery pattern in subjects with paraplegia to a push pattern in persons with tetraplegia. Level of SCI significantly affected the shoulder muscle recruitment patterns during wheelchair propulsion. Differences in rotator cuff and pectoralis major function require specific considerations in rehabilitation program design. |
| **Mulroy et al. 2005** | To document the effect of fore-aft seat position on shoulder joint kinetics. | (n=13) men with complete motor paraplegia propelled a test WC in 2 fore-aft seat positions during free, fast, and graded conditions. The seat-anterior position aligned the glenohumeral joint with the wheel axle and the seat-posterior position moved the glenohumeral joint 8 cm posteriorly. The right wheel of the test chair was instrumented to measure forces applied to the pushrim. An inverse dynamics algorithm was applied to calculate shoulder joint forces, external moments, and powers. | The superior component of the shoulder joint resultant force was significantly lower in the seat-posterior position. During graded propulsion, the posterior component of the shoulder joint force was significantly higher with the seat posterior. Peak shoulder joint moments and power were similar during free and fast propulsion. The seat-posterior position displayed increased internal rotation moment, decreased sagittal plane power absorption, and increased transverse plane power generation. This investigation provides objective support that a posterior seat position reduces the superior component of the shoulder joint resultant force. Consequently, this intervention potentially diminishes the risk for impingement of subacromial structures. |

| | | | |
|---|---|---|---|
| **Newsam et al. 1999** | To analyse 3D upper extremity motion during manual wheelchair propulsion in men with different levels od spinal cord injury | To compare three dimensional upper extremity motion during wheelchair propulsion in persons with 4 levels of spinal cord injury: low paraplegia (n=17), high paraplegia (n=19), C7 tetraplegia (n=16), and C6 tetraplegia (n=17). Upper extremity motion was recorded as subjects manually propelled a wheelchair mounted on a stationary ergometer. | Subjects with paraplegia had similar patterns suggesting that the wheelchair backrest adequately stabilizes the trunk in the absence of abdominal musculature. Compared with paraplegic subjects, those with tetraplegia differed primarily in the strategy used to contact the wheel. This was most evident among subjects with C6 tetraplegia who had greater wrist extension and less forearm pronation. |
| **Richter et al. 2007** | To investigate the natural stroke patterns of wheelchair users pushing on a level surface, to determine if users adapt their stroke patterns for pushing uphill, and to assess whether there are biomechanical advantages to one or more of the stroke patterns. | (n=26) manual wheelchair users with a spinal cord injury. Subjects pushed their own wheelchairs at self-selected speeds on a research treadmill set to level, 3º and 6º grades. Stroke patterns were measured using a motion capture system. Handrim biomechanics were measured using an instrumented wheel. Stroke patterns were classified for both level and uphill propulsion according to 1 of 4 common classifications: arcing, semi-circular, single-looping (SLOP), and double-looping (DLOP). Biomechanical outcomes of speed, peak handrim force, cadence, and push angle were all compared across stroke classifications using an analysis of variance. | Wheelchair users likely adapt their stroke pattern to accommodate their propulsion environment. Based on the large percentage of subjects who adopted the arcing pattern for pushing uphill, there may be benefits to the arcing pattern for pushing uphill. In light of this and other recent work, it is recommended that clinicians not instruct users to utilize a single stroke pattern in their everyday propulsion environments. |

| | | | |
|---|---|---|---|
| **Rodgers et al. 1994** | To investigate the wheelchair propulsion biomechanics of spinal cord injured (SCI), non-athletic wheelchair users. | (n=20) male paraplegic patients were videotaped during propulsion to fatigue on a stationary, instrumented wheelchair positioned on a roller with adjustable frictional resistance. | Peak handrim force was significantly correlated with concentric shoulder flexion and elbow extension isokinetic torques. Significant changes with fatigue were found in increased peak handrim force, decreased ulnar/radial deviation range of motion, and increased trunk forward lean. The highest calculated joint moments were found in shoulder flexion. Results suggest that potentially harmful changes occur with fatigue, and that the shoulder may be the most prone to musculotendinous-type overuse injury. |
| **Samuelsson et al. 2004** | To analyse the effects of rear-wheel position on wheelchair propulsion and seating aspects. With the hypothesis that seat inclination affects propulsion efficiency and seating in wheelchairs. | A randomized experimental crossover design was used to perform this analysis. (n=25) wheelchair users with paraplegia caused by a SCI were randomly selected from the records of the Unit of Neurological Rehabilitation at the University Hospital in Linköping, Sweden. Two activities were wheelchair propulsion on a treadmill and computer work for 30 minutes. | A simple correlation between wheelchair ergonomics and propulsion efficiency and seating comfort may not exist. Changing the position of the rear wheels and because of this changing, the weight distribution and seat angle of the wheelchair significantly affected propulsion ergonomics concerning push frequency and stroke angle. |

| | | | |
|---|---|---|---|
| **Schantz et al. 1999** | To monitor muscle activation and movement patterns of old injured and long experienced persons with paraplegia and tetraplegia during level free-wheeling propulsion. The subjects used their own wheelchairs, and three conditions were studied: self-chosen normal "everyday life" velocity, maximal velocity and maximally accelerated start. | Two groups: subjects with paraplegia (n= 4) and tetraplegia (n= 3). All subjects were physically active and experienced wheelchair users. The tests were done in the subjects' own wheelchairs and under free-wheeling conditions. The tasks studied were: self-chosen normal velocity, maximal velocity and maximally accelerated start. Muscle activation was registered by surface electromyography performed on several arm and shoulder muscles. The movement pattern was studied by goniometry of the shoulder and elbow joints, as well as by observing video recordings. Speed and arm cycle frequency were also recorded. | Results point to both similarities and differences in the movement pattern and muscle activation in individuals with para- and tetraplegia under different ambulation conditions. The differences are of such a magnitude that they are important enough to consider when teaching wheelchair techniques and developing rehabilitation programmes for different groups of patients with spinal cord injuries. |
| **Shimada, Boninger, Cooper 1998** | To characterise wheelchair propulsion stroke patterns by investigating joint accelerations, joint range of motions, wheelchair propulsion phases, and stroke efficiency. | (n=7) experienced wheelchair users (5 males, 2 females) were filmed using a three-camera motion analysis system. Each subject pushed a standard wheelchair fitted with a force-sensing pushrim (SMARTWheel) at two speeds (1.3 m/s and 2.2 m/s). | Three distinctly different stroke patterns: semi-circular (SC), single looping-over-propulsion (SLOP), and double looping-over-propulsion (DLOP), were identified from the kinematic analysis. Through our analysis of these patterns, SC was more biomechanically efficient than the other stroke patterns. |
| **Soltau et al. 2015** | To evaluate bilateral symmetry during manual wheelchair propulsion in a large group of subjects across different propulsion conditions. | 3D kinematics and handrim kinetics along with spatiotemporal variables were collected and processed from (n=80) subjects with paraplegia while propelling their wheelchairs on a stationary ergometer during three different conditions: level propulsion at their self-selected speed (free), level propulsion at their fastest comfortable speed (fast), and propulsion on an 8% grade at their level, self-selected speed (graded). | Results support the assumption of symmetry in manual wheelchair propulsion for studies that analyse groups of subjects without significant upper extremity pain or impairment. Small asymmetries likely exist in propulsion variables, and these may increase when propelling under more strenuous conditions. Thus, the validity of the symmetry assumption should be carefully considered in light of the specific research aims and methods. |

| | | | |
|---|---|---|---|
| **Tsai et al. 2012** | To investigate the effects of rear-wheel cambers on temporal-spatial parameters, joint angles, and propulsion patterns. | (n=12) inexperienced subjects participated in the study, no upper extremities musculoskeletal disorders. 8-camera 3D motion capture - markers attached to the wheelchair-user system during propulsion. Wheelchair had an instrumented wheel with cambers of 0°, 9°, and 15°, respectively, 1 m/s. average velocity. | Rear-wheel camber significantly affects: average acceleration, maximum end angle, trunk movement, elbow joint movement, wrist joint movement, propulsion pattern and joint range of motion.<br>For a 15° camber, the average acceleration and joint peak angles significantly increased. A single loop pattern (SLOP) was adopted by most of the subjects.<br>When choosing a wheelchair with camber adjustment, increase in joint movement and base of support should be considered there. |
| **van der Woude, Veeger, Rozendal 1989** | To study the effect of seat height on the cardiorespiratory system and kinematics in handrim wheelchair ambulation. | (n=9) non-wheelchair users participated in a wheelchair exercise experiment on a motor-driven treadmill. The subjects conducted five progressive exercise tests. After an initial try-out test, four tests were performed at different standardized seat heights of 100º, 120º, 140º, and 160º elbow extension. | Results showed an interrelationship between wheelchair seat height and both cardiorespiratory and kinematic parameters. With respect to the cardiorespiratory system. |
| **Veeger, van der Woude, Rozendal 1992** | To study the effect of tangential speed of the handrims independent of external power output on gross mechanical efficiency (ME). | (n=9) able-bodied subjects performed wheelchair exercise tests on a stationary ergometer. The ergometer allowed for measurement of torque and 3D forces on the rims and tangential velocity of the rear wheels. | It is suggested that an ineffective direction of forces on the rims might (partly) be responsible for the low ME and for a decrease in ME in relation to tangential handrim velocity. It is concluded that the use of handrims with a lower mechanical advantage will increase wheelchair propulsion efficiency. |
| **Vegter et al. 2013** | To compare the simultaneous outcomes of two different measurement-wheels attached to the different sides of the wheelchair, to determine measurement consistency within and between these instrumented wheels given the expected inter- and intra-limb variability as a consequence of motor control. | (n=9) able-bodied subjects received a three-week low-intensity handrim wheelchair practice intervention. They then performed three four-minute trials of wheelchair propulsion in an instrumented hand rim wheelchair on a motor-driven treadmill at a fixed belt speed. | A good agreement between both measurement-wheels was found at the level of the power output. This indicates a high comparability of the measurement-wheels for the different propulsion parameters. A high variability in forces and timing between the left and right side were found during the execution of this bimanual task, reflecting the human motor control process. |

| | | | |
|---|---|---|---|
| **Wang et al. 1995** | To document the 3D kinematic patterns of wheelchair propulsion across several selected speed conditions and to determine the critical kinematic changes in terms of the initial contact angle, the ratio between the drive and recovery phases, and the 3D linear and angular velocity patterns. | 3D kinematic features of wheelchair propulsion across four selected speeds were investigated based on (n=10) skilled male wheelchair athletes. | Results demonstrated that as the speed increased, the drive phase was performed faster while the range of the push-angle remained constant. More trunk forward lean motion resulted in a large initial contact angle in front of the top dead centre of the pushrim. Recovery involved a large range of vertical motion in terms of shoulder abduction and hyperextension in order to increase the distance over which a greater velocity could be developed. |